SCIENCE & TECHNOLOGY

ARS JOURNAL

A PUBLICATION OF THE AMERICAN ROCKET SOCIETY

VOLUME 30 NUMBER 8 AUGUST 1960

AUTOPILOT
OR
ANTENNA
PROBLEM • • ?

IF YOUR SPECS CALL FOR:

A miniature integrating gyro designed for economy, with superior off-null characteristics, low power consumption, and fast warm-up time . . .

THIS GYRO IS THE ANSWER

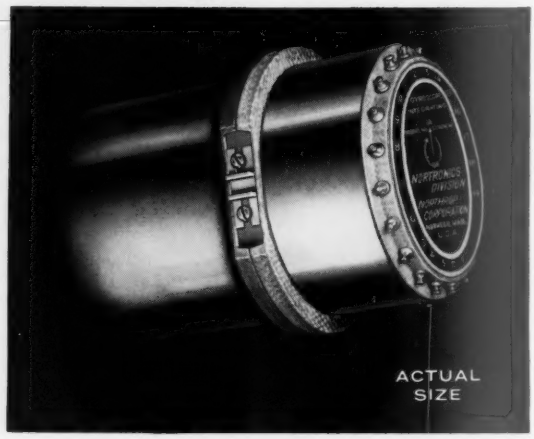

← GI-H5 miniature integrating gyro
Size ←
Cost ←
Perf →

MEASURED CHARACTERISTICS **1.** Total Drift: less than 5°/hour (uncompensated), less than 4°/hour per G. **2.** Storage Temperature: −65°F to +200°F (higher temperature models available). **3.** Extremely stable thermally, with warm-up time to 5% of damping from −65°F within 7 minutes. **4.** Characteristic Time Constant for 6 degree memory angle unit = 0.87 milliseconds. **5.** P.M. Torquer with better than 0.05% linearity and 1 rad/sec peak steady-state torque. Unpack it, put it in the system — it's ready to go. Availability — 90 days. Write or TWX for detailed test data on the GI-H5 (Norwood 835-U, or field offices listed below).

NORTRONICS
A Division of
NORTHROP CORPORATION

PRECISION PRODUCTS DEPARTMENT
NORWOOD, MASSACHUSETTS
Field Offices

Highway #46
Teterboro, New Jersey
Telephone: ATlas 8-1750
TWX-Hasbrouck Heights 871-U

2486 Huntington Drive
San Marino, California
Telephone: ATlantic 7-0461
TWX-Alhambra 9619-U

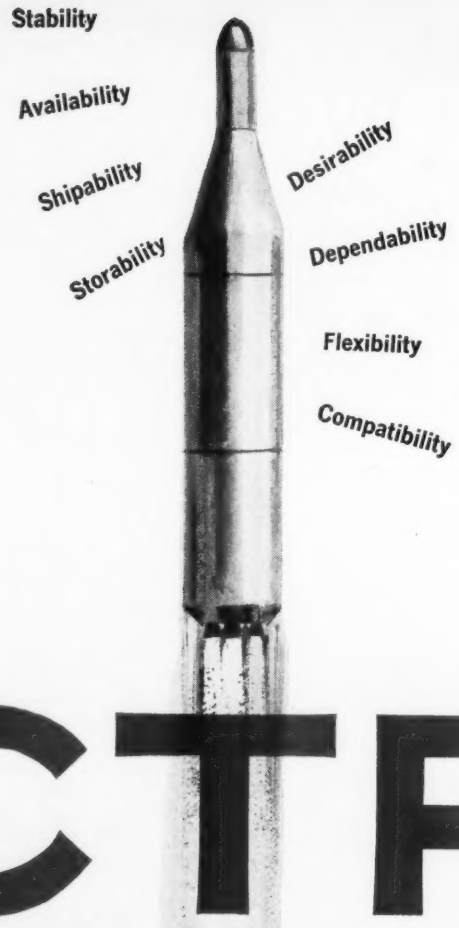

CTF

ideal storable oxidizer

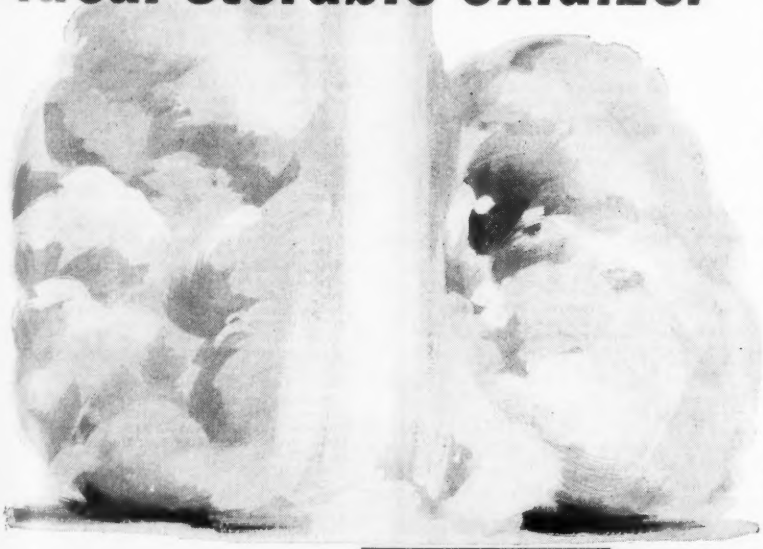

Investigate
the many advantages of Chlorine Trifluoride (ClF_3) as a rocket fuel oxidizer!

Desirability
—Chlorine Trifluoride is one of the most powerful rocket fuel oxidizers known. Its performance compares favorably with other oxidizers far more difficult to handle.

Properties
—CTF has many characteristics desirable in a storable propellant, with a wide liquid temperature range. It has a low freezing point (—105°F) and a moderate boiling point (53°F). Vapor pressure is 80 psia at 140°F.

Storability
—Unlike most liquid propellants, Chlorine Trifluoride requires no refrigeration. It is handled and stored safely and conveniently in standard steel cylinders. No special storing precautions necessary.

Availability
—CTF has been produced commercially by General Chemical for almost 10 years. Readily available in ton and 150-lb. steel cylinders and in smaller sizes.

Stability
—CTF has very high shock resistance; is shipped nationally via common carriers. It is thermally stable up to 450°F.

Dependability
—CTF gives predictable performance. In addition, CTF is hypergolic with hydrogen fuels over a wide range of pressures and temperatures.

Flexibility
—CTF can be used under all geographic and climatic conditions. No need for fixed supply points.

Compatibility
—CTF can be used satisfactorily with properly passivated steels, nickel alloys, copper and other common metals.

Density
—CTF's high density (1.825 gm/cc at 68°F or approximately 15.3 lbs./gallon) leads to outstanding density impulse values with a variety of rocket fuels.

Write today for a free copy of our technical bulletin, "Chlorine Trifluoride." Company letterhead, please.

First in Fluorine Chemistry

Allied Chemical

GENERAL CHEMICAL DIVISION
40 Rector Street, New York 6, N. Y.

ARS JOURNAL

A PUBLICATION OF THE AMERICAN ROCKET SOCIETY

American Rocket Society

500 Fifth Avenue, New York 36, N. Y.

Founded 1930

Scope of ARS JOURNAL

This Journal is devoted to the advancement of astronautics through the dissemination of original papers disclosing new scientific knowledge and basic applications of such knowledge. The sciences of astronautics are understood here to embrace selected aspects of jet and rocket propulsion, spaceflight mechanics, high speed aerodynamics, flight guidance, space communications, atmospheric and outer space physics, materials and structures, human engineering, overall system analysis, and possibly certain other scientific areas. The selection of papers to be printed will be governed by the pertinence of the topic to the field of astronautics, by the current or probable future significance of the research, and by the importance of distributing the information to the members of the Society and to the profession at large.

Information for Authors

Manuscripts must be as brief as the proper presentation of the ideas will allow. Exclusion of dispensable material and conciseness of expression will influence the Editors' acceptance of a manuscript. In terms of standard-size double-spaced typed pages, a typical maximum length is 22 pages of text (including equations), 1 page of references, 1 page of abstract and 12 illustrations. Fewer illustrations permit more text, and vice versa. Greater length will be acceptable only in exceptional cases.

Short manuscripts, not more than one quarter of the maximum length stated for full articles, may qualify for publication as Technical Notes or Technical Comments. They may be devoted to new developments requiring prompt disclosure or to comments on previously published papers. Such manuscripts are published within a few months of the date of receipt.

Sponsored manuscripts are published occasionally as an ARS service to the industry. A manuscript that does not qualify for publication, according to the above-stated requirements as to subject, scope or length, but which nevertheless deserves widespread distribution among jet propulsion engineers, may be printed as an extra part of the Journal or as a special supplement, if the author or his sponsor will reimburse the Society for actual publication costs. Estimates are available on request. Acknowledgment of such financial sponsorship appears as a footnote on the first page of the article. Publication is prompt since such papers are not in the ordinary backlog.

Manuscripts must be double spaced on one side of paper only with wide margins to allow for instructions to printer. Include a 100 to 200 word abstract. State the authors' positions and affiliations in a footnote on the first page. Equations and symbols may be handwritten or typewritten; clarity for the printer is essential. Greek letters and unusual symbols should be identified in the margin. If handwritten, distinguish between capital and lower case letters, and indicate subscripts and superscripts. References are to be grouped at the end of the manuscript and are to be given as follows. For journal articles: Authors first, then title, journal, volume, year, page numbers; for books: Authors first, then title, publisher, city, edition and page or chapter numbers. Line drawings must be clear and sharp to make clear engravings. Use black ink on white paper or tracing cloth. Lettering should be large enough to be legible after reduction. Photographs should be glossy prints, not matte or semi-matte. Each illustration must have a legend; legends should be listed in order on a separate sheet.

Manuscripts must be accompanied by written assurance as to security clearance in the event the subject matter lies in a classified area or if the paper originates under government sponsorship. Full responsibility rests with the author.

Preprints of papers presented at ARS meetings are automatically considered for publication.

Submit manuscripts in duplicate (original plus first carbon, with two sets of illustrations) to the Managing Editor, ARS JOURNAL, 500 Fifth Avenue, New York 36, N.Y.

ARS JOURNAL is published monthly by the American Rocket Society, Inc. and the American Interplanetary Society at 20th & Northampton Sts., Easton, Pa., U. S. A. Editorial offices: 500 Fifth Ave., New York 36, N. Y. Price: $12.50 per year, $2.00 per single copy. Second-class postage paid at Easton, Pa. This publication is authorized to be mailed at the special rates of postage prescribed by Section 132.122. Notice of change of address should be sent to the Secretary, ARS, at least 30 days prior to publication. Opinions expressed herein are the authors' and do not necessarily reflect the views of the Editors or of the Society.

Science non-fiction at Los Alamos

Is this the shape of things to come in Sherwood?

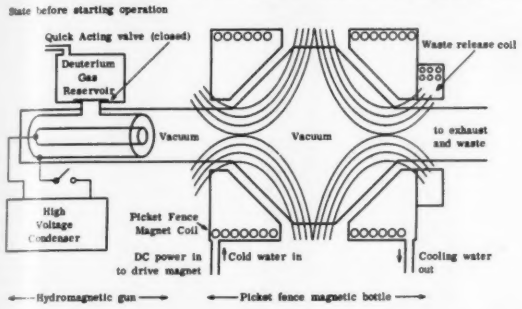

The cusped geometry or picket fence was proposed back in 1954 independently by Grad at N.Y.U. and Tuck at Los Alamos, to get around hydromagnetic instability of plasma-magnetic field interfaces. Nobody did much about it at the time. The pinch effect seemed to hold more promise, so why bother about a leaky picket fence? A large magnet to produce a DC picket fence geometry was built but laid aside. For several years the stabilized toroidal pinch (called Perhapsatron at Los Alamos) held the stage. But as our measuring techniques got better, the pinches began to show a most sinister behavior. An apparently stabilized pinch which should have been radiating energy at the rate of several kilowatts, turned out to be losing it at a rate of hundreds of megawatts. As we got the impurities out of the system, the losses seemed to go down. One pinch (Perhapsatron S-5) has seemed so clean we are trying to raise its temperature to thermonuclear levels by pouring in more power.

Then there appeared the spectre of plasma oscillations and their evil effects on magnetic confinement. In principle, plasma oscillations can thrive on the interaction of a fast wind of plasma electrons moving through a slower cloud of plasma ions. This makes things look bad for the pinch effect, because the plasma has to have a large electric current in it, and therefore an electron wind.

The Russians delivered the next blow. Trubnikov and Kondryatsev predicted an enormous cyclotron radiation flux from a plasma containing a magnetic field. This would ruin the chances for DD reactors, and make things tough even for DT reactors. Among other complications, a nearly perfect mirror would have to be placed around the inner wall of the plasma container to reflect the radiation back.

Then Rosenbluth and Drummond argued that when the angular distribution is considered, the radiation isn't really so bad—say 1/50th of what T and K say. Now Trubnikov has come right back with another paper that says it is five times worse than R and D said it was. The above theories are pretty simple—the real problem is exceedingly difficult theoretically. It may be quite a while before there is anything new in this direction.

Anyhow, the point is that DD reactors with magnetized plasmas now seem to be out. But some people, like Tuck, claim that DD reactors are the only ones that make sense, since a DT reactor which must carry on its back a monstrosity of a tritium recovery plant could never compete with fission power anyhow.

This brings us to the point that if we want to have a DD reactor, it has to have no magnetic field in its plasma. So all right, don't put a magnetic field in the plasma. Unfortunately, there aren't any magnetic confinement systems stable enough to hold a pure plasma, except one. You've guessed it—it's the picket fence.

So we went back to the warehouse and dusted off the magnet we built long ago. Already it is going full blast, a second one has been built and a third one is on its way. Of course, we aren't alone any more in this field. Small cusped geometries are being studied at General Atomic, Livermore, Stevens, Harwell, Utrecht and Kharkov. Pretty soon we will have only picket fences and plasma guns at Los Alamos, aside from a few Scyllas to study plasma at thermonuclear temperatures, unless old Perhapsatron S-5 does something pretty spectacular.

The diagram of Picket Fence I (above), run by D. Hagerman and J. Osher, shows how plasma is injected as a slug, strong enough to push through the magnetic field and spread out inside. (This is called entropy trapping, but that's another story). Does it work? Well, that depends. It's a lot more complicated than we thought. At first, we nearly died of joy when the plasma was shot in and seemed to stay around for ages in our time scale (1000 microseconds), emitting light in the process. But when a magnetic probe was inserted, the harsh truth was revealed—the containment lasted only a few microseconds. In other words, the long time period we thought we had observed was merely cold plasma emitting light by recombination.

Just lately, however, Messrs. Hagerman and Osher have cleaned things up to the point that hot plasmas are pushing the field aside strongly and are keeping the inside field pushed aside for very satisfying periods, like 50 microseconds. Also, if we keep the magnetic probe out of the way of the plasma, it stays around longer, which is what it should do. This particular picket fence is a horror to keep a vacuum in, as it is completely overrun with O rings. The next one will be baked. Fun, eh?

What about the leaks in the fence? It is pretty leaky, but we think we have an answer to that too, so watch for the story on the TLC picket fence one of these days.

For employment information write:
Personnel Director, Division 60-71

Dynamics of Liquids in Moving Containers

R. M. COOPER

Space Technology Laboratories, Inc.
Los Angeles, Calif.

MAN'S interest in the behavior of liquids in various containers is undoubtedly very old. The phenomena of liquid motion within a containing vessel presented a challenge as a natural curiosity to the hydrodynamicist of the past century, and continues to present difficulties for the engineer today. Civil engineers and seismologists have been very active, particularly since the early 1930's, in studying earthquake effects on large dams, oil tanks, water reservoirs and elevated water tanks. More recently, particularly with the advent of the jet age, the effects of fuel motion in partially full tanks have, of necessity, been included in some aircraft dynamic stability studies. With the appearance of the large liquid propelled rocket, where at least 90 per cent of the gross weight at liftoff is contributed by the liquid propellants, the forces and moments produced by the movement of large masses of liquids within their containers take on added importance. The exponential increase in the number of reports and papers on the subject of "sloshing," during the past decade is a reflection of this trend. It will be noted that, with the obvious exception of the work on "centrifugal slosh," only those papers have been surveyed here which consider the liquid to be subject to a gravitational force. Problems of bubble formation and growth, the behavior of liquids in free fall, vortex formation in draining tanks, and other related problems have not, in general, been included. Moreover, attention has been mainly restricted to the American literature, although some British, Russian and a few references in Japanese journals are included. The French, German and Italian literature, probably very rich in this field, remains relatively untouched.

An extensive bibliography pertaining to the general field of "water waves" (136)[1] and two "sloshing" literature surveys, containing many abstracts, are available (141,142). Attention is also directed to (45) for special studies pertaining to specific rocket vehicles.

It should be mentioned that a very large percentage of the reports cited here were carried out under Government contract and are available through the ASTIA offices.

Stationary Containers

The equations of motion of a perfect liquid were given by Euler in 1755 (71), but it was not until 1876 that the solution in its present-day form was given by Rayleigh (108) for the free oscillation of liquid in rigid rectangular and circular tanks of any uniform depth. The problem had been treated earlier by Poisson in 1828 for the circular basin, but the results were not interpreted because the theory of Bessel's functions had not been sufficiently developed at that time [(71) section 191]. The basic differential equations, linearization of the equations and boundary conditions, and solution by separation of variables for the circular and rectangular tanks of uniform depth are also given by Lamb [(71) sections 191, 257]. The technique has proved to be very well suited to cylindrical tanks of uniform depth, since the problem reduces to finding a solution of the two-dimensional wave equation. Thus, in addition to the solution for free oscillations of liquid in the complete circular cylindrical tank (71,108), results are available for the circular sector cross section (20,38,57,107,118); the complete annular cross section (15,19,33,54,57,117); the annular sector cross section, the so-called "ring-sector" tank (19,118); the elliptical cross section (37); the equilateral triangular cross section (57), and, of course, the rectangular cross section [(71) sections 191, 257]. Some numerical computations for the natural frequencies have been carried out for several annular tanks and for the "quarter tank," as a special case of the sector tank (15), based on the results given in (19 and 20). A general treatment of the cylindrical tank of arbitrary cross section has also been given (34,35) and is included as a special case of the completely arbitrary tank (134).

The separation of variables technique has been somewhat less fruitful for cases where the liquid depth is variable. A closed form solution has been obtained (49,51,73) for one eigenvalue in the case of the conical tank having a semi-apex angle $\alpha = \tan^{-1}\sqrt{m}$ $(m = 1,2,\ldots,)$ and the method has been generalized to apply to certain hyperboloidal tanks having these conical shapes as asymptotes (135). The other approach generally taken is to assume shallow water and two-dimensional flow (i.e., the so-called tidal wave theory) in order to obtain solutions. Under this assumption, the solution for free oscillation of liquid in a circular basin with a parabolically shaped bottom has been obtained exactly [(71) section 193], and an approximate solution has been obtained for the case of an elliptic basin with parabolically varying depth (46). An approximate solution is also given in (71) section 193 for an elliptically shaped basin of uniform depth.

One of the principal limitations in trying to apply the classical separation approach to some of these cases is the lack of a suitable coordinate system, in addition to the other difficulties encountered in treating three-dimensional problems. Because of this, other approaches have been put forward. It has been noted that when the tank is very deep, the bottom can be treated as flat regardless of the actual shape. On the other hand, if the tank is shallow the problem reduces to a two-dimensional one, as the variation with depth can be neglected. These two limiting cases have been employed, via a variational method, to obtain approximate solutions for tanks of

Received June 27, 1960.

[1] Numbers in parentheses indicate References at end of paper.

Dr. Cooper received the B.S.E. degree in 1948 and the M.S.E. and Ph.D. degrees from the University of Michigan in 1952 and 1956, respectively. He has worked at Chance Vought Aircraft, Inc., in its Dynamic Analysis Group and at Douglas Aircraft Co., Inc., as a design specialist in structures. Other papers published have been on dynamic and static problems of plates and shells. The author is currently Head of the Dynamics Section Research Group, Aeromechanics Laboratory at STL.

intermediate depth (72). Results have been obtained for conical tanks (72) and for a circular cylindrical tank with a conical bottom. Reasonably good agreement with experiment has been obtained. In another direction, integral equation techniques have been employed recently to obtain solutions for the circular canal and the spherical tank (32); solutions for some limiting cases are also treated in this reference by a variational method analogous to that given in (72). Other integral equation formulations have also been given, e.g., in (51) for the conical tank, which can be applied to other shapes as well, and in (136), vol. III, p. 354.

Moving Containers

In turning to examples of forced tank motion, the work mentioned previously by the seismologists should be noted. With two exceptions (58,88), the solutions which they have obtained are restricted to impulsive tank motions and neglect any free surface motion which occurs subsequent to the impulse (61,63,64,137). The case of impulsive tank motions has also been considered in (102). Under this restriction, the velocity potential is completely determinate, since either the potential or its normal derivative is specified on all of the fluid boundary surfaces; no "sloshing" can occur. The problem is similar in many respects to that for a completely enclosed liquid.

The equations of motion and the pressure equation for an ideal incompressible liquid referred to a moving coordinate system are given in (71,87 and 136). The velocity potential for the motion of a liquid completely filling an ellipsoidal envelope which is undergoing translation and rotation was given (independently) by Beltrami, Bjerknes and Maxwell in 1873 [(71) section 110]. A very detailed investigation of the motion of a rigid body having cavities completely filled with liquid was carried out by Zhukovskii (140) in 1885. It was shown that such a system could be replaced by an equivalent rigid body with a mass equal to the mass of the system, and having a certain moment of inertia.

The extension of Rayleigh's solution for liquid oscillations in an open rectangular tank to the case of small horizontal tank oscillation was given in the statement of a Royal Naval College examination question, prior to 1938 [quoted in (87) p. 423]. The case of small pitching oscillations of an open rectangular tank about a horizontal axis (located either above or below the tank boundaries, but intersecting the vertical axis of symmetry of the tank) was examined by Binnie (26) in 1941; the free surface boundary condition for this case is discussed in an appendix by Poole. The problem of the oscillation of liquid in a "moving silo" was apparently (105) treated by Pavlenko in 1936, in his book "The Rolling of Ships."

An active interest in the sloshing problem was generated in the aircraft industry around 1948 because of the flight behavior of certain high speed aircraft. Subsequently, some experimental work conducted by NACA in the free-flight wind tunnel at Langley field indicated the sloshing of water in an unbaffled spherical tank caused small amplitude, high frequency lateral oscillations to be superimposed on the normal oscillation of the model [(124), incidentally, this is one of the earliest references in which the term "sloshing" is applied to denote such fuel motion].

A comparatively crude beginning was made in 1950 toward devising a mechanical analog to represent fuel motion effects on aircraft dynamic stability (47). It was suggested that the liquid be replaced by a simple pendulum or a simple pendulum plus a fixed mass. The equations of motion for an aircraft with a number of spherical fuel tanks, wherein the fuel motion was approximated by the motion of solid pendulums, were subsequently set up (121) and used to study the interaction between these pendulums and the airplane. In evaluating the equivalent pendulum analogy as applied to rectangular and circular tanks, solutions were obtained for the case of steady-state sinusoidal horizontal oscillation of the tanks (74). The problem was re-examined next for the case of the rectangular tank undergoing steady-state oscillations in horizontal translation, pitch about a horizontal axis and roll about a vertical axis (48,48a); in (48a), Laplace transforms of all pertinent expressions are also given. A much more sophisticated and consistent mechanical analog, consisting of a fixed mass and an infinite number of undamped spring and mass systems, was also introduced. This model has since been used extensively but not exclusively in aircraft and missile dynamics analyses.

More recently, the rigid right circular cylindrical tank of uniform depth has been treated for small steady-state horizontal oscillations (9,17,44), arbitrary horizontal translation with acceleration small compared to the longitudinal (vertical) acceleration (66), and small steady-state pitch about a horizontal axis (9,17,44,119,120).

The solution for the full, capped circular cylindrical tank undergoing pitching motion has been considered (13,15,44, 140) and experimentally verified (36,139). The cylindrical tank of arbitrary cross section and uniform depth under both horizontal translation and pitch about a horizontal axis was treated (34) shortly after these results appeared, and a beginning was made toward the inclusion of viscous or "boundary layer" effects in the analysis. A formal solution for the pressure distribution, net forces and net moments due to liquid motion in tanks of arbitrary shape undergoing small horizontal oscillations and pitching has been given (134) in terms of certain integrals which can be evaluated either algebraically or numerically, depending on the particular problem. Results are also available, in terms of series of Mathieu functions, for the same forced motions of an elliptic cylindrical tank with flat bottom (37). A general treatment of the arbitrarily shaped tank undergoing forced motion has also been outlined in terms of the velocity potential (30). A Lagrangian equation formulation has been employed to obtain some results for the case of horizontal translation of the spherical tank and the circular canal (32). Very recently, the solutions, together with fairly extensive numerical results, have been given for the circular cylindrical sector tank and the ring sector tank (i.e., annular circular cylindrical sector tank) for the cases of horizontal oscillations in two directions, with pitch about two horizontal axes and roll about a vertical axis (19,20).

All of the theoretical studies cited here assume an incompressible liquid. Viscous effects, in the few places where assumed to exist at all, are restricted to narrow boundary layer regions for the case of the unbaffled tank. Moreover, with the exception of some studies of liquid oscillations in a rotating circular cylinder (69,70,80,81,84), all of the theoretical studies have assumed the flow to be irrotational with respect to an inertial frame of reference, since the fluid is acted on by a rotation-free force field (i.e., the gravitational field); it can be shown (71,87) that motion of the solid tank boundaries cannot produce rotational flow if the flow was initially irrotational. All of the results obtained are restricted to small free surface slopes, displacements and velocities, and consequently also to forcing frequencies which are not too near the natural frequencies of liquid oscillation, because of the assumptions of linearized boundary conditions and no damping. However, experimental studies indicate that these results may be applied reasonably close to resonance conditions (2) without large error. For an excellent discussion of the mathematical implications attendant on the linearization of the free surface boundary condition, see (129) chap. 2. Results are usually limited to those for the antisymmetrical sloshing modes having a single nodal diameter. In the case of the circular cylindrical tank, the orthogonality condition for trigonometric functions insures that this is the only class of motion which will contribute to the net horizontal force and moment exerted by the liquid on the tank. Exceptions to this, of course, are the sector and the ring sector tanks (19,20) where all classes must necessarily be included.

Experimental verifications of the theory of liquid oscillations began appearing simultaneously with the development of the theory. In the paper in which he discussed free oscillations of liquid in a circular cylindrical tank, Rayleigh also presented experimental results showing remarkable correlation with the theory (108). It is reassuring to know that succeeding investigators have generally arrived at similar conclusions for this case. Some experimental results together with a detailed discussion of the observed phenomena, by Guthrie (52), were available the year preceding Rayleigh's work. It may be of interest to note that some of the experimental difficulties which plagued Guthrie, such as the slow rotation or shifting of a nodal diameter, or the unexpected appearance of a symmetrical mode, have continued to occur. In the light of accumulated knowledge, the shifting of a nodal diameter was probably due to slightly out-of-round tanks (37), and a coupling between two classes of motion because of large amplitudes of motions may explain the unexpected modes (63) that were observed. [In a recent experiment, a small amount of ellipticity was deliberately introduced to insure that sloshing would occur in the desired direction (35).] Excellent correlation has been reported recently (2) between theoretical and experimental results for the case of steady-state horizontal oscillation of the right circular cylindrical tank [pressure distribution, net horizontal force and moment about an axis along the tank bottom, as well as resonant frequencies are reported (3,4)]. It is anticipated that similar results for other types of motion will be reported soon. The first few resonant frequencies have been investigated experimentally for the spherical tank and the circular canal (78), and again indicate excellent agreement with theory (32). The frequency response under impulsive tank motion has also been reported (63,88).

Viscous damping in smooth walled tanks has been found to have negligible effect on such properties as the natural frequencies (2,27,35,35a). However, damping can be a very critical part of the control and stability problem, particularly when the control system natural frequencies are close to the liquid sloshing natural frequencies; a good deal of work has been reported on this subject (45). A theoretical analysis of the damping produced by a ring baffle (86) has shown excellent agreement with experimental results (103,104). Other damping devices, such as floating cans and baffles of different sorts (2,5,17) have also been investigated experimentally. Finally, damping effects have been included in a control and stability analysis, in which the internal tank conditions do not permit a very rigorous treatment. Experimentally determined values for damping associated with each of the natural frequencies have been introduced into the theoretical results for the undamped system via the simple expedient of directly modifying the "resonance terms" in the denominator, so that they appear as in the case of a linear spring-mass-damper system (7,11). Precautions were taken to insure that the results reduced to the correct ones in the limiting cases of zero damping and "infinite damping," i.e., where there is no sloshing, so that the liquid behaved as if it were in a full, capped tank. An improved mechanical analog, wherein damping associated with rigid body rotation of the nonsloshing mass is included, is also forthcoming (60).

During the period from 1950 to the present, numerous contributions have appeared in the Russian literature. Although publication was apparently delayed until 1956 (at which time an extension for the case of an annular tank was added), the problem of the motion of a circular cylindrical tank partially filled with liquid was presented at a mechanics seminar of the Mathematical Institute of the Academy of Sciences in 1950. [See (102).] In 1951, the behavior of a rectangular tank undergoing small horizontal oscillations under an external elastic restoring force was treated, and some stability considerations were discussed (127); see (91 and 136) for additional comments. The general problems of motion of a rigid body containing liquid with a free surface and stability conditions have been treated extensively since 1952 (29,67,90, 91,93,100,105,114,115). The results have been applied to engineering problems, such as those encountered in ships, oscillations of pendulums containing liquid, and plane oscillations of rectangular and cylindrical tanks (89,92,94,95,101, etc.). More recently, two papers (96,99) have appeared wherein some higher order (i.e., nonlinear) wave amplitude and velocity effects are introduced.

Related Topics

Related topics which have been discussed include the disturbed motion of a liquid with a free surface in a rotating cylindrical tank [(69,70,71,80,81,84) sections 207 et seq.]. The natural frequencies of free surface oscillations of a rotating liquid relative to a rigid body rotation of constant angular velocity have been studied for a deep tank and the results applied to forced, transverse oscillations of the tank (84). Consideration has also been given to a non-full, rotating tank where centripetal acceleration is assumed to play the same role as that of gravity in the classical sloshing problem. The term "centrifugal slosh" has been coined to describe this case. The effective mass of a rotating annular cylinder subjected to an oscillation transverse to the spin axis has been given, and the mathematical aspects of the solution discussed (69,70,80,81). Another problem which has been treated is that of oscillation of liquid in connected tanks (8,16). Considerations of stability and stability criteria are included in (43,53,56).

The interaction between flexible tanks and liquid sloshing has also received notice. In most studies, a simple beam bending mode is assumed, and the sloshing is treated as a forced motion problem (10,97,98,106). Attempts have been made to include effects of wall bending (22,62,82,111); the frequencies and mode shapes of the coupled system have also been investigated (85,97,98,112).[2] Indications are that the effect of a free liquid surface on the first natural frequency of a liquid-filled free-free beam is to produce increases on the order of 25 per cent (85).

Summary

The small motion of an ideal liquid in a fixed or moving rigid container of simple geometrical shape is either known or methods are available for obtaining approximate but reasonable solutions. The effects of viscous damping and of certain damping devices have been studied. It is reasonable to expect that future results will include extensions of the theory to admit somewhat larger wave amplitudes and a better understanding of the interaction between the liquid and the flexible walls of its container.

References

1 Abramson, H. N., Martin, R. J. and Ransleben, G., "Application of Similitude Theory to the Problem of Fuel Sloshing in Rigid Tanks," 23 May 1958, TR no. 1, Contract: DA-23-072-ORD-1251, Southwest Research Institute, San Antonio, Texas.

2 Abramson, H. N. and Ransleben, G., "Simulation of Fuel Sloshing Characteristics in Missile Tanks by Use of Small Models," 20 March 1959, TR no. 3, Contract: DA-23-072-ORD-1251, Southwest Research Institute, San Antonio, Texas.

3 Abramson, H. N. and Ransleben, G., "Some Comparisons of Sloshing Behavior in Cylindrical Tanks With Flat and Conical Bottoms," 15 May 1959, TR no. 4, Contract: DA-23-072-ORD-1251, Southwest Research Institute, San Antonio, Texas.

4 Abramson, H. N. and Ransleben, G., "A Note on Wall Pressure Distributions During Sloshing in Rigid Tanks," 15 June 1959, TR no. 5, Contract: DA-23-072-ORD-1251, Southwest Research Institute, San Antonio, Texas.

5 Abramson, H. N. and Ransleben, G., "A Note on the Effectiveness of Two Types of Slosh Suppression Devices," 15 June 1959, TR no. 6, Contract: DA-23-072-ORD-1251, Southwest Research Institute, San Antonio, Texas.

6 Bauer, H. F., "Approximate Effect of Ring Stiffener on the Pressure Distribution in an Oscillating Cylindrical Tank Partly Filled With a Liquid." 12 September 1957, DA Memo no. 264, DA-M-114, Army Ballistic Missile Agency, Redstone Arsenal, Ala.

7 Bauer, H. F., "Damped Fluid Oscillations in a Circular Cylindrical

[2] For a treatment wherein the liquid is considered as a compressible fluid, see (24).

Tank Due to Bending Tank Walls," 16 May 1958, Rep. no. DA-TR-9-58, Army Ballistic Missile Agency, Redstone Arsenal, Ala.

8 Bauer, H. F., "Damped Oscillations in a Connected Fluid System," 1 May 1959, Rep. no. DA-TM-57-59, Army Ballistic Missile Agency, Redstone Arsenal, Ala.

9 Bauer, H. F., "Fluid Oscillations in a Circular Cylindrical Tank," 18 April 1958, Rep. no. DA-TR-1-58, Army Ballistic Missile Agency, Redstone Arsenal, Ala.

10 Bauer, H. F., "Fluid Oscillations in a Circular Cylindrical Tank Due to Bending of Tank Wall," 18 April 1958, Rep. no. DA-TR-3-58, Army Ballistic Missile Agency, Redstone Arsenal, Ala.

11 Bauer, H. F., "Fluid Oscillations in a Cylindrical Tank With Damping," 23 April 1958, Rep. no. DA-TR-4-58, Army Ballistic Missile Agency, Redstone Arsenal, Ala.

12 Bauer, H. F., "Fluid Oscillations of a Circular Cylindrical Tank Performing Lissajous-Oscillations," 18 April 1958, Rep. no. 2-58, Army Ballistic Missile Agency, Redstone Arsenal, Ala.

13 Bauer, H. F., "Force and Moment of a Liquid on a Rigidly Fixed Lid on the Free Fluid Surface Due to Translational and Rotational Oscillation of a Tank," 20 March 1959, Rep. no. DA-TN-25-59, Army Ballistic Missile Agency, Redstone Arsenal, Ala. (*Confidential*)

14 Bauer, H. F., "The Influence of Fluid in the Tanks on the Moments of Inertia of Jupiter AM 7 and AM 8," 31 March 1958, SA Memo no. 333, Rep. no. DA-M-1-58, Army Ballistic Missile Agency, Redstone Arsenal, Ala.

15 Bauer, H. F., "The Moment of Inertia of a Liquid in a Circular Cylindrical Tank," 23 April 1958, Rep. no. DA-TR-5-58, Army Ballistic Missile Agency, Redstone Arsenal, Ala.

16 Bauer, H. F., and Rheinfurth, M. H., "Oscillations in a Connected Fluid System," 9 April 1959, Rep. no. DA-TM-52-59, Army Ballistic Missile Agency, Redstone Arsenal, Ala. (*Confidential*)

17 Bauer, H. F., "Propellant Sloshing," 5 November 1958, Rep. no. DA-TR-18-58, Army Ballistic Missile Agency, Redstone Arsenal, Ala. (*Confidential*)

18 Bauer, H., F., "The Effective Moment of Inertia in Roll of Propellant and Roll Damping," Rep. no. DA-TR-67-59, Army Ballistic Missile Agency, Redstone Arsenal, Ala.

19 Bauer, H. F., "Free and Forced Fluid Oscillation in Circular Cylindrical Ring Sector Tanks," forthcoming report, Army Ballistic Missile Agency, Redstone Arsenal, Ala.

20 Bauer, H. F., "Free and Forced Fluid Oscillation in Circular Sector Tanks," forthcoming report, Army Ballistic Missile Agency, Redstone Arsenal, Ala.

21 Bauer, H. F., "Determination of Approximate First Natural Frequencies of Fluid in a Spherical Tank," Rep. no. DA-TN-75-58, Army Ballistic Missile Agency, Redstone Arsenal, Ala.

22 Baron, M. L. and Bleich, H. H., "The Dynamic Analysis of Empty and Partially Full Cylindrical Tanks. Part I. Frequencies and Modes of Free Vibration and Transient Response by Mode Analysis," May 1959, Final Report, DASA no. 1123A, 227 pp. Rep. published by Paul Weidlinger, Consulting Engr., N. Y., ASTIA no. 220236.

23 Berlot, R. R., "Production of Rotation in a Confined Liquid Through Translational Motion of the Boundaries," *J. Appl. Mech.*, vol. 26, Dec. 1950, pp. 513–516.

24 Berry, J. G. and Reissner, E., "The Effect of an Internal Compressible Fluid Column on the Breathing Vibrations of a Thin, Pressurized, Cylindrical Shell," *J. Aero. Sci.*, vol. 25, May 1958, pp. 288–294.

25 Binnie, A. M., "Self-Excited Oscillations in an Open Circular Water Tank," *Phil. Mag.*, vol. 46, 1955, pp. 327–337.

26 Binnie, A. M., "Waves in an Open Oscillating Tank," *Engineering*, vol. 151, 1941, pp. 224–226.

27 Birkhoff, G., "Liquid Oscillations in Static Containers," Memo GM-TN-12, 18 April 1956, Space Technology Laboratories, Inc., Los Angeles, Calif.

28 Bleich, H. H., "Longitudinal Forced Vibrations of Cylindrical Fuel Tanks," JET PROPULSION, vol. 26, no. 2, Feb. 1956, pp. 109–111.

29 Bolotin, V. V., "On the Motion of a Liquid in a Vibrating Container," *Prikl. Mat. Mekh.*, vol. 20, 1956, pp. 293–294.

30 Brooks, J. E., "Dynamics of Fluids in Moving Containers," Rep. GM04.4-26, 9 February 1959, Space Technology Laboratories, Inc., Los Angeles, Calif.

31 Brown, K. M., "Laboratory Test of Fuel Sloshing," 18 March 1954, Rep. Dev-782, Douglas Aircraft Co., Santa Monica, Calif.

32 Budiansky, B., "Sloshing of Liquids in Circular Canals and Spherical Tanks," *J. Aero Space Sci.*, vol. 27, May 1960, pp. 161–173.

33 Campbell, I. J., "Wave Motion in an Annular Tank," *Phil. Mag.*, Series 7, vol. 44, 1953, pp. 845–854.

34 Case, K. and Parkinson, W., "On the Motion of a Vessel Containing Fluid With a Free Surface," Memo, 8 February 1956, Space Technology Laboratories, Inc., Los Angeles, Calif.

35 Case, K. and Parkinson, W., "Damping of Surface Waves in an Incompressible Liquid," *J. Fluid Mech.*, vol. 2, 1957, pp. 172–184.

35a Case, K. and Parkinson, W., "The Damping of a Liquid in a Right Circular Cylindrical Tank," Memo GM45-75, 17 September 1956, Space Technology Laboratories, Inc., Los Angeles, Calif.

36 Chobotov, V. and Fowler, J., "Experimental Investigations of the Moment of Inertia in a Cylindrical Tank," Memo GM61.2-3, 18 February 1957, Space Technology Laboratories, Inc., Los Angeles, Calif.

37 Chu, W., "Sloshing of Liquids in Cylindrical Tanks of Elliptic Cross-Section," 26 September 1958, TR no. 2, Contract: DA-23-072-ORD-1251, Southwest Research Institute, San Antonio, Texas; *also* ARS JOURNAL, vol. 30, no. 4, April 1960, pp. 360–363.

38 Clark, C. D., "Natural Frequency Investigation for Propellant in Quarter Tank and Ring Tank Configuration," 28 August 1959, Rep. no. DA-TN-86-59, Army Ballistic Missile Agency, Redstone Arsenal, Ala.

39 Clark, C. D., "Effect of Propellant Oscillation on Saturn Roll Moment of Inertia," Rep. no. DA-TN-87-59, Army Ballistic Missile Agency, Redstone Arsenal, Ala.

40 Conrad, A., "Hydrodynamic Forces Induced in Fluid Containers by Earthquakes," Thesis, California Institute of Technology, Pasadena, 1956.

41 Ehrlich, L., "Exact Solutions for Sloshing Problems," Memo PA 2450/79, 22 September 1959, Space Technology Laboratories, Inc., Los Angeles, Calif.

42 Ewart, D. G., "Fuel Oscillation in Cylindrical Tanks and the Forces Produced Thereby," November 1956, G. W. Technical Note no. 2050, De Havilland Aircraft Co., Ltd., Great Britain.

43 Freed, L. E., "Stability of Motion of Conical Pendulums," Memo GM45.3-434, 16 October 1957, Space Technology Laboratories, Inc., Los Angeles, Calif.

44 Gleghorn, G. J., "Motion of Fluid in a Cylindrical Tank," 27 September 1955 (corrected as of 7 February 1957), Space Technology Laboratories, Inc., Los Angeles, Calif.

45 Gleghorn, G. J., "Pertinent Documents on Sloshing as of 16 October 1957," Memo GM42.6-11, 21 November 1957, Space Technology Laboratories, Inc., Los Angeles, Calif.

46 Goldsbrough, G. R., "The Tidal Oscillations in an Elliptic Basin of Variable Depth," Proc. Roy. Soc., London, Series A, vol. 130, 1930, pp. 157–167.

47 Graham, E. W., "The Forces Produced by Fuel Oscillation in a Rectangular Tank," 13 April 1950, Rep. SM-13748, Douglas Aircraft Co., Inc., Santa Monica, Calif.

48 Graham, E. W. and Rodriquez, A. M., "The Characteristics of Fuel Motion Which Affect Airplane Dynamics," *J. Appl. Mech.*, vol. 19, Sept. 1952, pp. 381–388.

48a Graham, E. W. and Rodriquez, A. M., "The Characteristics of Fuel Motion Which Affect Airplane Dynamics," Rep. SM14212, 27 November 1951, Douglas Aircraft Co., Inc., Santa Monica, Calif.

49 Green, J. W., "Further Remarks on Conical Sloshing," Memo PA/M-553/2, 28 May 1957, Space Technology Laboratories, Inc., Los Angeles, Calif.

50 Green, J. W., "On the Approximation to the Eigenvalues in a Sloshing Problem by the Eigenvalues of the Corresponding Discrete Problem," Memo PA-2450/1, 21 August 1959, Space Technology Laboratories, Inc., Los Angeles, Calif.

51 Green, J. W. and Landau, H. J., "A Third Note on Conical Sloshing," Memo PA/M-553/3, 19 August 1957, Space Technology Laboratories, Inc., Los Angeles, Calif.

52 Guthrie, F., "On Stationary Liquid Waves," *Phil Mag.*, Series 4, vol. 50, 1875, pp. 290–337.

53 Heist, E. K., "Equations of Motion of Missile With Sloshing," Memo GM-TM-146, 8 February 1956, Space Technology Laboratories, Inc., Los Angeles, Calif.

54 Hieatt, J. L., "Sloshing in a Tank Bounded by Concentric Cylinders," Memo GM42.6-507, 1 June 1959, Space Technology Laboratories, Inc., Los Angeles, Calif.

55 Hieatt, J. L. and Riley, J. D., "Digital Program for Fluid Sloshing in Tanks With Axial Symmetry," Rep. TM59-0000-00389, 30 September 1959, Space Technology Laboratories, Inc., Los Angeles, Calif.

56 Hinricks, K. and Kaufman, F. H., "Sloshing Stability Criteria for Vehicles With One Free Surface," Memo GM45.3-45, 12 July 1956, Space Technology Laboratories, Inc., Los Angeles, Calif.

57 Honda, K. and Matsushita, T., "An Investigation of the Oscillations of Tank Water," Scientific Reports Tôhoku Imperial University, First Series, vol. 2, 1913, pp. 131–148.

58 Housner, G. W., "Dynamic Pressures on Accelerated Fluid Containers," *Bull. Seismological Soc. Amer.*, vol. 47, no. 1, Jan. 1957, pp. 15–35.

58a Housner, G. W., "Earthquake Pressures on Fluid Containers," Tech. Rep. 8, Aug. 1954, Earthquake Research Lab., California Institute of Technology, Pasadena, Calif.

59 Howell, E. and Ehler, F. G., "Experimental Investigation of the Influence of Mechanical Baffles on the Fundamental Sloshing Mode of Water in a Cylindrical Tank," Rep. no. GM-TR-69, 6 July 1956, Space Technology Laboratories, Inc., Los Angeles, Calif.

60 Horn, G. J., "Contributions to an Improved Model for Sloshing," forthcoming report, Army Ballistic Missile Agency, Redstone Arsenal, Ala.

61 Hoskins, L. M. and Jacobsen, L. S., "Water Pressure in a Tank Caused by a Simulated Earthquake," *Bull. Seismological Soc. Amer.*, vol. 47, no. 1, Jan. 1957.

62 Hughes, W. G., "Flexure of Thin-Walled Circular Cylindrical Shells," R.A.E. TN-GW-525, Sept. 1959, Royal Aircraft Establishment, Great Britain.

63 Jacobsen, L. S. and Ayre, R. S., "Hydrodynamic Experiments With Rigid Cylindrical Tanks Subjected to Transient Motions," *Bull. Seismological Soc. Amer.*, vol. 41, no. 4, Oct. 1951, pp. 313–346.

64 Jacobsen, L. S., "Impulsive Hydrodynamics of Fluid Inside a Cylindrical Tank and of Fluid Surrounding a Cylindrical Pier," *Bull. Seismological Soc. Amer.*, vol. 39, 1949, pp. 189–204.

65 Jeffries, H., "Free Oscillations of Water in an Elliptical Lake," Proc. London Math. Soc., vol. 23, 1924.

66 Kachigan, K., "Forced Oscillations of a Fluid in a Cylindrical Tank," 4 October 1955, Rep. no. Zu 7-046, Convair, San Diego, Calif.

67 Kirchoff, G. and Hansemann, G., "Versuche über Stehened Schwingungen Des Wassers," *Ann. Physik Chem.* N. F., vol. 10, no. 246, 1880, pp. 337–347.

68 Krein, S. G. and Moiseyev, N. N., "On Vibrations of a Rigid Body Containing Liquid Having a Free Surface," *Prikl. Mat. Mekh.*, vol. 21, 1957, pp. 169–174. Also available as Space Technology Laboratories, Inc., translation STL-T-Ru-17, May 1960.

69 Knopp, M., "Centrifugal Sloshing," Memo PA-2297-02/2, 17 June 1959, Space Technology Laboratories, Inc., Los Angeles, Calif.

70 Knopp, M. and Troesch, B., "Centrifugal Sloshing," Memo PA-2297-02/1, 7 July 1959, Space Technology Laboratories, Inc., Los Angeles, Calif.

71 Lamb, H., "Hydrodynamics," Dover Publications, N. Y., 1945, sixth ed.

72 Lawrence, H. R., Wang, C. J. and Reddy, R. B., "Variational Solution of Fuel Sloshing Modes," JET PROPULSION, vol. 28, no. 11, Nov. 1958, pp. 729–736.

73 Levin, E., "Conical Sloshing," Memo PA/M-553/1, 5 April 1957, Space Technology Laboratories, Inc., Los Angeles, Calif.

74 Lorell, J., "Forces Produced by Fuel Oscillations," 6 October 1951, Progress Rep. 20-149, Jet Propulsion Laboratory, California Institute of Technology, Pasadena.

75 Lorell, J., "Effect of Fuel Sloshing on the Position of the Center of Rotation of a Missile," 14 February 1952, Rep. 20–65, Jet Propulsion Laboratory, California Institute of Technology, Pasadena.

76 Luskin, H. and Lapin, E., "An Analytical Approach to the Fuel Sloshing and Buffeting Problems of Aircraft," *J. Aeron. Sci.*, vol. 19, no. 4,

April 1952, pp. 217–228.

77 MacLaren, A. P. and Thirlwall, G. E., "Flight Trials on the Effects of Propellant Sloshing on the Motion of a Rocket Test Vehicle," R.A.E. Technical Memo GW-348, February 1959 (U.K. Restricted), Royal Aircraft Establishment, Great Britain.

78 McCarty, J. L. and Stephens, D. G., "Investigation of the Natural Frequencies of Fluids in Spherical and Cylindrical Tanks," NASA TN D-252, May 1960.

79 Merten, K. F. and Stephenson, B. H., "Some Dynamic Effects of Fuel Motion in Simplified Model Tip Tanks on Suddenly Excited Bending Oscillations," NACA TN 2789, Sept. 1952.

80 Miles, J. W., "Centrifugal Slosh," Memo GM59.8021.6-1, 19 February 1959, Space Technology Laboratories, Inc., Los Angeles, Calif.

81 Miles, J. W., "Centrifugal Slosh," Memo GM8021.6-2, 27 February 1959, Space Technology Laboratories, Inc., Los Angeles, Calif.

82 Miles, J. W., "Effect of Tank Flexibility on Fuel Sloshing," Memo GM61.4-11, 29 May 1957, Space Technology Laboratories, Inc., Los Angeles, Calif.

83 Miles, J. W. and Young, D., "Generalized Missile Dynamics Analysis–IV Sloshing," GM-TR-0165-00361, 7 April 1958, Space Technology Laboratories, Inc., Los Angeles, Calif.

84 Miles, J. W., "On Free Surface Oscillations in a Rotating Liquid," GM-TR-0165-00458, 18 August 1959, Space Technology Laboratories, Inc., Los Angeles, Calif.

85 Miles, J. W., "On the Sloshing of Liquid in a Flexible Tank," *J. Appl. Mech.*, vol. 25, June 1958, pp. 277–283.

86 Miles, J. W., "Ring Damping of Free Surface Oscillations in a Circular Tank," *J. Appl. Mech.*, vol. 25, June 1958, pp. 274–276.

87 Milne-Thomson, L. M., "Theoretical Hydrodynamics," Macmillan, London, 1950, third ed.

88 Morris, B. T., "A Laboratory Model Study of the Behavior of Liquid-Filled Cylindrical Tanks in Earthquakes," Thesis, Stanford University, June 1938.

89 Moiseyev, N. N., "Dynamics of a Ship Having a Liquid Load," *Izv. Akad. Nauk SSSR, Otd. Tekhn. Nauk*, no. 7, 1954, pp. 27–45. (In Russian.)

90 Moiseyev, N. N., "On Oscillations of a Heavy Ideal and Incompressible Liquid in a Container," *Doklady Akad. Nauk SSSR*, vol. 85, no. 5, 1952, pp. 963–966. (In Russian.)

91 Moiseyev, N. N., "The Motion of a Rigid Body With Cavities Partially Filled With an Ideal Liquid," *Doklady Akad. Nauk SSSR*, vol. 85, no. 4, 1952. (In Russian.)

92 Moiseyev, N. N., "On Two Pendulums Filled With Liquid," *Prikl. Mat. Mekh.*, vol. 16, 1952, pp. 671–678. (In Russian.)

93 Moiseyev, N. N., "The Problem of the Motion of a Rigid Body Filled With a Liquid Having a Free Surface," *Matematicheskii Sbornik*, vol. 32 (74), no. 1, 1953. (In Russian.)

94 Moiseyev, N. N., "The Problem of Small Oscillations of an Open Vessel With a Fluid Under the Action of an Elastic Force," *Ukrainian Mat. Zh.*, vol. 4, 1952, pp. 168–173. (In Russian.)

95 Moiseyev, N. N., "Some Questions of the Theory of Oscillation of Vessels With a Fluid," *Inzhenernyi Sbornik*, vol. 19, 1954, pp. 167–170. (In Russian.)

96 Moiseyev, N. N., "On the Theory of Nonlinear Vibrations of a Liquid of Finite Volume," *Prikl. Mat. Mekh.*, vol. 22, 1958.

97 Moiseyev, N. N., "On the Theory of Elastic Oscillations of a Fluid-Filled Body," *Doklady Akad. Nauk SSSR*, vol. 27, no. 1, 1959, pp. 53–56; *see also Soviet Physics*, vol. 4, no. 4, Feb. 1960.

98 Moiseyev, N. N., "On the Theory of Vibrations of Elastic Bodies With Liquid Cavities," *Prikl. Mat. Mekh.*, vol. 23, no. 5, 1959, pp. 862–878.

99 Narimanov, G. S., "Concerning the Motion of a Container Partially Filled With a Liquid Taking Into Account Large Motions of the Latter," *Prikl. Mat. Mekh.*, vol. 21, no. 4, 1957. (In Russian.) Also available as a Space Technology Laboratories, Inc., translation STL-T-Ru-18.

100 Narimanov, G. S., "Concerning the Motion of a Rigid Body With a Cavity Partially Filled With a Liquid," *Prikl. Mat. Mehk.*, vol. 21, no. 1, 1956, pp. 21–38. (In Russian.)

101 Narimanov, G. S., "Concerning the Motion of a Symmetrical Gyroscope, the Cavity of Which Is Partially Filled With Liquid," *Prikl. Mat. Mekh.*, vol. 21, 1957, pp. 696–700. (In Russian.)

102 Okhotsimskii, D. E., "On the Motion of a Rigid Body With a Cavity Partially Filled With a Liquid," *Prikl. Mat. Mekh.*, vol. 21, no. 1, 1956. (In Russian.) Also available as NASA translation NASA TT F-33, May 1960.

103 O'Neill, J. P., "Semi-Annual Report on Experimental Investigation of Sloshing," 1 July 1957–31 December 1958, TR-GM-0165-00582, Space Technology Laboratories, Inc., Los Angeles, Calif.

104 O'Neill, J. P., "Final Report on an Experimental Investigation of Sloshing," STL-TR-59-0000-09960, 4 March 1960, Space Technology Laboratories, Inc., Los Angeles, Calif.

105 Rabinovich, B. I., "Concerning Equations of Perturbed Motion of a Rigid Body Having a Cylindrical Cavity Partially Filled With a Liquid," *Prikl. Mat. Mekh.*, vol. 21, no. 1, 1956. (In Russian.)

106 Rabinovich, B. I., "Concerning Equations of Elastic Oscillations of Thin-Walled Bars Filled With Liquid Having a Free Surface," *Akad. Nauk SSSR Otd. Tekhn. Nauk, Izv. Mekh. i Mashinostr.*, July–Aug. 1959, pp. 63–68. (In Russian.) Also available as Space Technology Laboratories, Inc., translation STL-T-Ru-19.

107 Rayleigh, Lord, "Scientific Papers," six volumes published between 1869 and 1911.

108 Rayleigh, Lord, "On Waves," *Phil. Mag.*, Series 5, vol. 1, 1876, pp. 257–279.

109 Reese, J. R. and Sewall, J. L., "Effective Moment of Inertia of Fluid in Offset, Inclined, and Swept-Wing Tanks Undergoing Pitching Oscillations," NACA TN 3353, Jan. 1955.

110 Reese, J. R., "Some Effects of Fluid in Pylon-Mounted Tanks of Flutter," NACA RM L55F10, July 1955.

111 Reissner, E., "Complementary Energy Procedure for Vibrations of Liquid-Filled Circular Cylindrical Tanks," 19 June 1957, EM 7–9, GM TR-203, Space Technology Laboratories, Inc., Los Angeles, Calif.

112 Reissner, E., "Notes on Forced and Free Vibrations of Pressurized Cylindrical Shells Which Contain a Heavy Liquid With a Free Surface," AM no. 6–15, 1 November 1956, GM TR 87, Space Technology Laboratories, Inc., Los Angeles, Calif.

113 Richardson, A. R., "Stationary Waves in Water," *Phil. Mag.*, Series 6, vol. 40, 1920, pp. 97–110.

114 Rumiantsev, V. V., "Equations of Motion of a Rigid Body Having Cavities Partially Filled With a Liquid," *Prikl. Mat. Mekh.*, vol. 18, no. 6, 1954, pp. 719–728. (In Russian.)

115 Rumiantsev, V. V., "On Equations of Motion of a Rigid Body With a Cavity Filled With Liquid," *Prikl. Mat. Mekh.*, vol. 19, no. 1, 1955, pp. 1–12. (In Russian.)

116 Sandorff, P. E., "Principles of Design of Dynamically Similar Models for Large Propellant Tanks," NASA TN D-99, Jan. 1960.

117 Sano, K., "On the Seiches of Lake Tôya," Proc. Tôkyô Math-Phys. Soc., 2nd Series, vol. 7, 1913, pp. 17–22.

118 Sasaki, S., "On the Oscillations of Water in Circular-Sectorial and Ring-Sectorial Vessels," Scientific Reports Tôhoku Imperial University, First Series, vol. 3, 1914, pp. 257–270.

119 Schmitt, A. F., "Forced Oscillations of a Fluid in a Cylindrical Tank Undergoing Both Translation and Rotation," 16 October 1956, Rep. no. ZU 7-069, Convair, San Diego, Calif.

120 Schmitt, A. F., "Forced Oscillations of a Fluid in a Cylindrical Tank Oscillating in a Carried Acceleration Field-A Correction," 4 February 1957, Rep. no. ZU 7-074, Convair, San Diego, Calif.

121 Schy, A. A., "A Theoretical Analysis of the Effects of Fuel Motion on Airplane Dynamics," NACA TN 2280, Jan. 1951.

122 Sen, B. M., "Waves in Canals and Basins," Proc. London Math. Soc., Series 2, vol. 26, 1927, pp. 363–376.

123 Sewall, J. L., "An Experimental and Theoretical Study of the Effect of Fuel on Pitching-Translation Flutter," NACA TN 4166, Dec. 1957.

124 Smith, C., "The Effects of Fuel Sloshing on the Lateral Stability of a Free-Flying Airplane Model," NACA RM L8C 16, 29 June 1948.

125 Smith, K. W., "Present Work on the Effect of Fuel Sloshing in the Control of Ballistic Missiles," Note G/W/5/5027/KWS, June 1956, Royal Aircraft Establishment, Great Britain.

126 Smith, K. W., "Fuel Sloshing. Relation Between Surface Movement and Moving Mass Displacement for a Circular Tank," Aug. 1947, GW Dept., File Ref. GW/55027/KWS, Royal Aircraft Establishment, Great Britain.

127 Sretenskii, L. N., "The Oscillations of Liquid in a Moving Container," *Izv. Akad. Nauk SSSR Otd. Tekhn. Nauk*, 1951, pp. 1483–1494. (In Russian.)

128 Stafford, J., "The Oscillations of Liquid in a Circular Cylindrical Tank With Vertical Axis," June 1956, Publication no. TP 183, Saunders-Roe Ltd., Great Britain.

129 Stoker, J. J., "Water Waves—The Mathematical Theory With Applications," Interscience Publishers, Ltd., London, 1957.

130 Stokes, G. G., "On the Theory of Oscillatory Waves," Trans. Cambridge Phil. Soc., vol. 8, 1849, pp. 441–445; *also* Collected Math. and Physical Papers, vol. 1, Cambridge, 1880, pp. 197–229.

131 Strang, W. G., "Difference Solution of the Sloshing Eigenvalue Problem," Memo PA/2450/79, 13 August 1959, Space Technology Laboratories, Inc., Los Angeles, Calif.

132 Strang, W. G., "An Eigenvalue Bound by Finite Differences," Memo PA/2450/2, 18 June 1959, Space Technology Laboratories, Inc., Los Angeles, Calif.

133 Tamiya, S., "On the Dynamical Effect of Free Water Surface," *K. Zosen Kyokai*, vol. 103, 1958, pp. 59–67. (In Japanese.)

134 Trembath, N. W., "Fluid Sloshing in Tanks of Arbitrary Shape," R-GM-45.3-378, 28 August 1957, Space Technology Laboratories, Inc., Los Angeles, Calif.

135 Troesch, B., "Some New Exact Sloshing Solutions," Mathematical Analysis Dept. Numerical Note no. 132, 31 March 1959, Space Technology Laboratories, Inc., Los Angeles, Calif.

136 Wehausen, J. O., "Water Waves," Series 82, six volumes, Institute of Engineering Research, University of California, Berkeley.

137 Werner, P. W. and Sundquist, K. J., "On Hydrodynamic Earthquake Effects," Trans. Amer. Geophysical Union, vol. 30, no. 5, Oct. 1949, pp. 636–657.

138 Westergaard, H. M., "Water Pressures on Dams During Earthquakes," Trans. Amer. Soc. Civil Engrs., vol. 98, 1933, pp. 418–433.

139 Widmeyer, E. and Reese, J. R., "Moment of Inertia and Damping of Fluid in Tanks Undergoing Pitching Oscillations," NACA RM L53E01a, June 1953.

140 Zhukovskii, N. E., "On the Motion of a Rigid Body Having Cavities Filled With Homogeneous Liquid," in "Collected Works," vol. 2, Moscow State Publishing House of Technical Literature, 1949.

141 Sloane, M. N., "The Dynamics of the Sloshing Phenomenon," STL Bibliography no. 35, GM60.5111-5, April 1960, Space Technology Laboratories, Inc., Los Angeles, Calif.

142 Sweitzer, D., "Sloshing of Liquid Propellants," Astronautics Information Literature Search no. 67, Jet Propulsion Labs., California Institute of Technology, Pasadena, 1959. (*Confidential*)

Some Requirements for the Efficient Attainment of Range by Airborne Vehicles

M. ARENS[1]

Israel Institute of Technology
Haifa, Israel

The efficiency of attaining range using either a level cruise or ballistic trajectory can be evaluated by use of a suitable range factor for both trajectories. Use of this factor also allows comparison between aircraft using powerplants of different specific weight and fuel consumption. The ballistic trajectory is examined, and the region in which it is inherently superior to a level cruise trajectory is described as a function of cruising L/D and range. The optimum speeds for cruising flight are determined.

RECENT advances in powerplant technology and improvements in the aerodynamic characteristics of airborne vehicles at supersonic speeds foreshadow significant changes in the equipment to be used in future years for the transportation of payloads over Earth's surface. It is probable that present-day carriers, such as subsonic commercial transports and bombers as well as hypersonic ballistic missiles, will give way to more optimum airframe-powerplant combinations. The measure of the utility of a long range vehicle, or its optimizing criterion, is generally quite complex and is bound to vary with applications. It will in many cases include intangible considerations whose analytical formulation may be difficult, if not impossible. However, in almost all cases vehicle takeoff weight is a primary consideration strongly influencing other yardsticks, such as direct operating cost per ton-mile, development and production costs, etc. It will therefore be used as the optimizing criterion in this paper.

In selecting an aircraft for the accomplishment of a transport mission, the three primary parameters are the vehicle trajectory, the airframe and the powerplant. Thus for any specific airframe-powerplant combination there will generally be an optimum way of flying the desired mission. Or conversely, if the trajectory is specified it should be possible to find the particular airframe-powerplant combination giving the lowest takeoff weight for the accomplishment of the mission. Ideally, the variation of all three parameters should be studied independently in order to arrive at the optimum combination. This approach however is usually not tractable analytically, due to the large number of variables to be considered. An alternate approach is to determine the optimum trajectory for a series of vehicles, or to find the appropriate vehicles for a number of specified trajectories, and to select the best combination by comparing the results of the localized optimization procedures.

Trajectory Considerations

The now classical contributions of Miele (1–4)[2] to the application of the methods of the calculus of variations to trajectory optimization provide explicit solutions for restricted trajectories or for the case where some of the aircraft and powerplant variables are held constant. The solution to the general problem of finding the optimum aircraft for a specified mission must therefore be pieced together from a series of particular solutions. A simpler but less elegant method is to pre-select a number of possible trajectories, determine the optimum vehicle-powerplant combination for each trajectory, and arrive at a general solution by comparing the particular solutions. Using the latter approach, we arbitrarily choose the following possible trajectories for the attainment of long range missions:

1 *Ballistic*—Initial boost from sea level to burnout velocity required so that desired range is attained by subsequent unpowered flight without the use of aerodynamic lift, the unpowered portion of the trajectory being completely determined by Earth's gravitational field.

2 *Glide*—Initial boost from sea level to burnout velocity required so that desired range is attained by subsequent unpowered flight, using aerodynamic lift to glide to the destination.

3 *Skip*—Initial boost from sea level to burnout velocity required so that desired range is attained by subsequent unpowered flight, consisting of a sequence of ballistic paths connected by turns or skips using aerodynamic lift.

4 *Level cruise*—Continuously powered trajectory consisting of climb and acceleration to cruising speed and altitude followed by cruise at constant speed and lift to drag ratio.

Obviously a host of other trajectories are possible, such as, for example, those in which engine power is applied intermittently. But it may be anticipated that for any specific range requirement the best of the selected trajectories will be reasonably close to optimum.

Recently Allen (5) presented a comparison of ballistic, glide and skip trajectories for rocket powered aircraft. His results indicate that whereas there is no significant difference between these three trajectories if the L/D of the vehicles using aerodynamic lift is about 2, the glide and skip trajectories become increasingly superior to the ballistic trajectory as their L/D improves. Since the relative advantages of these trajectories can be assessed from (5), we will limit our attention to the ballistic and level cruise trajectories.

Received Aug. 17, 1959.

[1] Senior Lecturer, Department of Aeronautical Engineering.

[2] Numbers in parentheses indicate References at end of paper.

Comparison of Ballistic and Level Cruise Trajectories

For an aircraft cruising in an isothermal atmosphere at a speed V, at lift to drag ratio L/D, with a specific fuel consumption SFC, the change in aircraft weight W as a function of range S is given by the Breguet range equation (6)

$$W_1/W_2 = e^{\left[\frac{S/3600}{(V/SFC)(L/D)}\right]} \qquad [1]$$

If we wish to compare this with the change in weight of a vehicle flying a ballistic trajectory to cover the same range, we must first determine the required burnout velocity. Assuming an impulsive boost, the relation between burnout velocity and change in vehicle weight is given by (7)

$$V_b = Ig \ln W_1/W_2$$

or expressing the engine specific impulse in terms of the specific fuel consumption, and solving for the weight ratio

$$W_1/W_2 = e^{\left[\frac{V_b\,(SFC)}{3600\,g}\right]} \qquad [2]$$

Equation [2] can be put into a form similar to Equation [1]

$$W_1/W_2 = e^{\left\{\frac{S/3600}{\frac{V_b\cos\psi}{SFC}\left[\frac{(V_s/V_b)^2\,(S/R)}{\cos\psi}\right]}\right\}} \qquad [3]$$

where

$V_s = \sqrt{Rg_0}$, satellite velocity on Earth's surface
R = radius of Earth
ψ = launching angle

A comparison of Equations [3 and 1] leads to a natural definition of effective velocity V_{eff} and effective lift to drag ratio $(L/D)_{eff}$ for a ballistic vehicle as

$$V_{eff} = V_b \cos\psi$$

$$\left(\frac{L}{D}\right)_{eff} = \frac{(V_s/V_b)^2(S/R)}{\cos\psi}$$

Since there is an optimum launch angle ψ and burnout velocity V_b corresponding to each range S, the minimum ratio of vehicle weights is uniquely determined as a function of range. Fig. 1 shows the variation of effective velocity and effective L/D with range for a ballistic vehicle impulsively boosted through a drag-free atmosphere at optimum launching angles. The effective L/D increases with range as a result of the "lifting" effect of the centrifugal acceleration, and reaches a value of π for a range equivalent to half Earth's circumference. At this point the vehicle's effective velocity is 26,000 fps, the satellite velocity.

Comparison of Equation [1] with Equation [3] written in the form

$$W_1/W_2 = e^{\left[\frac{S/3600}{\frac{V_{eff}}{SFC}\left(\frac{L}{D}\right)_{eff}}\right]}$$

makes possible with the aid of Fig. 1 a direct evaluation of the relative merits of the ballistic and level cruise trajectories. It should be recalled that at this point we are comparing the performance of an impulsively boosted ballistic vehicle in a drag-free atmosphere with the performance of an airplane flying a powered cruising trajectory whose fuel expenditure in the acceleration and climb leg of the mission has been neglected, and whose cruise leg has been extended to the point of destination, rather than allowing for the deceleration prior to landing. Although, due to the assumption made, neither of the performance estimates is accurate, a comparison between them will properly describe their relative merits for many missions. An estimate of the fuel expenditure during the cruising airplane's acceleration leg will be treated later in this paper.

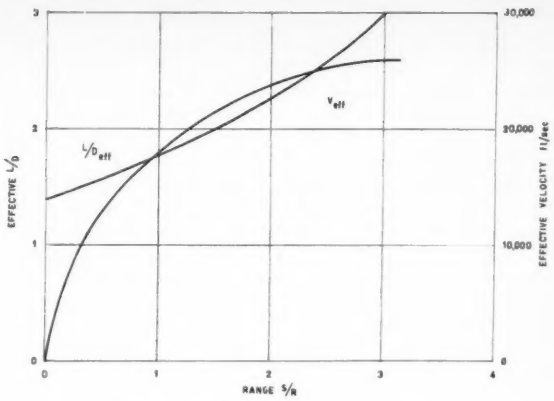

Fig. 1 Effective velocity and L/D of ballistic vehicles

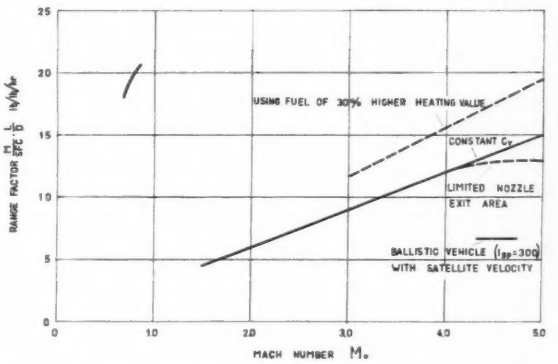

Fig. 2 Range factor for aircraft powered by airbreathing engines using hydrocarbon fuels

The path in which the largest value of $V/SFC \cdot L/D$ is obtained will lead to the smallest expenditure in vehicle weight, i.e., propellant, for any desired range. Since for the longer ranges the required burnout velocities can currently be attained only with rocket engines, it is instructive to compare the performance of level cruise vehicles using airbreathing engines with rocket powered ballistic vehicles. For the purpose of this comparison the attainable cruising L/D was assumed as 18 in subsonic flight and 6 in supersonic flight; the attainable engine specific fuel consumption was assumed as 0.8 lb/hr/lb in subsonic flight and 2 lb/hr/lb in supersonic flight. The latter assumption is based on use of turbofan engines for the subsonic regime, afterburning turbojets for supersonic flight below Mach 3.5 and ramjets beyond Mach 3.5. The efficiency of vehicles using the optimum engine in each speed range can be assessed by comparing their respective "range factors" $(M/SFC)(L/D)$. Such a comparison is shown in Fig. 2, as a function of flight Mach number. From Fig. 2 it is apparent that only limited regions of the flight speed spectrum are advantageous for the attainment of range using cruising trajectories: Firstly, the high subsonic range currently used by jet powered commercial transports and subsonic bombers, and secondly the high supersonic regime. The intervening speeds are inappropriate due to the combination of low aerodynamic and propulsive efficiencies. If reasonable engine exit area limitations are imposed, we may anticipate that the optimum supersonic cruising speed will lie between Mach 4 and 5. Although the range factor for subsonic flight is considerably better than the one for supersonic flight, it

should be recalled that for commercial transports the increased mileage obtainable from a supersonic transport would tend to balance the additional fuel expenditure (8). Most military applications require supersonic capability in any case, and an airplane designed for subsonic cruise and supersonic dash will have a subsonic L/D considerably worse than that shown in Fig. 2. For such airplanes, therefore, there would seem to be little advantage in cruising subsonically.

For comparative purposes Fig. 2 also shows the range factor for a ballistic vehicle operating at its maximum effective L/D, namely satellite velocity, using a rocket powerplant with a specific impulse of 300 sec. It is apparent that this is not an efficient means of obtaining range. It should be recalled, however, that this comparison neglects the effect of any differences in aircraft and engine structural weights. Should this effect be considered, the relative performance of the ballistic vehicle would improve, due to its higher structural efficiency.

Influence of Powerplant Weight

A complete evaluation of the effect of powerplant weight requires a knowledge of the specific weight of the powerplant (pounds of weight per pound of thrust), as well as the maximum thrust requirement of the mission. Although rocket powerplants, owing to their simplicity and higher combustion chamber pressures, have a sizable specific weight advantage over airbreathing powerplants in most of the flight speed spectrum, it should be recalled that whereas ballistic trajectories require a takeoff thrust at least equal to the vehicle takeoff weight, the equivalent thrust requirement for an airbreathing engine powering a level cruise airplane would generally be considerably less than half the vehicle weight.

A general criterion for powerplant superiority for a specific mission can be obtained by writing Equation [1] in the form

$$\frac{W_a}{W_1} + \frac{W_{PL}}{W_1} = e^{-\left[\frac{S/3600}{(V/SFC)(L/D)}\right]} - \frac{W_{PP}}{W_1} \qquad [4]$$

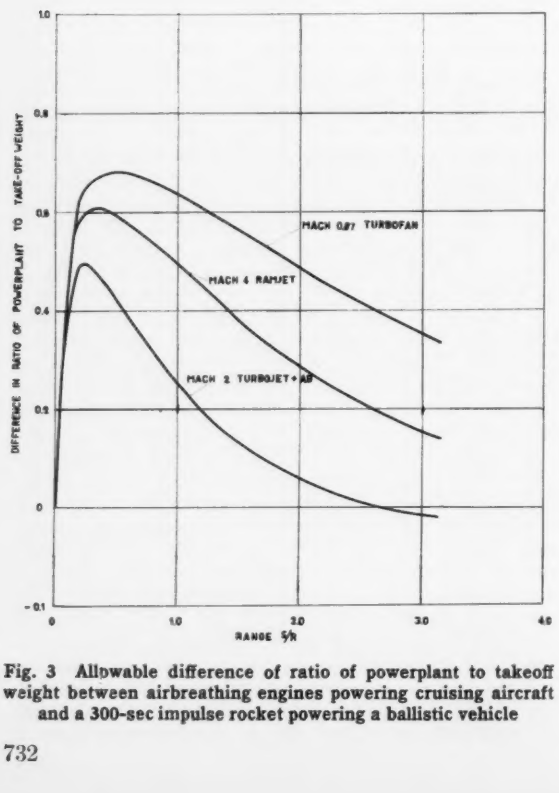

Fig. 3 Allowable difference of ratio of powerplant to takeoff weight between airbreathing engines powering cruising aircraft and a 300-sec impulse rocket powering a ballistic vehicle

where the "empty" weight of the vehicle at the conclusion of the cruise leg has been broken down into airframe structure weight W_a, powerplant W_{PP} and payload weight W_{PL}. The percentage of the vehicle takeoff weight allowed for structure and payload can be calculated by multiplying Equation [4] by W_1/W_0, the vehicle weight ratio for that part of the trajectory that precedes the cruise leg. For a ballistic trajectory this ratio is, of course, unity. For level trajectories with supersonic cruising speeds, it is of the order of 0.9.

If we neglect the fuel expenditure prior to entering the cruise leg, the criterion that a vehicle using powerplant A be superior to a vehicle using powerplant B is that

$$\frac{W_{PP_A}}{W_0} - \frac{W_{PP_B}}{W_0} < e^{-\left[\frac{S/3600}{\left(\frac{V}{SFC}\right)_A\left(\frac{L}{D}\right)_A}\right]} - e^{-\left[\frac{S/3600}{\left(\frac{V}{SFC}\right)_B\left(\frac{L}{D}\right)_B}\right]} \qquad [5]$$

If Equation [5] is written as an equality, it describes the break-even point between use of an efficient powerplant of high weight and an inefficient powerplant of low weight. The extent to which the low weight of rocket powerplants tends to overcome the poor propulsive and aerodynamic efficiency of rocket boosted ballistic vehicles may be judged from Fig. 3. The curves computed from Equation [5] show the allowable difference in weight between airbreathing powerplants for level cruise vehicles and a 300-sec specific impulse rocket used for a ballistic vehicle, for equal vehicle takeoff weights and assuming constant aircraft structure and payload weights. Assumptions regarding aerodynamic and propulsive parameters were the same as those discussed previously. It is seen that, except for extremely short ranges, the allowable powerplant weight differences for either the turbofan or ramjet powered level cruise vehicles are so large as to give them a decisive advantage over rocket propelled ballistic vehicles.

Acceleration to Cruising Velocity

For a sufficiently powered high speed vehicle, flying an optimum climb and acceleration path, the change in aircraft weight during the climb and acceleration leg can be approximated by

$$W_0/W_1 = e^{V(SFC)/3600\,g}$$

Using this approximation, the total change in weight for a level cruise vehicle covering a range S at a cruising speed V is, therefore

$$W_0/W_2 = e^{V(SFC)/3600\,g}\, e^{\frac{S/3600\,g}{(V/SFC)(L/D)}}$$

In this equation, the SFC during acceleration has been taken equal to the cruising SFC, an assumption which is justified for high speed cruise vehicles using airbreathing engines, and for rocket powered vehicles at all speeds. The range covered during acceleration has been neglected. This will usually be consistent with the previous assumptions of rapid acceleration and a small value of D/F, i.e., a large angle of climb. Upon rearranging the last equation we obtain

$$W_0/W_2 = e^{\frac{S/3600}{(V/SFC)(L/D)}\left[1 + \frac{(V/V_e)^2}{S/R}\frac{L}{D}\right]} \qquad [6]$$

It is now possible to compare the efficiency of the level cruise trajectory including the acceleration leg with a ballistic trajectory covering the same range. The condition that the level cruise trajectory be superior can be stated as

$$\frac{1 + \frac{(V/V_e)^2}{S/R}\frac{L}{D}}{\frac{V}{SFC}\frac{L}{D}} < \frac{1}{\frac{V_{eff}}{(SFC)_b}\left(\frac{L}{D}\right)_{eff}} = \frac{1}{\frac{V_b}{(SFC)_b}\left(\frac{V_e}{V_b}\right)^2\frac{S}{R}} \qquad [7]$$

where $(SFC)_b$ signifies the specific fuel consumption of the

ballistic vehicle powerplant. Equation [7] can be rearranged into the standard quadratic form

$$\left(\frac{V}{V_b}\right)^2 - \left(\frac{V}{V_b}\right)\frac{(SFC)_b}{(SFC)} + \left(\frac{V_s}{V_b}\right)^2 \frac{S/R}{L/D} < 0 \qquad [8]$$

The solution of Equation [8] written as an equality defines the conditions for which both trajectories are equally efficient, and is given by

$$\frac{V}{V_b} = \frac{1}{2}\frac{(SFC)_b}{(SFC)} \pm \frac{1}{2}\sqrt{\left[\frac{(SFC)_b}{(SFC)}\right]^2 - 4\left(\frac{V_s}{V_b}\right)^2 \frac{S/R}{L/D}} \qquad [9]$$

It is of interest to determine under what conditions a vehicle using a powerplant of given efficiency should fly a ballistic rather than a level cruise trajectory. If the *SFC* is not varied, Equation [9] becomes

$$\frac{V}{V_b} = \frac{1}{2} \pm \frac{1}{2}\sqrt{1 - 4\left(\frac{V_s}{V_b}\right)^2 \frac{S/R}{L/D}} \qquad [10]$$

This equation is plotted in Fig. 4, for three values of aircraft L/D, as a function of range. For the cruising velocities and ranges interior to any particular curve the level cruise trajectory is superior. It can be seen that as long as the cruising L/D is less than 4, the ballistic trajectory is always superior to a level cruise trajectory in which a powerplant of equal *SFC* is used. On the other hand, for an L/D of 8, the region of superiority of the level cruise trajectory extends to a range of 1.7 Earth-radii, or almost 7000 miles.

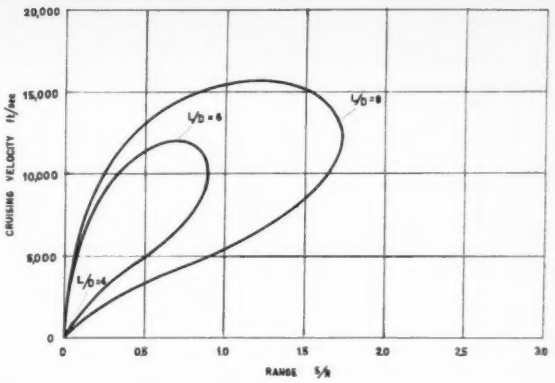

Fig. 4 Region of superiority of level cruise aircraft over ballistic vehicle

Optimum Cruising Velocity

If, as a first approximation, we neglect the change in aircraft lift to drag ratio and engine specific fuel consumption with Mach number in the supersonic regime, the range factor will be directly proportional to the cruising velocity. In other words, any increase in cruising speed will decrease the quantity of fuel expended during cruise. Increased cruising speeds, however, require larger fuel expenditures during the acceleration leg. Within the limits of validity of the approximations used in arriving at Equation [6], we can find an optimum cruising velocity by minimizing Equation [6]. This would be the velocity to which it pays to accelerate. Differentiating the exponent of the right-hand member with respect to velocity, one obtains after some manipulation

$$\frac{V^*}{V_s} = \sqrt{\frac{S/R}{L/D}} \qquad [11]$$

where V^* represents the optimum cruising velocity. This relation is plotted in Fig. 5 as a function of range. Included in Fig. 5 is a line obtained from Fig. 4, defining the break-even point between the level cruise and ballistic trajectory. Therefore, for a specific engine type, Fig. 5 shows the best cruising velocity for each range, as well as that range beyond which a ballistic trajectory should be used. As can be seen, the optimum cruising velocities are considerably beyond present airbreathing engine speed capabilities. This should lead us to expect, however, that extension of the maximum speeds of airbreathing engines will lead to more efficient means of attaining range.

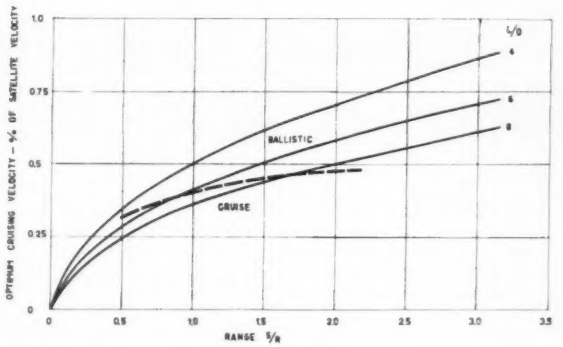

Fig. 5 Optimum cruising velocities

Conclusions

The high propulsive efficiency of airbreathing powerplants makes the attainment of range by jet powered aircraft flying level cruise trajectories more efficient than by rocket powered ballistic vehicles. For jet aircraft flying level trajectories, high subsonic velocities and Mach 4 to 5 supersonic velocities are the regions of highest range efficiency considering the current state of the art of airbreathing engines. If the efficient operation of airbreathing engines can be extended to hypersonic speeds, optimum cruising velocities will continue to increase, and the quantity of fuel required to transport a specified payload over a given distance can be expected to decrease below that required for today's best subsonic transports. The specific weight advantage of rocket engines is generally not sufficient to outweigh their high fuel consumption for use in long range vehicles.

An evaluation of ballistic trajectories indicates their inherent superiority to level cruise trajectories having the same type of powerplant if the attainable supersonic L/D is below 4. For a supersonic cruise L/D of 8, however, the ballistic trajectory is superior only for ranges exceeding 7000 miles.

Nomenclature

C_F = nozzle velocity coefficient
D = vehicle drag
g = acceleration of gravity
I = rocket specific impulse, sec
L = vehicle lift
R = Earth radius
S = range
SFC = engine specific fuel consumption, lb/hr/lb
V = vehicle velocity
W = vehicle weight
ψ = launch angle

Subscripts

0 = takeoff
1 = beginning of cruise leg
2 = end of cruise leg
a = airframe structure

b = burnout
eff = effective
PL = payload
PP = powerplant
s = satellite
$*$ = optimum

References

1 Miele, A., "Optimum Climbing Technique for Rocket-Powered Aircraft," JET PROPULSION, vol. 25, no. 8, Aug. 1955, p. 385.

2 Miele, A., "Stationary Conditions for Problems Involving Time Associated with Vertical Rocket Trajectories," *J. Aero/Space Sci.*, vol. 25, 1958, p. 467.

3 Miele, A., "Flight Mechanics and Variational Problems of a Linear Type," *J. Aero/Space Sci.*, vol. 25, 1958, p. 581.

4 Miele, A., "On the Brachistochronic Thrust Program for a Rocket Powered Missile Traveling in an Isothermal Medium," JET PROPULSION, vol. 28, no. 10, Oct. 1958, p. 675.

5 Allen, H. J., "Hypersonic Flight and the Reentry Problem," *J. Aeron. Sci.*, vol. 25, 1958, p. 217.

6 Perkins, C. D. and Hage, R. E., "Airplane Performance Stability and Control," John Wiley and Sons, Inc., N. Y., p. 186.

7 Sutton, G. P., "Rocket Propulsion Elements," John Wiley and Sons, Inc., N. Y., second ed., p. 380.

8 Oswald, W. B., "Applied Aerodynamics and Flight Mechanics," *J. Aeron. Sci.*, vol. 23, 1956, p. 469.

Continuously Powered Terminal Maneuver for Satellite Rendezvous

NORMAN E. SEARS Jr.[1]
and
PHILIP G. FELLEMAN[2]

Massachusetts Institute of Technology
Cambridge, Mass.

The concept of using a continuously powered maneuver to effect the terminal phase of a satellite rendezvous operation is discussed. The characteristics of several sample maneuvers are presented, including the transfer time, acceleration levels, characteristic velocity and thrust direction. These maneuvers include a non co-planar transfer between elliptic orbits as well as the simpler cases of co-planar maneuvers and circular orbits. The advantages of using continuously powered maneuvers are discussed as well as the parametric effects of the system constants on the characteristics of the maneuver.

THIS paper will describe the characteristics of a continuously powered maneuver for the terminal phase of a satellite rendezvous operation. Terminal phase shall mean that part of the rendezvous operation during which the final velocity and position corrections are made for two satellites that have been brought relatively close and have similar orbital characteristics. The terminal phase will start with the vehicles approximately 20 miles apart; the result of this phase will be that the two vehicles are within 50 ft of each other and have zero relative velocity.

Review of Rendezvous Maneuvers

Satellite rendezvous operations are potentially important to many forthcoming space missions. Three possibilities are:

1 The construction and supply of a space station designed to orbit the Earth.

2 The final phase of an interplanetary reconnaissance mission in which the reconnaissance vehicle would return to an orbit about the Earth and be met by a vehicle launched from the Earth, thus making it unnecessary to carry an aerodynamic re-entry body for the entire journey.

3 Rendezvous between two satellites orbiting the Earth in dissimilar orbits.

Several papers (1–5)[3] have been presented on possible methods that could be used to achieve rendezvous between orbiting vehicles. The general approach is to divide the problem into two parts: First, matching the respective orbital planes of the two vehicles, and second, effecting the co-planar transfer. Several possible trajectories have been proposed for the co-planar transfer. The most commonly suggested is the Hohmann or co-tangential ellipse trajectory, since it is a minimum fuel trajectory for transferring between two concentric circular orbits. It is also possible to make the co-planar transfer by the use of high energy trajectories, for example, intersecting elliptic, parabolic or hyperbolic trajectories. All of these trajectories are characterized by at least two impulsive thrust applications separated by long coasting periods.

In order to achieve successful rendezvous using maneuvers of this type, accurate knowledge of initial positions and velocities of the two satellite vehicles is required, and the impulsive thrust applications must be precisely controlled in time, magnitude and direction. After long unpowered coasting periods, uncertainties in initial conditions or errors in thrust application can result in significant position errors that cannot be corrected by a single impulsive thrust application. Although maneuvers of the minimum energy type are feasible for coarse navigation between widely separated satellite orbits, the accuracy requirements predicate the use of some method other than a single impulsive thrust to accomplish the final phase of the transfer. A continuously powered maneuver for this phase of the maneuver will be discussed in the following section.

Presented at the ARS Controllable Satellites Conference, MIT, April 30–May 1, 1959.

[1] Instrumentation Laboratory, Group Leader.

[2] Instrumentation Laboratory, Staff Engineer.

[3] Numbers in parentheses indicate References at end of paper.

Terminal Maneuver

For the purpose of illustrating the characteristics of the terminal maneuver, the initial conditions have been arbitrarily chosen: A range between the satellite and ferry of approximately 20 miles with velocities associated with either elliptic or circular orbits. Fig. 1 shows a co-planar example where the rendezvous vehicle's orbit is 10 miles below the satellite's orbit, and the rendezvous vehicle is about 20 miles away. In all of the examples given in this paper, it will be assumed that the satellite is at a 500-mile altitude at the start of each maneuver. The first examples will consider co-planar transfers in a circular orbit. Later examples will include both non co-planar and noncircular cases. The equations of motion for the co-planar problem are shown in Fig. 2 and apply to a body moving in a central force field. This assumption will hold throughout the rest of the paper. The equations of motion are presented in polar form, with radial acceleration being defined along the geocentric radius vector and circumferential acceleration at right angles to the radius vector. These directions and their coordinates are also shown in Fig. 2. Due to the coupling between the radial and circumferential axes that is inherent in the equations of motion, any acceleration applied along one axis, for example the circumferential direction, would result in both a change in the circumferential velocity and the radial velocity.

In order to achieve rendezvous, accelerations are required both to move the rendezvous vehicle toward the satellite and to fulfill the velocity requirement that the velocity vectors must match both in magnitude and direction at the time of contact or desired minimum range. Another way of stating these requirements is that the range rate must approach zero as the range approaches zero. Equations [1, 2 and 3] illustrate a set of forcing equations upon which a control system might be based

$$f_c = S_1[\dot{R} - f(R)]_c + S_2(RW_{LS})_c \quad [1]$$

$$f_r = S_3[\dot{R} - f(R)]_r + S_4(RW_{LS})_r \quad [2]$$

$$f_z = S_5[\dot{R} - f(R)_z + S_6(RW_{LS})_z \quad [3]$$

where

f_c, f_r, f_z = components of required acceleration
$\dot{R}$ = range rate along the line of sight
W_{LS} = angular velocity of the line of sight
R = range
$f(R)$ = desired range rate function
S_i = system sensitivity

Each of the forcing equations has two terms, each of which contains a component of the range rate vector. The first terms contain the component of the range rate vector along the line of sight ($\dot{R}$); the second terms contain the component perpendicular to the line of sight (RW_{LS}), which is equal to the range times the angular velocity of the line of sight. These two quantities may be readily measured from the rendezvous vehicle. Many functions $f(R)$ could satisfy the criterion of zero relative velocity at zero range. The particular function $f(R) = k\sqrt{R}$ has a further desirable property of requiring an almost constant deceleration of $k^2/2$ ft/sec^2 during the latter part of the maneuver. This property resulted in the choice of this particular function which will be used in all of the succeeding examples.

It should be noted at this point that control of the rendezvous operation from a ground station is virtually impossible, owing to the inaccuracies of the measuring equipment at such long distances and to the short time available to make these measurements. It is therefore felt that, for the accuracies needed to achieve a successful rendezvous, measurements must be made on board the rendezvous vehicle. It should also be noted that the Equations [1–3] imply continuous thrusting. This thrusting, moreover, must be variable in magnitude. These forcing equations have been substituted in the equa-

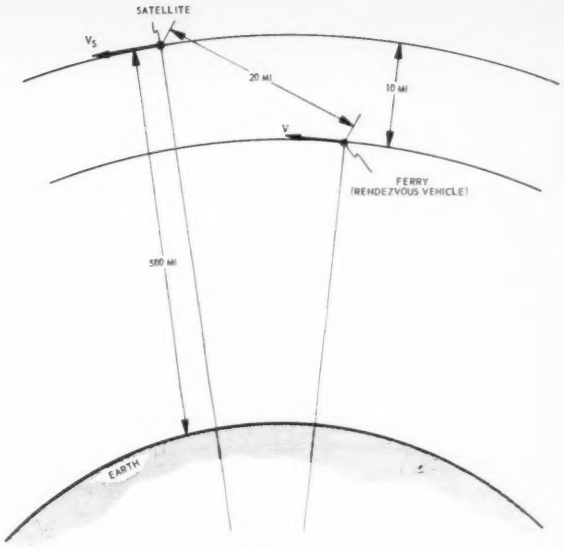

Fig. 1 Initial conditions for terminal phase

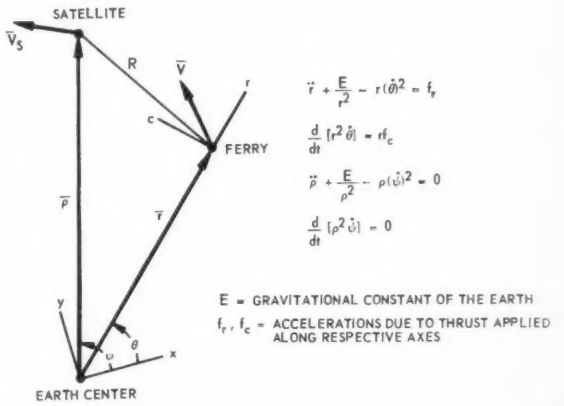

Fig. 2 Coordinate system and equations of motion (co-planar)

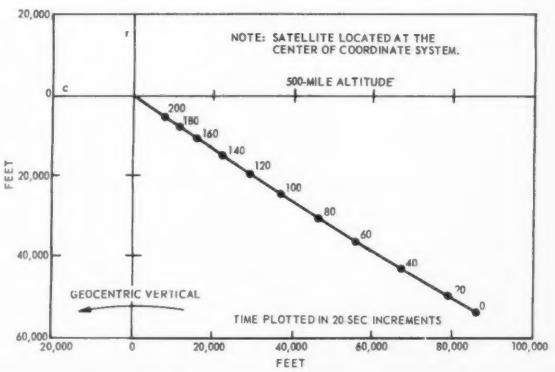

Fig. 3 Standard trajectory in satellite coordinate system

tions of motion shown on Fig. 2 and the problem simulated on an IBM 650 digital computer. The results of this simulation are demonstrated by several examples which follow.

Example 1: Co-Planar Maneuver Between Circular Orbits

The initial positions of the two vehicles are those shown in Fig. 1: Both vehicles have circular velocity at their respective altitudes. Fig. 3 is the trajectory of the rendezvous vehicle plotted in a coordinate system which is satellite-centered and rotating with the geocentric vertical. The dots along the trajectory represent 20-sec time increments. Though the path appears as a straight line to the scale drawn, there is some slight curvature at the beginning of the maneuver. Fig. 4 depicts the same path as would be seen by an inertial observer, with the curvature of the orbit and the scaling distance exaggerated in order to show the relative positions in inertial space. Again, 20-sec time increments are shown.

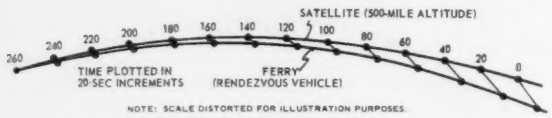

Fig. 4 Standard trajectory in inertial coordinates

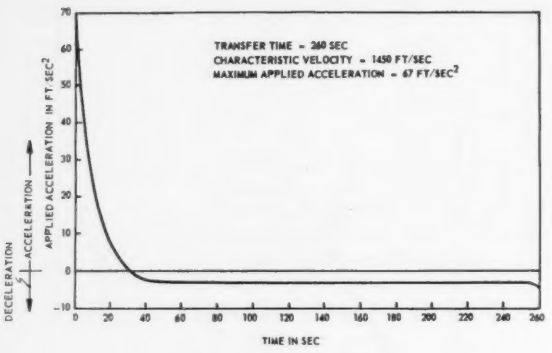

Fig. 5 Thrust profile

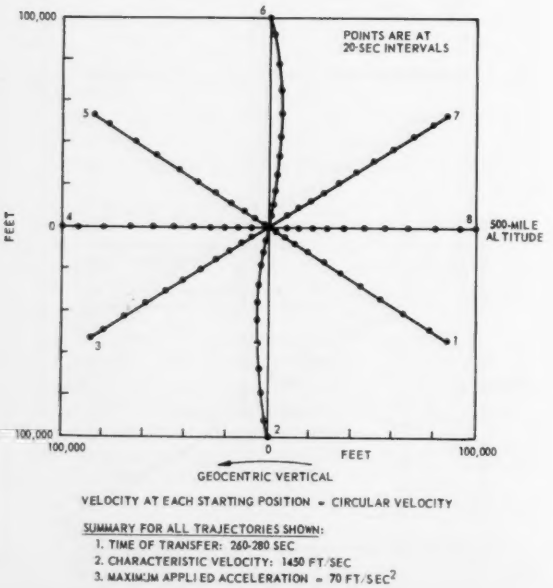

Fig. 6 Co-planar circular trajectories

Fig. 5 is the plot of the magnitude of the required acceleration vs. time. It will be assumed in these examples that the rendezvous vehicle achieves the required acceleration at all times. The high initial value of acceleration decreases rapidly and becomes a small negative value for the rest of the maneuver. This indicates that there is a short, high thrust level period of acceleration and a longer, low thrust level period of braking that continues to the end of the maneuver. The maximum required acceleration during the brief acceleration phase is determined by the difference between the actual vector relative velocity and that required by the control Equations [1–3]. The system sensitivities S_1–S_6 were equal to 0.1 sec^{-1} for this and following examples. During the deceleration or braking period the required acceleration level is essentially constant and equal to approximately $k^2/2$ due to the particular choice of desired range rate function $f(R) = k\sqrt{R}$ in Equations [1–3]. The scale factor k was equal to a value of 2.2 $ft^{1/2}$ sec^{-1} for these examples which resulted in a virtually constant deceleration of 2.5 fps^2.

It should be pointed out that the range of required accelerations, or equivalently, throttling capability, is determined by two factors: First, the peak accelerations resulting from the initial position and velocity conditions, and second, the value of constant deceleration level determined by the value of the scale factor k.

Fig. 6 shows several co-planar trajectories, all starting from the same initial range, but from different initial positions. In all cases, both the satellite and the rendezvous vehicle are initially in circular orbits. Trajectory 1 is the same as that shown in Fig. 3. All the trajectories have similar time of transfer, characteristic velocity and maximum acceleration levels. However, this would not be true if the initial ranges were much larger. Upon close examination of the figure, it may be seen that diagonally opposite trajectories, for example trajectories 1 and 5, are virtually identical. The

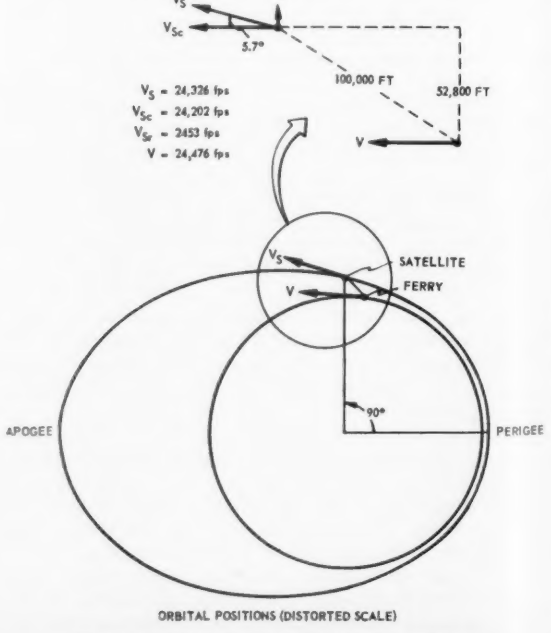

Fig. 7 Noncircular co-planar initial conditions

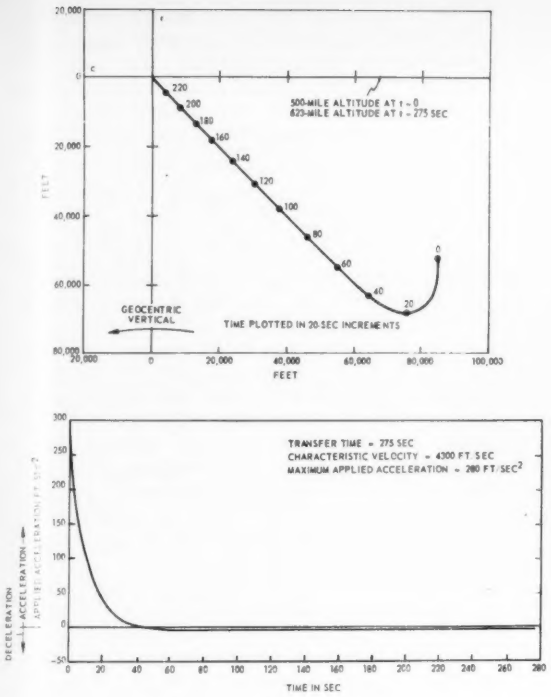

Fig. 8 Co-planar noncircular trajectory

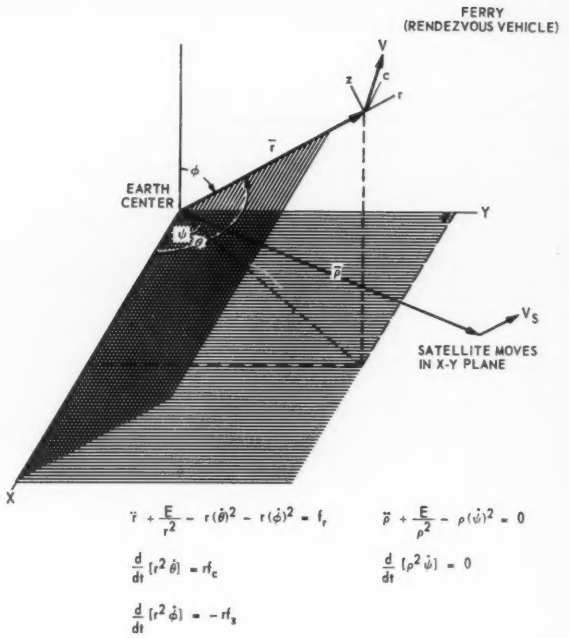

$$\ddot{r} + \frac{E}{r^2} - r(\dot{\theta})^2 - r(\dot{\phi})^2 = f_r \qquad \ddot{\rho} + \frac{E}{\rho^2} - \rho(\dot{\psi})^2 = 0$$

$$\frac{d}{dt}[r^2\dot{\theta}] = rf_c \qquad \frac{d}{dt}[\rho^2\dot{\psi}] = 0$$

$$\frac{d}{dt}[r^2\dot{\phi}] = -rf_z$$

Fig. 9 Equations of motion (non co-planar)

reason for this is that diagonally opposite starting positions have identical initial conditions of range rate. As before, 20-sec time increments are indicated along each trajectory.

Example 2: Co-Planar Maneuver Between Noncircular Orbits

Fig. 7 shows the initial conditions for a transfer involving a satellite in an elliptic orbit with an eccentricity of 0.1 at a true anomaly of 90 deg and a ferry vehicle in a circular orbit. In an expanded portion of the figure, the initial relative position and velocities of the two vehicles are shown, together with the magnitudes of the circumferential and radial velocity components. This figure is distorted in order to show the starting conditions of the terminal phase.

Fig. 8 shows the trajectory in the satellite reference coordinate system, and the thrust levels required during the maneuver. The satellite reference coordinate system on which the trajectory is plotted in Fig. 8 constantly changes altitude during the maneuver, starting at 500 miles and ending at 623 miles after the 275 sec required for the transfer maneuver. The time of the maneuver, the characteristic velocity and the maximum applied acceleration are also shown in Fig. 8. It should be noted here that the difference between the characteristic velocity of this maneuver and the characteristic velocity of Example 1, where both vehicles were in circular orbit (both maneuvers starting at the same initial range) results almost entirely from the radial velocity of the satellite that must be imparted to the ferry. The maximum applied acceleration is correspondingly greater for this noncircular case (280 fps² compared wtih 70 fps² for the circular problem), but the acceleration required for the braking phase is again constant at 2.5 fps².

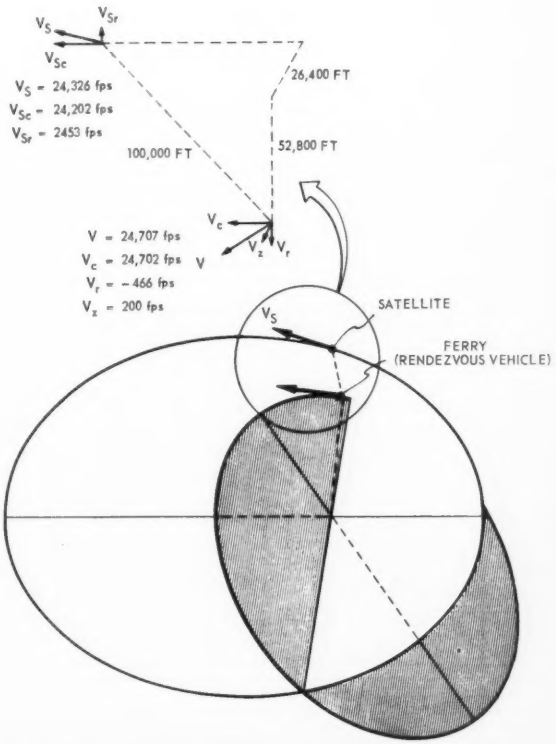

Fig. 10 Orbital positions for noncircular, non co-planar transfer

Example 3: Non Co-Planar Maneuver Between Noncircular Orbits

Fig. 9 shows a three-dimensional coordinate system and the equations of motion that are referred to this system. These equations have been simplified from the general equations of motion, since in the initial conditions considered here it is assumed that the angular separation between the orbital planes of the ferry and satellite is small. The third forcing equation (Eq. [3]) which is similar in form to the other two, applies to the orthogonal z direction.

This example includes noncircular as well as non co-planar conditions. Both the satellite and the ferry are in elliptic orbits with different eccentricities—the satellite orbit having an eccentricity of 0.1 and the ferry orbit having an eccentricity of 0.03. Fig. 10 shows the two orbits and the positions of the respective vehicles in their orbits, the scale again being distorted to show the initial conditions. The expanded portion of the figure shows the initial positions and velocities of the two vehicles together with the velocity components along the c, r, z axes. The components of the relative velocities are

$$V_{Sc} - V_c = -500 \text{ fps}$$
$$V_{Sr} - V_r = 2919 \text{ fps}$$
$$V_{Sz} - V_z = -200 \text{ fps}$$

The initial value of the range rate along the line of sight for this example is 1127 fps (that is, the vehicles are separating at this velocity).

Fig. 11 shows the trajectory as it would be seen from the satellite, projected onto the r-c plane and onto the c-z plane. The transfer time, characteristic velocity and maximum applied acceleration are again summarized for the maneuver (see Fig. 12). The increased characteristic velocity and required peak acceleration level, compared with the circular coplanar maneuver (see Fig. 5) and the noncircular co-planar maneuver (see Fig. 8), result from the large initial relative velocities; however, the deceleration during the braking phase is again constant at 2.5 fps^2.

The required thrust angles with respect to the line of sight for the preceding examples are plotted in Figs. 13. Fig. 13a shows the projection of this angle onto the r-c plane; Fig. 13b shows the projection onto the c-z plane. The rapid change in thrust angle shown in Fig. 13a is caused by the thrust changing from acceleration to deceleration. It should be noted that during the long deceleration period, the thrust angle remains relatively constant and directed away from the satellite.

In all of the preceding examples, the sensitivities that appear in the forcing equations were kept constant and equal to each other. No attempt has been made to optimize these constants or to determine whether a nonconstant sensitivity would result in lower characteristic velocities and maximum applied acceleration levels. If the sensitivities were increased, the trajectories would be similar; the only effect would be that the initial discrepancy between range rate and the desired range rate would be reduced sooner by the application of higher acceleration levels. This would result in a higher characteristic velocity for the entire maneuver, but the time required for transfer would remain essentially the same.

The transfer time is dependent on the initial range and the value chosen for the scale factor k. The transfer time is approximately proportional to the square root of the initial range and inversely proportional to k. The expression for transfer time can be written as

$$T = 2\sqrt{R}/k + g(S_i, k, R)$$

where

$$2\sqrt{R}/k \gg g$$

As previously stated, the function of range $f(R)$ in the forcing equations was chosen to be proportional to the square root of range. If the linear function $f(R) = kR$ had been chosen, the resulting transfer time could be written[4]

$$T = \frac{1}{k} \ln \left(\frac{R_0}{R_f} \right)$$

It can be seen from this equation that for rendezvous, i.e., $R_f = 0$, an infinite transfer time would be required. Practically, even a finite R_f would require extremely long transfer times and correspondingly higher characteristic velocities. For these reasons, a nonlinear function is indicated, and the square root was chosen for this discussion since it has the desirable characteristics previously described.

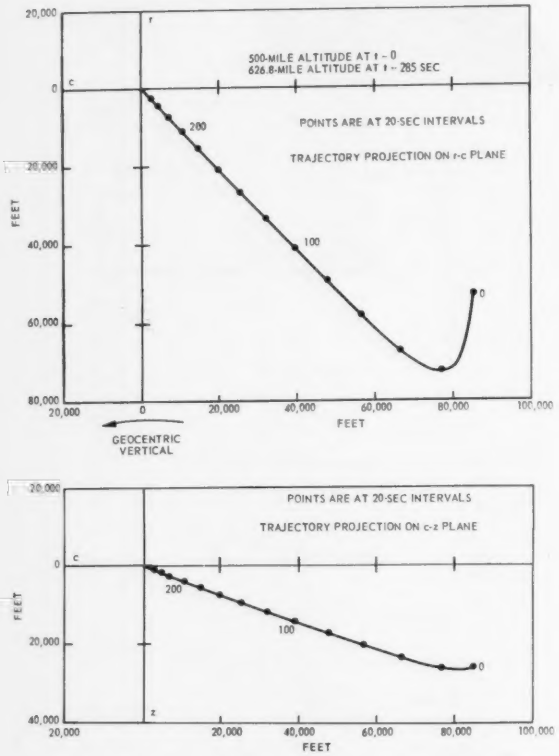

Fig. 11 Noncircular, non co-planar trajectory

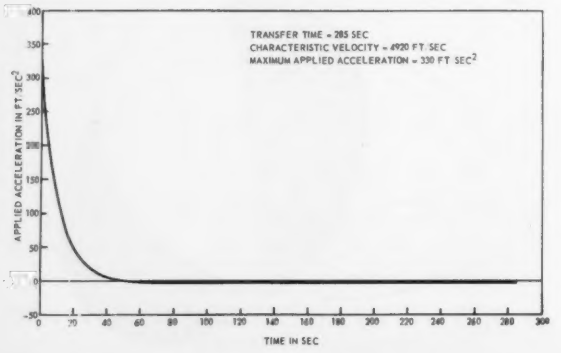

Fig. 12 Noncircular, non co-planar trajectory

[4] This expression is a correction to the paper as originally presented and was pointed out to the authors by B. P. Miller, Astro-Electronic Products Division, RCA, Princeton, N. J.

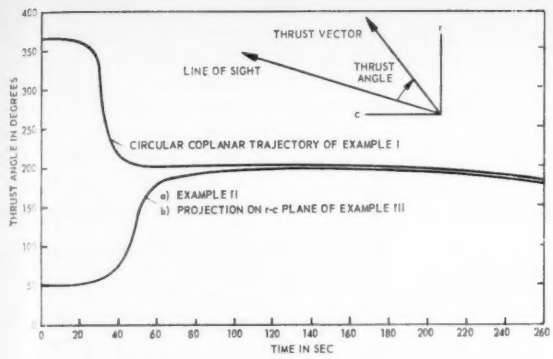

Fig. 13a Thrust angle profiles in the r-c plane

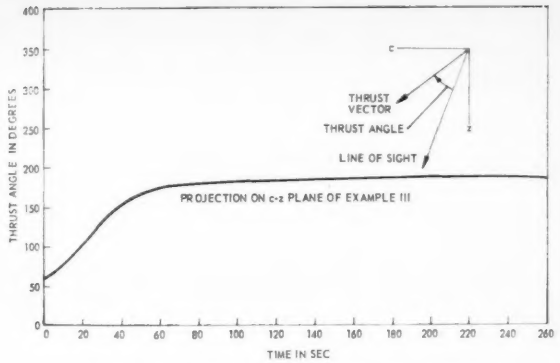

Fig. 13b Thrust angle profiles in the c-z plane

Summary

A continuously powered maneuver to be used for the terminal phase of a satellite rendezvous operation has been described. One advantage of a maneuver of this type is the possibility of continuously correcting deviations from the desired trajectory owing to measurement uncertainties. The maneuver described is based on the utilization of vehicle sensed line of sight information and is independent of ground derived data. The form of trajectory control based on the forcing equations (Eqs. [1–3]) and illustrated in the preceding examples, has the following characteristics (neglecting vehicle dynamics and assuming instantaneous acceleration response):

1 The time required to complete the maneuver is approximately equal to

$$T \sim 2\sqrt{R_0}/k$$

2 The maneuver naturally divides itself into two phases of acceleration, first, a brief period of acceleration toward the satellite, second, a longer period of braking to reduce the relative velocity to zero at the end condition. (Note: This initial acceleration period would not exist if there were an initial closing velocity equal to $k\sqrt{R}$ and W_{LS} equal to zero. Alternatively, if the initial velocity resulted in an even higher closing velocity, the acceleration would always be so as to reduce the relative velocity, i.e. braking.)

Initial acceleration phase: The maximum value of the acceleration in this phase is determined by the difference between the desired and actual initial conditions as well as by the system constants k and S_i.

Braking or deceleration phase: The required acceleration level during this phase is essentially constant in magnitude, owing to the choice of the desired range rate function $k\sqrt{R}$ and is equal to

$$|\bar{f}| = k^2/2$$

where

$$\bar{f} = \bar{f}_c + \bar{f}_r + \bar{f}_z$$

The maneuver described in this paper resulted in high characteristic velocities and wide variations in the required accelerations and thrust angles. This results from the particular choice of examples and initial conditions. In order to achieve a successful rendezvous between two orbiting vehicles, it is necessary to first accelerate and then decelerate one of the vehicles with respect to the other. It is possible to minimize the characteristic velocity using a continuously powered maneuver if a large closing velocity exists as an initial condition (6). In this case, the acceleration variation and thrust angle limits are considerably smaller than those presented here, and the characteristic velocity is essentially the same as that required merely to attain the desired orbit without regard to position matching.

Acknowledgment

This paper was prepared under the auspices of DSR Project 52-140, sponsored by the Weapons Guidance Laboratory of the Wright Air Development Center, through USAF Contract no. AF 33(616)-3892.

The publication of this report does not constitute approval by the Air Force of the findings or conclusions contained herein. It is published for the exchange and stimulation of ideas.

Nomenclature

X, Y, Z	=	Earth centered inertial coordinate system
r, c, z	=	vehicle centered coordinate system with r axis along the geocentric radius, and with the c axis parallel to the orbital plane of the satellite
$\bar{r}$	=	radius vector from the center of Earth to the rendezvous vehicle
θ	=	angle from X axis to $\bar{r}$
ϕ	=	angle from Z axis to $\bar{r}$
$\bar{\rho}$	=	radius vector from the center of Earth to the satellite
ψ	=	angle from X axis to $\bar{\rho}$
V	=	velocity of rendezvous vehicle
V_S	=	velocity of the satellite
f_r, f_c, f_z	=	specific force (thrust/unit mass) along the r, c or z axis, respectively
R	=	range from the rendezvous vehicle to the satellite
$\dot{R}$	=	range rate along the line of sight
W_{LS}	=	angular velocity of the line of sight
E	=	gravitational constant of the Earth ($E = 1.4072 \times 10^{16}$ ft^3/sec^2)
$f(R)$	=	desired range rate function
S_i	=	guidance system sensitivities
k	=	scale factor
T	=	transfer time

References

1 Gedeon, G. S., "Orbital Mechanics of Satellites," paper presented at the Western Regional Meeting of American Astronautical Society, Palo Alto, Calif., Aug. 18–19, 1958.

2 Lawden, D. F., "The Determination of Minimal Orbits," *J. Brit. Interplanet. Soc.*, vol. 2, no. 5, 1952.

3 Smith, R. A., "Establishing Contact Between Orbiting Vehicles," *J. Brit. Interplanet. Soc.*, vol. 10, no. 6, 1951.

4 Lawden, D. F., "Orbital Transfer via Tangential Ellipses," *J. Brit. Interplanet. Soc.*, vol. 2, no. 6, 1952.

5 Vargo, L. G., "Optimal Transfer Between Two Coplanar Terminals in a Gravitational Field," paper presented at the Western Regional Meeting of American Astronautical Society, Palo Alto, Calif., Aug. 18–19, 1958.

6 Felleman, P. G. and Sears, N. E., "A Guidance Technique for Achieving Rendezvous," paper presented at the IAS Symposium on Manned Space Stations, Los Angeles, Calif., April 1960.

Efficient Precision Orbit Computation Techniques[1]

R. M. L. BAKER Jr.,[2]
G. B. WESTROM,[3]
C. G. HILTON,[3]
R. H. GERSTEN,[3]
J. L. ARSENAULT[3]
and E. J. BROWNE[3]

Aeronutronic Div.,
Ford Motor Co.
Newport Beach, Calif.

A comparison is made of the methods of Cowell, Encke and the variation-of-parameters for the computation of high precision orbits. Analysis of the integration of an analytical three-body trajectory and an analytical low thrust spiral trajectory indicates the importance of decreasing the overall number of integration steps to avoid roundoff errors. Comparative computations demonstrate that Encke's method is preferable in the ballistic lunar trajectory, variation-of-parameters in the low thrust trajectory, and Cowell's method in the high thrust trajectory. The overall computational efficiency of Encke's and the variation-of-parameters method is also shown.

RECENTLY, engineers have been challenged with the problems of precision orbit computation techniques for the efficient numerical integration of space vehicle trajectories. The orbit computation problem is manifestly not a novel one, having been investigated rather thoroughly by celestial mechanics for many years.[4] Nevertheless, the conclusions reached to date are not general enough to answer the entire question, since the choice of method is dependent to a great degree upon the nature of the problem. For example, the problem of the motion of a minor planet or comet is not completely analogous to the problem of the motion of a low thrust interplanetary vehicle. For this reason, it is desirable to reopen the question of analytical technique and to determine the circumstances under which one technique is preferable to another. The computational techniques considered in this paper are two perturbational techniques, referred to as Encke's method and variation-of-parameters, and a direct integration of the accelerations called Cowell's method.

There is no a priori reason for preferring one of these methods to the exclusion of all the others. In the case of high perturbative forces, e.g., during high thrust, Cowell's method is probably superior. In the case when the perturbative forces are of small or moderate size over a restricted segment of the orbit, e.g., as for a lunar orbit and certain ballistic interplanetary trajectories, Encke's method seems superior. In the case of small perturbative forces acting throughout the entire trajectory, e.g., as during a low thrust interplanetary voyage, variation-of-parameters may be superior (3).[6] In the following sections these intuitive conclusions are substantiated by quantitative computations.

To evaluate quantitative results, it is necessary to delineate clearly between the errors resulting from truncation and those resulting from rounding in numerical integration. These errors affect the analysis in opposite ways; i.e., in evaluating a particular integral, the fewer integration steps employed, the less is the rounding error, but the greater is the truncation error and vice versa. It is sufficient to say that if truncation error is bounded to the same value for all methods tested, then the method exhibiting the fewest integration steps will be superior in point of accumulated error. The specific expressions relating these errors will be presented in the next section.

As has been frequently pointed out, the rounding error is not the only criterion to be considered in the choice of an integration technique. Encke's and, to an even greater degree, the variation-of-parameters techniques involve expressions that are much more complicated and often less symmetric than Cowell's simple formulas. Thus it is not immediately evident that a procedure yielding the fewest integration steps will be the most efficient in terms of computer time. Consequently, this paper will address itself to the question of overall computational efficiency as well as to accumulated errors.

The rationale to be followed involves the analysis of an analytically solvable three-body trajectory (synodic satellite) and a logarithmic spiral thrust trajectory, and the comparative computations of a ballistic lunar trajectory, a low thrust trajectory and a high thrust midcourse corrective maneuver. Each of these trajectories is computed by Cowell's, Encke's and the variation-of-parameters methods. Every effort is made to insure that the problem is identical for each method

Presented at the ARS Semi-Annual Meeting, June 8–11, 1959, San Diego, Calif.

[1] This research was supported in part by the U. S. Army under Contract DA-04-495-ORD-1389 monitored at Aeronutronic Division, Ford Motor Co., by the Army Ballistic Missile Agency.

[2] Lecturer, Assistant Professor of Astronomy, UCLA, also Staff Member, Aeronutronic. Presently on active duty with USAF at AFBMD. Member ARS.

[3] Staff Member.

[4] A summary of this prior work, a comparative analysis of several different methods of orbit computation, is presented in (18)[5] and in a 1958 paper by Porter (19).

[5] Numbers in parentheses indicate References at end of paper.

[6] The success of a variation-of-parameters method is dependent upon the proper choice of parameters; consequently, a more optimum choice of parameters might make this method more competitive with Encke's. Nevertheless, Encke's method will always prove to be superior where there exist moderate perturbative forces over a limited segment of a trajectory such that the resulting perturbative Encke displacements would still be small while the variation of the parameters would become relatively large.

and, furthermore, that the overall error is similarly bounded throughout the computation for each method. The deviations from the synodic satellite and spiral orbits specifically portray the direct relation between number of integration steps and integration error, and, consequently, their analysis is carried out first.

Computational Techniques

Perturbations

In all the integration techniques, Cowell's, Encke's and variation-of-parameters, perturbative acceleration terms are encountered. Perturbation theory has wide application in science and is particularly useful in areas where analytical solutions are difficult or impossible. Detailed discussions of perturbation theory are to be found in Moulton's book [(17), chap. 10] and in Herrick's [(9), chaps. 15–17]. A general discussion of perturbations in connection with astrodynamics is given by Herrick and Baker (11). The particular application of perturbation theory in this paper will be to those accelerations over and above the central force field of a two-body problem. These perturbative accelerations may be due to the gravitational attraction of other bodies, atmospheric or electromagnetic drag, oblateness of Earth and the moon, thrust, radiation pressure, relativity, etc.

The perturbations considered in this paper are: Oblateness of the Earth, lunar perturbations, solar perturbations and rocket thrust acceleration.

Oblateness of the Earth

If Earth were homogeneous in concentric spherical shells, its potential would be that of a point mass. The effects of the flattening of the poles and lack of symmetry about the Equator, however, manifest themselves as perturbative forces on bodies in the vicinity of Earth. These deviations from a spherical shape may be represented mathematically by a series of spherical harmonics. The precision by which the mathematical model corresponds to the physical one is, of course, dependent upon the accuracy with which the harmonic terms can be determined.

The second, third and fourth harmonic terms of Earth's gravitational field have been developed by Herrick [(9), chap. 18], Herrick and Walters (12), and Baker (3). The components of the perturbative terms of the second, third and fourth harmonics are[7]

$$\dot{r}_B^{\backprime} \begin{cases} \dot{x}_B^{\backprime} = -\dfrac{\mu x}{r^5}(J^{\backprime})(1-5\,U_z^2)-\mu H^{\backprime}\dfrac{xz}{r^7}(3-7\,U_z^2)-\dfrac{\mu x}{6r^7}(K^{\backprime})(3-42\,U_z^2+63\,U_z^4) & [1a] \\ \dot{y}_B^{\backprime} = \dfrac{(\dot{x}_B^{\backprime})}{x}\,y & [1b] \\ \dot{z}_B^{\backprime} = -\dfrac{\mu z}{r^5}(J^{\backprime})(3-5\,U_z^2)+\mu H^{\backprime}\dfrac{3}{5r^5}\left(1-10U_z^2+\dfrac{35}{3}U_z^4\right)-\dfrac{\mu z}{6r^7}(K^{\backprime})(15-70\,U_z^2+63\,U_z^4) & [1c] \end{cases}$$

Perturbation Due to the Sun and Moon

The perturbative terms due to the sun and moon can be written directly from the integrals for the n-body problem developed by Moulton (17) and others in texts on celestial mechanics. Using subscripts to denote the various bodies as indicated in the Nomenclature, the perturbative terms are from Herrick (9), chap. 15

$$\dot{r}_G^{\backprime} \begin{cases} \dot{x}_G^{\backprime} = m_1\left(\dfrac{x_{21}}{r_{21}^3}-\dfrac{x_{31}}{r_{31}^3}\right)+m_4\left(\dfrac{x_{24}}{r_{24}^3}-\dfrac{x_{34}}{r_{34}^3}\right) & [2a] \\ \dot{y}_G^{\backprime} = m_1\left(\dfrac{y_{21}}{r_{21}^3}-\dfrac{y_{31}}{r_{31}^3}\right)+m_4\left(\dfrac{y_{24}}{r_{24}^3}-\dfrac{y_{34}}{r_{34}^3}\right) & [2b] \\ \dot{z}_G^{\backprime} = m_1\left(\dfrac{z_{21}}{r_{21}^3}-\dfrac{z_{31}}{r_{31}^3}\right)+m_4\left(\dfrac{z_{24}}{r_{24}^3}-\dfrac{z_{34}}{r_{34}^3}\right) & [2c] \end{cases}$$

Thrust Perturbation

If the thrust is small compared to the central force, it is convenient to consider the thrust as a perturbative acceleration upon the vehicle. The perturbative components (see Fig. 1) due to the thrust are

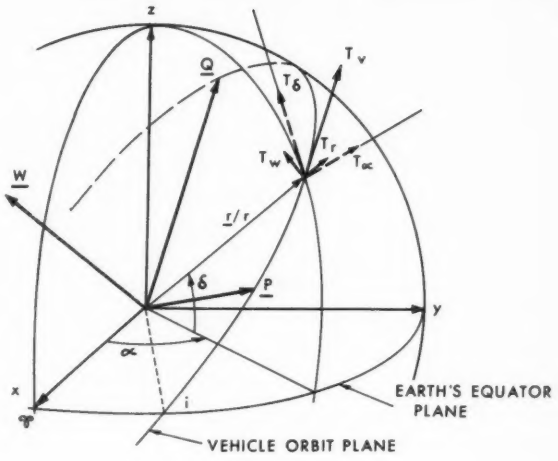

Fig. 1 Thrust components

$$\dot{r}_T^{\backprime} \begin{cases} \dot{x}_T^{\backprime} = T_r\dfrac{x}{r}-T_\delta\dfrac{xz}{r\sqrt{x^2+y^2}}-T_\alpha\dfrac{y}{\sqrt{x^2+y^2}} & [3a] \\ \dot{y}_T^{\backprime} = T_r\dfrac{y}{r}-T_\delta\dfrac{yz}{r\sqrt{x^2+y^2}}+T_\alpha\dfrac{x}{\sqrt{x^2+y^2}} & [3b] \\ \dot{z}_T^{\backprime} = T_r\dfrac{z}{r}+T_\delta\dfrac{x^2+y^2}{r} & [3c] \end{cases}$$

[7] The grave symbol (`) denotes a perturbative derivative with respect to time; see (2).

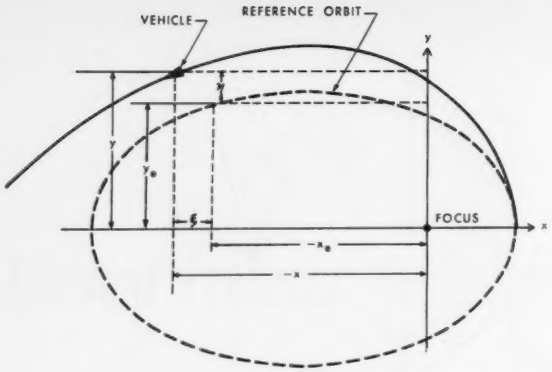

Fig. 2 Deviation from reference orbit

Total Perturbation

The total perturbative acceleration $\dot{r}^{\wedge}$ is the sum of the perturbations due to the oblateness of Earth $\dot{r}_B{}^{\wedge}$, the sun and moon $\dot{r}_G{}^{\wedge}$, and rocket thrust $\dot{r}_T{}^{\wedge}$

$$\dot{r}^{\wedge} \begin{cases} \dot{x}^{\wedge} = \dot{x}_T{}^{\wedge} + \dot{x}_B{}^{\wedge} + \dot{x}_G{}^{\wedge} & [4a] \\ \dot{y}^{\wedge} = \dot{y}_T{}^{\wedge} + \dot{y}_B{}^{\wedge} + \dot{y}_G{}^{\wedge} & [4b] \\ \dot{z}^{\wedge} = \dot{z}_T{}^{\wedge} + \dot{z}_B{}^{\wedge} + \dot{z}_G{}^{\wedge} & [4c] \end{cases}$$

where $\dot{x}^{\wedge}$, $\dot{y}^{\wedge}$, $\dot{z}^{\wedge}$ refer to the total perturbative components.

Drag and radiation pressure perturbations, perturbations resulting from the planets and perturbations due to the triaxial figure of the moon have been neglected.

Cowell's Method

Cowell's method involves the direct integration of the total acceleration, central as well as perturbative, acting on a vehicle. The necessity of carrying a large number of significant figures due to the large central force term is an obvious disadvantage of the method. The resulting decrease in the size of the integration step, particularly in the region of a large central force, makes the method tedious for hand calculations.

The advent of the high speed computing machine is responsible for a considerable revival of the method. The coordinates of the five outer planets, for example, were determined at the Watson Laboratories utilizing Cowell's method (6). The Themis Code, developed at the University of California Radiation Laboratory, is an IBM 704 program of Cowell's method for interplanetary orbits (23). For precision orbit work, roundoff error tends to limit the usefulness of programs based upon Cowell's method. Even with "double precision programs" accuracy is lost. Since tabular information, such as the coordinates of the planets, is not available to more than seven or eight significant figures, the interpolations (even with a series of dummy digits added to the tabulations) will always involve random interpolation and rounding errors for more entries into the tables.

In Cowell's method, the equations of motion, which must be integrated twice to obtain position coordinates, are

$$\ddot{x} = -(\mu x/r^3) + \dot{x}^{\wedge} \quad [5a]$$

$$\ddot{y} = -(\mu y/r^3) + \dot{y}^{\wedge} \quad [5b]$$

$$\ddot{z} = -(\mu z/r^3) + \dot{z}^{\wedge} \quad [5c]$$

where $\ddot{x}$ is the acceleration with respect to the arbitrary time unit, as discussed in (13). The central force term in the x direction is defined by $-\mu x/r^3$. The total perturbative term in the x direction due to bulge, thrust and other bodies is $\dot{x}^{\wedge}$. The accelerations in the y and z directions are defined in an analogous manner.

Encke's Method

Over a hundred years ago, the German astronomer Encke proposed a method of handling special perturbations which has proved to be well suited to slightly perturbed orbits, such as ballistic lunar trajectories.[8] Encke's method differs from Cowell's in that differential accelerations due to perturbations are integrated rather than the total accelerations. More specifically, one calculates the deviation from a two-body reference orbit. Fig. 2 shows the relationship between the reference orbit and the actual path of the vehicle.

Let x, y, z denote the actual position of the object, x_e, y_e, z_e the position on the reference orbit, and ξ, η, ζ the departure from the reference orbit. One can obtain the following relationships

$$\xi \triangleq x - x_e \qquad x \rightarrow y, z \qquad \xi \rightarrow \eta, \zeta \quad [6]$$

The differential acceleration between actual and reference positions of the rocket can be expressed as

$$\frac{d^2\xi}{dt^2} = \mu k^2 \left(\frac{x_e}{r_e{}^3} - \frac{x}{r^3} \right) + \dot{x}^{\wedge} \qquad x \rightarrow y, z \quad [7]$$

The first term on the right-hand side is obviously the difference between the reference orbit and the actual path, and $\dot{x}^{\wedge}$ represents the total perturbational component.

In contrast to Cowell's method, therefore, only the differential *accelerations* due to perturbations are integrated to obtain departures from a two-body orbit. These departures are then added onto the coordinates of the rocket as found from the two-body orbit to obtain the actual position of the rocket. Taking cognizance of the fact that only differential accelerations are integrated instead of total accelerations, it is possible to take larger steps of integration. A careful choice of the reference orbit is necessary in order to make the method most efficient.

The actual formulas which are used in the calculations utilizing Encke's method were developed by Herrick [(9), chap. 15].

The Variation-of-Parameters Method

The variation-of-parameters or variation-of-elements method differs from the Encke method in that there is a continuous rectification of the reference orbit. The reference motion of the object in question is represented by a set of parameters that, in the absence of perturbative forces, would remain constant with time. As an example, astronomers often employ elements specifying the elliptical two-body motion of an object as the reference motion. They then integrate the variation of some of these parameters, such as the semimajor axis a, eccentricity e, the time of perifocus passage T and the orientation angles of the orbit plane. Often, certain vectorial elements proposed by Herrick (8), rather than these parameters, are integrated. Perturbative forces will then cause these parameters to vary, and the differential equations of motion are formulated in terms of these orbit parameters or functions thereof. These differential equations are integrated in the computations of this paper by the technique discussed by Herrick in (9), chap. 18.

Alternatively, it is possible to choose a different form for the reference or gross motion. One might, for example, include part of the perturbative forces caused by the nonspherical shape of Earth, and employ for the gross motion a solution

[8] Extensive studies utilizing Encke's method have been conducted by various companies, including Aeronutronic, Douglas Aircraft Co., Convair Astronautics, Republic Aviation, Systems Corporation of America, and a number of others.

found by Garfinkel (7). When drag force predominates, as in the case of entry, it is sensible to discard entirely a gravitational gross motion and employ a rectilinear gravity-free drag orbit instead, as in (2).

The formulas utilized in the variation-of-parameters method were developed by Herrick [(9), chap. 17]. Care must be exercised to choose an appropriate set of parameters for the most efficient use of the variation-of-parameters method.

Error Control

Introduction

The essential feature of numerical integration is the representation of the integrand as a polynomial of finite order. This may be done by a Taylor series expanded about any point at which the value of the integrand is tabulated. The coefficient derivatives of such a series can be expressed in terms of antecedent tabular values of the integrand or the finite differences between these values. Evidently, the error due to the finiteness of the series, *the truncation error*, is reduced by taking a small interval of tabulation, i.e., a small step size. In the Runge-Kutta integration technique, intermediate values of the integrand are computed. The truncation error of the formula used is of the order of the fourth derivative.

The rounding error, due to the finite number of digits carried, increases with the number of computations. The number of computations necessarily increases when the step size is reduced. Certain procedures have been suggested by Herrick (10) to limit the accumulation of rounding error, but, for any one method, the fewer steps, the less error is incurred.

The following sections discuss both truncation and rounding error, and an analytical check is provided in the last section to illustrate the principles involved.

Runge-Kutta Integration Procedure

The choice of the "modified" Runge-Kutta method of integration was based on the fact that its advantages (21) over other techniques were useful in this comparison. In a study such as this, it is of primary importance to be able to integrate up to a point specified in advance. This ability, the ease with which Runge-Kutta starts the integration, and the convenience of interval size change are some of the benefits derived from the use of this routine. It must be mentioned here that this method does not arrive at a true estimate for the truncation error. In this comparison, the emphasis is placed on consistency between the methods, and since this estimate remains constant, it does not appear to be a disadvantage.

A variation of the Runge-Kutta integration technique has been devised (22) to include error estimation and automatic interval size control.

In the comparison of the perturbation techniques, namely, Cowell's, Encke's and variation-of-parameters, the same error control must be applied to each method. By employing the same numerical integration technique, in this case the so-called modified Runge-Kutta method, the truncation error remains constant if it is applied to similar integrals. If the integrals are different, as in this study, then, when absolute error control is considered, the error control must be kept on the same parameters. In Cowell's method, the integrals are x, y, z and $\ddot{x}, \ddot{y}, \ddot{z}$; in Encke's method ξ, η, ζ and $\ddot{\xi}, \ddot{\eta}, \ddot{\zeta}$; and in variation-of-parameters, these are $\boldsymbol{a}(a_x, a_y, a_z)$ and $\boldsymbol{b}(b_x, b_y, b_z)$, n and M. Any one set could have been adopted as the basis for comparison, but for convenience, Cowell's integrals for determining position (x, y, z) and velocity $(\dot{x}, \dot{y}, \dot{z})$ were utilized. The comparison is made on the number of integration steps needed in each of the methods, since roundoff errors accumulate with the number of steps.

Rounding Error

Numerical computations are necessarily limited in accuracy to a finite number of digits. The error incurred in rounding the result of each computation is propagated through the whole subsequent computation. Further, the accuracy of computation is limited by the number of digits in the input information or by errors inherent in that information. Automatic computing machinery and programs should be so constructed as to minimize the accumulation of roundoff, but, even so, the end places of the numbers produced will contain rounding error which grows generally with the amount of computation producing the numbers.

This problem is especially serious in numerical integrations, since the errors generated at any step are propagated to the end of the integration. Integration is essentially a process of summation. Thus, an actual error in one integrand value will appear in all subsequent single integrals. The same error at each step would result in a linear increase with the number of steps. If the double integral is taken, the absolute error in the double integral will be the original error times the number of steps since the commission of the error. This argument really applies only to blunders. Of course, we are only concerned here with statistical errors. Both rounding and truncation errors are distributed presumably in a Gaussian fashion about zero. Instead of a variation with the number of steps in a single integration, the variation of the mean error is with the square root of the number of steps. In double integration, the variation is with the three-halves power of the number of steps (5, 20).

Although Cowell's method involves the least computation per step, the integrand is the total acceleration, which may change rapidly. Therefore, a small step size is necessary to limit truncation error, since the integrals, position and velocity, change their leading figures rapidly. By reducing the integrals to the departures from two-body values, Encke's method can carry additional significant digits at the expense of more computation per step. The variations of the parameters are slower yet, thus enabling the use of large intervals at the expense of yet more extensive computation per step. The major error is introduced in the integration rather than in auxiliary computation.

The employment of double precision calculations to counteract end figure error is not only wasteful of computing time but is of no real value if tables are to be entered and interpolated at each integration step. If the tables are accurate, e.g., to six significant figures, the addition of 14 more dummy figures will not counteract the basic random interpolation or roundoff error.

As Miner (16) points out, the rounding error in floating point arithmetic is large relative to that in fixed point computation. But fixed point arithmetic involves coded scaling operations for the most precise results. Some loss of generality of the program results unless the scaling factors can be treated as input parameters.

Calculations

Analytical Solutions

To establish the precisions of the various orbit integration techniques, it is desirable to compare these results with analytical solutions. Most of the problems of interest cannot be solved analytically; hence it is only possible to make a comparison with some very specialized analytical solutions. One such solution is a special case of the three-body problem solved by Lagrange and discussed by many authors, e.g., Klemperer and Benedikt (15). A selenoid (or "synodic") satellite is defined as an Earth satellite moving with the same angular velocity as the moon. The satellite maintains a constant position with respect to the Earth-moon system (see Fig. 3). One drawback of this three-body solution is that the relative distances between the bodies remain constant. A solution in-

volving a physically meaningless system of *fixed* masses, due to Euler [see Whittaker (24)], might have been employed instead; however, since it is the magnitude of the perturbative accelerations that is of interest, not the change in acceleration, this analytical solution was not employed. In fact, such a variable perturbative acceleration would have clouded the estimate of truncation error.

Since the general three-body solution is very complex, the following simplifying assumptions are made in order to make the analytical solution more manageable: The satellite has zero mass, all perturbations except those due to the moon are neglected and the assumption of a circular orbit for the moon. These assumptions are, of course, not demanded by the numerical integration techniques.

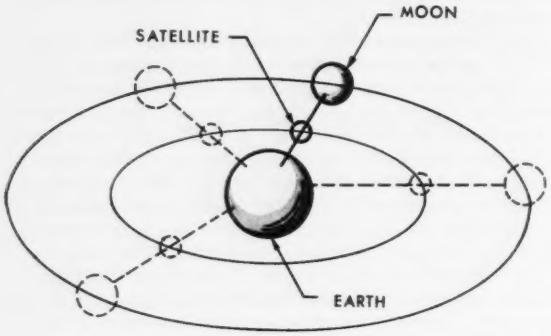

Fig. 3 Synodic satellite

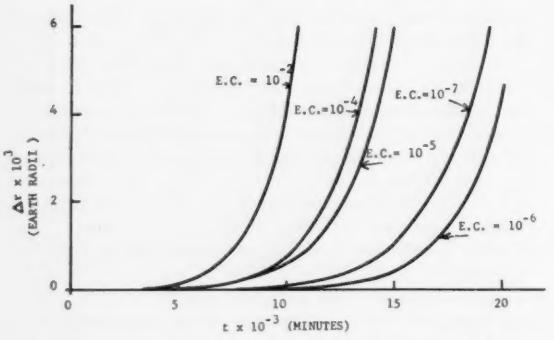

Fig. 4 Analytical solution vs. Cowell's method (synodic satellite)

Of the five solutions possible, the one in which the satellite is at inferior conjunction is chosen, since the perturbation due to the moon is largest for this position. The fact that this is not a stable point is an advantage, since it is then possible to compare the time at which a satellite departs from the starting position in a particular integration technique. If one chose a stable point, such as one of the sextile points [see Klemperer and Benedikt (15)] there might be a tendency to oscillate about the point. [The numerical description of this analytical orbit may be found in (4 and 14).]

The orbit was integrated utilizing Cowell's method with error control varied from 10^{-2} to 10^{-7} on position and velocity. Encke's method was not used for this orbit, since the choice of a reduced mass for Earth reduces the integrals to zero, yielding a solution which is always identical with the analytical solution. Similarly, utilizing the variation-of-parameters technique with a proper choice of constants reduces the perturbations to zero.

In order to check the error control the orbit was integrated with the variation-of-parameters method choosing an artificial reference orbit such that the integrals would not go to zero. This variation-of-parameters method naturally does not compare well with Cowell's in regard to the number of steps required.

Fig. 4 shows the departures from the analytical orbit utilizing various error controls (*E. C.*) with Cowell's method. Due to the instability of the orbit, the departure is rather rapid as soon as the satellite leaves the equilibrium point. The relation of the error control to the point of departure is discussed in the last section.

A second analytical solution considered was one of low thrust. There have been numerous references in the literature regarding low thrust trajectories. One such low thrust trajectory capable of a closed form analytical solution has been discussed by Bacon (1). This trajectory is a logarithmic spiral in an inverse-square gravitational field (see Fig. 5). [The numerical description of this analytical orbit may also be found in (4 and 14).]

Perturbation techniques again yield a perfect solution with the proper choice of reference orbits. Hence, results are presented in Fig. 6 only for Cowell's method for various values of error control.

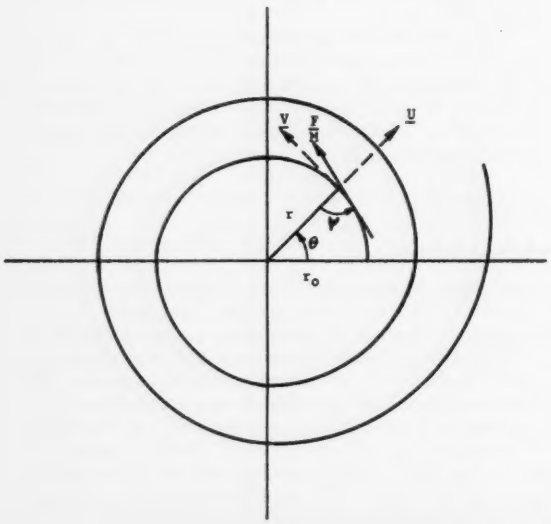

Fig. 5 Logarithmic spiral (low thrust)

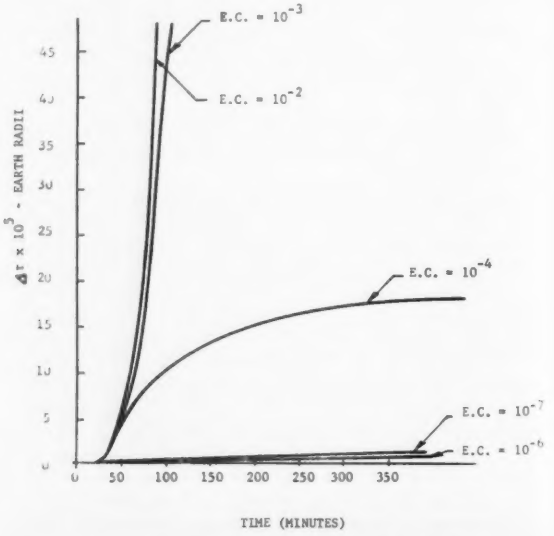

Fig. 6 Logarithmic spiral (Cowell's method)

Ballistic Lunar Trajectory

A standard $3\frac{1}{4}$-day ballistic lunar trajectory (see Fig. 7) for which Encke's method has been used in sensitivity studies for lunar impact[9] was compared with variation-of-parameters and Cowell's methods. The perturbations include the second and fourth harmonics of the Earth potential, lunar and solar perturbations. The constants used in these trajectories are listed in the Nomenclature.

Comparisons were made at the same distance from Earth to the rocket for different orbit computation techniques utilizing various error controls.

Low Thrust Trajectory

With the recent emphasis on electrical propulsion there is considerable interest in the efficient numerical integration of low thrust satellite and interplanetary orbits (see Fig. 8). This class of orbits involves small accelerations over long periods of time.

Two trajectories with thrust about equal to 10^{-5} and 10^{-6} Earth radii/$(k_e^{-1}$ min$)^2$ were determined by direct integration and perturbational techniques. The perturbations are limited to thrust for a more direct comparison.

High Thrust Corrective Maneuver

The uncertainties in the constants, e.g., Earth flattening, masses, solar parallax and burnout conditions make purely ballistic interplanetary and lunar trajectories impractical without midcourse correction.

Two trajectories with thrust about equal to 10^{-1} and 10^{-2} Earth radii/$(k_e^{-1}$ min$)^2$ were compared as in the low thrust case with the same initial conditions. Since the corrective thrust (see Fig. 9) was applied at a rather great distance from Earth's surface, the perturbative thrust level was considerably higher than the basic acceleration due to gravity in both cases.

Conclusions

Rounding vs. Truncation Error

Selection of a particular error control for any trajectory necessitates a compromise between rounding and truncation error. As can be seen from the computations plotted in Figs. 10 and 11 the rounding errors surpass truncation errors as the number of integration steps is increased. As shown in Fig. 10, rounding error caused by an excessive number of integration steps produces a continuous departure from the analytical three-body orbit. For any one error control this departure is continuous due to the fact that the integration is carried out about an unstable libration point. On the other hand, in the case of the spiral trajectory (Fig. 11) the rounding error for an excessive number of steps results in an oscillation and not a departure. This oscillation is caused by the fact that the logarithmic trajectory is a stable one.

The foregoing analyses substantiate the well-known tradeoff between truncation and roundoff error, but it is noteworthy to observe how quickly (within 120 steps) roundoff error becomes a major factor in the accuracy of the computations.

Orbit Computation Techniques for Particular Trajectories

In view of the relatively large effect of roundoff error, as pointed out in the previous section, it is desirable to select a method which minimizes the number of required integration steps to compute a high precision orbit. Table 1 indicates the number of integration steps or number per hour (in real time) to accomplish various trajectories utilizing all three in-

[9] The Aeronutronic High Precision Lunar Trajectory Determination Computer Program, Aeronutronic publication U-378.

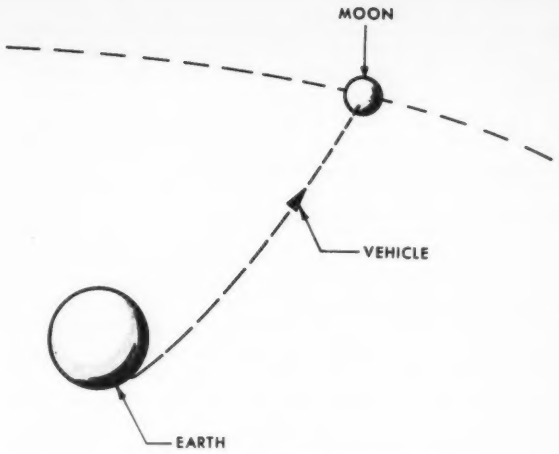

Fig. 7 Ballistic lunar trajectory

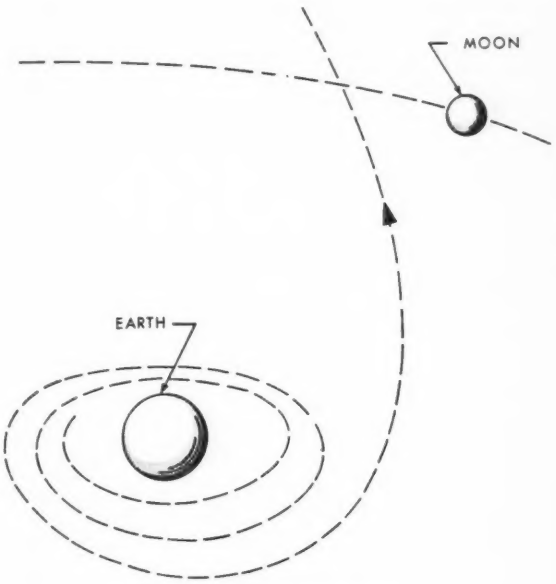

Fig. 8 Low thrust trajectory

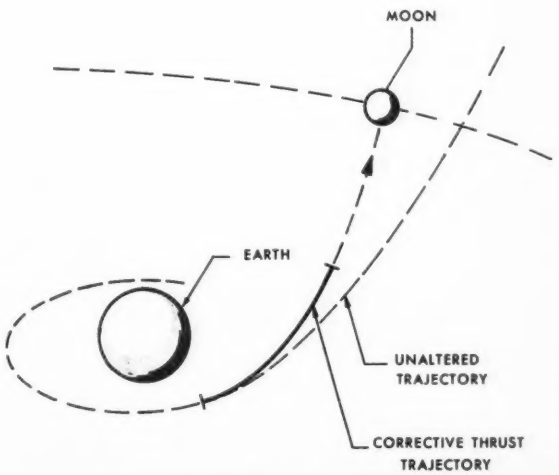

Fig. 9 High thrust corrective maneuver

tegration techniques. It is self-evident from Table 1 that the statements made in the introduction are valid in that the proper choice of computational technique for high precision computations is dependent upon the nature of the problem; e.g., Encke's is preferable in the ballistic lunar trajectory,[10] variation-of-parameters in the low thrust trajectory and Cowell's method in the high thrust trajectory.

Overall Computational Efficiency

The overall computational efficiency of a particular technique must be judged both with respect to accumulated error and required computational time. One other factor that may be of some importance is the flexibility of a given computational procedure. Cowell's method is evidently the most flexible of the computational methods that can be employed. The disadvantage of its use, however, in high precision orbit computations as compared with other more special perturbational techniques is manifest. The complexity of equations required in perturbational methods is reflected in the increased time needed for the computer to carry out a given iteration. Nevertheless, the nearly 10 to 1 decrease in number of steps required constitutes an advantage inherent in the use of perturbational methods, for the first two of the forementioned cases, that is considerably more significant than the increased machine time required. This conclusion is particularly valid since the use of perturbational methods increases machine time by at most 50 per cent per iteration. Studies are now underway to compare these methods on the computation of minor planet orbits.

[10] Note that in Encke's method the orbit should probably be rectified after about 45 Earth-radii to yield an overall 10:1 advantage over Cowell's method.

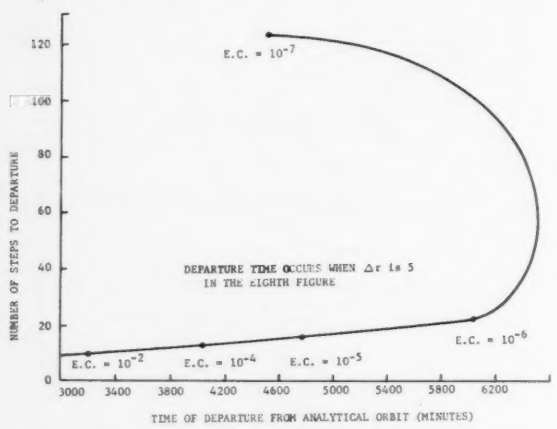

Fig. 10 Synodic satellite (Cowell's method)

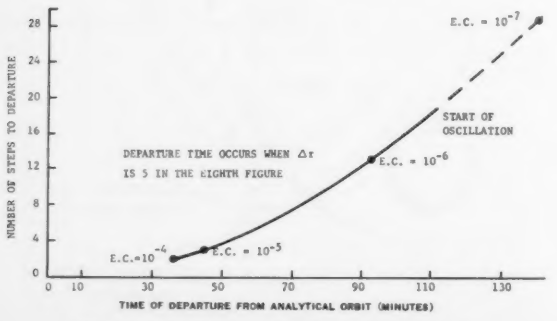

Fig. 11 Logarithmic spiral (Cowell's method)

Table 1 Number of integration steps for orbit computation techniques for particular trajectories

Trajectory		Cowell	Variation-of-parameters[a]	Encke
ballistic lunar	steps to 45 radii	132	57	14
	steps to impact	190	...	49
low thrust, steps/hr		7	0.75	4.5
high thrust, steps/hr		8	30	...

[a] The high eccentricity of the lunar ballistic orbit caused this particular form of the variation-of-parameters to take a rather excessive number of steps.

Nomenclature

The following nomenclature, in general, adheres to the standard notation of celestial mechanics. Each of the motions under study are referred to an equatorial coordinate system with the x-axis pointed toward the vernal equinox (e.g., mean equinox of 1950.0), the z-axis directed toward the north celestial pole and the y-axis directed such that a right-handed system is formed.

The definitions of the terms utilized in the analysis are listed below. The grave signs ($\grave{}$) represent time derivatives caused by perturbations, in this analysis caused by thrust, Earth's bulge and the gravitational influence of the sun and moon. Dots represent nonperturbative time derivatives, e.g., $dx/d\tau = \dot{x} + x\grave{}$.

The unit of length is Earth's equatorial radius (6.37814×10^6 m); the unit of time is the k_e^{-1} min (equal to 13.447052 min), and the unit of mass is Earth's mass (5.975×10^{27} gm).

Vectors

$\boldsymbol{a}$ = vector directed to perigee, having a scalar value equal to the eccentricity with components a_x, a_y, a_z

$\boldsymbol{b}$ = vector in the orbit plane perpendicular to $\boldsymbol{a}$, in the direction of motion, having a scalar value equal to the product of the eccentricity and the square root of the semilatus rectum (parameter) of the orbit, with components b_x, b_y, b_z

$\boldsymbol{P}$ = unit vector directed to perigee with components P_x, P_y, P_z

$\boldsymbol{Q}$ = unit vector in the orbit plane perpendicular to $\boldsymbol{P}$, in the direction of motion when the vehicle is at perigee

$\boldsymbol{r}$ = radius vector with components x, y, z directed from the origin (geocenter) to the missile

$\boldsymbol{r}_e$ = radius vector with components x_e, y_e, z_e directed from the origin (geocenter) to the hypothetical unperturbed position of the vehicle on the reference orbit (employed in Encke's method)

$\dot{\boldsymbol{r}}\grave{}$ = perturbative derivative of $\dot{\boldsymbol{r}}$ (in this case caused by thrust, Earth's bulge and gravitational influence of the sun and moon) with components $\dot{x}\grave{}$, $\dot{y}\grave{}$, $\dot{z}\grave{}$

$\boldsymbol{T}$ = thrust per unit mass (for discussion of components see scalars)

$\boldsymbol{U}$ = unit vector in the direction of $\boldsymbol{r}$ with components U_x, U_y, U_z, i.e., $U_x = x/r$, $x \rightarrow y, z$

$\boldsymbol{V}$ = transverse unit vector in the orbit plane perpendicular to $\boldsymbol{U}$ in the direction of motion

$\boldsymbol{W}$ = unit vector perpendicular to the orbit plane forming a right-handed system with $\boldsymbol{P}$ and $\boldsymbol{Q}$ (or $\boldsymbol{U}$ and $\boldsymbol{V}$) and with components W_x, W_y, W_z

Scalars

a = semimajor axis of the orbit

e = eccentricity of the orbit

E = eccentric anomaly for an elliptical orbit

$E.C.$ = error control

m = mass in terms of the mass of the central body

M = mean anomaly with initial value of M_0, radians
n = mean motion of the vehicle
p = semilatus rectum (parameter) of the orbit, i.e., $p = r^4\dot{\psi}^2 = a(1 - e^2)$
T = time of perigee passage
T_r, T_v, T_w = components of thrust per unit mass in a right-handed coordinate system directed along the U, V, W vectors, respectively
T_α = component of thrust per unit mass in the positive α direction (see Fig. 1)
T_δ = component of thrust per unit mass in the positive δ direction (see Fig. 1)
α = right ascension of the vehicle
δ = declination of the vehicle
μ = mass of Earth; $\mu = m_{\text{Earth}} = 1$ for the units utilized
ξ, η, ζ = differences between the computed true coordinates x, y, z and the two-body reference coordinates x_c, y_c, z_c, respectively; also used to denote distances to synodic satellite
τ = modified time defined by the equation $\tau = k_e(t - t_0)$

Subscripts

1 = sun
2 = vehicle
3 = Earth
4 = moon
B = bulge perturbation
G = perturbation due to the sun and moon
T = thrust perturbation

Constants

m_1 = $0.332{,}448 \times 10^6$ (sun's, in Earth masses)
m_2 = 0 (vehicle's)
m_3 = 1 (Earth's)
m_4 = 0.012,288,8 (moon's)
k_e = geocentric gravitational constant = 0.074,365,740 for the units used
$J\backslash$ = coefficient of the second harmonic of Earth's potential = $1.623\,41 \times 10^{-3}$
$H\backslash$ = coefficient of the third harmonic of Earth's potential = 6.0×10^{-6}
$K\backslash$ = coefficient of the fourth harmonic of Earth's potential = 9.09×10^{-6}

References

1 Bacon, R. H., "Logarithmic Spiral: An Ideal Trajectory for the Interplanetary Vehicle with Engines of Low Sustained Thrust," *Amer. J. Physics*, March 1959, vol. 27, p. 164.

2 Baker, R. M. L., Jr., "Application of Astronomical Perturbation Techniques to the Return of Space Vehicles," ARS JOURNAL, March 1959; "Encke's and the Variation of Parameters Methods as Applied to Re-Entry Trajectories," *J. Amer. Astron. Soc.*, vol. 6, no. 1, Spring 1959.

3 Baker, R. M. L., Jr., "High Precision Orbit Determination," Monthly Progress Report, Aeronutronic, Newport Beach, Calif., Nov. 1958; Appendix B, Dec. 1958.

4 Baker, R. M. L., Jr. and Makemson, M. W., "An Introduction to Astrodynamics," Academic Press, N. Y., 1960.

5 Brouwer, D., "On the Accumulation of Errors in Numerical Integration," *Astron. J.*, vol. 46, 1937, p. 149.

6 Eckert, W. J., Brouwer, D. and Clemence, G. M., Astronomical Papers Prepared for the Use of the American Ephemeris and Nautical Almanac, vol. 12, "Coordinates of the Five Outer Planets," 1653–2060, U. S. Govt. Printing Office, Washington, D. C., 1951.

7 Garfinkel, B., "On the Motion of a Satellite of an Oblate Planet," Ballistic Research Lab. Rep. no. 1018, Aberdeen Proving Ground, Md., 1957.

8 Herrick, S., "A Modification of the 'Variation-of-Constants' Method for Special Perturbations," *Pub. Astron. Soc. Pacific*, vol. 60, no. 356, 1948, pp. 321–323.

9 Herrick, S., "Astrodynamics and Rocket Navigation," Van Nostrand, to be published in 1961.

10 Herrick, S., "Step-by-Step Integration of $\ddot{x} = f(x, y, z, g)$ Without a Corrector," in *Mathematical Tables and Other Aids to Computation*, vol. 5, 1951, p. 61.

11 Herrick, S. and Baker, R. M. L., Jr., "Recent Advances in Astrodynamics," JET PROPULSION, Oct. 1958, vol. 28, no. 10, pp. 649–654.

12 Herrick, S. and Walters, L. G., "The Influence of the Earth's Potential Field on a Nearly Circular Satellite," Technical Note, U-326, Aeronutronic, Newport Beach, Calif., Jan. 9, 1959.

13 Herrick, S., Baker, R. M. L., Jr. and Hilton, C. G., "Gravitational and Related Constants for Accurate Space Navigation," in "Proc. VIIIth International Astronautical Congress, Barcelona, 1957," Springer Verlag, Vienna, 1958, pp. 197–235; University of California, Los Angeles, Astronomical Papers, no. 24, vol. 1, pp. 297–338.

14 "High Precision Orbit Determination," Final Report, Aeronutronic, Newport Beach, Calif., Pub. no. U-583, Sept. 28, 1959.

15 Klemperer, W. B. and Benedikt, E. T., "Selenoid Satellites" in "Proc. VIIIth International Astronautical Congress, Barcelona, 1957," Springer Verlag, Vienna, 1958.

16 Miner, W. E., "Analysis of Computational Accuracy of Lunar Probe Decks in use at ABMA," ABMA Rep. no. DA-TN-16-59.

17 Moulton, R. F., "An Introduction to Celestial Mechanics," second ed., MacMillan Co., N. Y., 1956.

18 "Planetary Coordinates for the Years 1960–1980," Her Majesty's Stationery Office, London, pp. vii-xix.

19 Porter, J. G., "A Comparative Study of Perturbation Methods," *Astron. J.*, vol. 63, no. 10, 1958, pp. 405–406.

20 Schlesinger, F., "On the Errors in the Sum of the Number of Tabular Quantities," *Astron. J.*, vol. 30, Sept. 1917, p. 183.

21 Schlesinger, S., "High Precision Orbit Determination," Appendix B, Monthly Progress Rep., Aeronutronic, Newport Beach, Calif., Jan. 1959.

22 Schlesinger, S., "Integration Methods for Differential Equations," Pub. no. U-348, Aeronutronic, Newport Beach, Calif.

23 Vienop, E. and Brady, J. L., "The Themis Code; an Astronomical Numerical Integration Program for the IBM 704," Rep. no. 5242, University of California Radiation Laboratory, May 28, 1958.

24 Whittaker, E. T., "Analytical Dynamics," Cambridge University Press, 1944, pp. 94–99.

1960 ARS Meeting Schedule

Date	Meeting	Location	Abstract Deadline
Aug. 15–20	11th International Astronautical Congress	Stockholm, Sweden	Past
Sept. 27–30	Power Systems Conference	Santa Monica, Calif.	Past
Oct. 10–12	Human Factors and Bioastronautics Conference	Dayton, Ohio	Past
Nov. 3–4	Electrostatic Propulsion Conference	Monterey, Calif.	Past
Dec. 5–8	ARS Annual Meeting and Astronautical Exposition	Washington, D.C.	Aug. 25

Send all abstracts to Meetings Manager, ARS, 500 Fifth Ave., New York 36, N.Y.

Three-Dimensional Drag Perturbation Technique

ROBERT M. L. BAKER Jr.[2]

University of California
Los Angeles, Calif.

This paper extends the analysis of the application of an astronomical special perturbation technique to the entry of space vehicles (into a resistive medium) to three dimensions. Furthermore, perturbations resulting from the asphericity of Earth and the rotation of Earth's atmosphere have been explicitly included, and the effects of ablation, cross winds and lift are considered. Use of the variation-of-parameters perturbation technique allows for the more efficient and accurate computation of a large class of entry orbits.

REALISTIC analyses of space vehicle entry should be formulated in three dimensions. Thus, the basic two-dimensional equations given in (2)[3] of a gravity-free drag "intermediary" orbit for special perturbations (numerical integration) require extension. The analyses found in the referenced work will not be repeated; however, the following notational changes should be noted: The symbols, x, $x^{\backprime}$, y, $y^{\backprime}$, $\dot{y}$, $\dot{y}^{\backprime}$ and P in (2) are replaced in this paper by x_ω, $x_\omega{}^{\backprime}$, y_ω, $y_\omega{}^{\backprime}$, $\dot{y}_\omega$ ($\equiv\dot{s}$), $\dot{y}_\omega{}^{\backprime}$ ($\equiv\dot{s}^{\backprime}$) and P_1, respectively. The specific analytical representation of the atmosphere density function $\mu D_0{}^2\sigma\gamma(\sigma) = \mu D_0{}^2(C_0 + C_2r^2 + C_4r^4 + \ldots)$ has been replaced by a more general $f(r)$ in this paper. The subscript ω refers to a coordinate system rigidly attached to the orbit plane with the x_ω axis directed to the perigee. (The equations will be established in geocentric form; however, extension to any planetocentric form will be obvious.) Other notation is given in the Nomenclature included at the end of this paper.

For convenience the elements of the gravity-free drag orbit have been introduced here in a vectorial format in a fashion analogous to the formulation of the variation of parameters carried out in classical celestial mechanics (8). These vectorial elements, phrased in the standard nomenclature introduced by Adams and Comrie in 1922 (1) and found in (13), p. 155, are given as follows

$$\boldsymbol{a} \triangleq x_\omega \boldsymbol{P} \qquad [1]$$

$$\boldsymbol{b} \triangleq \boldsymbol{Q} \qquad [2]$$

See Fig. 1 for the definition of the $\boldsymbol{P}$ and $\boldsymbol{Q}$ unit vectors.

Perturbation Equations

Eight perturbation equations (one for each of the three equatorial x, y and z components of the vectors $\boldsymbol{a}$ and $\boldsymbol{b}$, plus Eqs. [5 and 6]) are integrated with y_ω as the independent variable. They are

$$\boldsymbol{a} = \boldsymbol{a}_0 + \int_{y_{\omega_0}}^{y_\omega} \boldsymbol{a}'\,dy_\omega \qquad [3]$$

$$\boldsymbol{b} = \boldsymbol{b}_0 + \int_{y_{\omega_0}}^{y_\omega} \boldsymbol{b}'\,dy_\omega \qquad [4]$$

$$P_1 = \int_{y_{\omega_0}}^{y_\omega} P_1'\,dy_\omega \qquad \text{(initially, } P_1 \text{ is zero)} \qquad [5]$$

and, *if* the time is required, e.g., for the determination of longitude

$$\tau = \tau_0 + \int_{y_{\omega_0}}^{y_\omega} \frac{dy_\omega}{\dot{y}_\omega + y_\omega{}^{\backprime}} \qquad [6]$$

Although singularities in the foregoing formulas do not arise in either ascent or descent drag orbits, they will emerge if one attempts to reproduce a drag-free gravity orbit. In this case it becomes clear, after a little thought, that $\dot{y}_\omega + y_\omega{}^{\backprime}$ (being the speed of the object relative to the perturbed x_ω axis) will

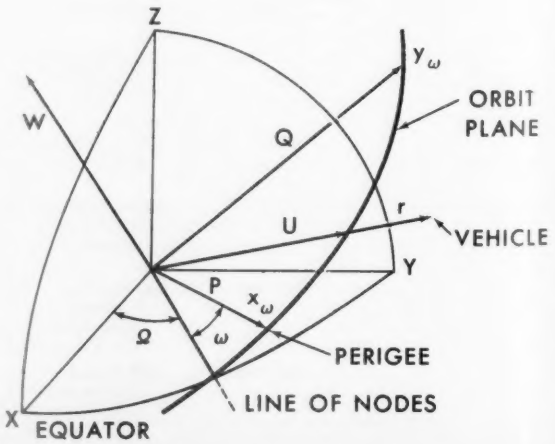

Fig. 1 Orientation vectors

Received July 1, 1959.

[1] This research was supported in part by the U. S. Army under Contract DA-04-495-ORD-1389 monitored at Aeronutronic Systems, Inc., by the Army Ballistic Missile Agency and by the U. S. Air Force under Contract AF 49 (638)-498 monitored at UCLA by AFOSR.

[2] Lecturer, Assistant Professor of Astronomy; also Staff Member, Aeronutronic Div., Ford Motor Co., Newport Beach, Calif. Presently on active duty with USAF at AFBMD. Member ARS.

[3] Numbers in parentheses indicate References at end of paper.

pass through zero twice during a complete revolution on an elliptical Keplerian orbit. Consequently, when $\dot{y}_\omega + y_\omega{}^\wedge$ becomes small, it is necessary to switch over to the following alternate formulas that have τ as independent variable

$$\boldsymbol{a} = \boldsymbol{a}_0 + \int_{\tau_0}^{\tau} \boldsymbol{a}^\wedge d\tau \quad (\boldsymbol{a}^\wedge = x_\omega \boldsymbol{P}^\wedge + x_\omega{}^\wedge \boldsymbol{P}) \qquad [3a]$$

$$\boldsymbol{b} = \boldsymbol{b}_0 + \int_{\tau_0}^{\tau} \boldsymbol{b}^\wedge d\tau \quad (\boldsymbol{b}^\wedge = \boldsymbol{Q}^\wedge) \qquad [4a]$$

$$P_1 = \int_{\tau_0}^{\tau} P_1{}^\wedge d\tau \qquad [5a]$$

$$(P_1{}^\wedge = \{\dot{y}_\omega{}^\wedge/(A\dot{y}_\omega + B) + y_\omega{}^\wedge f(r) + [f(r_0) - f(r)](\dot{y}_\omega + y_\omega{}^\wedge)\})$$

and

$$y_\omega = \int_{\tau_0}^{\tau} (\dot{y}_\omega + y_\omega{}^\wedge) d\tau \qquad [7]$$

where $r_0 \triangleq \sqrt{x_{\omega_0}{}^2 + y_{\omega}{}^2}$.

Under certain circumstances (of low inertial speed $\dot{y}_\omega$ or high lift), $\dot{y}_\omega + y_\omega{}^\wedge$ may be negative. In this case the object is receding from the x_ω axis and the integration should be carried in the negative direction. The upper limit on the integrals should, therefore, be set after an inspection of the sign of $\dot{y}_\omega + y_\omega{}^\wedge$.

A check on Equations [3 and 4] is obtained by determining how closely the dot product relations $\boldsymbol{a}\cdot\boldsymbol{b} = 0$ and $\boldsymbol{b}\cdot\boldsymbol{b} = 1$ hold. Equation [6] need only be integrated if time τ is required explicitly, e.g., if the longitude of the sub-vehicle point is to be computed. The employment of y_ω as independent variable also allows for a simple scheme for the termination of the integration at any given height. This procedure is particularly convenient when the simulation of a vehicle configuration change, triggered by a barometric switch, is involved.

The integrands of Equations [3, 4 and 5] are of the form

$$\boldsymbol{a}' = (x_\omega \boldsymbol{P}^\wedge + x_\omega{}^\wedge \boldsymbol{P})/(\dot{y}_\omega + y_\omega{}^\wedge) \qquad [8]$$

$$\boldsymbol{b}' = \boldsymbol{Q}^\wedge/(\dot{y}_\omega + y_\omega{}^\wedge) \qquad [9]$$

$$P_1{}' = P_1{}^\wedge/(\dot{y}_\omega + y_\omega{}^\wedge) \quad (\text{note that } |\boldsymbol{P}| \neq P_1) \qquad [10]$$

$$y_\omega{}^\wedge = \left(\frac{x_\omega{}^2}{\dot{s}r}\right) \dot{r}^\wedge - \left(\frac{x_\omega y_\omega}{\dot{s}r}\right) r\dot{v}^\wedge \qquad [11]$$

$$\dot{s} \equiv \dot{y}_\omega = \left(\dot{s}_0 + \frac{B}{A}\right) \times \exp\,[-AF(x_{\omega_0}, y_{\omega_0}, y_\omega) + AP_1] - \frac{B}{A} \qquad [12]$$

$$\dot{s}^\wedge \equiv\equiv \dot{y}_\omega{}^\wedge = (\dot{\boldsymbol{r}}_D{}^\wedge + \dot{\boldsymbol{r}}_\oplus{}^\wedge)\cdot\boldsymbol{Q} \qquad [13]$$

Equation [12] can be recognized as Equation [42] of (2) with the series for $\sigma\gamma(\sigma)$ generalized to $f(r)$. Equations [10 and 12] are derived in Appendix A. The vectors $\dot{\boldsymbol{r}}_D{}^\wedge$ and $\dot{\boldsymbol{r}}_\oplus{}^\wedge$ in Equation [13] are perturbative accelerations caused by unaccounted for drag (crosswind and lift) accelerations and the gravitational field of Earth, respectively; and $\dot{r}^\wedge$ and $r\dot{v}^\wedge$ are the radial and transverse components of perturbative acceleration, respectively. $\boldsymbol{P}^\wedge$ and $\boldsymbol{Q}^\wedge$ are formed by the relations

$$\boldsymbol{P}^\wedge = \boldsymbol{Q}\bar{w}^\wedge - \boldsymbol{W}\bar{q}^\wedge \qquad [14]$$

$$\boldsymbol{Q}^\wedge = \boldsymbol{W}\bar{p}^\wedge - \boldsymbol{P}\bar{w}^\wedge \qquad [15]$$

$$\bar{p}^\wedge \triangleq r\dot{b}^\wedge/\dot{s} \qquad [16]$$

$$\bar{q}^\wedge \triangleq (y_\omega/x_\omega\dot{s})r\dot{b}^\wedge \qquad [17]$$

$$\bar{w}^\wedge \triangleq -v^\wedge = \omega^\wedge \qquad [18]$$

where

$r\dot{b}^\wedge$ = perturbative acceleration directed normal to the orbit plane (orthogonal component) and includes accelerations occasioned by the equatorial bulge and by the rotation of Earth's atmosphere, etc.
b = angle measured up from the orbit ($\boldsymbol{P} - \boldsymbol{Q}$) plane
$\boldsymbol{W}$ = unit vector normal to the orbit plane (see Fig. 1)

Consequently, $\boldsymbol{W} = \boldsymbol{P} \times \boldsymbol{Q}$. Equations [14 through 18] are derived in chapter 17 section H of (10), where the quantity $\sqrt{p}\,\boldsymbol{W} = \boldsymbol{r} \times \dot{\boldsymbol{r}}$ is associated with $x_\omega\,\dot{s}\boldsymbol{W}$.

From Equation [13] of (2) it can be shown that

$$x_\omega{}^\wedge = -\left(\frac{x_\omega y_\omega}{\dot{s}r}\right)\dot{r}^\wedge + \left(\frac{y_\omega{}^2}{\dot{s}r}\right) r\dot{v}^\wedge \qquad [19]$$

while

$$\omega^\wedge = x_\omega{}^\wedge/y_\omega \qquad [20]$$

Components of Perturbative Accelerations

The radial, transverse, orthogonal and tangential components [the tangential component introduced by Moulton (12)] are, respectively

$$\begin{aligned} \dot{r}^\wedge &= (\dot{\boldsymbol{r}}_\oplus{}^\wedge + \dot{\boldsymbol{r}}_D{}^\wedge)\cdot\boldsymbol{U} \\ r\dot{v}^\wedge &= (\dot{\boldsymbol{r}}_\oplus{}^\wedge + \dot{\boldsymbol{r}}_D{}^\wedge)\cdot\boldsymbol{V} \\ r\dot{b}^\wedge &= (\dot{\boldsymbol{r}}_\oplus{}^\wedge + \dot{\boldsymbol{r}}_D{}^\wedge)\cdot\boldsymbol{W} \\ \dot{s}^\wedge &= (\dot{\boldsymbol{r}}_\oplus{}^\wedge + \dot{\boldsymbol{r}}_D{}^\wedge)\cdot\boldsymbol{Q} \quad (\text{see Eq. [13]}) \end{aligned} \qquad [21]$$

In Equations [21] $\boldsymbol{U}$ is a unit vector directed along $\boldsymbol{r}(\boldsymbol{U} = \boldsymbol{r}/r)$, and $\boldsymbol{V}$ is a unit vector in the orbit plane perpendicular to $\boldsymbol{U}(\boldsymbol{V} = \boldsymbol{W} \times \boldsymbol{U})$. The components of $\dot{\boldsymbol{r}}_\oplus{}^\wedge$ are

$$\dot{\boldsymbol{r}}_\oplus{}^\wedge \begin{cases} \dot{x}_\oplus{}^\wedge = -\dfrac{x}{r^3} - \dfrac{x}{r^5} J_\oplus(1 - 5U_z{}^2) - \dfrac{xz}{r^7} H_\oplus(3 - 7U_z{}^2) - \dfrac{x}{6r^7} K_\oplus(3 - 42U_z{}^2 + 63U_z{}^4) + \ldots \\ \dot{y}_\oplus{}^\wedge = \dot{x}_\oplus{}^\wedge y/x \\ \dot{z}_\oplus{}^\wedge = -\dfrac{z}{r^3} - \dfrac{z}{r^5} J_\oplus(3 - 5U_z{}^2) + \dfrac{3H_\oplus}{5r_2}\left(1 - 10U_z{}^2 + \dfrac{35}{3}U_z{}^4\right) - \dfrac{z}{6r^7} K_\oplus(15 - 70U_z{}^2 + 63U_z{}^4) + \ldots \end{cases} \qquad [22]$$

where $\boldsymbol{a}^\wedge$, $\boldsymbol{b}^\wedge$ and $P_1{}^\wedge$ are given in Equations [3a, 4a and 5a] and

$$F(x_{\omega_0}, y_{\omega_0}, y_\omega) \triangleq \int_{y_{\omega_0}}^{y_\omega} f(r_0) dy_\omega$$

i.e., it is the analytical part of the integral.

where $U_z = z/r$, and $J_\oplus$, $H_\oplus$ and $K_\oplus$ are the coefficients of the second, third and fourth harmonics of Earth's gravitational field (their numerical values may be found in the Nomenclature). Because of the choice of the units of surface circular satellite speed, these equations are dimensionless and do not contain the mass factor explicitly.

The x, y and z components of perturbative acceleration $\dot{\boldsymbol{r}}_D{}^\wedge$

resulting from lift and residual drag accelerations are

$$\dot{\boldsymbol{r}}_D \searrow \begin{cases} \dot{x}_D \searrow = -D_0 \dot{s}^2 \left(\left[\mu\gamma(\nu)\sigma(H)\gamma(\sigma)\nu \frac{\nu_x}{\dot{s}^2} - \mu \left(A + \frac{B}{\dot{s}} \right) \frac{f(r)}{D_0^2} Q_x \right] - \mu\gamma(\nu)\sigma(H)\gamma(\sigma) \times \right. \\ \qquad \left. \frac{\nu^2}{\dot{s}^2} \frac{C_L}{C_{D_0}} \left\{ \left(U \times \frac{\nu}{\nu} \right)_x \sin \xi + \left[\frac{\nu}{\nu} \times \left(U \times \frac{\nu}{\nu} \right) \right]_x \cos \xi \right\} \right) \\ x \rightarrow y, z \end{cases} \quad [23]$$

(For low altitudes the magnitudes of $\dot{\boldsymbol{r}}_D \searrow$ can be greatly reduced by changing to a rotating coordinate system, i.e., by setting $\dot{\theta} = 0$ in Eq. [25] and by adding in the coriolis and centrifugal terms.) In Equation [23], $\gamma(\nu)$ gives the true variation of the drag coefficient with Mach number and is obtained from a linear interpolation of a table of sonic speed vs. height and γ vs. Mach number; and $\sigma(H)$ is the density ratio and is obtained by *exponential* interpolation of a model atmosphere with argument height H. $\gamma(\sigma)$ gives the transitional variation of the drag coefficient with density and is obtained from Equation [2] of (3) with the inclusion of a nonunity value of the accommodation coefficient (see Appendix B)

$$\gamma(\sigma) = C_D/C_{D_0} = a + b \exp\left[-c\sigma(H)\right] \quad [24]$$

where a, b and c are coefficients discussed in (6) and in Appendix B (their numerical values may be found in the Nomenclature). C_L is the lift coefficient (C_L will be a function of the angle between the flow and the normal to the surface),[4] and ξ is the bank angle. A variation of the drag coefficient resulting from the reaction of ablated atoms might also be included; see Equations [13 to 18] of (4). The x subscript in Equation [23] denotes the x component of the cross-product vector.

The velocity of the vehicle relative to a rotating atmosphere including cross winds is obtained from

$$\boldsymbol{\nu} \begin{cases} \nu_x = \dot{x} + y\dot{\theta} + q(\cos\alpha \sin\phi' \cos A + \sin\alpha \sin A) \\ \nu_y = \dot{y} - x\dot{\theta} + q(\sin\alpha \sin\phi' \cos A - \cos\alpha \sin A) \\ \nu_z = \dot{z} - q \cos\phi' \cos A \end{cases} \quad [25]$$

where

$\dot{x}, \dot{y}, \dot{z}$ = components of the velocity of the vehicle in equatorial coordinates

q = speed of the cross wind measured in a framework rotating with Earth's angular rate (all speeds in units of surface circular satellite speed)

$\dot{\theta}$ = 0.058,834,470

ϕ' = geocentric latitude of the "geocentric sub-vehicle point" ($\phi' = \sin^{-1} z/r$)

α = right ascension of the satellite ($\sin\alpha = y/\sqrt{x^2 + y^2}$ and $\cos\alpha = x/\sqrt{x^2 + y^2}$)

A = azimuth *from* which the wind is coming; see (17)

A and q are to be obtained by linear interpolation of tables with argument height H. In nearly equatorial orbits the discrepancy between ν and $\dot{s}$ (and hence the "perturbation") becomes larger as $\dot{s}$ decreases, and the rotating coordinate system is indicated. For feasibility and sensitivity studies, however, it is possible to set $\dot{\theta} = 0$ without including the coriolis and centrifugal force terms.

The height of the vehicle above an oblate Earth (in Earth radii a_e) is given by

$$H = r - 1 + f \sin^2\phi' + \frac{f^2}{2}\left(\frac{1}{r} - \frac{1}{4}\right)\sin^2 2\phi' + \ldots \quad [26]$$

[4] See (7) for a discussion of transitional lift. In particular note from Fig. 6, pp. 15–19, that the lift/drag ratio varies between 0 and 0.15. The lift can, therefore, be legitimately considered as a perturbation on the drag orbit (at least in the transitional regime).

where f is the Earth's flattening.[5] Note that this "height" is measured along a normal from the surface of the spheroid to the vehicle and not along a normal from the geoid. Such a discrepancy is not serious and only amounts to a few feet at most.

The variation of μ (and perhaps of the area ratio) can be obtained by an ablation formula or from a separate integration of the mass loss per unit time [see (4)], whereas ξ and C_L are obtained from tables. The constants A and B are computed by a fit of $\gamma(\dot{s})$ to $A + B/\dot{s}$ under the approximation that $\nu = \dot{s}$ and c_s = a constant 310 m per sec for supersonic motion [or for motion prior to the maximum value of $\gamma(\dot{s})$]; and B is zero with A fitted to the mean value of $\gamma(\dot{s})$ for subsonic motion.

Latitude, Longitude and Entry Angle

Given the right ascension α of the vehicle in radians and the time t in minutes

$$t = \tau(13.447{,}052) \text{ min} \quad [27]$$

the longitude of the "sub-vehicle point" measured eastward from the Greenwich meridian λ_E is

$$\lambda_E = \alpha(57.295{,}779) - 15\theta_{g_0} - (0.250{,}684{,}48)(t - t_0) \quad [28]$$

in degrees and decimals. It should be noted that negative angles found in Equation [28] are to be interpreted as positive third or fourth quadrant angles. θ_{g0} is the initial Greenwich sidereal time measured in hours and decimals of an hour.

The geodetic latitude (measured positive in the northern hemisphere) is computed from

$$\phi = \left\{ \tan^{-1}\left[\frac{1}{(1-f)^2} \tan\phi' \right] \right\} 57.295{,}779 \quad [29]$$

in degrees and decimals [see (17) p. 166 for a more precise ϕ].

If ζ is the entry angle between the velocity of the vehicle relative to the atmosphere $\boldsymbol{\nu}$ and the local vertical $\boldsymbol{Z}$[6]; then

$$\cos\zeta = \boldsymbol{\nu} \cdot \boldsymbol{Z}/\nu \quad [30]$$

The components in an equatorial system of the unit vector $\boldsymbol{Z}$ are

$$Z_x = \frac{x}{r}\frac{\cos\phi}{\cos\phi'}$$

$$Z_y = \frac{y}{r}\frac{\cos\phi}{\cos\phi'}$$

$$Z_z = \sin\phi$$

Initial Conditions

The initial condition will be given (at time t_0 and Greenwich sidereal time θ_{g0}) as position and velocity in an equatorial coordinate system, i.e., as x_0, y_0, z_0 and $\dot{x}_0$, $\dot{y}_0$, $\dot{z}_0$. Because the

[5] The height in geometric meters is $Z = a_e H$.

[6] Strictly speaking, $\boldsymbol{Z}$ is here defined as the local *geodetic* vertical reckoned at the "geocentric sub-vehicle point."

coefficients in F may be modified at different atmospheric levels, the program may have to be initialized several times during the computation. Given position and velocity, it is possible to obtain

$$\boldsymbol{Q}_0 = \boldsymbol{r}_0/\dot{s}_0 \qquad \text{(i.e., } Q_{x_0} = \dot{x}_0/\dot{s}_0,\ x \rightarrow y,\ z) \qquad [31]$$

$$\boldsymbol{W}_0 = \boldsymbol{r}_0 \times \boldsymbol{r}_0/r_0{}^2\dot{v}_0 \qquad (r_0\dot{v}_0 = \sqrt{\dot{s}_0{}^2 - \dot{r}_0{}^2}) \qquad [32]$$

$$\boldsymbol{P}_0 = \boldsymbol{Q}_0 \times \boldsymbol{W}_0 \qquad [33]$$

$$y_{\omega_0} = \boldsymbol{Q}_0 \cdot \boldsymbol{r}_0 \qquad \text{(note that } y_{\omega_0} \text{ will be negative for entry)} \qquad [34]$$

$$\dot{y}_{\omega_0} = \dot{s}_0 = (\dot{x}_0{}^2 + \dot{y}_0{}^2 + \dot{z}_0{}^2)^{1/2} \qquad [35]$$

$$x_{\omega_0} = \boldsymbol{P}_0 \cdot \boldsymbol{r}_0 \qquad [36]$$

and by definition

$$\dot{x}_{\omega_0} = 0$$

As checks, one might compute how closely the relation

$$x_0{}^2 + y_0{}^2 + z_0{}^2 = x_{\omega_0}{}^2 + y_{\omega_0}{}^2$$

holds.

Equations [1 and 2] are then employed to compute the initial x, y and z components of $\boldsymbol{a}_0$ and $\boldsymbol{b}_0$ and the integration may begin. From the integrations indicated in Equations [3, 4 and 5], $\boldsymbol{P}$, $\boldsymbol{Q}$, x_ω, y_ω and $\dot{y}_\omega$ can be computed, and x, y, z and $\dot{x}$, $\dot{y}$, $\dot{z}$ can be obtained from

$$\begin{aligned} x &= x_\omega P_x + y_\omega Q_x \\ \dot{x} &= \dot{y}_\omega Q_x \qquad (x \rightarrow y,\ z) \end{aligned} \qquad \ldots\ldots\ldots\ldots\ldots\ldots\ldots\ldots\ldots\ldots [37]$$

thus another integration cycle can be computed.

Although this gravity-free orbit procedure has been found to be particularly advantageous and superior to Cowell's method [see (2, 5 and 17)] in the integration of high speed meteorite, grazing braking-ellipse and high mass/area quotient entry orbits, it has not been found to be particularly efficient for the computation of entry from satellite orbits of low mass/area or high lift vehicles. Even in these cases, however, its superiority to Cowell's method is manifest.

Appendix A: Derivation of Perturbation Equations

From the basic equation of motion discussed in (2)

$$\frac{d\dot{y}_\omega}{d\tau} = -\mu_0 D_0{}^2 \left(A + \frac{B}{\dot{y}_\omega}\right) \sigma\gamma(\sigma)\dot{y}_\omega{}^2 + \dot{y}_\omega{}^\backslash \triangleq$$

$$-\left(A + \frac{B}{\dot{y}_\omega}\right) f(r)\dot{y}_\omega{}^2 + \dot{y}_\omega{}^\backslash \qquad [A\text{-}1]$$

therefore

$$\frac{dy_\omega}{d\tau}\frac{d\dot{y}_\omega}{dy_\omega}\frac{1}{(A + B/\dot{y}_\omega)\dot{y}_\omega{}^2} = -f(r) + \frac{\dot{y}_\omega{}^\backslash}{(A + B/\dot{y}_\omega)\dot{y}_\omega{}^2} \qquad [A\text{-}2]$$

But

$$dy_\omega/d\tau = \dot{y}_\omega + y_\omega{}^\backslash$$

so that

$$\int_{\dot{y}_{\omega_0}}^{\dot{y}_\omega} \frac{d\dot{y}_\omega}{(A\dot{y}_\omega + B)} = -\int_{y_{\omega_0}}^{y_\omega} f(r_0)dy_\omega - \int_{y_{\omega_0}}^{y_\omega} [f(r) - f(r)_0]dy_\omega + \int_{y_{\omega_0}}^{y_\omega} \frac{\dot{y}_\omega{}^\backslash dy_\omega}{(A + B/\dot{y}_\omega)\dot{y}_\omega{}^2} - \int_{\dot{y}_{\omega_0}}^{\dot{y}_\omega} \frac{y_\omega{}^\backslash d\dot{y}_\omega}{(A + B/\dot{y}_\omega)\dot{y}_\omega{}^2} \qquad [A\text{-}3]$$

where $r_0{}^2 \triangleq x_{\omega_0}{}^2 + y_\omega{}^2$. Of course

$$\frac{d\dot{y}_\omega}{dy_\omega} = \frac{d\dot{y}_\omega}{d\tau}\frac{d\tau}{dy_\omega}$$

and, consequently

$$d\dot{y}_\omega = \left(\frac{d\dot{y}_\omega}{d\tau}\right)\frac{dy_\omega}{(\dot{y}_\omega + y_\omega{}^\backslash)}$$

Hence, the last three integrals of Equation [A-3] combine to form the integral of the perturbative component (Eq. [5a])

$$\int_{y_{\omega_0}}^{y_\omega} \left\{\left[\dot{y}_\omega{}^\backslash - \frac{y_\omega{}^\backslash}{(\dot{y}_\omega + y_\omega{}^\backslash)}\left(\frac{d\dot{y}_\omega}{d\tau}\right)\right] \times \frac{dy_\omega}{(A\dot{y}_\omega{}^2 + B\dot{y}_\omega)} - [f(r) - f(r_0)]\right\} dy_\omega \triangleq \int_{y_{\omega_0}}^{y_\omega} P_1{}'dy_\omega \equiv P_1$$

the integrand of which reduces to

$$P_1{}' = \frac{[\dot{y}_\omega{}^\backslash/(A\dot{y}_\omega + B) + y_\omega{}^\backslash f(r)]}{(\dot{y}_\omega + y_\omega{}^\backslash)} - [f(r) - f(r_0)] \qquad [A\text{-}4]$$

where $\dot{y}^\backslash \equiv \dot{s}^\backslash$ and $\dot{y}_\omega \equiv \dot{s}$. Thus

$$\int_{\dot{y}_{\omega_0}}^{\dot{y}_\omega} \frac{d\dot{y}_\omega}{(A\dot{y}_\omega + B)} = -\int_{y_{\omega_0}}^{y_\omega} f(r_0)dy_\omega + \int_{y_{\omega_0}}^{y_\omega} P_1{}'dy_\omega \qquad [A\text{-}5]$$

may be integrated so that Equation [12] is determined, i.e.

$$\dot{s} \equiv \dot{y}_\omega = \left(\dot{y}_{\omega_0} + \frac{B}{A}\right) \times$$

$$\exp\left[-AF(x_{\omega_0}, y_{\omega_0}, y_\omega) + AP_1\right] - \frac{B}{A} \qquad [A\text{-}6]$$

As an example, if

$$f(r_0) = \mu_0 D_0{}^2 \sum_{i=-n}^{i=n} C_i r_0{}^i$$

then

$$F(x_{\omega_0}, y_{\omega_0}, y_\omega) = \mu_0 D_0{}^2 \sum_{i=-n}^{i=n} Y_i$$

where

$$Y_{-2} = \frac{C_{-2}}{x_{\omega_0}}\left[\tan^{-1}\left(\frac{y_\omega}{x_{\omega_0}}\right) - \tan^{-1}\left(\frac{y_{\omega_0}}{x_{\omega_0}}\right)\right]$$

$$Y_{-1} = C_{-1}\left[\log_e\left(\frac{y_\omega + \sqrt{x_{\omega_0}{}^2 + y_\omega{}^2}}{y_{\omega_0} + \sqrt{x_{\omega_0}{}^2 + y_{\omega_0}{}^2}}\right)\right]$$

$$Y_0 = C_0(y_\omega - y_{\omega_0})$$

$$Y_1 = \left(\frac{C_1}{2}\right)\left[y_\omega\sqrt{y_\omega{}^2 + x_{\omega_0}{}^2} - y_{\omega_0}\sqrt{y_{\omega_0}{}^2 + x_{\omega_0}{}^2} + x_{\omega_0}{}^2 \log_e\left(\frac{y_\omega + \sqrt{x_{\omega_0}{}^2 + y_\omega{}^2}}{y_{\omega_0} + \sqrt{x_{\omega_0}{}^2 + y_{\omega_0}{}^2}}\right)\right]$$

$$Y_2 = C_2[x_{\omega_0}{}^2(y_\omega - y_{\omega_0}) + (\tfrac{1}{3})(y_\omega{}^3 - y_{\omega_0}{}^3)] \qquad \ldots\ldots\ldots\ldots\ldots\ldots\ldots\ldots\ldots\ldots [A\text{-}7]$$

Experience has shown that the employment of Y_0 and Y_{-2} (or Y_2) is adequate [i.e., $C_0 + C_{-2}/r^2$ or $C_0 + C_2r^2$ provides an adequate fit of $\sigma\gamma(\sigma)$]. See the Nomenclature for comments concerning C_i. Alternately, one might choose the bilinear function

$$f(r_0) = \mu D^2(1 - br_0{}^2)/(fr_0{}^2 - c)$$

so that

$$F = \frac{(1 - bc/f)}{2G} \log_e \left[\frac{(G^2/f - y_\omega G)}{(G^2/f - y_\omega G)}\right] - \frac{by_\omega}{f}\Bigg|_{y_{\omega 0}}^{y_\omega}$$

for $f(fx_{\omega_0}^2 - c) < 0$ or

$$F = \frac{(1 + bc/f)}{G} \tan^{-1}\left(\frac{y_\omega f}{G}\right) - \frac{by_\omega}{f}\Bigg|_{y_{\omega 0}}^{y_\omega}$$

for $f(fx_{\omega_0}^2 - c) > 0$, where

$$G^2 \triangleq f(fx_{\omega_0}^2 - c) \qquad G \triangleq +\sqrt{G} \qquad \text{[A-8]}$$

Appendix B: Transitional Satellite Drag

The transitional behavior of the drag coefficient is considered here only for completeness, since a satellite during its entry phase traverses the transitional drag regime rather quickly. Nevertheless, the overall importance of transitional drag during the balance of the lifetime of the satellite is evident, and Equation [24] should be employed in any precise determination of satellite motion.

In the case of satellites and re-entry capsules having relatively "smooth" surfaces, as contrasted with porous and microscopically rough meteoritic surfaces, it may well be that the value of the accommodation coefficient α should not be assumed to be unity as in (3), Equation [A-3]. Apparently, the earlier published experimental results, which seemed to indicate values of the accommodation coefficient near unity (16), should be revised. In particular, Hurlbut (11) and Schamberg (15) have recently suggested a much lower value of the accommodation coefficient based upon a model due to Baule (1914) and a single collision per surface interaction [pp. 51, 52 of (15)]. On the basis of this model, Schamberg adopts an accommodation coefficient of about 0.5 for molecular nitrogen incident on aluminum; however, the facts that the surface of the satellite is not entirely "clean" and that the experimental data on accommodation are quite preliminary, suggest that the accommodation coefficient can only be bounded between 0.3 and unity.

As pointed out by Schaaf (14) the dissociation of oncoming nitrogen molecules (requiring about 9.7 ev per dissociation) would completely soak up the incident kinetic energy of the molecules. Thus, the emitted nitrogen atoms would be completely accommodated to the surface temperature of the satellite ($\alpha = 1$), or perhaps to a temperature below that of the surface.[7] In addition to the dissociation, α also depends upon the angle of incidence. It becomes obvious, therefore, that the overall average accommodation coefficient for a given body must be considered as a summation of various processes, most of which tend to push α toward unity.

In view of the uncertainty in the accommodation coefficient, Equations [5 and 6] of (3)[8] should be extended according to Equations [7 and 8] of (6) (of course, satellite surface temperatures are, by necessity, low enough so that $T_s \times 2.17 \times 10^{-3} \ll m_s\dot{y}^2$). Employing these more general formulas with an accommodation coefficient of 0.5, $j = 3$ and $m_s \cong 28.5$ (m_s is more properly a function of height H), we find that

$$B \cong 3.07 \times 10^5 \sigma d \qquad \text{[B-1]}$$

$$bc \cong 1.64 \times 10^5 (C_{L_0}/C_{DF}) d \qquad \text{[B-2]}$$

where

B = transitional drag parameter
d = diameter (of the vehicle), cm

see (6). These formulas are good to order $(\bar{V}_s/\dot{y})^2$, where $\bar{V}_s$ is the average speed of the emitted molecules.

[7] If the emitted atoms left with an average speed *below* that of a gas issuing forth at the satellite surface temperature, then the emitted atoms would tend to shield the surface, and the onset of transitional flow would occur even more rapidly!

[8] The sign of E_1 in Equation [1] of (3) was incorrect, and the equation should be revised to read: $C_D = 2[1 - D_1B + (E_0 - E_1B)\ \bar{V}_s/\dot{y}]$.

Hence, in MKS units for an arbitrary α

$$a \cong 1 \qquad \text{[B-3]}$$

$$b \cong C_{DF}/C_{D_0} - 1 \qquad \text{[B-4]}$$

$$c \cong \frac{C_{DF}}{C_{D_0} b} \sqrt{\frac{A_0}{1 - \alpha}}\ (4.93 \times 10^6 + 1.132 \times 10^7 \sqrt{1 - \alpha}) \qquad \text{[B-5]}$$

The free molecule flow value of the drag coefficient C_{DF} is obtained by taking the limit of C_D as $B \to 0$, e.g., for a blunt body

$$C_{DF} = 2(1 + E_0\bar{V}_s/\dot{y}) \cong 2(1 + 0.354\sqrt{1 - \alpha}) \qquad \text{[B-6]}$$

See Equation [5] of (6).

Acknowledgments

The author gratefully acknowledges the assistance of Jeannine L. Arsenault, C. G. Hilton and James Enright who have checked through the paper with care, and Larry Sashkin who added many useful suggestions and was instrumental in coding the IBM 650 program.

Nomenclature

For the most part the following notation is standard in celestial mechanics and can be found in (1, 8, 13 and 17).

A = constant fitted to the Mach number variation of the drag coefficient with a mean sonic speed $\cong 1$; also the azimuth of the direction from which the wind is coming
A_0 = initial projected frontal area of the vehicle, m²
a = coefficient in Equation [24] $\cong 1$
a_e = Earth's equatorial radius, 6,378,145 m. [Obtained from (9), p. 313, Eq. F3, with the inclusion of the more recently determined value of f']
$\boldsymbol{a}$ $\triangleq x_\omega \boldsymbol{P}$
B = constant fitted to Mach number variation of the drag coefficient with a mean sonic speed $\cong c_s(C_{DT}/C_{D_0} - 1) = 0.0392\ [C_{DT}/C_{D_0} - 1]$ for $c_s = 310$ m per sec; also the transitional parameter in Appendix B
b = coefficient in Equation [20] $\cong C_{DF}/C_{D_0} - 1$. (See Appendix B)
b = angle measured up from the orbit plane in the $\boldsymbol{W}$ direction
$\boldsymbol{b}$ $\triangleq \boldsymbol{Q}$
C_i = constants obtained by a fit of $\sigma\gamma(\sigma)$ to $\sum_{i=-n}^{i=n} C_i r^i$ over different atmospheric levels about one scale height in width. Above a maximum altitude C_i is set equal to zero. [C_i is fitted to $\sigma(H)$, where $H = r - r_c$, and r_c is the geocentric distance of Earth's surface near the point of entry. Note that r_c, and hence the fit, is dependent upon the latitude of the entry area]
C_{D_0} = reference (hypersonic continuum) value of the drag coefficient (0.92 for a sphere or 1.5 for a typical entry capsule)
C_{DF} = free molecule flow value of the drag coefficient, i.e., value at $B = 0$. (See Appendix B)
C_{DT} = maximum value of the transonic drag coefficient $\cong 1.06$ at $M = 1.2$ for a sphere, and $\cong 1.54$ at $M = 2.5$ for a typical entry capsule
C_L = lift coefficient
c = coefficient in Equation [24]. (See Appendix B)
c_s = local sonic speed (in terms of surface circular satellite speed)
D_0^2 $\triangleq C_{D_0} A_0 \rho_0 V_{c_0}^2/2g_0 m_0$
d = diameter, cm
F = $\int_{y_{\omega 0}}^{y_\omega} f(r_0)dy_\omega$
$f(r)$ = $\mu_0 D_0^2 \sigma\gamma(\sigma)$ expressed analytically
f = Earth's flattening, 1/298.3. (Personal communications from J. A. O'Keefe, A. Eckels and L. G. Jacchia, 1958)
G = function derived in Appendix A

g_0 = acceleration of gravity at unit distance, 9.780,320 m per sec^2

H = altitude above an oblate Earth, Earth radii a_e. (See Eq. [26])

$H_\oplus$ = coefficient of the third harmonic of Earth's gravitational potential = 6.04×10^{-6}. (See Eq. [22])

$J_\oplus$ = coefficient of the second harmonic of Earth's gravitational potential = 1623.41×10^{-6}. (See Eq. [22])

j = number of nontranslational degrees of freedom excited in the collision process (taken as 3)

$K_\oplus$ = coefficient of the fourth harmonic of Earth's gravitational potential = 6.37×10^{-6}. (See Eq. [22])

M = Mach number, v/c_s

m = mass of the space vehicle, kg

m_e = atomic weight of the emitted atmospheric molecules, $\cong 28.5$

n = largest power of the polynomial employed to fit C_t (usually 2)

P_1 = quantity defined by Equations [5, 5a and 10]

$\boldsymbol{P}$ = unit vector directed from the geocenter to perigee (x_ω axis)

$\boldsymbol{Q}$ = unit vector lying in the orbit plane perpendicular to $\boldsymbol{P}$ (y_ω axis)

q = speed of the cross wind measured in a framework rotating with Earth's angular rate (in terms of surface circular satellite speed V_{c0})

r = radius vector from the geocenter to the vehicle, Earth radii a_e

r_0 = $+\sqrt{x_{\omega 0}^2 + y_{\omega^2}}$

$\dot{r}_{g\diagdown}$ = perturbative acceleration occasioned by Earth's gravitational field including equatorial bulge effects. (See Eq. [28])

$\dot{r}_{D\diagdown}$ = perturbative acceleration occasioned by lift and residual drag acceleration. (See Eq. [29])

$\dot{s}$ = speed of the space vehicle with respect to an inertial frame. By definition all speed is directed along the $y_\omega(\boldsymbol{Q})$ axis and hence $\dot{s} \equiv \dot{y}_\omega$ (units of surface circular satellite speed)

t = time = $\tau(13.447{,}052)$ min

$\boldsymbol{U}$ = unit vector along the radius vector to the vehicle, i.e., $\boldsymbol{U} = \boldsymbol{r}/r$

$\boldsymbol{V}$ = unit vector in the orbit plane perpendicular to $\boldsymbol{U}$, i.e., $\boldsymbol{V} = \boldsymbol{W} \times \boldsymbol{U}$

$\bar{V}_e$ = average speed of the molecules emitted from the surface of the satellite

V_{c0} = surface circular satellite speed, 7905.258 m per sec

v = true anomaly

$\boldsymbol{W}$ = unit vector perpendicular to both $\boldsymbol{P}$ and $\boldsymbol{Q}$

x, y, z = equatorial coordinates oriented according to some specified equinox and Equator, in units of equatorial radii a_e

Y_i = functions derived in Appendix A

Z = altitude in geometric meters = Ha_e

$\boldsymbol{Z}$ = unit vector in the direction of the zenith. (Note $\boldsymbol{Z} \neq |\boldsymbol{Z}|$)

α = right ascension of the space vehicle, radians, = $\tan^{-1}(y/x)$; also the accommodation coefficient in Appendix B

$\gamma(v)$ = $C_D(v/c_s)/C_{D0}$, the drag coefficient variation with Mach number

$\gamma(\sigma)$ = $C_D(\sigma)/C_{D0}$, the drag coefficient variation in the transitional regime

ζ = entry angle. (See Eq. [30])

θ_{g0} = initial Greenwich sidereal time in hours and decimals of an hour

$\dot{\theta}$ = constant reflecting the rotational speed of the Earth, 0.058,834,470

λ_E = longitude of the sub-vehicle point measured positive eastward from the Greenwich meridian in degrees and decimals

μ $\triangleq m_0/m$

$\boldsymbol{v}$ = velocity of the space vehicle with respect to a rotating atmosphere (units of surface circular satellite speed). (See Eq. [25])

ξ = bank angle

ρ = atmospheric density, kg/m^3

ρ_0 = "sea-level" atmospheric density, 1.225 kg/m^3

σ $\triangleq \rho/\rho_0$

τ = time variable given in units corresponding to those of Earth radii and surface circular satellite speed, i.e., in units of 13.447,052 min

ϕ = geodetic latitude in degrees and decimals

ϕ' = geocentric latitude, radians

ω = argument of perigee

Superscripts

$(\cdot)$ = ordinary time derivative. Gives speeds in terms of surface circular satellite speed V_{c0}

$(\diagdown)$ = perturbative time derivative

$(')$ = perturbative derivative with y_ω as the independent variable; also the geocentric latitude

Subscripts

D = drag

E = measurement eastward

L = lift

0 = initial condition or value

x, y, z = the x, y or z components (in an equatorial coordinate system) of vector quantities such as the cross-product vectors in Equations [23]

ω = relates a coordinate to the orbit plane

i, j, k = running indexes

$\oplus$ = Earth

References

1 Adams, C. E., "Calculation of a Comet's Coordinates," *J. Brit. Astron. Assoc.*, vol. 32, 1922, pp. 231–234; Comrie, L. J., "Note on Dr. Adams' Paper and the Computation of Ephemerides," *J. Brit. Astron. Assoc.*, vol. 32, 1922, pp. 234–241.

2 Baker, R. M. L., Jr., "Application of Astronomical Perturbation Techniques to the Return of Space Vehicles," ARS JOURNAL, vol. 29, no. 3, March 1959, pp. 207–211.

3 Baker, R. M. L., Jr., "Transitional Aerodynamic Drag of Meteorites," *Astrophys. J.*, vol. 129, no. 3, 1959.

4 Baker, R. M. L., Jr., "Sputtering as It Is Related to Hyperbolic Meteorites," *J. Appl. Phys.*, vol. 30, no. 4, 1959, pp. 550–555.

5 Baker, R. M. L., Jr., Westrom, G. B., Hilton, C. G., Arsenault, J. L., Gersten, R. H. and Browne, E. J., "Efficient Precision Orbit Computation Techniques," ARS JOURNAL, vol. 30, no. 8, Aug. 1960, pp. 740–747.

6 Baker, R. M. L., Jr., "The Effect of Accommodation on the Transitional Drag of Meteorites," *Astrophys. J.*, vol. 130, no. 3, 1959.

7 Charwat, A. F., "Lift and Pitching Moment in Near-Free-Molecule Flow," Rand Rep. R-339, Rand Corp., Santa Monica, June 1959

8 Herrick, S., "A Modification of the 'Variation-of-Constants' Method for Special Perturbations," *Pub. Astron. Soc. Pacific*, vol. 60, no. 356, 1948, pp. 321–323.

9 Herrick, S., Baker, R. M. L., Jr. and Hilton, C. G., "Gravitational and Related Constants for Accurate Space Navigation," Univ. of Calif., Los Angeles. Astronomical Papers, vol. 1, no. 24, pp. 297–338.

10 Herrick, S., "Astrodynamics," Van Nostrand Co., Inc., 1961.

11 Hurlbut, F. C., "Note on Surface Interaction and Satellite Drag," Rand Rep. R-339, Rand Corp., Santa Monica, June 1959.

12 Moulton, F. R., "An Introduction to Celestial Mechanics," Macmillan Co., Inc., N. Y., 1914.

13 "Planetary Coordinates for the Years 1800–1940," Her Majesty's Nautical Almanac Office, London, 1933.

14 Schaaf, S. A., "Aerodynamics of Satellites," Rand Rep. R-399, Rand Corp., Santa Monica, June 1959.

15 Schamberg, R., "A New Analytic Representation of Surface Interaction for Hyperthermal Free Molecule Flow with Application to Neutral-Particle Drag Estimates of Satellites," Rand Rep .RM-2313, Rand Corp., Santa Monica, Jan. 1959.

16 Wiedemann M. and Trumpler, P., "Thermal Accommodation Coefficient," Trans. ASME, vol. 68, 1946, pp. 57–64.

17 Baker, R. M. L., Jr. and Makemson, M. W., "An Introduction to Astrodynamics," Academic Press, N. Y., 1960.

Flame Stabilization on a Porous Plate

ALAN Q. ESCHENROEDER[1]

Cornell University
Ithaca, N. Y.

The position and stability of the flame in a boundary layer with uniform mixture injection from a porous flat plate parallel to a uniform air stream were determined experimentally. Propane-air flames were observed over a free stream velocity range of 10 to 42 fps and a range of mass equivalence ratios for the injected mixture from 1.09 to 4.76. Both the average and time variant distances from the leading edge to the beginning of the flame were measured at various free stream air mass fluxes, injection mass fluxes and injected mixture compositions. A correlation of nondimensional flameholding distance with mixture composition was obtained.

THE WIDE gap between normal burning velocities and average flow velocities in certain high intensity combustion chambers requires the use of flameholding devices. The functioning of these devices usually depends on the creation of a recirculation zone which provides compatibility between chemical reaction times and fluid residence time.

In an effort to reduce the dissipative losses which arise from recirculation, it has been proposed that the boundary layer on a heated plate could serve as a flameholding region. Investigations varying from incidental observations to comprehensive studies of this type of phenomenon are found in the literature (1–9).[2] In their third chapter, Ziemer and Cambel (7) give a review of the main contributions.

The hot plate method of flame stabilization is based on an enhancement of chemical reactivity and a thickening of the boundary layer due to heat transfer away from the surface. In the present work, a somewhat different approach is taken. Mass transfer rather than heat transfer is utilized for thickening the boundary layer. Moreover, fuel is mixed only with the injected air and not with the main stream. Related applied problems in addition to flameholding in internal flows are suggested by this configuration, e.g., flames associated with mass transfer cooling, erosive burning of solid propellants and external burning for lift augmentation.

Boundary layer theory may be employed to describe the flow without chemical reaction upstream from the flameholding region or with a fully developed diffusion flame downstream from the flameholding region (10). The mechanism of the ignition point itself, however, is such that the boundary layer conditions no longer generally apply (8) due to large values of the molecular transport of species and energy in the streamwise direction. Unlike the case of combustion on a heated surface, the ignition and flame stability on the porous plate are governed largely by the streamwise transport components. Significant nondimensional parameters can be found from theoretical developments, but a detailed study of the phenomena is best performed through experiment.

Analyses (10–12) have demonstrated that an appropriate choice of nondimensional quantities may be as follows: Square root of distance $\sqrt{\xi} \equiv (\rho_0 v_0/\rho_1 U_1)(\rho_1 U_1 x/\mu_1)^{1/2}$; fuel concentration $m_f \equiv$ mass concentration of fuel species in the injected mixture. $\rho_0 v_0$ is the injection mass flux at the porous surface; $\rho_1 U_1$ is the free stream mass flux; x is the flameholding distance, and μ_1 is the free stream viscosity. The distance parameter, which contains flow variables, is taken as the dependent variable, and the fuel concentration, which reflects the chemical nature of the system, is considered as the independent variable. The latter can be normalized to yield the *mass* equivalence ratio Φ_m, the ratio of $m_{f\,(\text{injected})}$ to $m_{f\,(\text{stoichiometric})}$.

Design of the Experiment

A low speed tunnel with a 3 × 6-in. test section was used for the experiments. The general layout of the tunnel is shown schematically in Fig. 1. Tubular straighteners and screens (20, 40, 60, 80 and 100 mesh) in the 18 × 21-in. calming section created uniform flow conditions in the test section. The tunnel was placed in parallel with a bypass line so that throttling would not cause surging in the blower. The air stream velocity through the test section was determined by measuring the pressure drop over the nozzle between the calming section and the test section. The range of free stream velocity for combustion experiments was 10 to 42 fps.

A short section of duct with porous stainless steel walls was placed between the nozzle throat and the test section. Suction through these walls removed the small amount of retarded fluid which had built up on the nozzle walls. The need for continuous, smooth boundary layer removal precluded the use of a suction slot. Because the actual boundary layer thickness at the leading edge of the test section was never zero, a means of compensating the results to simulate a true leading edge was developed analytically.

The test section itself had Pyrex plates for side walls along the 3-in. dimension, and a porous slab made of bonded alumina particles for a bottom wall along the 6-in. dimension. The porous slab extended 10 in. in the streamwise direction. Mixtures of propane and air were admitted to the porous wall from a chamber below the wall. The porous plate was constant in thickness and permeability, and a constant pressure was maintained at the inlet to the pores, thereby insuring uniform injection. Initial lighting of the flames was done with a spark gap igniter. The propane and injected air flows were measured with rotameters calibrated by a wet gas meter.

Calibrations and performance tests were run after each component was assembled to the apparatus, and many velocity profiles were obtained in order to study the boundary layer

Received Sept. 21, 1959.

[1] Presently Associate Aeronautical Engineer, Aerodynamic Research Department, Cornell Aeronautical Laboratory, Inc., Buffalo, N. Y. Member ARS.

[2] Numbers in parentheses indicate References at end of paper.

flow at various points. Measured values of the velocity gradient at the wall and the boundary layer thickness with blowing agreed with the theoretical predictions (11), although the profile shapes were not in full agreement. The transition Reynolds numbers at the various levels of the blowing ratio $\rho_w v_w / \rho_1 U_1$ were found by the impact tube method described in Appendix C of (13) and compared rather well with those of other investigators.

Flameholding distances were measured visually by sighting along the flame front and determining an average distance with an ordinary scale. In addition, time-resolved photographic measurements of the same quantity were made by the streak photographic technique. In order to do this, a horizontal slit, which limited the flame image to the streamwise direction, was placed in the Schlieren beam passing through the test section side walls. Vertical film motion was imparted by a drum camera while the slit was photographed. A repetitive flash unit, collimated parallel with the masking slit, provided 20-millisec timing marks.

Two-Dimensional Laminar Flames

Laminar burning could be obtained with equivalence ratios ranging from 1.09 to 4.76. However, flames with relatively straight fronts free from longitudinal wrinkles were observed only in the range 1.09 to 1.67. Flame instability fixed the lower limit, and the appearance of irregularities along the flame front approximately established the upper limit. All of the flames were bifurcated, having a rich blue-green branch along the wall and a hazy bluish diffusion-fed branch farther out in the stream. The two branches joined in a smooth two-dimensional nose at the flameholding location. The bifurcated flame phenomenon can be likened to the double-cone bunsen flame with rich hydrocarbon-air mixtures. In that case, the carbon burns to its first oxidation state in the bright inner cone resulting in reactive products consisting mainly of hydrogen and carbon monoxide in amounts approximating a water-gas equilibrium. The outer cone is a diffusion flame in which these species react with the oxygen from the ambient air. Understandably, the outer branch of the bifurcated boundary layer flame was less luminous at the lower end of the fuel concentration range than at the upper. Expansion of the injected gas due to the heating in the inner branch caused spreading of the outer branch into the stream at a slope as large as 1 in 8. The inner branch clung closely to the porous surface except at the richer mixtures, indicating that the mass burning rate of the inner flame was adjusted to the normal flow rate by means of heat transfer to the wall as in the one-dimensional case investigated by Botha and Spalding (14). The flames always held in a region of nearly vanishing shear, theoretically $\sqrt{\xi} \geq 0.827$, and the heat transfer from the inner branch to the free stream was probably small relative to that to the injected mixture because the gas between the branches was at very high temperatures.

The sharp appearance of the flame over its entirety seemed to indicate that laminar boundary layer flow was preserved in downstream regions where turbulent flow had prevailed in earlier calibration runs with no combustion. Stabilization of the flow could conceivably occur from heat transfer and from vorticity arising from the flame system acting in opposition to the vorticity due to viscous effects. In view of the fact that blowing from the surface generally destabilizes the boundary layer, this is indeed an interesting effect.

Fig. 2 is a plot of the square root of the nondimensional flameholding distance vs. the mass equivalence ratio for each of the two-dimensional flames. On the average, reproducibility was 6.3 per cent for identical flow settings, an error analysis (13) predicting a maximum error in $\sqrt{\xi}$ of $\pm 7\frac{1}{2}$ per cent for visual and ± 5 per cent for photographic observations. The points display a nearly linear dependence of the distance parameter upon the injected mixture strength. The photographic runs are grouped especially well about such a line.

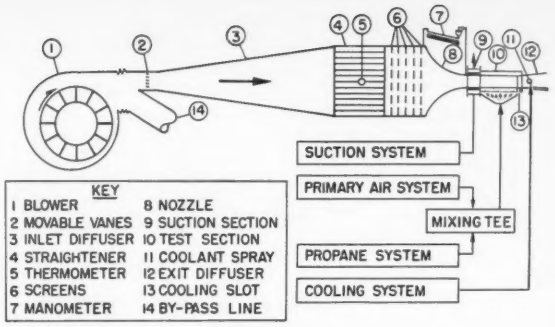

Fig. 1 General arrangement of apparatus

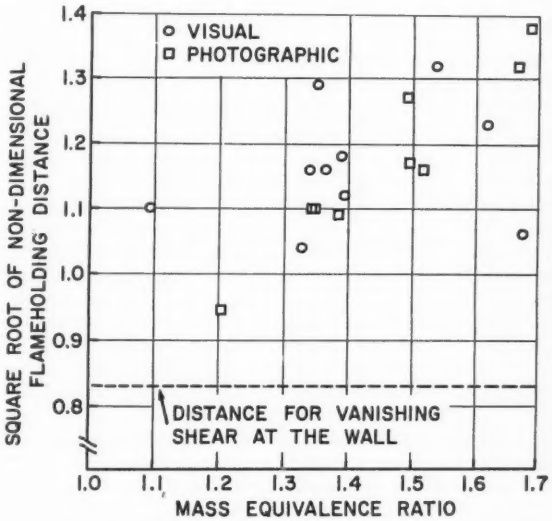

Fig. 2 Square roots of experimental flameholding distances for two-dimensional laminar flames

An extension of the mean of the data to the stoichiometric concentration ($\Phi_m = 1$) would approximately intersect the theoretical boundary layer blowoff value of the distance parameter. Such a limiting condition is described in (10) as surface combustion because the flame receives sufficient oxygen from the injected mixture and, therefore, does not seek a position where it will receive some of its oxygen from the free stream. With richer mixtures, the flame moves away from the wall and stabilizes farther downstream than with the stoichiometric mixture. A crude explanation is that the critical boundary velocity gradient is lower for rich mixtures causing the flame to hold at a greater distance from the leading edge. Attempts to employ boundary layer theory for formulating flame stability criteria are met with severe difficulty for two reasons:

1 The second derivatives in downstream distance, which are neglected in the boundary layer simplifications, play a major role in the ignition region at the beginning of the flame.

2 Even without combustion, the boundary layer theory is of questionable applicability (11,15) in the blowoff region where the shear approaches zero. Since the flame holds near the blowoff distance, both inaccuracies arise simultaneously. A method of overcoming the first inaccuracy has been proposed (13) using the equations developed by Emmons (16), but the second difficulty enumerated previously prevents the development of a meaningful stability theory.

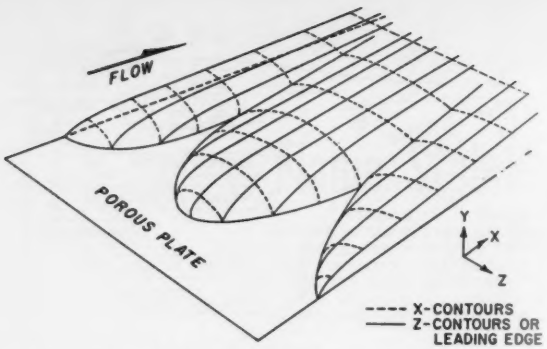

Fig. 3 A form of nonisotropic flame observed experimentally

The 10 streak photographic records revealed interesting oscillatory behavior of the flame. The records taken with horizontal Schlieren knife edge gave somewhat sharper resolution of the flame than those taken with vertical knife edge, but oscillations occurred in either case. Repetitive spark photographs of an early pilot run were taken with mixture flow through the plate immediately after a flame was intentionally extinguished. All visible features of the flow appeared steady, so that the oscillation probably arises from the strong coupling between the flow and the flame. This check was needed because the destabilizing effect of blowing without combustion could be reasonably suspected to be the sole cause of the oscillation. Frequencies of 15 to 25 cps occurred in the regime of two-dimensional flames. A certain amount of regularity in frequency and wave form was exhibited within each record over many cycles, but only approximate trends were apparent from run to run. In the range $1.33 < \Phi_m < 1.50$, the amplitudes were at a maximum and the frequencies at a minimum. Since the flame flashed back all the way to the leading edge in some of the records, the distance parameter in Fig. 2 was calculated consistently for the extremal downstream flame location for the photographic runs.

Gross (3) has reported that flame oscillations in the boundary layer on an impermeable streamlined plate in a uniform stream of combustible mixture occur at a frequency of 20 to 30 cps in the range $1.09 < \Phi_m < 1.50$. Similarly, Ziemer and Cambel (7) experimented with flame stabilization on a heated plate in a combustible stream and reported random oscillations of 14 to 30 cycles within a single run at $\Phi_m = 0.92$. Both investigations employed propane-air mixtures. The similarity of these findings with the results of the present work suggests that there may be some subtle connection between the flame-holding mechanisms in the widely different cases of the impermeable plate in a mixture stream and the porous plate feeding mixture into an air stream.

Among the various runs, the downstream speed of flame motion observed on the streak records ranged from about one to three times the upstream speed. Gross observed in his experiment that the movement toward the leading edge took place at about four times the speed of movement toward the trailing edge, but Ziemer and Cambel observed no regular relationship between upstream and downstream flame motion.

Nonisotropic Flames

The majority of the flames observed had a series of cusps along their nose portions, these cusps persisting as longitudinal wrinkles in the outer branch of the flame. A perspective sketch of a double-cusp configuration is shown in Fig. 3. These flames occurred mainly in the mixture range of $1.68 < \Phi_m < 4.76$. The bright inner branch burned along the wall at the leaner end of this mixture range, but burned at a slight distance from the wall at the rich end. The luminosity of the inner branch decreased, and that of the outer branch increased with increasing fuel concentration. No wrinkles appeared in the inner flame. Again, the downstream portions of the combustion region appeared to be in a laminar flow except in the extreme cases of turbulent contamination described in the following.

Such behavior is a form of nonisotropic flame propagation which manifests itself in cellular flames when there is burning into a uniform mixture. The literature contains analyses and experiments explaining and describing the latter phenomenon (17). The fuel concentration at which the waviness becomes noticeable is somewhat higher than that observed in cellular flame experiments (14) because of the dilution action of the free stream air. With different mixtures, different sizes and numbers of cusps appeared, but the shape of each cusp was always basically the same as that illustrated in Fig. 3. In the vicinity of $\Phi_m = 1.7$, there were several shallow cusps. As the mixture was enriched the cusps became less numerous, but deeper in the downstream direction. Occasionally, there were large cusps with a fine structure of very small cusps superimposed on them. The configuration depicted in Fig. 3 was the steadiest of all and was obtained in the range $2.0 < \Phi_m < 2.7$. Above this range, the central salient began receding downstream with richer mixtures until it vanished leaving one deep central cusp. In some runs, the one- and two-cusp configurations alternated at a low frequency without any change in flow settings. Transition to turbulent boundary layer flow took place slightly upstream from the root of the single cusp when it became deep enough. The resulting disturbances propagated and grew along the sides of the cusp in the upstream direction causing unsteadiness in the flame. When the mixture was enriched above about $\Phi_m = 3.35$, a large downstream portion of the flame broke into extensive oscillations until the two sides of the flame no longer held. At the upper limit of fuel concentration, the burning oscillated so violently that it blew off the plate.

Generally, nonisotropic flames interact strongly with the approaching stream. In a plane paralleling the plate and including the flame, the flow is accelerated in advance of the cusps and decelerated in advance of the salients. This aerodynamic effect and other preferential diffusion effects in regions of sharp flame curvature have been discussed fully in the literature, e.g., (17).

The nonisotropic results cannot be properly shown on Fig. 2 because the distance parameter is based on two-dimensional flow theory and the nonisotropic flames are inherently three-dimensional at their fronts. Nevertheless, measurements were taken, and the distance parameter was calculated for the shortest distance from the leading edge to each flame front. The values thus obtained scatter from $\sqrt{\xi} = 0.74$ to $\sqrt{\xi} = 2.30$. It should be mentioned, however, that only one out of 71 points was upstream from the distance at which shear approaches zero according to two-dimensional theory.

The curved structure of the nose of the flame did not leave a clear impression on streak photographs, but rather two smudgy regions—one coincident with the salients and the other with the cusps. Several records show clearly the turbulent contamination, described previously, as a series of heavy lines, indicating a disturbance of high intensity and scale. The nature of this flame motion is entirely different from that of the oscillatory flames. The turbulent contamination acts randomly at higher frequency and amplitude than the regular oscillations. In the range $1.68 < \Phi_m < 3.35$, there was very little flame movement of any kind.

Turbulent Flames

A study of laminar burning was the central objective of the investigation, but a few incidental observations of turbulent flames are worthy of mention. Since the variation of transi-

tion Reynolds number with blowing ratio $\rho_0 v_0/\rho_1 U_1$ had been determined for the apparatus without combustion, cases in which the boundary layer flow approaching the flame was turbulent over the entire plate width could be recognized. Only flames occurring in this condition are called turbulent flames in the present work. Although the richer nonisotropic flames appeared to be violently unsteady over their entire fronts, the origin of the disturbance was localized in the deepest portion of the cusp. This disturbance spread over the flame front and the approach flow by the mechanism described in the last section. Perhaps this distinction between turbulent flames and disturbed laminar flames seems tenuous, but it was always easily recognized in the experiments. The scale of the irregularities was much greater and the disturbance frequency was lower with the rich nonisotropic flames than with the turbulent flames. Furthermore, little if any nonisotropy was observable in the turbulent flame fronts. They were rather straight in the gross sense, but had a fine scale noise-like disturbance superimposed on them.

There was never a smooth transition from one mode of burning to the other, but rather a sudden jump when tunnel air velocity was increased beyond a certain level. At mixtures richer than $\Phi_m = 3.35$, the unsteady laminar burning persisted up to complete blowout with increasing air velocity. Detailed quantitative data were not secured for the jump phenomenon, but with leaner mixtures, borderline cases were observed in which either laminar or turbulent flames could stabilize at the same flow settings depending upon the manner of approaching the settings.

Three flames which had just jumped to the turbulent state and four flames which had just blown past the trailing edge of the test plate during gradual increases in tunnel air speed were observed. Thus, both extremes of the turbulent range of the apparatus were investigated. The results are plotted in Fig. 4 which also includes a shaded region indicating laminar flame runs. The transition line, which was determined without combustion, divides the diagram into laminar and turbulent boundary layer flow regimes. The criterion of the effective disappearance of laminar shear (11,12) is $(\rho_0 v_0/\rho_1 U_1) \times (\rho_1 U_1 x/\mu_1)^{0.5} = 0.827$, and the corresponding condition governing the turbulent regime according to the measurements reported by Hacker (18) is $(\rho_0 v_0/\rho_1 U_1)(\rho_1 U_1 x/\mu_1)^{0.2} = 0.08$. The relationship of the turbulent points to the latter flow condition resembles that of the laminar points to the former criterion. The two-dimensional laminar flame results lie near the bottom of the shaded area. The points for flames that had just jumped are near the transition line, but are definitely in the turbulent regime. Viewed as a whole, the information presented in Fig. 4 confirms that the flames described in the preceding sections were indeed laminar by the criterion presented here. Several attempts were made to investigate the region where the laminar boundary layer blowoff locus approaches the transition line, but no flames could be stabilized for a blowing ratio of less than 0.00684.

Conclusions

Two types of laminar flames were observed: Two-dimensional and nonisotropic. Only the former can be fairly correlated by the boundary layer distance parameter, but the latter are comparable with the cellular flames observed by other experimenters. All but one of the nonisotropic flames held downstream from the laminar boundary layer blowoff. The turbulent contamination of the cusps was almost certainly reinforced by the inherent flow instability of the boundary layer profile with blowing. It was, therefore, something more complicated than a pure case of the so-called "flame generated turbulence" which depends only on the ability of the flame to distribute, amplify and feed back local velocity fluctuations. The flameholding distance increased with richer mixtures, but flame stabilization was not possible with mixtures leaner than about $\Phi_m = 1.09$. Large amplitude periodic oscillations of the laminar two-dimensional flames occurred near the stoichiometric end of the range $1.09 < \Phi_m < 1.68$. Laminar nonisotropic flames were observed in the range $1.68 < \Phi_m < 4.76$. Extensive contamination of the flame with disturbances set the upper limit of mixtures. The performance of turbulent flames relative to turbulent boundary layer blowoff tends to parallel that in the laminar case. This suggests that the blowing away of the boundary layer limits flameholding ability in the turbulent case much in the same way it does in the laminar case.

Acknowledgment

The author is grateful to Professors D. G. Shepherd and D. E. Ordway at Cornell University for their guidance and encouragement throughout the work. Thanks are also due the Ford Instrument Co. and the Visking Corp. for their generous fellowship support.

Nomenclature

m_f = mass of fuel species in the injected mixture per unit mass of injected mixture
U_1 = free stream velocity
v_0 = normal velocity at plate surface
x = downstream distance along the plate
μ_1 = free stream viscosity
ξ = nondimensional downstream distance
ρ_0 = density at plate surface
ρ_1 = density at free stream conditions
Φ_m = equivalence ratio based on mass fractions

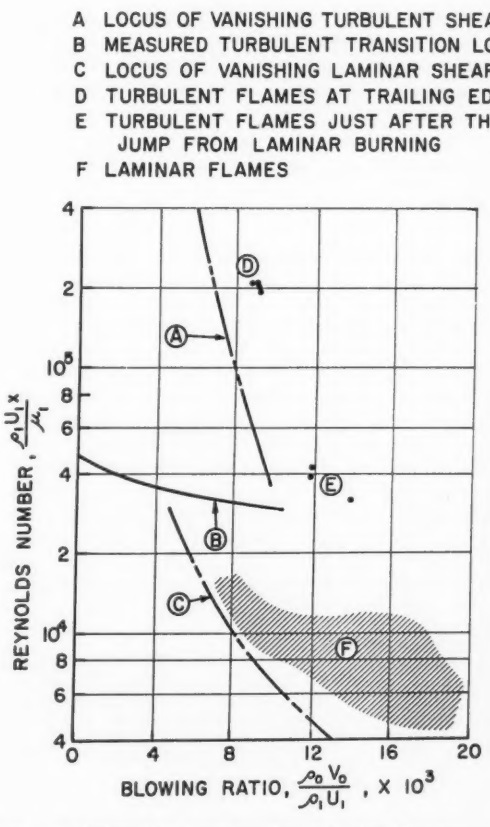

Fig. 4 Relationship of combustion and flow phenomena on a plot of Reynolds number vs. blowing ratio

References

1 Gilbert, M., Haddock, G. and Metzler, A., "A Study of Combustion in a Flowing Gas," NACA TN 1037, April 1946.

2 Tsien, H., "Instruction and Research at the Daniel and Florence Guggenheim Jet Propulsion Center," JOURNAL OF THE AMERICAN ROCKET SOCIETY, no. 81, June 1950, p. 62.

3 Gross, R. A., "Aerodynamics of a Two Dimensional Flame," Harvard University, Combustion Tunnel Laboratory, Interim Technical Rep. no. 2, June 1952.

4 Toong, T. Y., "Ignition and Combustion in a Laminar Boundary Layer Over a Hot Surface," in "Sixth International Symposium on Combustion," Reinhold Publishing Co., N. Y., 1957, pp. 532–540.

5 Wójcicki, S., "Flame Stabilisation in the Boundary Layer," Bull. de l'Academie Polonaise des Sciences, Series 4, no. 4, 1956, pp. 293–294.

6 Hottel, H. C., Toong, T. Y. and Martin, J. J., "Flame Stabilization in a Boundary Layer," Project Squid Technical Rep. no. MIT-13-P, MIT, Cambridge, Oct. 1956.

7 Ziemer, R. W. and Cambel, A. B., "Boundary Layer Combustion," Northwestern University, Gas Dynamics Laboratory Rep., Dec. 1956.

8 Dooley, D. A., "Ignition in the Laminar Boundary Layer of a Heated Plate," in "1957 Heat Transfer and Fluid Mechanics Institute," Stanford University Press, Stanford, pp. 321–342.

9 Toong, T. Y., Davis, J. W., Barkah, K., Sellman, E. W., Snyder, J. E. and Harper, G. F., "Ignition in a Boundary Layer over a Hot Surface," ARS preprint no. 520-57, Dec. 1957.

10 Eschenroeder, A. Q., "Combustion in the Boundary Layer on a Porous Surface," to be published in *J. Aero/Space Sci.*

11 Lew, H. G. and Fanucci, J. B., "An Exact Solution of the Laminar Boundary Layer with Zero Pressure Gradient and Homogeneous Injection," Pennsylvania State University, Technical Rep. no. 6, July 1955.

12 Eschenroeder, A. Q., "The Compressible Laminar Boundary Layer with Constant Injected Mass Flux at the Surface," *J. Aero/Space Sci.*, vol. 26, no. 11, Nov. 1959, pp. 762–763.

13 Eschenroeder, A. Q., "Flame Stabilization in the Boundary Layer on a Porous Flat Plate," Doctoral Thesis, Cornell University, Ithaca, N. Y., 1959.

14 Botha, J. D. and Spalding, D. B., "The Laminar Flame Speed of Propane/Air Mixtures with Heat Extraction from the Flame," Proc. Royal Soc., Series A, vol. 225, 1954, pp. 71–96.

15 Emmons, H. W. and Leigh, D. C., "Tabulation of the Blasius Function with Blowing and Suction," Gt. Britain Aeronautical Research Council Rep. no 15,966, June 1953.

16 Emmons, H. W., "Theoretical Aerothermodynamics," in "1958 Heat Transfer and Fluid Mechanics Institute," Stanford University Press, Stanford, pp. 1–14.

17 Markstein, G. H., "Instability Phenomena in Combustion Waves," in "Fourth Symposium on Combustion," Williams and Wilkins, Baltimore, 1953, pp. 44–59.

18 Hacker, D. S., "Turbulent Boundary Layer with Mass Addition," General Electric Co., Evendale, Ohio, Aircraft Gas Turbine Division, R56AGT215, May 1956.

Technical Notes

Luminosity and Pressure Oscillations Observed With Longitudinal and Transverse Modes of Combustion Instability[1]

M. J. ZUCROW,[2] J. R. OSBORN[3] and A. C. PINCHAK[4]

Purdue University, Lafayette, Ind.

Combustion pressure oscillations were observed in two experimental gaseous bipropellant rocket motors. The geometries of the two motors were different so that one rocket motor tended to exhibit only the longitudinal mode while the other displayed only transverse modes of oscillations. The local pressure and the luminosity of the combustion gases were simultaneously recorded while the rocket motors were operating with combustion pressure oscillations. The results indicate that the reaction mechanism which sustains the longitudinal mode is similar to the aerothermodynamic interaction which supports the transverse modes of combustion pressure oscillation. In addition, the results are in agreement with and support the "shock or pressure wave" mechanism of combustion pressure oscillations as postulated by Zucrow and Osborn.

Received Oct. 5, 1959.

[1] The research reported herein was sponsored by the Office of Naval Research, Power Branch, Department of the Navy, under Contract N7onr-39418. Reproduction in full or in part is permitted for any use of the United States Government.

[2] Atkins Professor of Engineering. Fellow Member ARS.

[3] Associate Professor of Mechanical Engineering. Member ARS.

[4] Research Assistant. Student Member ARS.

Apparatus and Instruments

THE ROCKET motor utilized in the longitudinal mode investigations had a combustion chamber diameter of $3\frac{3}{8}$ in. and a length of $16\frac{1}{4}$ in. A motor having a diameter of 7 in. and a length of only 2 in. was employed in the transverse mode experiments. Both motors burned premixed gaseous propellants which entered the combustion chamber through a "showerhead" type injector. A complete description of the experimental equipment may be found in (2 and 3).[5]

Photocon pressure transducers were employed to detect the pressure oscillations, and a photomultiplier tube (RCA type 931A) observed the luminosity variations. The photomultiplier tube had an "S-4" cathode surface which was primarily sensitive to the blue region of the visible spectrum. In the "longitudinal motor," the pressure and luminosity transducers were located at the same axial position, and in the "transverse motor" on the same imaginary radius.

Longitudinal Mode Results

Fig. 1 illustrates typical luminosity and pressure oscillations observed with the longitudinal mode of combustion pressure oscillations. The two rapid pressure rises on the leading edge of the pressure wave are indicative of the incidence and reflection of the shock front at the injector face. The luminosity, however, increases along a smooth curve, and no indication of pressure wave reflection is found in the light intensity trace. The phase shift between the two waves of Fig. 1 was approximately one quarter of the period of oscillation (290 microsec). With the premixed methane-air and the premixed ethane-air propellant combinations the wave shapes were similar to those of Fig. 1 (premixed ethylene and air), and the $\frac{1}{4}$-cycle phase shift between the two waves was also found.

[5] Numbers in parentheses indicate References at end of paper.

EDITOR'S NOTE: The Technical Notes and Technical Comments sections of ARS JOURNAL are open to short manuscripts describing new developments or offering comments on papers previously published. Such manuscripts are usually published without editorial review within a few months of the date of receipt. Requirements as to style are the same as for regular contributions (see masthead page).

For all three propellant combinations, the maximum amplitudes of the pressure and luminosity oscillations were approximately 75 per cent of the mean chamber pressure and mean light intensity level, respectively.

Transverse Mode Results

Fig. 2 depicts some typical wave forms found with transverse mode oscillations. From frequency measurements, the basic transverse mode was found to be the first circumferential mode. Fig. 2 also indicates that the pressure wave does not reflect from the chamber wall as it moves through the chamber in a circumferential direction. The very high amplitude indicates a strong pressure wave, but the slow initial rise reveals that the pressure wave is not a shock wave. Although the pressure oscillation has sharp well-defined peaks, the luminosity wave is smooth and appears very similar in shape to the luminosity trace of Fig. 1 which depicts that for the longitudinal mode. The frequency of the oscillations is higher in the case of the transverse modes, but the phase shift between the two waves remains approximately $\frac{1}{4}$-cycle of oscillation (approximately 95 microsec).

Much stronger oscillations were found with the transverse modes. In some cases the peak to peak amplitude of the pressure waves was greater than twice the mean chamber pressure. The luminosity amplitudes increased in a corresponding manner.

Fig. 3 shows a strong high frequency transverse mode (approximately 19,000 cps) superimposed upon the basic transverse mode (approximately 2700 cps). In this test run the light intensity variations correlated with the pressure oscillations for both the basic and the superimposed transverse modes. From pressure data alone, the existence of the high frequency transverse mode (19,000 cps) is somewhat doubtful because of the dynamic response characteristics of the pressure transducers. However, the existence of the luminosity oscillations which correlate with the pressure oscillations of the high frequency mode conclusively establishes the existence of that mode. In addition, an estimate of the relative magnitudes of the basic and high frequency transverse modes may be obtained by comparing the sizes of their luminosity waves.

Fig. 4 illustrates the regions in which luminosity oscillations were observed. This chart is only for oscillations of the transverse mode. Similarly shaped stability regions were also found for the longitudinal mode oscillations (3).

Discussion of Results

The slow rise of the main portion of the light intensity trace as depicted in Figs. 1 and 2 is to be expected. When the shock or pressure wave passes through the combustion zone, the temperature immediately rises. However, this rise in temperature cannot instantaneously increase the chemical reaction rates because of the many intermediate reactions inherent in the combustion of hydrocarbons. Consequently, the overall reaction rate only gradually increases. When the reaction rate is at its maximum, the chemiluminescence radiation is greatest. Other experimenters have discussed this.

Gaydon (4) states that in the combustion zone of gases, radiation is emitted which cannot be entirely attributed to thermal radiation alone. He concludes that increases in the reaction rate produce a larger number of excited atomic species per unit time. This in turn produces an increase in the radiation flux which is quite significant in the visible region where the photomultiplier tube is sensitive.

Markstein (5) also reached this conclusion from his experiments also conducted using a 931A photomultiplier tube. He found that the radiation does not immediately increase with the passage of the shock front, but rather rises along a smooth continuous curve similar to the luminosity variation of Figs. 1 and 2.

From these considerations it may be concluded that the luminosity variation can be considered as an indication of the instantaneous chemical reaction rate.

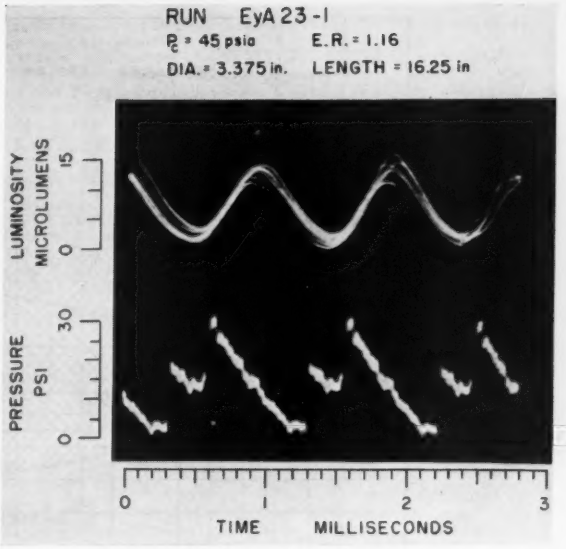

Fig. 1 Oscillogram for ethylene and air

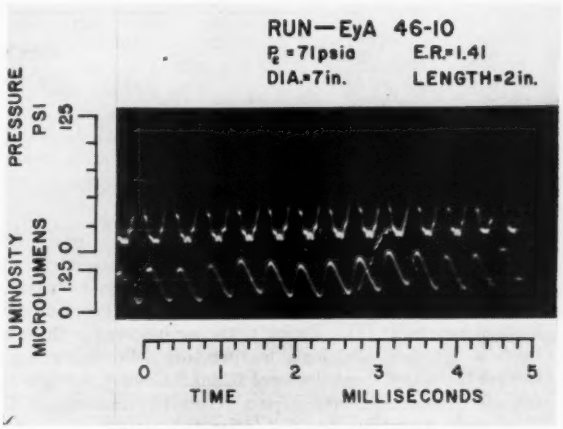

Fig. 2 Oscillogram for ethylene and air

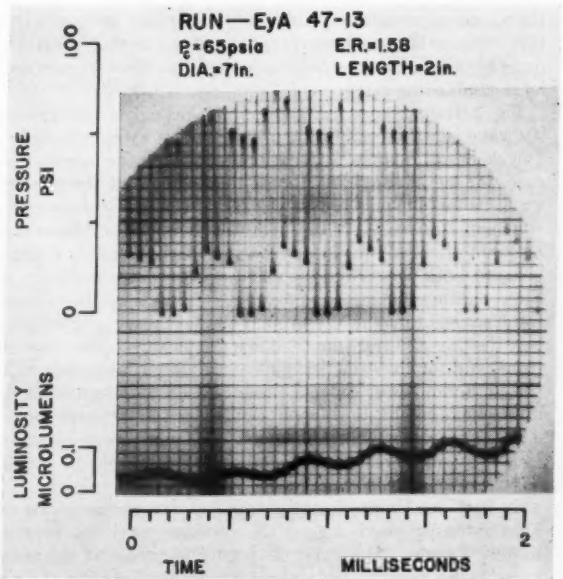

Fig. 3 Oscillogram for ethylene and air

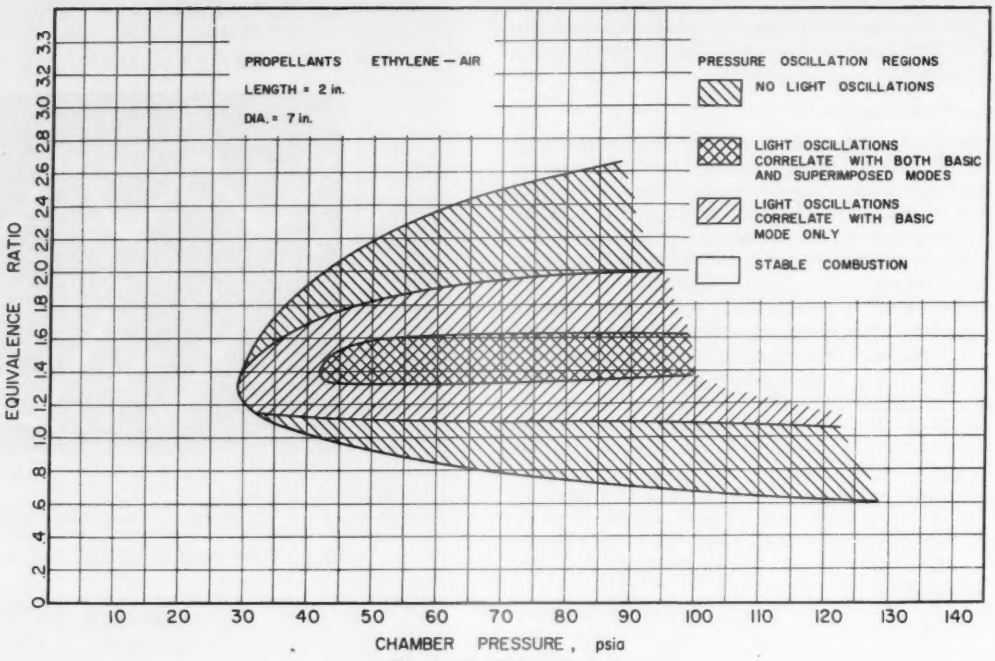

Fig. 4 Stability regions

Phase Shift Between the Two Waves

Fig. 1 (longitudinal mode) illustrates that the light intensity waves lag the pressure waves by approximately one quarter of the period. This lag of the luminosity variation is in accordance with the postulated shock wave theory of combustion instability (1). Owing to the lag inherent in the combustion kinetics, the high temperature field immediately behind the shock front does not instantaneously increase the overall combustion rate. As a result the increase in the luminosity would be expected to lag the passage of the pressure wave. The major conclusion which can be drawn from the aforementioned phase shift is the fact that the passing of the shock wave causes an increase in burning rate, which in turn sustains the shock wave. Thus, it can be stated that the pressure wave is the cause rather than the effect of increased local combustion rates.

Fig. 2 (transverse mode) shows that the peak of the luminosity wave lags the peak of the pressure wave by approximately $\frac{1}{4}$ cycle or approximately 95 microsec. As in the longitudinal case, the lag of the light intensity indicates that the pressure wave causes an increase in the local chemical reaction rate which in turn sustains the pressure wave. The phase shift between the two waves can be interpreted in this manner because both the radiation and pressure detectors were located on the same imaginary radius. That is, as the pressure front sweeps tangentially around the periphery of the chamber, the pressure transducer senses the passage of the pressure front, and for the same imaginary radius but at a later time, the photomultiplier detects the increased radiation from the intensified combustion zone following the pressure front. Thus, it was concluded that the transverse mode was sustained by an aerothermodynamic "feedback system" similar to that of the longitudinal mode.

In both the longitudinal mode and the transverse mode the light intensity wave lagged the pressure wave by approximately $\frac{1}{4}$ cycle. However, the higher frequency of the transverse mode necessitates a shorter time lag between the two waves, or a shorter time for the chemical reaction rate to reach its maximum value. In order that this time be reduced, the unburned propellants must be in a "higher ordered state of preparation" (6). That is, they must be raised to a high temperature and the local concentrations must constitute a proper range of the equivalence ratio (see Fig. 4). If these conditions are satisfied, then the unburned propellants are closer to the condition of self-accelerating combustion. Hence, when the pressure front again passes through the "prepared" unburned propellants, the temperature rise owing to the shock front "triggers" the reaction into an accelerated rate. The accelerated reaction then consumes the local propellants at a rapid rate and exhausts the local stored chemical energy content of the gases.

At this point the transport phenomena demonstrate their importance, because the burned propellants must flow out and the unburned propellants must replace them if the returning pressure front is to be amplified or the oscillations sustained. In addition, the unburned propellants must be rapidly heated by convective heat transfer from the recirculated combustion gases so as to put them in the "higher ordered state of preparation." (It should be noted that the "order of preparation" refers only to that portion of the propellants which are not consumed prior to the return of the pressure front.) Thus, if the transport phenomena are considerably altered, the magnitude and type of the combustion pressure oscillations will also undergo radical changes. Additional data are now being prepared to demonstrate these effects.

Conclusion

The longitudinal and transverse modes of combustion pressure oscillations are essentially a manifestation of an aerothermodynamic interaction in a combustion process. That is, a shock wave or pressure wave passes through the unburned and burning propellants, thereby increasing the pressure and temperature field behind the shock front, and thus causing an acceleration in the local combustion rate. In turn, the extra energy release resulting from the accelerated combustion sustains the shock or pressure wave.

The chemical interaction in tranverse mode oscillations was quite similar to the interaction in the longitudinal mode. However, the transport interaction effects were considerably different merely because of the differences in the geometry.

Acknowledgment

The authors wish to acknowledge R. L. Walters and J. M. Bonnell for their aid in conducting the experimental program.

References

1 Zucrow, M. J. and Osborn, J. R., "An Experimental Study of High Frequency Combustion Pressure Oscillations," JET PROPULSION, vol. 28, no. 10, Oct. 1958, pp. 654–659.

2 Osborn, J. R. and Schiewe, R. M., "An Experimental Investigation of High Frequency Combustion Pressure Oscillations in a Gaseous Bipropellant Rocket Motor," Purdue University Rep. no. I 58–1, June 1958.

3 Osborn, J. R. and Pinchak, A. C., "Investigation of Aerothermodynamic Interaction Phenomena in Combustion Pressure Oscillations," Purdue University Rep. no. I 59–2, June 1959.

4 Gaydon, A. G. and Wolfhard, H. G., "Flames, Their Structure, Radiation and Temperature," Chapman and Hall, Ltd., London, 1953, chap. IX, pp. 193–215.

5 Markstein, G. H., "A Shock-Tube Study of Flame Front-Pressure Wave Interaction," in "Sixth Symposium (International) on Combustion," Reinhold Publishing Corp., N. Y., 1957, pp. 387–398.

6 Ellis, H. B. and Pickford, R. S., "High-Frequency Combustion Instability," Aerojet-General TN-17, Aerojet-General Corp., Azusa, Calif., Sept. 1956. *(Confidential)*

Experimental Studies With Small-Scale Ion Motors[1]

C. R. DULGEROFF[2]

Rocketdyne Div., North American Aviation, Inc., Canoga Park, Calif.

R. C. SPEISER[3] and A. T. FORRESTER[4]

Electro-Optical Systems, Inc., Pasadena, Calif.

In an experimental program we have operated cesium surface ionization ion sources in ion motor configurations. Ion beam power and thrust levels per unit ionizer area up to 177 w per cm² and 5.6 × 10^{-4} lb per cm² have been achieved. In mass utilization studies it was found that 70 per cent of the cesium used reached the collector as high energy ions, and over 90 per cent was ionized at the ionizer. The injection of electrons into the ion beam for neutralization purposes was accomplished by the operation of a thermionic emitter near the exit aperture of the motor, the electrons being accelerated into the beam by the ion space charge fields.

ONE OF several methods of electrical propulsion involves the electrostatic acceleration of ions. The cesium surface ionization source used with this type of propulsion device has the following advantages (1)[5]:

1 Only one species of ions is formed, and that at a well-defined surface and with small thermal energies—factors which allow very good focusing of the beam.

2 Neutral (unaccelerated) particles constitute only a small fraction of the exhaust.

3 The power required to ionize the cesium is mainly that required to maintain the ionizer at operating temperature and can be made a small fraction of the power delivered to the exhaust.

4 The device would be capable of long periods of unattended operation.

5 The weight of the device would be low.

Although the experiments reported in this paper were on a small scale, they cover many of the phenomena of significance to the development of practical size ion motors.

Presented at the ARS 14th Annual Meeting, Washington, D.C., Nov. 16–20, 1959.

[1] This research was supported by AFOSR Contract AF49(638)-351 and WADC Contract AF 33(616)-5927.

[2] Principal Scientist. Member ARS.

[3] Senior Physicist. Member ARS.

[4] Principal Scientist. Member ARS.

[5] Numbers in parentheses indicate References at end of paper.

Apparatus

The test system (Fig. 1) is an 8-in. diameter, 2-ft long vacuum tank with the ion device mounted on an insulator at one end and an ion beam collector mounted on the other end. Two types of collectors were used—a calorimetric beam power measuring collector and a beam thrust measuring system using pendulum-type supports and a displacement transducer. The collectors could be biased as could be grids mounted directly in front of them.

A typical small-scale ion motor (Fig. 2) has a heated cesium reservoir, a needle valve and a delivery tube ending in a $\frac{3}{16}$-in. diameter porous tungsten ionizer. The ionizer is bounded by a field shaping electrode which also encloses a resistance heating element and radiation shielding.

An initial acceleration followed by a deceleration was accomplished by operating the ionizer at a positive potential

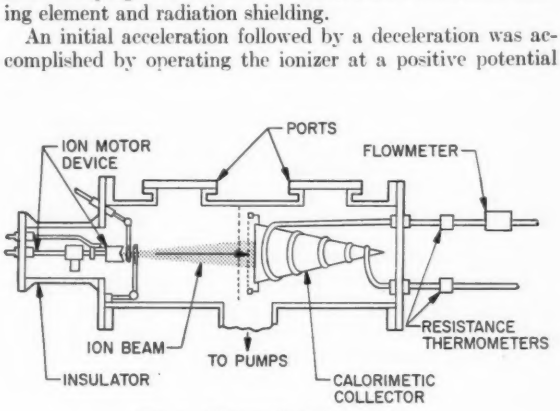

Fig. 1 Schematic of test system

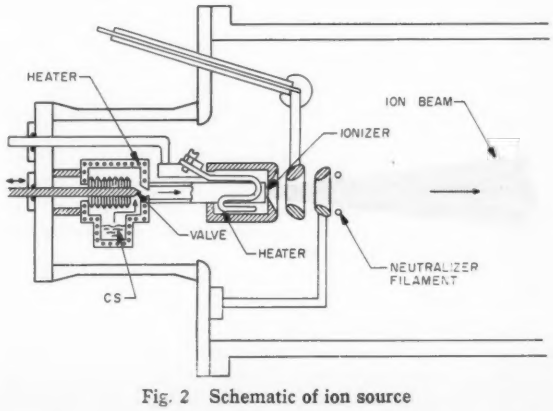

Fig. 2 Schematic of ion source

and an accelerating electrode at a negative potential relative to the exit, and neutralizing electrodes which were held near ground potential. Although the voltage across the accelerating gap was the sum of the two potentials, the net accelerating voltage was the potential of the ionizer alone. The cesium ion perveance of this circular aperture system was approximately 10^{-9} amp/$v^{3/2}$, depending on electrode spacing. The accelerating gap is about the same size as the ionizer diameter. To provide for electrical neutralization of the beam, a thermionic electron emitter was placed around the periphery of the ion beam at the exit aperture of the electrode system.

Experimental Results

Currents and focusing

Cesium ion beams up to 2.1 milliamp, corresponding to a current density of about 12 milliamp per cm^2 at the ionizer, were generated at 15-kv net acceleration potential. This was with a porous tungsten ionizer of 70 per cent theoretical density operated at about 1575K. In general, it was not necessary to operate the neutralization filament in order to get a collimated beam. Presumably neutralization, in this case, occurs as a result of the trapping of secondary electrons in the space charge trough built up by the ions. True ion current measurements were calculated from beam power measurements.

Collimation of the beam was quite good. Total beam divergence angles under 12 deg were usually observed, and angles as low as 8 deg total spread were achieved. These angles are obtained from photographs such as that of Fig. 3 which shows the ion beam during operation of the motor.

In operation of the accelerate-decelerate system, it was found that beam currents greater than those corresponding to space charge limitations based on the net accelerating voltage could be produced. However, the currents were less than those corresponding to the space charge limited values based on the total voltage across the accelerating gap. In general, for a given net accelerating voltage (potential of source), the beam current increased as the total potential across the accelerating gap was increased up to voltages some three or four times the net acceleration voltage. Thus, even with a $\frac{1}{4}$-in. accelerating gap, a current density of 4 milliamp per cm^2 was easily achieved at 4-kv net acceleration voltage.

Sputtering and secondary electrons

A sputtering ratio of 10 nickel atoms per incident 10-kv cesium ion was determined from the erosion of the nickel grid in front of the collector. This is in good agreement with other data (2) on sputtering by heavy ions and indicates the necessity of good focusing to prevent extreme erosion of the electrodes.

Secondary electron emission due to ion bombardment was measured by putting small (<100 v) voltages between the collectors and the grids mounted immediately in front of them. It was ascertained that at zero bias about one half of the directly measured collector current was due to electrons leaving the collector. With biases set so that electrons would be accelerated away from the collector, it was found that the secondary electron emission coefficient for a cesium contaminated graphite collector (used in the thrust measuring system) ranged from 1.3 for 2-kv cesium ions to 5 for 12-kv cesium ions. We would expect these values to be valid for the graphite accelerating electrode used in the source, and they may be approximately valid for most materials after long bombardment with cesium ions.

Mass efficiency

An extended duration run to determine a cesium utilization factor was made with a net acceleration voltage of 9 kv and an ion beam current averaging 1.22 milliamp as derived from the calorimetric collector beam power measurements. This run lasted 30.66 hr giving 37.3 milliamp-hr of cesium ions to the collector. Since the 0.265 gm of cesium consumed corresponds to 53 milliamp-hr of cesium ions, approximately 70 per cent of the cesium used reached the collector as high energy ions. From considerations of the currents measured at the electrodes and grids, it was ascertained that about 90 per cent of the cesium was ionized at the ionizer.

Fig. 3 Ion beam

Neutralization

It was found that the current could be easily neutralized by operation of the thermionic electron emitter surrounding the exit aperture of the electrode system. In beam neutralization tests, collector power measurements remained unchanged, whereas the directly measured collector current could be decreased to zero or even made to go negative by further increasing the temperature of the thermionic emitter. This is not surprising, because although the electrons are drawn into the beam by small space charge fields, they have much higher velocities than the ions. Since the dimensions of the laboratory apparatus are small compared to the distance required for the electrons and ions to equilibrate, at equal currents there is still a net positive space charge.

Thrust

Thrust measurements were made by measuring the force of the ion beam on a pendulum suspended collector plate as previously indicated. The theoretical expression for thrust (assuming cesium ions are accelerated) is given by

$$F = 3.73 \times 10^{-4} IV^{1/2}$$

where

F = thrust, lb
I = ion beam current, amp
V = net accelerating potential, v

The measured thrusts were found to be in agreement with this relationship for thrusts up to 100 micropounds which corresponds to over $\frac{1}{2}$ millipound per cm^2 of ionizer area.

Conclusions

In general the experimental results support the consideration of this scheme as a promising method of space propulsion. The cesium surface ionization system provides well-behaved ion motor operation with performance characteristics close to theoretical values. The current densities are adequate for practicable propulsion devices with high mass efficiency, and the simple neutralization scheme appears to be practical, although neutralization tests are not conclusive in the necessarily limited dimensions of laboratory systems. The experimental studies reported in this paper indicate that no major technological "breakthroughs" are necessary for the development of practical cesium surface ionization ion motors.

References

1 Forrester, A. T. and Speiser, R. C., "Cesium-Ion Propulsion," ASTRONAUTICS, vol. 4, no. 10, Oct. 1959, p. 34.

2 Massey, H. S. W. and Burhop, E. H. S., "Electronic and Ionic Impact Phenomena," Oxford University Press, 1952, pp. 583–589.

Ionospheric Structure Above Fort Churchill, Canada, From Faraday Rotation Measurements

RAYMOND E. PRENATT[1]

Ballistic Research Laboratories, Aberdeen Proving Ground, Md.

Integrated electron content in the ionosphere above Fort Churchill, Manitoba, Canada, has been computed for a number of sounding rocket firings during the IGY. The method used involves the determination of the Faraday rotation of the 76.06 mc DOVAP tracking signal transmitted from the rocket. The expression relating Faraday rotation to integrated electron content is given, and the technique for measuring Faraday rotation using DOVAP spin records is described. Integrated electron content for two of the flights evaluated to date is presented with particular reference to some of the more interesting or unexpected results obtained.

Faraday Rotation

FARADAY rotation refers to the rotation of the plane of polarization of an electromagnetic wave when it traverses a birefringent medium, such as the ionosphere. Considering propagation approximately along the magnetic field (quasi-longitudinal propagation) of a linearly polarized signal whose frequency is much higher than the collision and gyromagnetic frequencies, one obtains the following expression for the rate of Faraday rotation with distance along the ray path

$$\frac{d\Omega}{dr} = -\frac{e^3\mu_0 N_e H \cos\phi}{2m^2 c_0 \epsilon_0 \omega^2}$$

From this is obtained the expression for total Faraday rotation along the ray path

$$\Omega = -\frac{e^3\mu_0}{2m^2 c_0 \epsilon_0 \omega^2}\int_{r_1}^{r_2} N_e H \cos\phi \, dr$$

where H, $\cos\phi$ and N_e may vary along r. Using a flat Earth approximation this equation may be written

$$\Omega = -\frac{e^3\mu_0}{2m^2 c_0 \epsilon_0 \omega^2}\int_{h_1}^{h_2} N_e H \cos\phi \sec\theta \, dh$$

Furthermore, for small horizontal ranges, $\cos\phi$ and $\sec\theta$ are essentially constant along the ray path. Using a single effective value of H then, the equation takes its final form

$$\Omega = -\frac{e^3\mu_0 H \cos\phi \sec\theta}{2m^2 c_0 \epsilon_0 \omega^2}\int_{h_1}^{h_2} N_e dh$$

Measurement of Faraday Rotation

The amount of Faraday rotation is taken as the difference between the rocket spin as measured by DOVAP[2] and an assumed true spin. During the vacuum portion of the flight of a stable rocket, the true spin rate should be constant. However, an examination of the DOVAP spin records shows that, in general, the measured spin rate is not constant during the vacuum portion of the flight. This is shown in Fig. 1. At two points in time when the rocket is at the same altitude (ascending and descending), low in the ionosphere but above any significant drag, the true total spin is taken equal to the DOVAP total spin. These are shown in Fig. 1 as points A and B which define the true spin vs. time. The difference between the true spin and the DOVAP spin at any time is the amount of Faraday rotation between the rocket and the receiving station at that time.

Integrated Electron Content

An ORDVAC[3] program has been used to compute integrated electron contents for several IGY flights at Fort

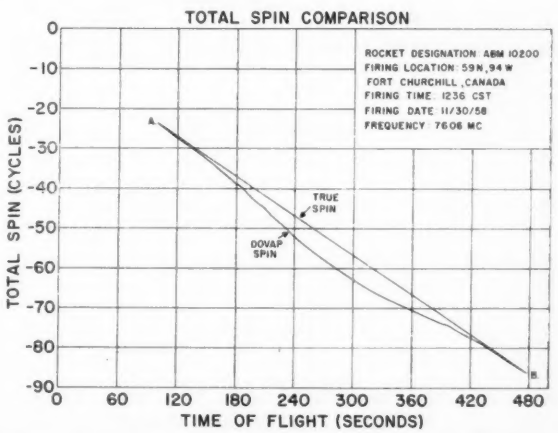

Fig. 1 Comparison of assumed true rocket spin and apparent spin as measured at the launch site DOVAP station

---

Presented at the ARS 14th Annual Meeting, Washington, D. C., Nov. 16–20, 1959.

[1] Physicist, Applied Physics Branch, Ballistic Measurements Laboratory. Member ARS.

[2] DOVAP (Doppler Velocity And Position) is a Doppler tracking system designed at Ballistic Research Laboratories and used for determining precision trajectories of missiles and sounding rockets at a number of ranges throughout the U. S. and at Fort Churchill, Manitoba, Canada.

[3] The ORDVAC (Ordnance Variable Automatic Computer) is a high speed electronic digital computer designed and constructed by the University of Illinois for the Computing Laboratory of the Ballistic Research Laboratories.

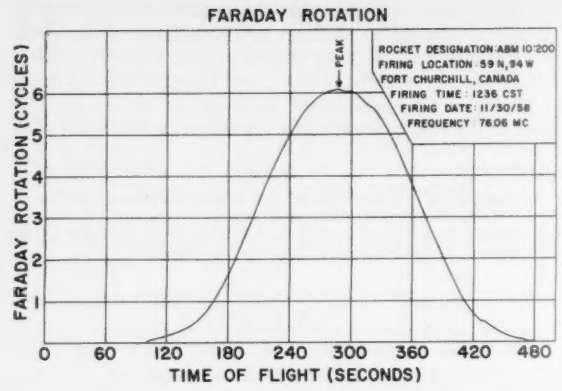

Fig. 2 Faraday rotation vs. time of flight from Spaerobee rocket ABM 10.200

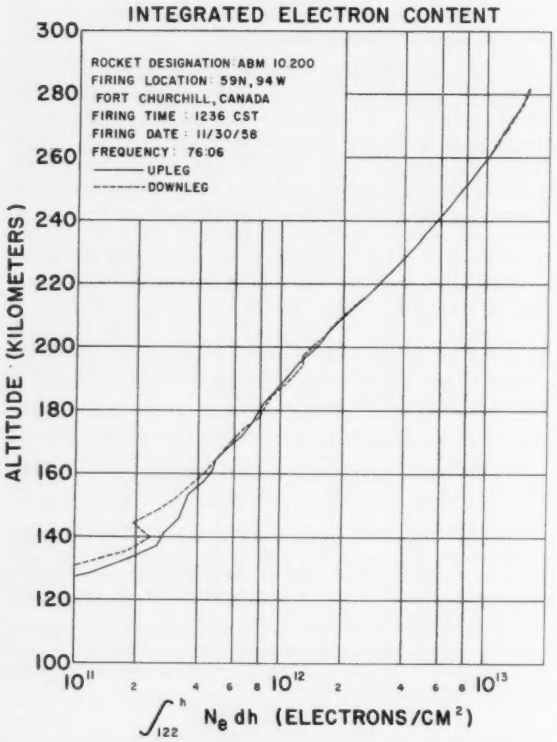

Fig. 3 Total electron content vs. altitude during flight of Spaerobee ABM 10.200

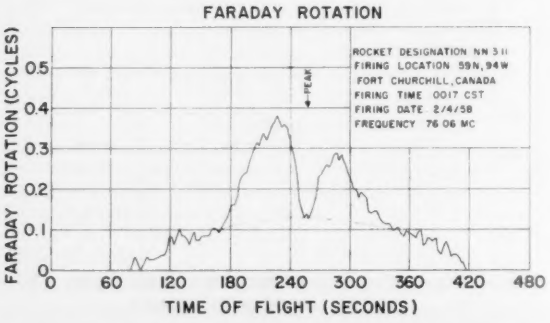

Fig. 4 Faraday rotation vs. time of flight from Aerobee-Hi rocket NN 3.11

Churchill. Fig. 2 shows the Faraday rotation vs. time obtained from the spin record, shown in Fig. 1, obtained during the flight of Spaerobee rocket ABM 10.200 on Nov. 30, 1958. From this, the integrated electron content in Fig. 3 was computed. Since this flight reached one of the highest altitudes attained at Fort Churchill during the IGY, both the Faraday rotation and the corresponding electron content are several times those normally encountered.

Figs. 4 and 5 are plots of Faraday rotation and associated electron content vs. time for Aerobee-Hi NN3.11, fired Feb. 4, 1958. Since this flight took place shortly before midnight, both the Faraday rotation and electron content are more than an order of magnitude less than those for ABM 10.200. At the time of the flight of NN3.11, the ionosphere exhibited a condition known as Spread F. This is a poorly understood phenomenon which is believed to be associated with extreme turbulence in the ionosphere. Of particular interest in this flight is the possible evidence of horizontal ionospheric inhomogeneity which the data show. A normal midnight ionosphere might give the results shown by the dotted lines in Figs. 4 and 5. It appears, however, that at $X + 180$ sec (200 km) the rocket entered a cloud of more intense ionization, since both Faraday rotation and associated electron content began to increase rapidly. Near peak altitude, while moving with a horizontal velocity of 150 m per sec, the rocket crossed a break or discontinuity about 7.5 km wide in the electron cloud as indicated by the 65 per cent decrease in both Faraday rotation and total electron content. Shortly after peak the rocket re-entered a highly ionized region from which it emerged at $X + 350$ sec (200 km).

Similar results were obtained by another type of analysis employed by Ballistic Research Laboratories to determine electron densities. In this method the DOVAP trajectory is compared with a computed vacuum trajectory and electron densities are computed from the differences in velocity. In this case, at the time of the decrease in Faraday rotation, the DOVAP velocity relative to the vacuum velocity showed an unexpected increase. This effect corresponds to an increase in the relative rate of change of phase path length such as that which would be observed if the average electron density along the ray path, and therefore total electron content, were to decrease. As the decrease in Faraday rotation, this effect also recovers shortly after peak altitude.

In an effort to find an alternative explanation for the observed data, a number of possible sources of error or misinterpretation of the data have been considered, but each such source so far examined would affect only one of the analysis techniques described above.

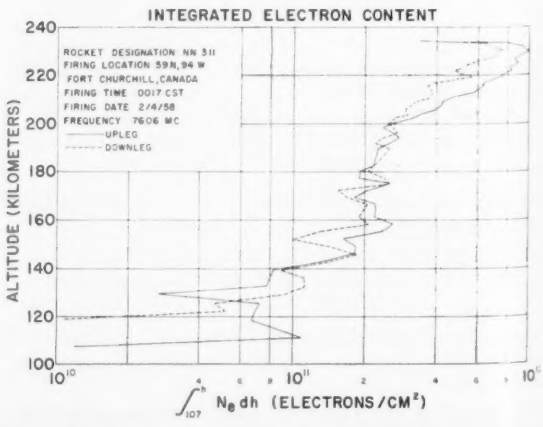

Fig. 5 Total electron content vs. altitude during flight of Aerobee-Hi NN3.11

Acknowledgment

The author is indebted to J. Carl Seddon of the Goddard Space Flight Center, NASA, for several stimulating discussions of a number of IGY flights at Fort Churchill including that of NN 3.11.

Nomenclature

Ω = Faraday rotation, radians

e, m = charge and mass of the electron, respectively
ϵ_0, μ_0 = permittivity and permeability of free space, respectively
c_0 = velocity of light in free space
ω = radian frequency at the transmitted signal
N_e = electron density, electrons per m^3
H = magnetic field intensity, ampere turns per m
ϕ = angle between transmission path and the magnetic field
θ = angle between transmission path and the vertical
dr, dh = incremental path length and altitude, respectively

Approximate Free Molecule Aerodynamic Characteristics[1]

D. M. SCHRELLO[2]

North American Aviation, Inc., Columbus, Ohio

Expressions for the free molecule lift, drag and static pitching moment of an arbitrary body of revolution are derived under the restriction that the average normal component of the molecular speed ratio over the exposed body surface be greater than or equal to unity. It is shown that no assumptions about the nature of the molecular reflection process are required, so that the results are applicable to specular as well as diffuse reflection. A consequence of the restriction is that a minimum permissible speed ratio exists for any given body shape, below which the approximate results are formally not applicable. For most blunt bodies, however, this lower limit is found to be of the order of 2.0. A comparison of the present results with Gustafson's "Newtonian-diffuse" theory shows the present results to contain an additional term of order $1/S_\infty^2$ which significantly improves the agreement between the approximate and exact drag coefficients at low values of the molecular speed ratio.

IT IS now well known that the exact solution for the aerodynamic forces and moments on an arbitrary inclined body in free molecule flow is not readily expressible in analytical form. This circumstance is a result chiefly of the complicated integrals which must be evaluated in the process of integrating the exact pressures and shearing stresses over the body surface. In order to obtain results for body shapes not currently amenable to exact analysis, it has been necessary to develop approximate techniques, such as those presented by Gustafson (1)[3] and Schamberg (2). These approximate methods generally require rather restrictive assumptions about the nature of the molecule-surface interaction process and/or the range of values of the molecular speed ratio which is of interest.

In particular, the assumption that the random molecular velocity is negligible in comparison to the vehicle velocity (the hyperthermal assumption) is somewhat questionable at the highest altitudes for which the neutral particle forces and moments on a satellite may still predominate over those due to other influences. For example, if an altitude of about 1000 miles is taken as a tentative upper limit of the neutral particle free molecule flow regime (2) then, based upon Minzer's 1959 atmosphere (3), a satellite in a circular orbit at this altitude is found to move with a speed ratio of about 3.7, which appears too low to justify the hyperthermal assumption. Moreover, since the details of the molecule-surface interaction are still lacking, it appears desirable to eliminate all unnecessary assumptions about the nature of this process.

The method presented here introduces assumptions which are believed to be less restrictive than those made previously. Nonetheless, these assumptions allow relatively simple closed form results to be obtained. The chief restriction imposed is that the average normal component of molecular speed ratio over the exposed body surface must be greater than or equal to unity. This restriction is made as a result of expanding the Gaussian error function which appears in the exact free molecule pressure and shearing stress coefficients and neglecting second-order terms in these expressions. It implies a definite, minimum, free stream speed ratio for any given body shape above which the results apply, but for most blunt bodies of interest, this minimum is found to be about 2.0.

Approximate Pressure and Shearing Stress Coefficients

The pressure and shearing stress on an element of surface exposed to a free molecule flow which is in Maxwellian equilibrium are given by (4)

$$p = \frac{\rho V_\infty^2}{2S_\infty^2}\left\{\left(\frac{2-\sigma_N}{\sqrt{\pi}}S_N + \frac{\sigma_N}{2}\sqrt{\frac{T_W}{T_\infty}}\right)e^{-S_N^2} + \left[(2-\sigma_N)\left(S_N^2+\frac{1}{2}\right) + \frac{\sigma_N\sqrt{\pi}}{2}\sqrt{\frac{T_W}{T_\infty}}S_N\right][1+\mathrm{erf}(S_N)]\right\}$$

$$\tau = \frac{\rho V_\infty^2}{2S_\infty^2}\sigma_T\frac{S_T}{S_N}\left\{\frac{S_N}{\sqrt{\pi}}e^{-S_N^2} + S_N^2[1+\mathrm{erf}\,(S_N)]\right\} \qquad [1]$$

The Gaussian error function appearing in these expressions may be rearranged and integrated by parts to yield

$$\mathrm{erf}\,(S_N) = 1 - \frac{e^{-S_N^2}}{S_N\sqrt{\pi}} + \frac{1}{\sqrt{\pi}}\int_{S_N}^{\infty} e^{-t^2}\frac{dt}{t^2} \qquad [2]$$

Denoting the last term in this expression by $\epsilon(S_N)$ and substituting Equation [2] into Equations [1] lead to

$$p = \rho_\infty V_\infty^2\left\{\left[(2-\sigma_N)\left(\frac{S_N}{S_\infty}\right)^2 + \frac{\sigma_N\sqrt{\pi}}{2S_\infty}\sqrt{\frac{T_W}{T_\infty}}\left(\frac{S_N}{S_\infty}\right) + \frac{2-\sigma_N}{2S_\infty^2}\right]\left[1+\frac{1}{2}\epsilon(S_N)\right] - \frac{2-\sigma_N}{4\sqrt{\pi}}\frac{e^{-S_N^2}}{S_N^3}\left(\frac{S_N}{S_\infty}\right)^2\right\}$$

$$\tau = \rho_\infty V_\infty^2\sigma_T\frac{S_T}{S_N}\left(\frac{S_N}{S_\infty}\right)^2\left[1+\frac{1}{2}\epsilon(S_N)\right] \qquad [3]$$

Received Dec. 17, 1959.

[1] This work is a condensation of North American Aviation, Inc. Rep. no. NA 59H-345, Aug. 17, 1959.

[2] Research Specialist, Engineering Research Section.

[3] Numbers in parentheses indicate References at end of paper.

which apply to elements of surface which are exposed directly to the free stream flow. For shielded elements, the corresponding expressions are identical to Equations [3] with S_N replaced by $-S_N$ and $[1 + \epsilon(S_N)/2]$ replaced by $\epsilon(S_N)/2$. If the restriction $S_N \geq 1$ is made, then it is not difficult to show that

$$\frac{1}{2}\epsilon(S_N) \cong O\left(\frac{e^{-S_N^2}}{4S_N^3\sqrt{\pi}}\right) \ll 1$$

and terms of this order may be neglected in comparison to unity. With this restriction, the forces on exposed elements of surface become

$$\frac{p}{\rho_\infty V_\infty^2} \cong (2 - \sigma_N)\left(\frac{S_N}{S_\infty}\right)^2 + \frac{\sigma_N\sqrt{\pi}}{2S_\infty}\sqrt{\frac{T_W}{T_\infty}}\left(\frac{S_N}{S_\infty}\right) + \frac{2 - \sigma_N}{2S_\infty^2}$$

$$\frac{\tau}{\rho_\infty V_\infty^2} \cong \sigma_T \frac{S_T}{S_N}\left(\frac{S_N}{S_\infty}\right)^2 \qquad [4]$$

whereas a comparison of Equations [3] and the corresponding equations for shielded surfaces leads to the conclusion that $p \cong \tau \cong 0$ is consistent with Equations [4] for these surfaces.

According to the formal restriction that $S_N \geq 1$, the approximate free molecule forces and moments on any body must be obtained by integrating Equations [4] only over that portion of the exposed surface for which $S_N \geq 1$. This poses certain practical difficulties regarding the limits of integration. To the order of the approximation, however, it is sufficient to satisfy the restriction $S_N \geq 1$ in the mean over the exposed body surface rather than at each point. This introduces little error, since the contribution to the overall aerodynamic forces and moments made by those portions of the surface for which $0 \leq S_N \leq 1$ is generally small. In this case, integration of Equations [4] may proceed over the entire exposed body surface, with the results subject only to the condition that

$$\frac{1}{\eta}\int\int_\eta S_N(t)dt \geq 1 \qquad [5]$$

Approximate Force and Moment Integrals

The approximate pressure and shearing stress expressions obtained in the foregoing may now be integrated over the exposed surface of an arbitrary body of revolution. The procedure is straightforward but laborious. Cylindrical polar coordinates x, r, φ are defined, where x is the distance along the body axis measured from the nose, $r(x)$ is the equation of the body surface, and φ is the meridian angle measured from the plane containing S_∞ and x, with $\varphi = 0$ taken downward. Equations [4] are then substituted into general integral expressions for the lift, drag and static nose pitching moment (including the contributions of the tangential stresses), and the integration over φ performed. Due account must be taken of the limits of integration, which change from $0 \leq \varphi \leq \pi$ for $r' \geq \tan\alpha$ to $0 \leq \varphi \leq \cos^{-1}(-r'/\tan\alpha)$ for $r' \leq \tan\alpha$. For simplicity, the coefficients σ_N, σ_T and T_W are regarded as constants, but it is evident that this assumption is not essential. The results of this lengthy process may be expressed in coefficient form as

$$C_D = \frac{2\pi}{A_R}\int_0^l \left[2(2 - \sigma_N - \sigma_T)\frac{\zeta^2\sin^2\alpha}{1 + \zeta^2\tan^2\alpha} f(\zeta) + \frac{\sigma_N\sqrt{\pi}}{S_\infty}\sqrt{\frac{T_W}{T_\infty}}\frac{\zeta^2\sin^2\alpha}{\sqrt{1 + \zeta^2\tan^2\alpha}} g(\zeta) + \left(\frac{2 - \sigma_N}{S_\infty^2} + 2\sigma_T\right)\zeta h(\zeta)\sin\alpha\right] r\,dx \qquad [6]$$

$$C_L = C_D\cot\alpha - \frac{2\pi}{A_R\cos\alpha} \times \int_0^l\left[2(2 - \sigma_N - \sigma_T)\frac{\zeta^2\sin^2\alpha}{1 + \zeta^2\tan^2\alpha} g(\zeta) + \frac{2 - \sigma_N}{S_\infty^2}\zeta m(\zeta) + \left(\frac{\sigma_N\sqrt{\pi}}{S_\infty}\sqrt{\frac{T_W}{T_\infty}}\frac{\zeta^2\sin\alpha}{\sqrt{1 + \zeta^2\tan^2\alpha}} + 2\sigma_T\cos^2\alpha\zeta\right)h(\zeta)\right] r\,dx \qquad [7]$$

$$C_{m_0} = -\frac{2\pi}{A_R l_R}\int_0^l \left(\left\{2(2 - \sigma_N - \sigma_T)\frac{\zeta^2\sin^2\alpha}{1 + \zeta^2\tan^2\alpha}[f(\zeta) - g(\zeta)] + \frac{\sigma_N\sqrt{\pi}}{S_\infty}\sqrt{\frac{T_W}{T_\infty}}\frac{\zeta^2\sin\alpha}{\sqrt{1 + \zeta^2\tan^2\alpha}}[g(\zeta) - h(\zeta)] + \frac{2 - \sigma_N}{S_\infty^2}\zeta[h(\zeta) - m(\zeta)]\right\}(r\zeta\tan\alpha + x) + 2\sigma_N\zeta\sin^2\alpha\left[\left(x - \frac{r\zeta}{\tan\alpha}\right)h(\zeta) + \frac{r\zeta}{\tan\alpha}g(\zeta)\right]\right) r\,dx \qquad [8]$$

where $\zeta \equiv r'/\tan\alpha$, and the functions f, g, h and m are given by

$$f(\zeta) \equiv \frac{1}{\pi}\left[\left(1 + \frac{3}{2\zeta^2}\right)\cos^{-1}(-\zeta) + \frac{1}{\zeta}\left(\frac{11}{6} + \frac{2}{3\zeta^2}\right)\sqrt{1 - \zeta^2}\right], \quad \zeta \leq 1; \quad f(\zeta) \equiv 1 + \frac{3}{2\zeta^2}, \quad \zeta \geq 1$$

$$g(\zeta) \equiv \frac{1}{\pi}\left[\left(1 + \frac{1}{2\zeta^2}\right)\cos^{-1}(-\zeta) + \frac{3}{2\zeta}\sqrt{1 - \zeta^2}\right], \quad \zeta \leq 1; \quad g(\zeta) \equiv 1 + \frac{1}{2\zeta^2}, \quad \zeta \geq 1$$

$$h(\zeta) \equiv \frac{1}{\pi}\left[\cos^{-1}(-\zeta) + \frac{1}{\zeta}\sqrt{1 - \zeta^2}\right], \quad \zeta \leq 1; \quad h(\zeta) \equiv 1, \quad \zeta \geq 1$$

$$m(\zeta) \equiv \frac{1}{\pi}\cos^{-1}(-\zeta), \quad \zeta \leq 1; \quad m(\zeta) \equiv 1, \quad \zeta \geq 1 \qquad [9]$$

Equations [9] define a set of universal functions for an arbitrary body of revolution in free molecule flow and are shown plotted in Fig. 1.

The remaining integration of Equations [6–8] may be performed once the variations $\zeta(x)$ and $r(x)$ are known for any particular body.

The condition that the average normal component of the molecular speed ratio must be greater than or equal to unity is obtained from Equation [5] as

$$S_\infty\sin\alpha\int_0^l \zeta h(\zeta) r\,dx \geq \int_0^l \sqrt{1 + \zeta^2\tan^2\alpha}\; m(\zeta) r\,dx \qquad [10]$$

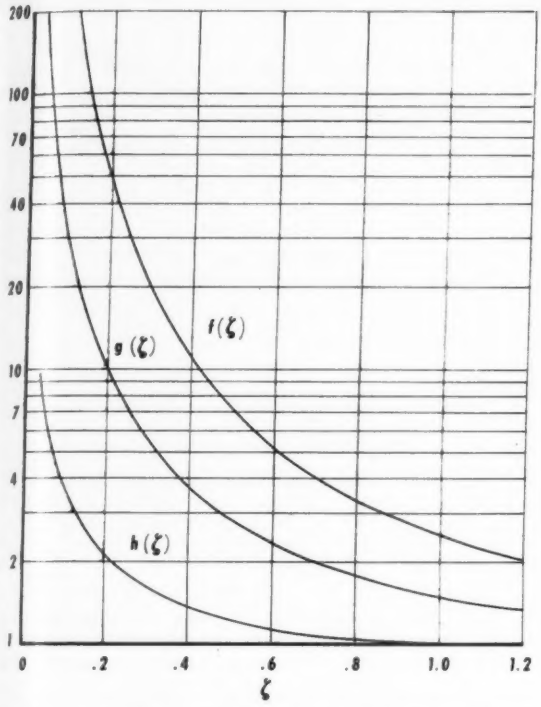

Fig. 1 **Approximate free molecule flow functions for a body of revolution**

from which a minimum permissible value of S_∞ may be determined for any given value of α for the particular body shape of interest.

It is noted in Equations [4] that if $\sigma_N = 1$, $\sigma_T = 0$ and the limit $S_\infty \to \infty$ is taken while S_N/S_∞ remains finite, the usual Newtonian pressure coefficient for hypersonic continuum flow results; namely, $p/\rho_\infty V_\infty^2 = (S_N/S_\infty)^2$ and $\tau = 0$. Thus, by the appropriate choice of constants, the general force and moment integrals developed in the foregoing may be directly applied to hypersonic continuum flow calculations. It is also noted that Gustafson's Newtonian-diffuse results (1) may be recovered from the more general results presented above by setting $\sigma_N = \sigma_T = 1$ and neglecting terms of order $(1/S_\infty)^2$.

Results for Several Elementary Shapes

The approximate expressions given are now applied to several elementary bodies of revolution at angle of attack.

Right-circular cylinder: In this case, $\zeta \equiv 0$ and Equations [6–8] simplify greatly. For example, from Equation [8], the approximate pitching moment about the nose, neglecting end effects and based upon the transverse area $2rl$ and the total length l, is

$$C_{m_0} = -\frac{2}{3}\left(2 - \sigma_N + \frac{\sigma_T}{2}\right)\sin^2\alpha - \frac{\sigma_N\pi^{3/2}}{8S_\infty}\sqrt{\frac{T_W}{T_\infty}}\sin\alpha - \frac{2-\sigma_N}{2S_\infty^2} - \sigma_T\frac{\pi r}{2l}\sin\alpha\cos\alpha \quad [11]$$

which is found to compare favorably with the exact result presented in (1). By the criterion of Equation [10], this result is formally applicable for all $S_\infty \geq \pi/2\sin\alpha$.

Right-circular cone: With δ the cone semivertex angle, ζ is constant and equal to $\tan\delta/\tan\alpha$. The approximate results for this case may be readily obtained from Equations [6–8]. For example, the drag coefficient referred to the base area is found to be

$$C_D = 2(2 - \sigma_N - \sigma_T)\sin^2\delta\cos^3\alpha f(\zeta) + \frac{\sigma_N\sqrt{\pi}}{S_\infty}\sqrt{\frac{T_W}{T_\infty}}\sin\delta\cos^2\alpha g(\zeta) + \left(\frac{2-\sigma_N}{S_\infty^2} + 2\sigma_T\right)h(\zeta)$$

Similar results are found for C_L and C_{m_0}. The criterion of applicability for the conical body becomes, from Equation [10]

$$S_\infty \geq m(\zeta)/h(\zeta)\sin\delta\cos\alpha$$

which indicates that for semivertex angles in excess of 25 deg, the theory is applicable for all molecular speed ratios greater than about 2.6.

Sphere: The results for the sphere-segment are extremely lengthy and will not be presented here. However, for a complete sphere, the approximate drag (based on the projected area) obtained from Equation [6] is simply

$$C_D = (2 + \sigma_T - \sigma_N) + \frac{2-\sigma_N}{S_\infty^2} + \frac{2}{3}\frac{\sigma_N\sqrt{\pi}}{S_\infty}\sqrt{\frac{T_W}{T_\infty}}$$

which is formally applicable for all $S_\infty \geq 2$, but agrees well with the exact results to considerably lower values.

Acknowledgment

The author is indebted to Dr. S. T. Chu of The Ohio State University for review of this material prior to publication.

Nomenclature

A_R	= body reference area
C_L, C_D, C_{m_0}	= lift, drag and static nose pitching moment coefficients
f, g, h, m	= universal functions for approximate free molecule forces and moments
l_R	= body reference length
p, τ	= surface pressure and shearing stress
S	= molecular speed ratio, ratio of vehicle speed to most probable molecular speed
T	= absolute temperature
V	= velocity
x, r, φ	= cylindrical coordinates for a body of revolution
α	= angle of attack
$\epsilon(S_N)$	= remainder in expansion of Gaussian error function $\equiv \frac{1}{\sqrt{\pi}}\int_{S_N}^{\infty} e^{-t^2}\frac{dt}{t^2}$
ζ	= body slope parameter $= r'/\tan\alpha$
η	= total body surface area exposed to free stream flow
ρ	= mass density
σ_N, σ_T	= normal and tangential momentum exchange coefficients

Subscripts

N	= component normal to element of surface
T	= component tangent to element of surface
W	= wall or surface value
∞	= free stream value

References

1 Gustafson, W. A., "Aerodynamic Moments on Bodies Moving at High Speed in the Upper Atmosphere," ARS JOURNAL, vol. 29, no. 4, April 1959, pp. 301–303.

2 Schamberg, R., "A New Analytic Representation of Surface Interaction for Hyperthermal Free-Molecule Flow with Application to Satellite Drag," 1959 Heat Transfer and Fluid Mechanics Symposium preprint, Stanford University Press, June 1959.

3 Minzer, R. A., "Higher Atmospheric Densities and Temperatures Demanded by Satellite and Recent Rocket Measurements," ARS preprint 781–59, 1959.

4 Talbot, L., "Free Molecular Flow Forces and Heat Transfer for an Infinite Circular Cylinder at Angle of Attack," *J. Aeron. Sci.*, vol. 24, no. 6, June 1957, pp. 458–459.

Evaluation of Coasting Flight of an Ascending Satellite Vehicle for Circular Orbits

A. D. COHEN[1] and H. H. RHODES[2]

General Electric Co., Malta Test Station, Ballston Spa, N. Y.

The evaluation of satellite ascent paths may be facilitated by the use of parametric curves. Graphs are presented which relate conditions at the beginning of the coasting portion to those existing when the vehicle attains a horizontal attitude.

IN FIG. 1 a sketch identifying the various parameters at stage burnout, prior to the start of the coasting period, is shown. With the thrust equal to zero and no lift or drag forces acting, the summation of forces may be taken in a direction tangent to the flight path and perpendicular to the flight path

$$M\frac{dV}{dt} = Mg_0\left(\frac{R_0}{R}\right)^2 \sin\epsilon \qquad [1]$$

$$MV\frac{d\epsilon}{dt} = \frac{MV^2}{R}\cos\epsilon - Mg_0\left(\frac{R_0}{R}\right)^2\cos\epsilon \qquad [2]$$

Also

$$V\sin\epsilon = dR/dt \qquad [3]$$

Combining Equations [1 and 3], the following will result

$$-VdV = g_0(R_0/R)^2\,dr \qquad [4]$$

Integrating equations between the start of the coasting period *bo* and the termination of the coasting period *c*, the result is

$$\frac{V_{bo}^2 - V_c^2}{2} = R_0^2 g_0\left[\frac{1}{R_{bo}} - \frac{1}{R_c}\right] \qquad [5]$$

In Equation [5], the value of V_{bo} and R_{bo} will usually be known from a computer program, or they may be estimated by other techniques. Combining Equations [1, 2 and 3] and rearranging terms, the following may be written

$$\tan\epsilon d\epsilon = \frac{dR}{R} + \frac{dV}{V} \qquad [6]$$

Integrating Equation [6], there results

$$\frac{\cos\epsilon_{bo}}{\cos\epsilon_c} = \frac{R_c V_c}{R_{bo} V_{bo}} \qquad [7]$$

Combining Equations [5 and 7] and solving for V_c, the following equation may be obtained

$$V_c = \frac{R_0^2 g_0\cos\epsilon_c}{R_{bo}V_{bo}\cos\epsilon_{bo}} - \sqrt{\left(\frac{R_0^2 g_0\cos\epsilon_c}{R_{bo}V_{bo}\cos\epsilon_{bo}}\right)^2 - \frac{2R_0^2 g_0}{R_{bo}} + V_{bo}^2} \qquad [8]$$

If a circular orbit is desired, $\cos\epsilon_c = 1$ and V_c may be computed directly from Equation [8].

Shown in Fig. 2 is a typical plot of V_c as a function of ϵ_{bo} and V_{bo} for $R_{bo} = 4060$ miles. A family of curves for other values of R_{bo} may be computed in a similar manner.

From Equation [7], the altitude at the end of the coasting flight may be expressed as

$$h_c = (R_c - R_0) = \left(\frac{R_{bo}V_{bo}\cos\epsilon_{bo}}{V_c\cos\epsilon_c} - R_0\right) \qquad [9]$$

Received March 11, 1960.

[1] Systems and Operations Specialist. Member ARS.

[2] Systems Engineer. Member ARS.

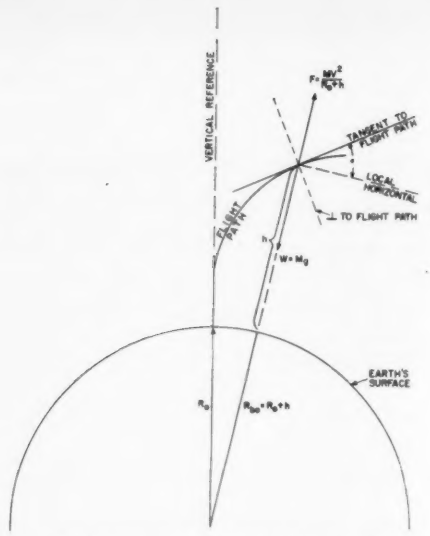

Fig. 1 Trajectory nomenclature relative to Earth

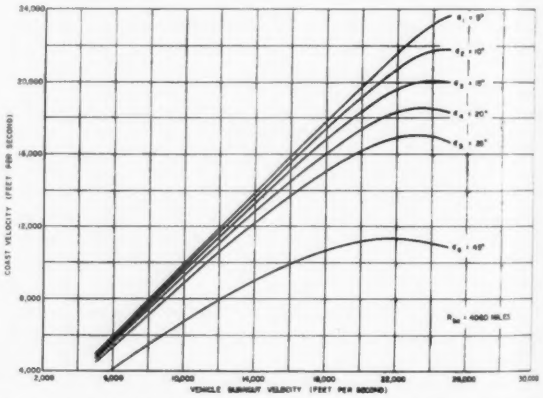

Fig. 2 Coast velocity as a function of vehicle burnout velocity

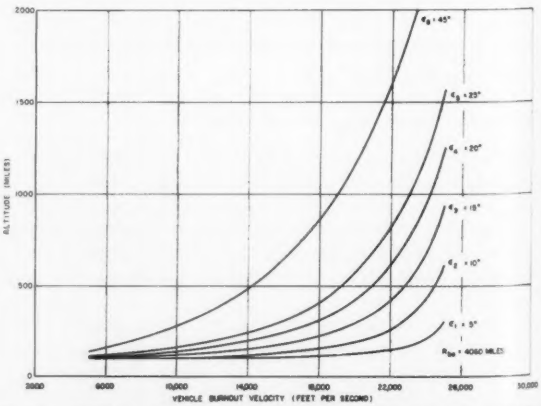

Fig. 3 Altitude at end of coasting as a function of vehicle burnout velocity

Fig. 3 is a plot of h_c for $R_{bo} = 4060$ miles and $\cos \epsilon_c = 1$ for values of ϵ_{bo} and V_{bo}.

Illustrative Example

Assume that a trajectory calculation has yielded the following results at stage burnout: $R_{bo} = 4060$ miles; $V_{bo} = 18{,}000$ fps, and $\epsilon_{bo} = 15$ deg. For ϵ_c equal to zero deg, determine the conditions at the end of the coast.

From Fig. 2 at $V_{bo} = 18{,}000$ fps and $\epsilon_{bo} = 15$ deg, V_c is found to be 16,800 fps. The altitude at the end of coast is found from Fig. 3 to be 220 miles. Thus, the altitude gain in coasting is $220 - (4060 - 3960) = 120$ miles, and the decrease in velocity is 1200 fps. The firing of the final stage occurs at the end of coast, and the velocity increment supplied by it is the difference between the orbital velocity and V_c.

Nomenclature

M = mass
V = velocity
t = time
g_0 = Earth gravity at surface
R_0 = radius of Earth
R = distance to vehicle from center of Earth
ϵ = flight angle with respect to local horizontal of Earth's surface
h = altitude above surface of Earth
d = differential operator

Subscripts

bo = burnout
c = coast

Use of the Construction Parameter in Staging Optimization

A. D. COHEN[1]

General Electric Co., Malta Test Station, Ballston Spa, N. Y.

In the recent literature on staging optimization, the solutions have required a knowledge of the hardware weight staged in order to obtain the construction parameter. This parameter has been assumed as a constant, but as is shown here, the value is, in reality, a function of the stage size. A method of incorporating this factor into the solution is presented.

IN THE several articles appearing in recent months on staging optimization, a constant value of the ratio of hardware weight jettisoned to stage weight, or construction factor, has been assumed (1–4).[2] The dependency of this factor upon the size of the stage will be shown, and a method for incorporating this into the solution is suggested. For the purpose of this analysis, the nomenclature of (2) will be adopted.

Basically, the system of equations presented in (2) will permit the solution of λ_n for each stage, such that the overall payload-to-launch-weight ratio $\Lambda = M_1/M_{01}$ will be obtained. As part of the input data, the value of θ_n is required. θ_n is defined as the stage construction factor, or the ratio of the weight of the stage that is jettisoned prior to ignition of the subsequent stage divided by the launch weight of the jettisoned stage. Thus

$$\theta_n = M_{en}/M_{0n} \qquad [1]$$

The items that comprise M_e are the powerplant, tankage, missile structure, interstage structure and unexpended propellant weight.

Powerplant weight: This weight can be approximated by $K_1 \times F_{Ln}$, where K_1 may be readily determined by the designer.

Tankage weight: Simple design analysis will show that the tankage weight is equal to $K_2 \times V_{pn}$. The propellant volume may be expressed as

$$V_{pn} = \frac{M_{pn}}{\rho_{pn}} = \frac{\dot{M}_{pn} t_n}{\rho_{pn}} = \frac{F_{Ln} t_n}{I_{Ln} \rho_{pn}} \qquad [2]$$

The tankage weight then becomes equal to $K_2 F_{Ln} t_n / I_{Ln} \rho_{pn}$.

Structure weight: The structural weight is equal to $K_3 \times F_{Ln}$, and the value of K_3 should be known to the designer.

Interstage structure weight: Design analysis will show that this weight is proportional to the stage payload weight and is equal to $K_4 \times M_{0(n+1)}$.

Unexpended propellant weight: The weight of the unexpended propellant may be expressed as a function of the initial propellant weight or $K_5 \times W_{pn}$. This may also be expressed, following the pattern of Equation [2], as $K_5 F_{Ln} t_n / I_{Ln}$.

Substituting the various component weight items into Equation [1]

$$\theta_n = \frac{M_{en}}{M_{0n}} = \frac{K_1 F_{Ln}}{M_{0n}} + \frac{K_2 F_{Ln} t_n}{I_{Ln} \rho_{pn} M_{0n}} + \frac{K_3 F_{Ln}}{M_{0n}} + \frac{K_4 M_{0(n+1)}}{M_{0n}} + \frac{K_5 F_{Ln} t_n}{I_{Ln} M_{0n}} \qquad [3]$$

In (2), λ_n has been defined as $M_{0(n+1)}/M_{0n}$. Also the launch-thrust-to-launch-weight ratio will usually be given for each stage. Designating the ratio F_{Ln}/M_{0n} as K_6, Equation [3] may be expressed as

$$\theta_n = K_6 \left[(K_1 + K_3) + \frac{t_n}{I_{Ln}} \left(\frac{K_2}{\rho_{pn}} + K_5 \right) \right] + K_4 \lambda_n \qquad [4]$$

In order to eliminate the burning time t_n from Equation [4], the stage mass ratio may be expressed as

$$\frac{M_{0n}}{M_{0n}\theta_n + M_0(n+1)} = \frac{M_{0n}}{M_{0n} - M_{pn}} = \frac{M_{0n}/F_{Ln}}{M_{0n}/F_{Ln} - t_n/F_{Ln}} \qquad [5]$$

Equation [5] may be solved for t_n, after appropriate substitutions, to yield

$$t_n = (I_{Ln}/K_6)(1 - \theta_n - \lambda_n) \qquad [6]$$

Substituting Equation [6] into Equation [4], and solving for θ_n will result in

$$\theta_n = \frac{K_6(K_1 + K_3) + K_4\lambda_n + (K_2/\rho_{pn} + K_5)(1 - \lambda_n)}{1 + K_2/\rho_{pn} + K_5} \qquad [7]$$

From Equation [7], it may be seen, that after substitution of the appropriate values of K and the known values of I_{Ln} and ρ_{pn}, the expression will reduce to the form

$$\theta_n = K' + K''\lambda \qquad [8]$$

where K' and K'' are functions of K_{1-6}, I_{Ln} and ρ_{pn}.

Thus θ_n has been shown to be a function of λ_n. From (2), it may be seen that the solution for the various λ_n is one of trial and error. Since θ_n is dependent upon λ_n, an additional iterative loop is necessary. The system of equations is readily programmed on a digital computer, so that accurate answers can be obtained rapidly.

Received March 11, 1960.

[1] Systems and Operations Specialist. Member ARS.

[2] Numbers in parentheses indicate References at end of paper.

Nomenclature

F_{Ln} = stage launch thrust, lb
I_{Ln} = stage launch specific impulse, sec
K_{1-6} = dimensionless constants
M_{en} = stage jettison weight, lb
M_{0n} = stage launch weight, lb
$M_{0(n+1)}$ = payload of the nth stage, lb
M_{pn} = propellant weight, lb
$\dot{M}_{pn}$ = propellant flow rate, lb per sec
t_n = stage burning time, sec
V_{pn} = stage propellant volume, ft^3
λ_n = stage payload parameter = $M_{0(n+1)}/M_{0n}$
ρ_{pn} = mean propellant bulk density, lb per ft^3
θ_n = construction parameter = M_{en}/M_{0n}

References

1 Weisbord, L., "A General Optimization Procedure for N-Staged Missiles," JET PROPULSION, vol. 28, no. 3, March 1958, pp. 164–167.
2 Subotowicz, M., "The Optimization of the N-Step Rocket With Different Construction Parameters and Propellant Specific Impulses in Each Stage," JET PROPULSION, vol. 28, no. 7, July 1958, pp. 460–463.
3 Hall, H. H. and Zambelli, E. D., "On the Optimization of Multistage Rockets," JET PROPULSION, vol. 28, no. 7, July 1958, pp. 463–465.
4 Builder, Carl H., "General Solution for Optimization of Staging of Multistaged Boost Vehicles," ARS JOURNAL, vol. 29, no. 7, July 1959, pp. 497–499.

Free Molecule Flow Over Nonconvex Bodies[1]

IRA M. COHEN[2]

Princeton University, Princeton, N. J.

THE CLASSICAL free molecule flow (1)[3] has to date been developed only for flow about convex surfaces. In the usual analysis, all molecules are considered to be incident (on the surface) from, and return to, the free stream. This note will generalize the free molecule analysis to a consideration of arbitrary surfaces.

The interaction of molecules with the surface will be idealized as follows: Molecules will be re-emitted *isotropically* with an energy corresponding to the body temperature. The first requirement is fundamental; the second may be dropped, as will be indicated in the following.

The incident gas stream is considered to consist of molecules of a single species only. The body temperature T_b is assumed to be sufficiently far from absolute zero to avoid cold wall paradoxes (2), and is constant over the body surface and with time. It is assumed that for each surface element, the mass flux incident is equal to the mass flux re-emitted ($\nu_i = \nu_r$); i.e., neither surface poisoning nor trapping of gas molecules is permitted.

The incident number flux on a unit of surface about a point $\bar{X}_1$ in a nonconvex region of an arbitrary body is given by

$$\nu_i(\bar{X}_1) = \nu_\infty(\bar{X}_1) + \nu_b(\bar{X}_1)$$

where

$\nu_\infty(\bar{X}_1)$ = incident number flux from the free stream
$\nu_b(\bar{X}_1)$ = contribution to $\nu_i(\bar{X}_1)$ by molecules re-emitted from the body surface

ν_∞ may be calculated as a function of body geometry and speed ratio. ν_b is expressed as an integral of the molecular number flux re-emitted from the body over the entire nonconvex surface.

Consider two elements of surface on an arbitrary body. See Fig. 1. Denote the argument point by $\bar{X}_1$ and the parameter point by $\bar{X}_2$. With the assumption of isotropic re-emission (cosine law), the molecular number flux emitted by dA_2 that is intercepted by dA_1 is

$$dA_1 d\nu_b(\bar{X}_1) = \frac{\cos\phi_1 \cos\phi_2}{\pi r_{1\text{-}2}^2} \nu_r(\bar{X}_2) dA_2 dA_1$$

But $\nu_r(\bar{X}_2)$ is equal to $\nu_i(\bar{X}_2)$ so that the incident number flux is given by

$$\nu_i(\bar{X}_1) = \nu_\infty(\bar{X}_1) + \int_{A_2} K(\bar{X}_1, \bar{X}_2)\nu_i(\bar{X}_2) dA_2 \qquad [1]$$

where

$$K(\bar{X}_1, \bar{X}_2) = \frac{\cos\phi_1 \cos\phi_2}{\pi r_{1\text{-}2}^2} = K(\bar{X}_2, \bar{X}_1)$$

It has recently been brought to the author's attention that Equation [1] had been derived in 1956 by DeMarcus (4). DeMarcus credits Clausing (5) with the first formulation of the problem in terms of an integral equation in 1929. Both DeMarcus and Clausing were concerned with the flow of extremely rarefied gases through pipes.

The symmetry of K with respect to interchanging parameter point and argument point means that the fraction of mass flux emitted by dA_2 about $\bar{X}_2$ that is received by dA_1 about $\bar{X}_1$ *is the same* as the fraction of mass flux emitted by dA_1 that is received by dA_2.

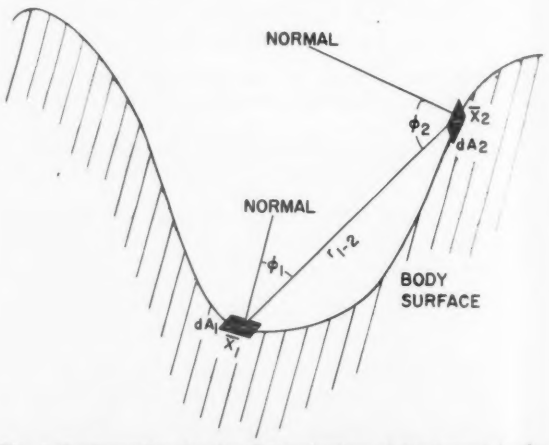

Fig. 1 Configuration for the determination of the kernel in the number flux integral equation

Received March 11, 1960.
[1] This work was supported by the Daniel and Florence Guggenheim Foundation and the Air Force Office of Scientific Research, ARDC, Fluid Mechanics Division under Contract AF 49(638)-465.

[2] Graduate Student, Department of Aeronautical Engineering.
[3] Numbers in parentheses indicate References at end of paper.

Equation [1] is a Fredholm integral equation, the solution of which may be written in the form (3)

$$\nu_i(\bar{X}_1) = \nu_\infty(\bar{X}_1) - \int_{A_2} \tilde{K}(\bar{X}_1, \bar{X}_2)\nu_\infty(\bar{X}_2)dA_2$$

where $\tilde{K}$ is the resolvent kernel.

The momentum and energy fluxes at the body surfaces will now be calculated. At any point in space, in particular on the body surface, the incident mass momentum and energy fluxes may be expressed as the sum of two contributions: One an integral over the solid angle subtended at the point by outer space, the other an integral over the solid angle subtended by the body. See Fig. 2. Then we may write by analogy to the convex body analysis (2)

$$\nu_i(\bar{X}_1) = \int_{-\infty}^{\infty}\int_{-\infty}^{\infty}\int_0^{\infty} c_z f(\bar{c})d\bar{c} = \iint_{\Omega_1} \sin\varphi\cos\psi\left[\int_0^{\infty} c^3 f^{(1)}(c,\omega)dc\right]d\omega + \iint_{\Omega_2} \sin\varphi\cos\psi\left[\int_0^{\infty} c^3 f^{(2)}(c,\omega)dc\right]d\omega \qquad [2]$$

where $d\omega = \sin\varphi\, d\varphi\, d\psi$.

In Equation [2] the left-hand side has been written in the usual free molecule rectangular coordinate system and the right-hand side is expressed in terms of spherical polar coordinates. The integral over Ω_1 gives ν_∞. $f^{(1)}(c, \omega)$ is usually assumed to be a Maxwellian velocity distribution with respect to an observer moving with the mass velocity of the stream U. The integral over Ω_2 yields ν_b. However, $f^{(2)}$ is unknown and must be found so that the equations for momentum and energy flux analogous to Equation [2] may be written. ν_b is known from the solution of Equation [1]. It is assumed that molecules are re-emitted from the surface with a Maxwellian distribution of molecular speeds with respect to an observer on the surface. Then

$$f^{(2)}(c) = \frac{N_b(\bar{X}_1)}{(2\pi RT_b)^{3/2}}\exp\left(-\frac{c^2}{2RT_b}\right) \qquad [3]$$

where N_b is to be determined. From the second half of Equations [2 and 3]

$$\nu_b(\bar{X}_1) = \iint_{\Omega_2} \sin\varphi\cos\psi\left[\int_0^{\infty} c^3\frac{N_b(\bar{X}_1)}{(2\pi RT_b)^{3/2}}\exp\left(-\frac{c^2}{2RT_b}\right)dc\right]d\omega =$$

$$N_b(\bar{X}_1)\sqrt{\frac{RT_b}{2\pi}}\left(\frac{1}{\pi}\iint_{\Omega_2}\sin\varphi\cos\psi d\omega\right) = N_b(\bar{X}_1)\sqrt{\frac{RT_b}{2\pi}}B(\bar{X}_1)$$

We may denote $\nu_b(\bar{X}_1)/\sqrt{(RT_b/2\pi)}$ by n_b, the number density at the argument point of molecules re-emitted elsewhere from the body. Consequently

$$N_b(\bar{X}_1) = n_b(\bar{X}_1)/B(\bar{X}_1) \qquad [4]$$

Equations [3 and 4] determine $f^{(2)}$ uniquely as a function of c the absolute molecular speed and $\bar{X}_1$ the argument point. Incidentally, if Ω_2 is a hemisphere, $B(\bar{X}_1) = 1$. This suggests that to calculate the contribution to momentum and energy transfer due to molecules re-emitted from the body at the argument point

$$f^{(2)}(c) = \frac{n(\bar{X}_1)}{(2\pi RT_b)^{3/2}}\exp\left(-\frac{c^2}{2RT_b}\right) \qquad n(\bar{X}_1) = \frac{\nu_r(\bar{X}_1)}{\sqrt{RT_b/2\pi}}$$

be defined so that

$$\nu_r(\bar{X}_1) = \iint_{\Omega_2} \sin\varphi\cos\psi\left[\int_0^{\infty} c^3 f^{(2)}(c)dc\right]d\omega = \nu_i(\bar{X}_1)$$

If the model of surface interaction did not require that molecules be re-emitted with an energy corresponding to the body temperature, i.e., if thermal accommodation with the body surface were not perfect, the integral equation [1] would have to be solved by iteration to determine $f^{(2)}$. With each of the terms in the infinite sum arising from the iteration is associated the fraction of molecular flux that has struck the surface once, twice, three times and so on before incidence at the argument point. The mass flux fractions thus separated have an energy depending on some thermal accommodation coefficient and the number of collisions suffered with the body surface. An equation such as Equation [3] may be written for each *component* of the mass flux and $f^{(2)}$ would then be given as an infinite sum over collisions with the body surface.

The momentum and energy transfer at the surface are now calculated.

1 Normal momentum (pressure)

$$p = p_i + p_r \qquad p_i = m\int_{-\infty}^{\infty}\int_{-\infty}^{\infty}\int_0^{\infty} c_z^2 f(\bar{c})d\bar{c}$$

$$p(\bar{X}_1) = m\iint_{\Omega_1}\sin^2\varphi\cos^2\psi\left[\int_0^{\infty} c^4 f^{(1)}dc\right]d\omega + m\iint_{\Omega_2}\sin^2\varphi\cos^2\psi\left[\int_0^{\infty} c^4 f^{(2)}dc\right]d\omega + m\iint_{\Omega_3}\sin^2\varphi\cos^2\psi\left[\int_0^{\infty} c^4 f^{(3)}dc\right]d\omega$$

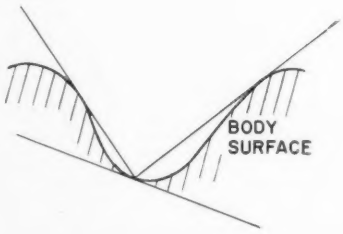

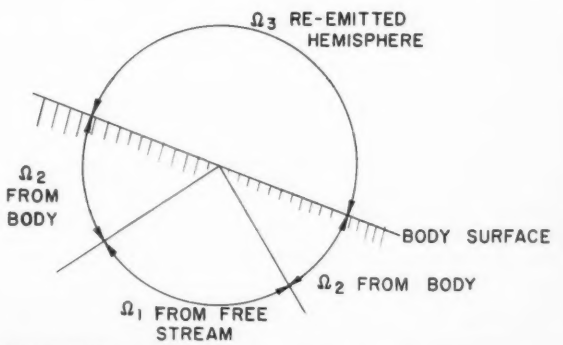

Fig. 2 Domains of integration

2 Tangential momentum (shear)

$$\tau = \tau_i = -m \int_{-\infty}^{\infty} \int_{-\infty}^{\infty} \int_{0}^{\infty} c_x c_y f(\bar{c}) d\bar{c}$$

Because of isotropic re-emission, the contribution to shear at the surface arising from re-emitted molecules is zero

$$\tau = -m \iint_{\Omega_1} \sin^2 \varphi \cos \psi \sin \psi \left[\int_0^{\infty} c^4 f^{(1)}\, dc \right] d\omega - m \iint_{\Omega_2} \sin^2 \varphi \cos \psi \sin \psi \left[\int_0^{\infty} c^4 f^{(2)}\, dc \right] d\omega$$

3 Translational energy flux

$$E_{tr} = E_{tr,i} - E_{tr,r} \qquad E_{tr,i} = \frac{1}{2} m \int_{-\infty}^{\infty} \int_{-\infty}^{\infty} \int_{0}^{\infty} c_z (\bar{c} \cdot \bar{c}) f(\bar{c}) d\bar{c}$$

$$E_{tr}(\bar{X}_1) = \frac{1}{2} m \iint_{\Omega_1} \sin \varphi \cos \psi \left[\int_0^{\infty} c^5 f^{(1)} dc \right] d\omega + \frac{1}{2} m \iint_{\Omega_2} \sin \varphi \cos \psi \left[\int_0^{\infty} c^5 f^{(2)} dc \right] d\omega - \frac{1}{2} m \iint_{\Omega_3} \sin \varphi \cos \psi \left[\int_0^{\infty} c^5 f^{(3)} dc \right] d\omega$$

In these equations, m is the mass of a single molecule. The rate of heat transfer to the body may be calculated by including the contribution to energy transfer by internal degrees of freedom. This may easily be found if equipartition of energy is assumed. The procedure is analogous to that of (2).

The case of a hemisphere or any portion of a sphere with the concave surface facing upstream provides a simple example. In this case, $K(\bar{X}_1, \bar{X}_2) = 1/4\pi R^2 = \text{constant}$, where R is the spherical radius. Since the integral kernel is constant, Equation [1] has a simple solution

$$\nu_i(\bar{X}_1) = \nu_\infty(\bar{X}_1) + \lambda \int_{A_2} \nu_\infty(\bar{X}_2)\, d\left(\frac{A_2}{R^2}\right)$$

where

$\lambda = [4\pi - A/R^2]^{-1}$

A = surface area of the body

For a hemisphere, $A = 2\pi R^2$, and thus $\lambda = 1/2\pi$.

Acknowledgment

Acknowledgment is gratefully extended to Prof. W. D. Hayes for many helpful suggestions.

References

1 Tsien, H. S., "Superaerodynamics, Mechanics of Rarefied Gases," *J. Aeron. Sci.*, vol. 13, no. 12, Dec. 1946.

2 Hayes, W. D. and Probstein, R. F., "Hypersonic Flow Theory," Academic Press, N. Y., 1959, chap. X.

3 Hildebrand, F. B., "Methods of Applied Mathematics," Prentice Hall, Englewood Cliffs, N. J., 1952, p. 430.

4 DeMarcus, W. C., "The Problem of Knudsen Flow," U. S. Atomic Energy Commission, Rep. K-1302, 1956, ORGDP.

5 Clausing, P., "On the Steady Flow of Very Rarefied Gases," *Physica*, vol. 9, 1929, p. 65. (In Dutch.)

High Temperature Critical Systems

HARRY L. REYNOLDS[1]

Lawrence Radiation Laboratory, Livermore, Calif.

NUCLEAR propulsion systems require very high temperature reactors. The temperatures required are far above the temperatures of power reactors now in use or contemplated for the near future. At the present time, reasonably satisfactory calculation procedures exist for predicting critical masses, power distributions and other neutronic properties of room temperature reactors. A large number of room temperature critical experiments have been carried out to normalize and check the calculation procedures. However, the prediction of room temperature critical masses remains risky.

If the moderating materials are at high temperature, the calculations are further complicated. Neutrons will slow down only to the temperature of the moderator where cross sections are less well known than at room temperature. The physics of the slowing down process, when the neutron energy is close to the thermal energy of the moderating material, is quite complicated because of molecular and crystalline effects. This slowing down process must be better understood in order to accurately predict cold-to-hot critical mass differences. Doppler broadening of resonance cross sections will increase, adding to the complications. Temperature differences in the reactor will result in neutrons increasing in energy when they pass from a cold to a hot region. This is particularly true in some propulsion reactors which have reflectors very much colder than the core. Thus neutrons must be followed not only from the fission energy to thermalization, but also from one thermal energy to another. Until recently, very little experimental information existed to assist in the evaluation of criticality calculations at elevated temperatures.

Over the past few years, this laboratory has been involved in the measurement of critical masses for "clean" systems at room temperature. A "clean" system is a critical assembly of very simple geometry, such as a rectangular parallelepiped containing only the fuel and moderating materials. Great efforts are made to remove extraneous factors from the measurement, such as neutron reflection from the building floor and walls, and the effect of nonhomogeneities. The critical mass of the resulting system can be calculated using existing procedures without approximations, and the validity of the physics of the calculation can be verified. Until these measurements were made, most existing critical measurements were of systems duplicating proposed reactors. The complexities of these systems made it difficult to determine whether errors in calculations were due to the reduction of the complex system to a calculable system or to the calculation procedure itself.

The moderating materials used in these "clean" experiments

Presented at the ARS 14th Annual Meeting, Washington, D. C., Nov. 16–20, 1959.

[1] Assistant Division Leader.

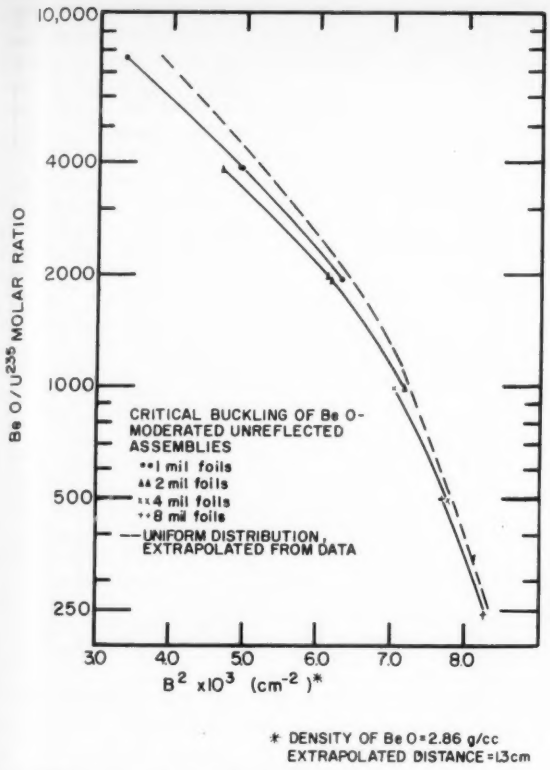

Fig. 1 Typical results for bare unreflected systems of homogeneous BeO and U^{235}

were graphite, beryllium and beryllium oxide, all useful materials for high temperature propulsion reactors. Typical results for bare unreflected systems of homogeneous BeO and U^{235} are shown in Fig. 1. The BeO density is 2.86 gm per cc. The BeO to U^{235} atomic ratio is plotted vs. B^2, the buckling. The buckling is defined by the following wave equation

$$\nabla^2\phi + B^2\phi = 0$$

where ϕ is the neutron flux. From this curve, one can obtain the critical mass for any shape and size unreflected BeO moderated system with U^{235} mixed homogeneously with the moderator. For a rectangular system

$$B^2 = \left(\frac{\pi}{a + 2\lambda}\right)^2 + \left(\frac{\pi}{b + 2\lambda}\right)^2 + \left(\frac{\pi}{c + 2\lambda}\right)^2$$

where

a, b, c = dimensions of the system
λ = extrapolation length

The experiments were done with thin uranium foils. The flux inside of the foils is less than at the exterior, owing to absorption of the neutrons as they progress into the foils. This is known as self-shielding. The effect of the self-shielding was evaluated by first determining the buckling with a given foil thickness with the foils spaced uniformly. The foil thickness was then halved together with the spacing. An extrapolation to a homogeneous distribution of fuel could then be made. This data is shown in the figure.

A special facility known as "Hot Box" has been constructed at Jackass Flats at the Nevada test site to study high temperature critical assemblies. In all essentials, the facility duplicates the usual critical assembly facility except that it is contained in a large oven or enclosure which can be elevated in temperature with a selected atmosphere. Uranium foils,

Fig. 2 Nevada test site showing Hot Box at left and control building at right

Fig. 3 Exterior of the oven

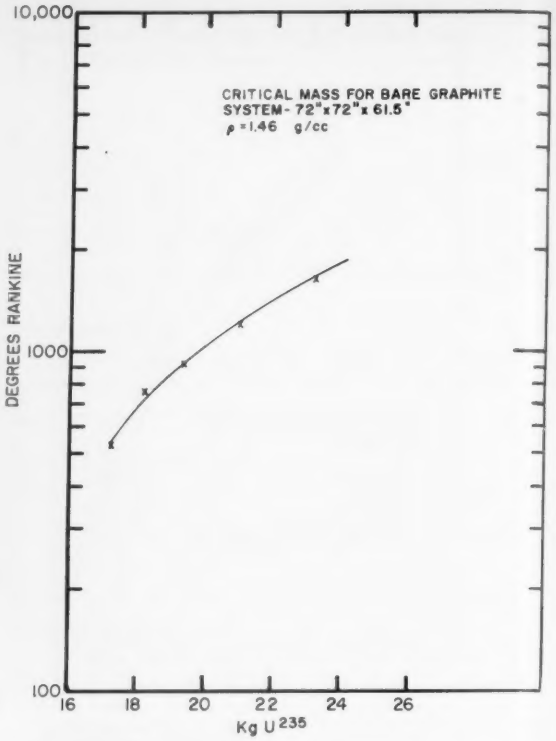

Fig. 5 Results of graphite moderated core 72.0 × 72.0 × 61.5 in. Graphite density 1.46 gm per cc. Each gram of U^{235} associated with 0.85 gm of stainless steel and 0.07 gm of U^{238}

Fig. 4 Inside of oven with graphite system partially assembled

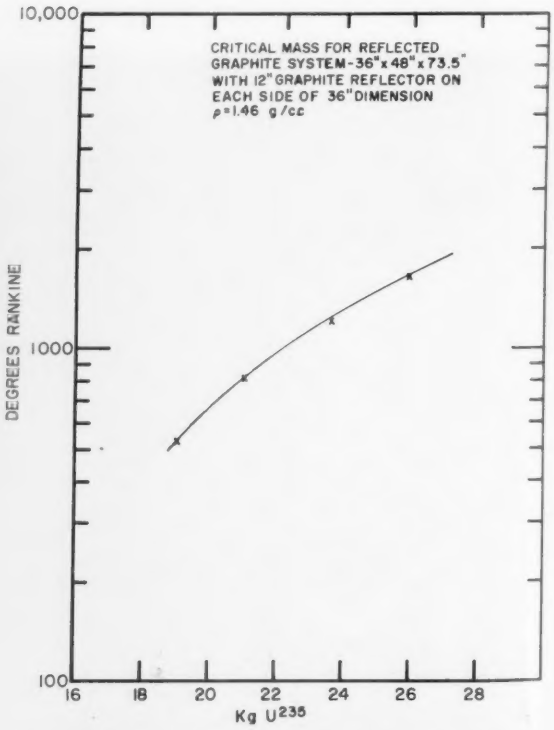

Fig. 6 Graphite moderated core 36.0 × 48.0 × 73.5 in. with 12-in. reflector

together with blocks of moderating materials, are assembled on a low mass table at room temperature, and then raised to higher temperature as a unit by passing externally heated gas through the moderator and oven. Critical masses and power distributions may be measured from room temperature up to 1200 F. Although this temperature does not approach that required for propulsion reactors, it is sufficiently high to determine if calculation procedures are adequate for estimating the effect of temperature changes. If the change in critical mass from room temperature to 1200 F can be properly calculated, there should be no difficulty in extending the calculations to higher temperatures.

Some of the proposed experiments which can be carried out with the Hot Box are:

1 The critical mass and fluxes of bare nonreflected systems with various solid moderators will be determined as a function of temperature.

2 The critical mass and fluxes of reflected systems with various moderators, reflectors, porosities and geometries will be determined as a function of temperature.

3 The effect of nonuniform temperature distribution upon critical mass and power distribution will be studied.

4 The effect of structural poisons, such as zirconium or stainless steel, will be observed.

5 Methods of reactivity temperature compensation will be studied.

6 Temperature coefficients of reactivity will be measured.

The test site is shown in Fig. 2. The critical assembly is located 1300 ft to the left of the control building. The exterior of the oven is shown in Fig. 3. The oven walls are approximately 0.2 mean-free-path thick, so neutron reflection from the walls is not a factor for consideration. The low mass table in the oven which supports the critical assemblies and isolates them from the floor is large enough for a critical assembly 10 × 10 × 8-ft high. Heat can be added to the assemblies at the rate of 600 kw, and the largest systems require approximately 12 hr to be heated to 1200 F. The maximum gas flow rate through an assembly is 30,000 cfm.

The inside of the oven is shown in Fig. 4. A partially assembled graphite system is on the low mass table. The control vanes, which consist of boron nitride encased in stainless steel, can be seen entering the graphite from the top. The number of vanes in each arm of the cross can be varied, but all vanes in an arm move together. The stainless steel encased uranium foils are inserted in the slots between the graphite blocks. Wires pass from the foils through the oven walls, so that foils may be removed from outside the oven. Heating and cooling air passes vertically through holes in the graphite. The tube in the center of the system is for the insertion and removal of a neutron source.

The experimental procedure is as follows. The critical mass at room temperature is determined for a particular system. An estimate of the additional fuel that will be required for criticality at the elevated temperature is made. Then the additional fuel is added with the control vanes inserted. The reactor is heated to the desired temperature and the control vanes removed. If there is too much fuel present for the system to be just critical at the elevated temperature, fuel elements can be removed by pulling wires from outside the oven. If the amount of fuel is not sufficient for criticality, the temperature can be reduced until the system is critical. Power distribution measurements can be made by irradiating uranium foils in the reactor and then counting the foils for the induced activity.

Criticality in the Hot Box was attained for the first time in February 1959. The concept of studying "clean" systems has been continued in this facility. Since then a graphite moderated bare unreflected system, a graphite moderated graphite reflected system, and several BeO moderated bare unreflected systems have been studied. At the present time a BeO moderated graphite reflected system is under study. The graphite reflector is maintained at a temperature 800 deg lower than the BeO core. Further studies of more complicated systems will be underway shortly.

Results for the two graphite measurements will be given here. The first system was graphite moderated with dimensions of 72.0 × 72.0 × 61.5 in. The graphite density was 1.46 gm per cc. Each gram of U^{235} was associated with 0.85 gm of stainless steel and 0.07 gm of U^{238}. The results are shown in Fig. 5. The temperature is plotted in degrees Rankine vs. the critical mass in kilograms of U^{235}. Data were obtained at five different temperatures. The critical mass at 1200 F is 35 per cent larger than at room temperature if the fuel is in the form of 2-mil thick uranium foils. Consideration must be given to the fact that as the temperature increases the effective cross section of the uranium decreases; thus, the self-shielding of the foil will decrease with temperature. At the higher temperature there are effectively more uranium atoms per foil, since the absorption per atom is not as large. For a homogeneous system, the necessary uranium increase to become critical at the high temperature would be larger than the 35 per cent by approximately 10 per cent.

The second system was a graphite moderated core 36.0 × 48.0 × 73.5 in. with a 12-in. reflector placed on each side of the 36-in. dimension of the core. The graphite density was the same, and the fuel was associated with the same impurities. The results of this experiment are given in Fig. 6. In this case the increase in temperature required an increase in U^{235} fuel content of 36 per cent. Again the fuel was in the form of 2-mil thick foils.

The results of these measurements should be useful to anyone designing reactors for propulsion. Further details concerning any of the measurements or calculations mentioned may be obtained from the author.

Aerodynamic Heating Charts for Solid Propellant Rocket Motors

GERALD R. GUINN[1]

Thiokol Chemical Corp., Redstone Division, Huntsville, Ala.

The solutions for transient temperatures in a semi-infinite composite solid when the heat input is approximated by a fifth-degree polynomial of time are presented. These solutions have been numerically evaluated and are presented in charts from which the temperature history at several locations in a typical liner-propellant combination can be computed for a given aerodynamic heating input.

KAYE and Yeh (1)[2] have presented a method of determining the temperatures in an insulated flat plate for unidirectional heat flow when the heat flux is a constant or a linear function of time. Using the design charts of (1), Sutton (2) has suggested a method of solution for an aerodynamic heating input that is expressed as a fifth-degree polynomial function of time. The charts of (1) can be used to compute the temperatures of the chamber wall of a large solid propellant rocket motor when the aerodynamic heat input is small and the chamber wall is thermally thick. However, if the wall is thermally thin enough to offer little resistance to heat flow, the insulated flat plate solution is not applicable because of the larger proportion of heat escaping to the liner and the propellant grain.

Wassermann (3,4) has obtained a solution for a two-layer semi-infinite solid; however, the heat input of his solution represented a triangular function of time. Since the heat input of a missile may assume functions that are not conveniently represented by the triangular heat input, it became necessary to arrive at a solution with a greater freedom of choice for the input function.

A solution is presented herein that will compute the temperature in the liner and propellant grain for a heat input that is expressed as a fifth-degree polynomial in time. It is assumed that there is no thermal lag in the chamber wall and that the thermal layer in the propellant is thin relative to the radius of the motor.

Discussion

The coordinates of the system are shown in Fig. 1. The equations representing the temperatures in the liner and the propellant are

$$\frac{\partial T_1(x, t)}{\partial t} = \alpha_1 \frac{\partial^2 T_1(x, t)}{\partial x^2} \qquad (0 < x \leq a) \qquad [1]$$

$$\frac{\partial T_2(x, t)}{\partial t} = \alpha_2 \frac{\partial^2 T_2(x, t)}{\partial x^2} \qquad (a \leq x < \infty) \qquad [2]$$

The boundary condition at the heated surface is

$$-k_1[\partial T_1(0, t)/\partial x] = Q(t) \qquad [3]$$

where the heat input is the fifth-degree polynomial

$$Q(t) = \sum_{s=0}^{5} q_s t^s \qquad [4]$$

The conditions at the interface for no interface resistance to heat flow are

$$k_1 \frac{\partial T_1(a, t)}{\partial x} = k_2 \frac{\partial T_2(a, t)}{\partial x} \qquad [5]$$

$$T_1(a, t) = T_2(a, t) \qquad [6]$$

The condition in the semi-infinite propellant is

$$T_2(x, t) = 0 \qquad (x \to \infty) \qquad [7]$$

The initial condition is

$$T_1(x, 0) = T_2(x, 0) = 0 \qquad [8]$$

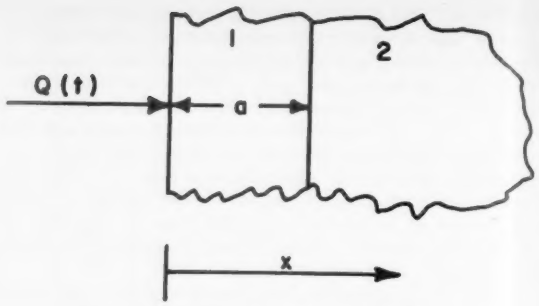

Fig. 1 Nondimensional heat flow system

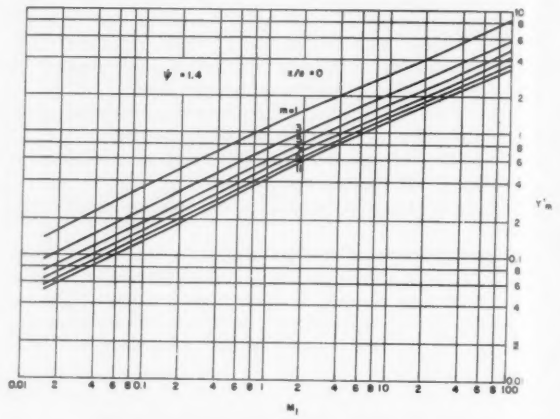

Fig. 2 Parameters at case-liner interface

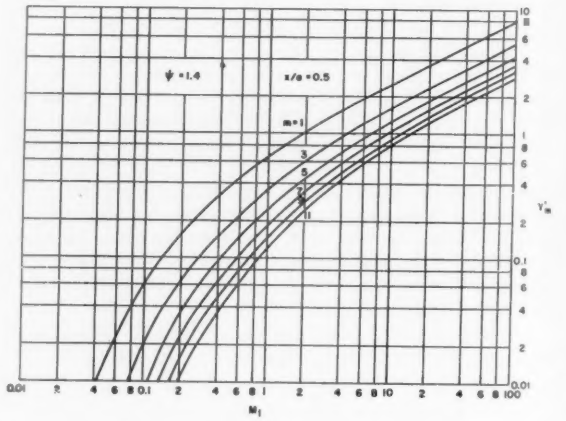

Fig. 3 Parameters at liner midplane

Received March 3, 1960.

[1] Analytical Engineer. Member ARS.

[2] Numbers in parentheses indicate References at end of paper.

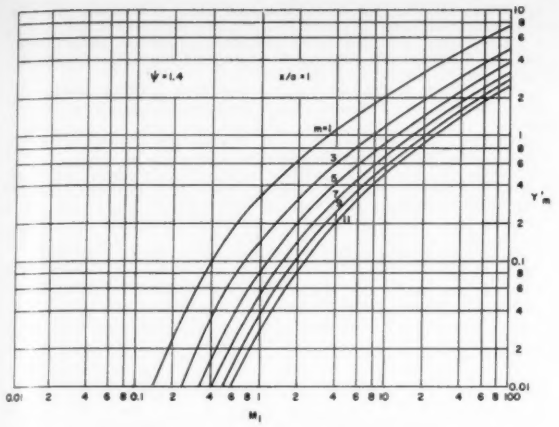

Fig. 4 Parameters at liner-propellant interface

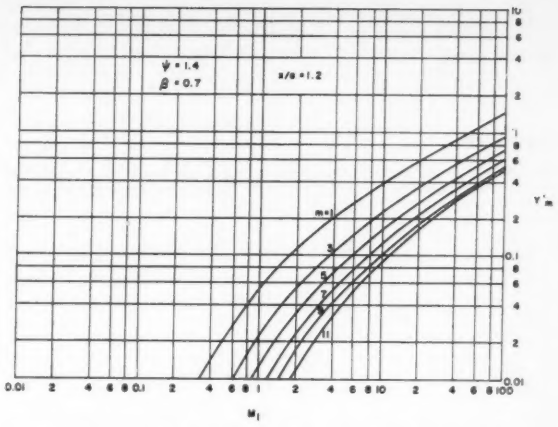

Fig. 5 Parameters in propellant at 20 per cent of liner thickness

The solution to Equations [1 through 8] was obtained through the use of the Laplace transforms (5). The transformed temperature in the liner is

$$\bar{T}_1(x, p) = \frac{\bar{Q}(p)}{k_1 q_1} \times \left[\left(\frac{\cosh aq_1 + \psi \sinh aq_1}{\sinh aq_1 + \psi \cosh aq_1} \right) \cosh xq_1 - \sinh xq_1 \right] \quad [9]$$

and for the propellant

$$\bar{T}_2(x, p) = \frac{\bar{Q}(p)e^{-q_s(x-a)}}{k_1 q_1} \times \left[\left(\frac{\cosh aq_1 + \psi \sinh aq_1}{\sinh aq_1 + \psi \cosh aq_1} \right) \cosh aq_1 - \sinh aq_1 \right] \quad [10]$$

In order to convert back into T,t coordinates, it is necessary to place a restriction upon the relative values of the thermal properties of the two materials. Since the liner is the better insulator of the two, the restriction will therefore be $k_2 > k_1$. The inverse Laplace transforms of Equations [9 and 10] give the final form for the temperatures. The temperature in the liner is

$$T_1(x, t) = \frac{a}{k_1} \sum_{s=0}^{5} q_s t^s Y_{2s+1} + T_i \quad [11]$$

and in the propellant

$$T_2(x, t) = \frac{2a}{(\psi - 1)k_1} \sum_{s=0}^{5} q_s t^s Y''_{2s+1} + T_i \quad [12]$$

where T_i is now the constant initial temperature and

$$Y'_m = 2^m \left(\frac{m-1}{2} \right)! \sqrt{M_1} \left[\sum_{n=0}^{\infty} \frac{(-1)^n}{A^n} i^m \operatorname{erfc} \frac{2n + x/a}{2\sqrt{M_1}} - \sum_{n=0}^{\infty} \frac{(-1)^n}{A^{n+1}} i^m \operatorname{erfc} \frac{2n + 2 - x/a}{2\sqrt{M_1}} \right] \quad [13]$$

$$Y''_m = 2^m \left(\frac{m-1}{2} \right)! \sqrt{M_1} \times \sum_{n=0}^{\infty} \frac{(-1)^n}{A^{n+1}} i^m \operatorname{erfc} \frac{2n + 1 + \beta(x/a - 1)}{2\sqrt{M_1}} \quad [14]$$

when the index $m = 1, 3, 5$, etc., and where i^m erfc is the mth repeated integral of the complementary error function.

To facilitate computation, the functions Y'_m and Y''_m have been numerically evaluated for $\beta = 0.7$ and $\psi = 1.4$. These values were selected as being representative of the thermal properties of composite high energy solid propellants and their corresponding liners. See Figs. 2–6.

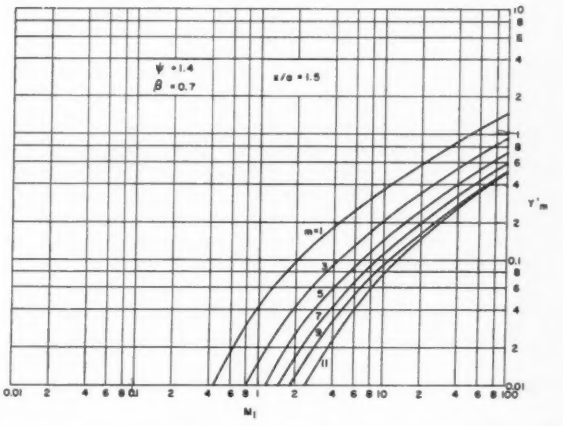

Fig. 6 Parameters in propellant at 50 per cent of liner thickness

Investigation of Equation [13] will reveal that if an insulated flat plate is assumed ($k_2 = 0$), Y'_m will be identical with the Z_m function of (1 and 6). It is also interesting to note from the charts that for $M_1 < 0.1$, the two functions converge for $x/a = 0$, because the heat escaping to the propellant does not affect the surface temperature in such a short time; therefore the liner is effectively an insulated plate.

Nomenclature

α	=	thermal diffusivity
x	=	distance from heated surface
t	=	time
T	=	temperature
Q	=	heat rate per unit area
q_s	=	arbitrary constant
a	=	liner thickness
$\bar{T}$	=	transformed temperature
p	=	transformed time
$\bar{Q}$	=	transformed heat rate
k	=	thermal conductivity

$\psi = (k_2/k_1)\sqrt{\alpha_1/\alpha_2}$
$A = (\psi + 1)/(\psi - 1)$
$M_1 = \alpha_1 t/a^2$
$\beta = \sqrt{\alpha_1/\alpha_2}$

References

1 Kaye, J. and Yeh, V. M., "Design Charts for Transient Temperature Distribution Resulting From Aerodynamic Heating at Supersonic Speeds," *J. Aeron. Sci.*, vol. 22, 1955, pp. 755–786.

2 Sutton, G. W., "On One-Dimensional Heat Conduction With an Arbitrary Heating Rate," *J. Aeron. Sci.*, vol. 24, 1957, pp. 854–855.

3 Wassermann, B., "One-Dimensional Heat Conduction Into a Double-Layer Slab Subjected to a Linear Heat Input for a Small Time Interval," *J. Aeron. Sci.*, vol. 24, 1957, pp. 924–925.

4 Wassermann, B. and Nolan, E. J., "Heat Flow in a Composite Slab," General Electric Co., Thermodynamics Technical Memo no. 44, May 7, 1957.

5 Carslaw, H. S. and Jaeger, J. G., "Conduction of Heat in Solids," Oxford University Press, London, second ed., 1959 chap. 12.

6 Jordan, W. Y., "An Analytical Procedure for Calculating Transient Temperature Distribution in Flat Plates Exposed to High Heating Rates," Army Ballistics Missile Agency Rep. DS-TN-97, Oct. 3, 1957.

Stress-Strain Equations for Case-Bonded Solid Propellant Grains[1]

CHARLES H. PARR[2]

Rohm & Haas Co., Redstone Arsenal Research Division, Huntsville, Ala.

Equations expressing elastic stresses and strains in a three-material, composite, hollow, circular cylinder representing a case-bonded propellant grain, liner and motor case are developed for loading conditions consisting of internal pressure, arbitrary radial temperature gradient and volumetric changes.

IN THE past few years a number of solutions for the stress and/or strain distribution in a simplified model of a propellant grain under a variety of loading conditions have been published (1–5).[3] All of these solutions were typified by the assumptions of axial symmetry, infinite length and infinitesimal elasticity. The usefulness of these solutions is enhanced by the use of stress concentration factors, such as those found by Ordahl and Williams (6) and Williams (7).

The present solution of the stress-strain distribution in an infinite, elastic, hollow, circular cylinder with a three-material composite wall was derived in a general form which included loadings of internal pressure, volume change and axially symmetric temperature gradients.[4] The model used in the analysis consisted of three axially symmetric cylinders bonded at their respective interfaces which correspond to the motor case, liner and propellant grain of the rocket. The solution was assumed to be valid in the region of the cylindrical section of the motor which is free of end effects. The end effects caused by both mechanical and thermal deviations from the model would be principally confined to distances of about one web thickness from each end of the motor. There were no limitations on the thickness of the liner and case, such as have been imposed in other analyses. Included in the solution was an axial stress term which could be varied to account for differences in nozzle diameter and which could account approximately for axial acceleration forces. All physical properties and dimensions of the three materials were arbitrary, although no temperature dependence was allowed. The usual assumptions of infinitesimal elasticity were inherent in the analysis.

Received March 2, 1960.

[1] This work was sponsored by the Army Ordnance Corps under Contract no. DA-01-021-ORD 5135.

[2] Scientist, Engineering Research Group.

[3] Numbers in parentheses indicate References at end of paper.

[4] The general solution to the thermal stress portion of this problem was evidently first published by Gatewood (8).

Analysis

Consider an elastic isotropic material which undergoes a linear dimensional change expressed by a function

$$\beta = \delta + \alpha T$$

where

- δ = linear expansion factor (for instance, dimensional change caused by a phase change)
- αT = change in linear dimension due to expansion with temperature
- α = linear coefficient of thermal expansion
- T = temperature change from some initial datum temperature distribution

For composite bodies, this datum temperature is most conveniently taken as that at which no stresses are induced in the body by differential thermal expansion. This condition cannot always be satisfied with a uniform temperature distribution for a composite body of three or more materials, and the factor δ may be used to adjust the stress state to the selected uniform base temperature. The stress-strain relations may be written

$$\epsilon_\theta - \beta = \frac{\sigma_\theta}{E} - \nu\left(\frac{\sigma_r}{E} + \frac{\sigma_z}{E}\right)$$

$$\epsilon_r - \beta = \frac{\sigma_r}{E} - \nu\left(\frac{\sigma_\theta}{E} + \frac{\sigma_z}{E}\right)$$

$$\epsilon_z - \beta = \frac{\sigma_z}{E} - \nu\left(\frac{\sigma_r}{E} + \frac{\sigma_\theta}{E}\right) \qquad [1]$$

where

- ϵ = strain related to dimensional change
- $(\epsilon - \beta)$ = strain related to stress
- σ = stress
- E = elastic modulus
- ν = Poisson's ratio

Subscripts θ, r, z refer to a cylindrical coordinate system.

It can be shown (9) that in an infinite circular cylinder subject to nonshear boundary tractions and temperature gradients independent of θ and z, the cylinder is in a state of generalized plane strain, and the stresses may be expressed in the form

$$\frac{\sigma_r}{E} = B - D\frac{R^2}{r^2} - \Delta \qquad [2]$$

$$\frac{\sigma_\theta}{E} = B + D\frac{R^2}{r^2} + \Delta - \frac{\beta}{1-\nu} \qquad [3]$$

where

B, D = constants to be evaluated from the boundary conditions

R = normalizing radius

$$\Delta = \frac{1}{(1-\nu)r^2}\int_{r_i}^{r} \beta\rho d\rho$$

r_i = inner radius

The strains corresponding to the stresses expressed by Equations [2 and 3] are, from Equation [1]

$$\epsilon_\theta = (1+\nu)[(1-2\nu)B + D(R^2/r^2) + \Delta] - \nu\epsilon_z \quad [4]$$

$$\epsilon_r = (1+\nu)\left[(1-2\nu)\,B - D\frac{R^2}{r^2} - \Delta + \frac{\beta}{1-\nu}\right] - \nu\epsilon_z \quad [5]$$

The axial strain ϵ_z is constant and must be evaluated from the boundary conditions. The axial stress σ_z may also be expressed from Equations [1, 2 and 3] as

$$\frac{\sigma_z}{E} = \epsilon_z - \frac{\beta}{1-\nu} + 2\nu B \quad [6]$$

Equations [1 through 6] apply to each of the three layers of the composite cylinder resulting in seven unknown constants to be evaluated: B_1, D_1, B_2, D_2, B_3, D_3 and ϵ_z. The axial strain ϵ_z is a constant and the same constant for all three materials. This, in effect, means that plane sections remain plane.

Using subscripts 1, 2 and 3 to indicate inner (propellant), middle (liner) and outer (case) layers, respectively, the following boundary conditions may be written to determine the seven unknown constants

$$(\sigma_r)_1 = -p \qquad r = a \quad [7a]$$

$$(\sigma_r)_1 = (\sigma_r)_2 \qquad r = b \quad [7b]$$

$$(\epsilon_\theta)_1 = (\epsilon_\theta)_2 \qquad r = b \quad [7c]$$

$$(\sigma_r)_2 = (\sigma_r)_3 \qquad r = c \quad [7d]$$

$$(\epsilon_\theta)_2 = (\epsilon_\theta)_3 \qquad r = c \quad [7e]$$

$$(\sigma_r)_3 = 0 \qquad r = d \quad [7f]$$

$$2\pi\int_a^d \sigma_z\rho d\rho = \pi\lambda p a^2 \quad [7g]$$

Here p is the internal pressure in the motor, and a, b, c and d are radii of the propellant inner surface, the propellant-liner interface, the liner-case interface and case outer surface, respectively. The indicated integration in boundary condition [7g] must be performed separately for each material, the sum of the three integrals being the indicated integral.

Boundary conditions [7b, 7c, 7d and 7e] insure continuity of the body at the interfaces. Boundary condition [7g] insures equilibrium of the composite cylinder in the axial direction. The factor λ is used to adjust the longitudinal forces in a motor system. For instance, $\lambda = 1$ represents an unvented pressure vessel, whereas $\lambda = 0$ represents a fully vented vessel. For a more detailed discussion see (3) p. 33.

Applying boundary conditions [7] to Equations [2, 4 and 6], and letting the normalizing radius R equal b results in the following relations between the constants

$$B_1 - \frac{b^2}{a^2}D_1 = -\frac{p}{E_1} \quad [8a]$$

$$B_1 - D_1 - \frac{E_2}{E_1}B_2 + \frac{E_2}{E_1}D_2 = \Delta_1 \quad [8b]$$

$$(1+\nu_1)(1-2\nu_1)B_1 + (1+\nu_1)D_1 - (1+\nu_2)(1-2\nu_2)B_2 - (1+\nu_2)D_2 + (\nu_2-\nu_1)\epsilon_z = -(1+\nu_1)\Delta_1 \quad [8c]$$

$$B_2 - D_2\frac{b^2}{c^2} - \frac{E_3}{E_2}B_3 + \frac{E_3}{E_2}D_3\frac{b^2}{c^2} = \Delta_2 \quad [8d]$$

$$(1+\nu_2)(1-2\nu_2)B_2 + (1+\nu_2)D_2\frac{b^2}{c^2} - (1+\nu_3)(1-2\nu_3)B_3 - (1+\nu_3)D_3\frac{b^2}{c^2} + (\nu_3-\nu_2)\epsilon_z = -(1+\nu_2)\,\Delta_2 \quad [8e]$$

$$B_3 - D_3(b^2/d^2) = \Delta_3 \quad [8f]$$

$$\nu_1 B_1\frac{E_1}{E_3}\left(1-\frac{a^2}{b^2}\right) + \nu_2 B_2\frac{E_2}{E_3}\left(\frac{c^2}{b^2}-1\right) + \nu_3 B_3\left(\frac{d^2}{b^2}-\frac{c^2}{b^2}\right) + \frac{\epsilon_z}{2}\left[\frac{E_1}{E_2}\left(1-\frac{a^2}{b^2}\right) + \frac{E_2}{E_3}\left(\frac{c^2}{b^2}-1\right) + \left(\frac{d^2}{b^2}-\frac{c^2}{b^2}\right)\right] = \frac{\lambda p a^2}{2E_3 b^2} + \frac{E_1}{E_3}\Delta_1 + \frac{E_2}{E_3}\frac{c^2}{b^2}\Delta_2 + \frac{d^2}{b^2}\Delta_3 \quad [8g]$$

---

where

$$\Delta_1 = \frac{1}{(1-\nu_1)b^2}\int_a^b \beta\rho d\rho$$

$$\Delta_2 = \frac{1}{(1-\nu_2)c^2}\int_b^c \beta\rho d\rho$$

$$\Delta_3 = \frac{1}{(1-\nu_3)d^2}\int_c^d \beta\rho d\rho$$

These seven equations may be solved directly for the seven constants (B_1, D_1, B_2, D_2, B_3, D_3, ϵ_z) in terms of the parameters λ, p/E_1, E_2/E_1, E_2/E_3, a/b, c/b, d/b, ν_1, ν_2, ν_3, Δ_1, Δ_2 and Δ_3. Equations [2 through 6] can then be used to determine the stresses and strains in each layer. For hand calculation this process is time consuming and can be more easily carried out on an electronic digital computer using matrix methods. Results of a study to determine the effects of liner physical properties on the stress-strain distribution in propellant grains were obtained in this manner (10).

References

1 Rohm & Haas Co., "Quarterly Progress Report on Interior Ballistics," no. P-55-1, Feb. 1955. (*Confidential*)

2 Rohm & Haas Co., "Quarterly Progress Report on Weapons Research," no. P-56-12, July 1956. (*Confidential*)

3 Rohm & Haas Co., "Quarterly Progress Report on Weapons Research," no. P-57-5, April 1957.

4 Zwick, S. A., "Thermal Stresses in an Infinite, Hollow Case-Bonded Cylinder," JET PROPULSION, vol. 27, no. 8, Aug. 1957, p. 872.

5 Ungar, E. E. and Shaffer, B. W., "Thermal Stresses in Long Cylindrical Case-Bonded Propellant Grains," New York University, College of Engineering Research Division, Sept. 1958.

6 Ordahl, D. D. and Williams, M. L., "Preliminary Photoelastic Design Data for Stresses in Rocket Grains," JET PROPULSION, vol. 27, no. 6, June 1957, p. 657.

7 Williams, M. L., "Some Thermal Stress Design Data for Rocket Grains," ARS JOURNAL, vol. 29, no. 4, April 1959, p. 260.

8 Gatewood, B. E., "Note on the Thermal Stresses in a Long Circular Cylinder of m + 1 Concentric Materials," *Quart. Appl. Math.*, vol. 6, 1948, p. 84.

9 Timoshenko, S. and Goodier, J. N., "Theory of Elasticity," McGraw-Hill, N. Y., 2nd ed., 1951, article 135.

10 Rohm & Haas Co., "Quarterly Progress Report on Engineering Research," no. P-59-23, Jan. 1960.

Conformal Transformation of a Solid Propellant Grain With a Star-Shaped Internal Perforation Onto an Annulus[1]

HOWARD B. WILSON Jr.[2]

Rohm & Haas Co., Redstone Arsenal Research Division, Huntsville, Ala.

THE ANALYSIS of stress and temperature problems for solid propellant rocket motor grains may be simplified by conformally mapping the complicated geometry of the grain into a more tractable form. This note describes the approximate transformation onto an annulus of the cross section of a cylindrical grain having a circular external boundary and an n-pointed star-shaped internal boundary, such as is employed in case-bonded applications. The transformation gives a particularly good representation in the vicinity of the star tip which is of primary importance in stress analysis problems.

The transformation which conformally maps the z plane with a hole having n axes of symmetry onto the ζ plane with a circular hole is of the form

$$z = A\zeta + \frac{B}{\zeta^{n-1}} + \frac{C}{\zeta^{2n-1}} + \frac{D}{\zeta^{3n-1}} + \frac{E}{\zeta^{4n-1}} + \dots \qquad [1]$$

where

$$z = x + iy$$
$$\zeta = \xi + i\eta = \rho e^{i\theta}$$

When the coefficients $A, B, C, \dots$ are of comparable absolute magnitude and the absolute value of ζ is greater than 1, the terms

$$\frac{B}{\zeta^{n-1}} + \frac{C}{\zeta^{2n-1}} + \frac{D}{\zeta^{3n-1}} + \frac{E}{\zeta^{4n-1}} + \dots$$

may be neglected, and circles in the ζ plane are mapped approximately onto circles in the z plane. Therefore the same transformation may be used to map onto an annulus a propellant grain having an internal boundary with n star points and a circular outer boundary. The circle $|\zeta| = 1$ is mapped onto the internal boundary of the grain and the circle $|\zeta| = R_3/A$ is mapped approximately onto the circle $|z| = R_3$ which corresponds to the external boundary of the grain. The transformation is illustrated in Fig. 1.

In this note, only the four-term mapping function

$$z = A\zeta + \frac{B}{\zeta^{n-1}} + \frac{C}{\zeta^{2n-1}} + \frac{D}{\zeta^{3n-1}} \qquad [2]$$

is considered. The coefficients A through D are determined from the following conditions:

1 $z = R_1$, which corresponds to the tip of the star point, is mapped onto $\zeta = 1$.

2 $z = R_2 e^{i\pi/n}$, which corresponds to the tip of the inverse star point, is mapped onto $\zeta = e^{i\pi/n}$.

3 The ratio of the width of the star point at two locations is specified.

4 The radius of curvature at the star tip is specified.

Condition 1 gives

$$R_1 = A + B + C + D \qquad [3]$$

Condition 2 gives

$$R_2 e^{i\pi/n} = Ae^{i\pi/n} + \frac{B}{e^{i\pi(n-1)/n}} + \frac{C}{e^{i\pi(2n-1)/n}} + \frac{D}{e^{i\pi(3n-1)/n}} =$$

$$(A - B + C - D)e^{i\pi/n}$$

Received March 9, 1960.

[1] This work was sponsored by the U. S. Army Ordnance Corps under Contract no. DA-01-021-ORD 5135.

[2] Scientist, Engineering Research Group.

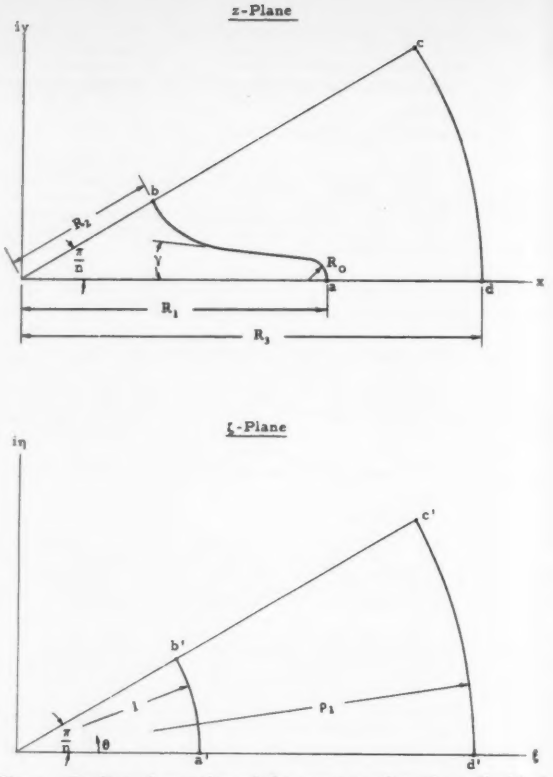

Fig. 1 Conformal mapping of the cross section of a cylindrical grain having a circular external boundary and an n-pointed star-shaped internal boundary onto an annulus

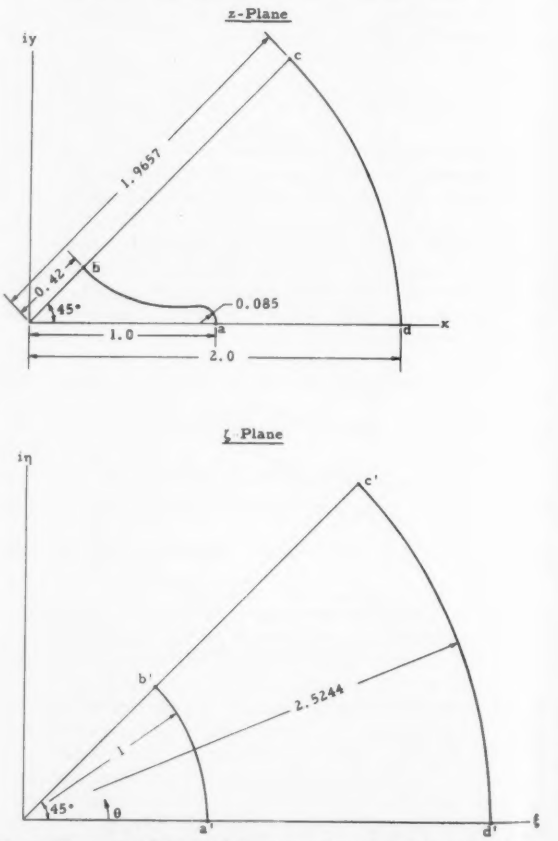

Fig. 2 Example of the conformal mapping of a grain with a four-pointed star onto an annulus

or

$$R_2 = A - B + C - D \qquad [4]$$

Let y_k be the imaginary part of the image in the z plane of the point $\zeta = e^{i\theta_k}$. Then

$$y_k = A \sin(\theta_k) - B \sin[(n-1)\theta_k] - C \sin[(2n-1)\theta_k] - D \sin[(3n-1)\theta_k]$$

Let $0 < \theta_1 < \theta_2 < \pi/n$, and let β be a number greater than or equal to 1 where $\beta = y_2/y_1$. Then condition 3 gives

$$A[\sin(\theta_2) - \beta \sin(\theta_1)] - B\{\sin[(n-1)\theta_2] - \beta \sin[(n-1)\theta_1]\} - C\{\sin[(2n-1)\theta_2] - \beta \sin[(2n-1)\theta_1]\} - D\{\sin[(3n-1)\theta_2] - \beta \sin[(3n-1)\theta_3]\} = 0 \qquad [5]$$

The choice of θ_1, θ_2 and β is arbitrary within the limits specified in the foregoing. For a given choice of θ_1 and θ_2, the angle 2γ between opposite sides of the star point is zero when $\beta = 1$ and increases with β.

Since the circle $\zeta = e^{i\theta}$, $0 \leq \theta \leq 2\pi$, is mapped onto the internal boundary of the propellant grain, the radius of curvature at any point of this boundary may be expressed as a function of θ. If δ is the radius of curvature at any point then

$$\delta = [(x')^2 + (y')^2]^{3/2}/[x'y'' - y'x'']$$

The primes denote differentiation with respect to θ. For $\theta = 0$

$$x' = y'' = 0$$

$$x'' = -[A + (n-1)^2 B + (2n-1)^2 C + (3n-1)^2 D]$$

$$(y')^2 = [A - (n-1)B - (2n-1)C - (3n-1)D]^2$$

Therefore if R_0 is the radius of curvature at the tip of the star point, condition 4 gives

$$R_0 = \frac{[A - (n-1)B - (2n-1)C - (3n-1)D]^2}{[A + (n-1)^2 B + (2n-1)^2 C + (3n-1)^2 D]} \qquad [6]$$

The solution of Equations [3–6] is straightforward. Since Equations [3, 4 and 5] are linear, they may be solved for B, C and D in terms of A. These solutions substituted into Equation [6] give a quadratic equation for the determination of A. For each of the two values of A resulting from the solution of the quadratic, a set of B, C and D values may be determined which will satisfy all the conditions specified. Since the smaller value of A usually gives a mapping function which is not conformal, the larger value of A is chosen. B, C and D are then determined from Equations [3, 4 and 5].

Consider a numerical example for a grain with a four-pointed star. Let $R_0 = 0.085$, $R_1 = 1.0$, $R_2 = 0.42$, $R_3 = 2.0$, $\beta = 1.0$, $\theta_1 = 25$ deg and $\theta_2 = 30$ deg. Equations [3–6] become

$$A + B + C + D = 1.0$$

$$A - B + C - D = 0.42$$

$$A[\sin(30°) - \sin(25°)] - B[\sin(90°) - \sin(75°)] - C[\sin(210°) - \sin(175°)] - D[\sin(330°) - \sin(275°)] = 0$$

and

$$0.085[A + 9B + 49C + 121D] = [A - 3B - 7C - 11D]^2$$

Solution of these equations as outlined gives

$$A = 0.7855$$
$$B = 0.2758$$
$$C = -0.0755$$
$$D = 0.0142$$

A plot of the internal boundary of the propellant grain is shown in Fig. 2. The radius of curvature near the star tip is nearly constant, and the sides of the star point are parallel. The circle $\zeta = \rho_1 e^{i\theta}$, $0 \leq \theta \leq 2\pi$, is mapped onto the external grain boundary of radius R_3. The value of ρ_1 may be determined by solving the equation

$$R_3 = A\rho_1 + \frac{B}{\rho_1^3} + \frac{C}{\rho_1^7} + \frac{D}{\rho_1^{11}}$$

This may be done most easily by the use of Newton's method with an initial approximation of $\rho_1 = R_3/A$.

For the example considered, when $R_3 = 2.0$ it is found that $\rho_1 = 2.5244$. Note that the point $\zeta = 2.5244\, e^{i\pi/4}$ is mapped onto the point $z = 1.9657\, e^{i\pi/4}$ so that the external boundary of the propellant grain deviates from a circle by 1.73 per cent of the radius.

As the number of star points in the grain is increased, it may be necessary to use more terms in the mapping function unless the ratio R_2/R_1 is increased. More terms may be added by using additional linear equations of the form [5], with associated changes in Equations [3–6]. Increasing the number of linear equations in the system still results in a quadratic equation for the determination of A.

New Patents

George F. McLaughlin, *Associate Editor*

Liquid storage tank (2,922,287). R. S. Rae, Santa Monica, Calif., assignor to the Garrett Corp.

Inner and outer shells spaced to form a cooling passage between. A mixture of gas in the passage passes through a gas circulating passage in heat exchange relationship with the substance passing through the delivery line.

Airborne evaporate cooling system (2,922,291). D. W. Fox and R. M. Rivello, Silver Spring, Md., assignors to the U. S. Navy.

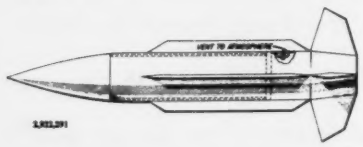

Coolant enclosed in closed containers positioned between outer and inner skins of a missile. Structures cooperating with the containers and missile skin to form channels venting to ambient pressures.

Propulsion system (2,923,126). M. Precaul, Paris, France, assignor to Société Technique de Recherches Industrielles et Mécaniques.

Rocket with cylindrical tubular powder blocks forming a propulsive charge located in the body. Blocks are spaced from the body, and from front and rear cages in the body.

Pressure ratio measuring instrument (2,923,153). S. Westman, Inglewood, Calif., assignor to the Garrett Corp.

Counterweight connected to a beam so as to develop a force vector equal and opposite to the force vector developed by the instrument in response to linear acceleration.

Vertical takeoff aircraft with jettisonable auxiliary engine (2,923,495). H. P. G. von Zborowski, Brunoy, France.

Ring-like container propelling unit releasably fixed to an aircraft for applying thrust. Unit includes jet power plant and a limited amount of fuel housed in the wing-sectioned ring.

Tracking device (2,923,826). C. H. Brumley, Penfield, N. Y., assignor to Bausch & Lomb Optical Co.

System for continuously directing an axis of a positionable mechanism upon an object to be tracked, and for maintaining this relationship.

Model satellite system (2,924,033). D. H. Lanctot, Malibu, Calif., assignor to Don-Lan Electronics Co.

Hollow illuminated rotating globe representing Earth, supported on a hollow tube. A base contains a blower to supply air into the globe at a pressure higher than ambient air. A hole in the globe supplies a jet of air to support a sphere spaced from the globe.

Resonance combustion apparatus (2,924,071). T. P. de Paravicini, Shepton Mallet, England, assignor to Normalair, Ltd.

Thermodynamically controlled gas circuit. Air from the upstream opening is admitted so long as the upstream pressure exceeds the downstream pressure. Reverse flow is repelled when the downstream pressure is greater.

Insulated storage container (2,924,351). G. F. Hawk and G. S. Kiester, Bryan, Ohio, assignors to Aro Equipment Corp.

Spherical-spaced wall container for holding liquid oxygen. The inner sphere is maintained in dimensional balance within the outer sphere, and the space between is evacuated to provide a vacuum

Tandem rocket launcher (2,930,288). F. C. Janah, Dallas, Texas, assignor to Chance Vought Aircraft, Inc.

Launching tubes aligned in tandem. A deflector door in the space between tubes block the aft tube and protects the aft rocket from blast effects of the forward rocket. The door is moved out of the space to permit the aft rocket free passage through the forward tube.

Ammonium nitrate composite propellant (2,930,683). B. R. Adelman, Waco, Texas, assignor to Phillips Petroleum Co.

Solid rocket propellant charge comprising ammonium nitrate and a rubber binder. The resulting mixture is formed into charges and cured at a temperature range of 175 to 180 F.

Propellant combination (2,930,684). I. A. Kanarek, Los Angeles, Calif., assignor to North American Aviation, Inc.

Liquid fluorine in liquid oxygen and a liquid organic fuel consisting of gasoline, ethyl alcohol, triethylamine and ethylenediamine.

Rocket launcher (2,931,273). A. J. Weatherhead Jr., Shaker Heights, Ohio, assignor to The Weatherhead Co.

Seven rocket tubes arranged in a hexagonal cluster with two of the tubes in a bottom row, two in the top row, and three in the middle row, all in contact with the middle tube of the middle row.

Air intake structure (2,934,893). F. W. Streeter, Reform, Ala., assignor to Westinghouse Electric Corp.

Supersonic jet propulsion engine with outer and inner tubular shells defining a primary air passageway. The inner shell has a central inlet passageway which may be blocked by leaf members.

Fuel supply and flame stabilizer (2,934,894). R. A. B. Lang, Lloydtown, Ontario, Canada, assignor to Orenda Engines, Ltd.

Jet engine afterburner having a second fuel ejection means to discharge fuel axially of a chamber in the tailcone.

Variable area propelling nozzle and thrust spoiler (2,934,986). M. Kadosch and J. H. Bertin, Neuilly-sur-Seine, France, assignors to SNECMA Co.

Auxiliary slot-like nozzle extending along the outlet periphery of a propulsive nozzle. An auxiliary jet issues inwardly across the jet stream to exert a throttling and constricting action.

Noise suppressor (2,935,842). A. L. Highberg and J. M. Tyler, South Coventry, Conn., assignors to United Aircraft Corp.

Radially spaced discharge slots comprising stationary and rotary members. The rotary members may be rotated to a noise suppression position to form a continuation of the stationary unit slots.

Combustion motor starting and signal means (2,935,843). R. P. Haviland, Key West, Fla., assignor to General Electric Co.

Frangible member supported in the path of combustion gases. Pressure surge through the nozzle will fracture the member, open an electrical circuit, and increase the flow of reactant.

System for feeding combustion fluids to rocket motors (2,935,844). H. D. Parks and R. W. Porter, Schenectady, N. Y., assignors to General Electric Co.

Automatic acceleration operated selector for choosing appropriate valves to be closed. The selector operating the valves is controlled by a fluid system.

Automatic injection system for self-igniting propellants (2,935,845). K. K. Neuhoefer, Monroe, N. Y., assignor to the U. S. Army.

First outlet nozzles pass hypergolic fluids at normal input pressure after a predetermined time from starting, and serially interconnect chambers leading from ducts to second outlet nozzles.

Reaction motor feed system (2,935,846). J. Neale and C. F. Malcolm Jr. (Member ARS), Long Valley, N. J., assignors to Thiokol Chemical Corp. (Corporate Member ARS).

Reservoir containing propellant and connected to a heat adder chamber containing admixed gases. A conduit connects the reservoir to the combustion chamber.

Rocket engine testing and launching apparatus (2,925,013). H. R. Santora, G. P. Lunday and J. A. Benson (Member ARS), Van Nuys, Calif., assignors to North American Aviation, Inc.

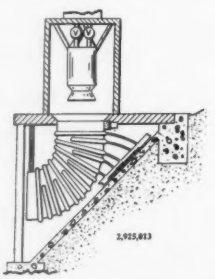

Flame deflector receiving the exhaust of a rocket engine. Water manifolds extend around the structure at various intervals. Water is supplied at pressures and amounts based on a predetermined impingement pressure and temperature of the exhaust.

EDITOR'S NOTE: Patents listed above were selected from the Official Gazette of the U. S. Patent Office. Printed copies of patents may be obtained from the Commissioner of Patents, Washington 25, D. C., at a cost of 25 cents each; design patents, 10 cents.

Book Reviews

Ali Bulent Cambel, Northwestern University, *Associate Editor*

Principles of Analog Computation, by George W. Smith and Roger C. Wood, McGraw-Hill Book Co., Inc., New York, 1959, 234 pp. $7.50.

Reviewed by E. A. TRABANT
Purdue University

As stated in the authors' preface, "For those interested in the detailed design of analog-computer components, this book will not prove to be adequate." However, the coverage of analog computation techniques is thorough with many fine examples drawn from the fields of particle dynamics and servomechanisms. For those with some knowledge of electronics and the equivalent background of a senior or first year graduate student in the physical and mathematical sciences the text should prove to be adequate for an understanding of the principles presented. When necessary, step-by-step procedures are used; however, unnecessary details are held to a minimum.

The first three chapters contain a description of the basic components of an analog computer, elementary techniques for the solution of problems and some details on the analysis of linear systems on an analog computer. The fourth chapter uses the diode in the simulation of nonlinear systems; the fifth chapter covers the application of the relay comparator. Fundamental implicit-function techniques with examples is the subject of the sixth chapter. There follows a treatment of arbitrary-function generators. Some relatively new techniques are discussed with respect to diodes.

The text is thorough in its coverage, accurate in fundamentals and well arranged for study.

Theory of Mechanical Vibrations, by Kin N. Tong, John Wiley and Sons, Inc., New York, 1960, xii + 348 pp. $9.75.

Reviewed by DANA YOUNG
Yale University

It was only a little over thirty years ago that the first text in the U.S.A. dealing with mechanical vibrations was published. At that time, only a small handful of engineering schools offered a course in vibrations. Since then, quite a few excellent texts on this subject have been written, and the course offerings in this field have multiplied manyfold.

In a limited sense, a vibration is simply a periodic motion, but the engineering study of vibrations goes far beyond this and covers many aspects of the dynamic behavior of mechanical, acoustical and electrical systems. As engineering technology has advanced, the field of mechanical vibrations has continued to grow in interest and scope. A generation ago the majority of applications were in connection with rotating machinery. Since then, the range of application has extended to include a wide variety of problems in airplane dynamics, rockets and missiles, automatic control systems, servomechanisms, shock isolation, impact loadings, stress wave propagation, blast effects, random excitation, dynamics of soils, hydraulic and acoustic transients, and many others.

As vibration problems in engineering have increased in scope and complexity, there has arisen a need for more sophisticated methods of analysis, and these have developed along many lines to include such topics as operational transform methods, variational principles, impedance concepts, stochastic processes, nonlinear mechanics and visoelastic effects. There has also arisen the need for a clear understanding of the classical theory of linear elastic systems as related to the mathematics of eigenvalue problems. It is this latter phase of vibration theory that this book emphasizes.

The first two chapters deal with one and two degree of freedom systems. The treatment of these simple systems is necessarily somewhat similar to that in other vibration texts, although the author has naturally introduced some reorientation in viewpoint.

Chapter 3 deals with multidegree of freedom systems using matrix theory throughout. Particular attention is given to general principles and their application to such topics as orthogonality of eigenvectors, Rayleigh's quotient, semidefinite systems, matrix iteration, the enclosure theorem and electrical analogs. Only brief attention is given to the solution of specific problems. The summation convention (as used in tensor notation) is introduced in parallel with the matrix notation, although no use is made of this convention in developing the theory. Governing equations are derived from the energy expressions using the concept of conservation of energy rather than the powerful and more generally useful Lagrangian equations.

The fourth and last chapter treats of the vibration of elastic bodies, using as principal examples the longitudinal vibrations of bars and the lateral vibrations of Bernoulli-Euler beams. This chapter contains a fairly general theoretical discussion of the orthogonality properties of eigenfunctions, Rayleigh's quotient and the Rayleigh-Ritz method.

This book is intended to be primarily a textbook for beginning graduate students and, as such, is an interesting and worthwhile addition to existing texts on mechanical vibrations. It is not a direct substitute for the others but does provide some excellent supplementary material. It will require an experienced instructor to give life and meaning to the generalizations, and to point out the broad and exciting scope of engineering vibration problems that are not mentioned in this text. Surprisingly few bibliographical references are given.

Design and Performance of Gas Turbine Power Plants, edited by W. R. Hawthorne and W. T. Olson, Vol. XI of "High Speed Aerodynamics and Jet Propulsion," Princeton University Press, Princeton, N.J., 1960, 563 pp. $15.

Reviewed by SERGE GRATCH
Northwestern University

Jointly with its companion volume, "Aerodynamics of Turbines and Compressors," this treatise is intended to give a comprehensive coverage of the aircraft gas turbine power plant. From some points of view, the book is eminently successful in its purpose. The various aspects of the subject are discussed quite competently by recognized authorities in the field. The judicious selection of topics gives a balanced picture of the relative importance of various branches of science and engineering in the design, development and performance studies of gas turbine power plants. It is unfortunate that, as has been the case with other volumes of this series, publication was delayed so much after the initial preparation of drafts that the book is already about five years out of date. Nevertheless this treatise would be a welcome addition to the library of anyone concerned with gas turbines.

This volume consists of a brief general introduction, followed by three main sections devoted, respectively, to combustion chamber design, mechanical and metallurgical aspects, and performance of gas turbine power plants. Several of the chapters have very general interest, in fields not necessarily restricted to the subject of the book. For instance, the section on experimental techniques (by H. C. Hottel and G. C. Williams) could well be adopted as a textbook on experimental methods for high temperature research. The section on mechanics of materials for gas turbine applications (by E. Orowan and C. R. Soderberg) is an excellent summary of the engineering aspects of the behavior of metals at high temperature. Some of the other sections are definitely of lower caliber. For instance, it might have been better if the rather naive discussion of thermodynamic principles presented in the last section of the book had been omitted altogether, particularly since the same subject matter is treated so much more fully in other volumes of the same series.

An Introduction to Fluid Mechanics and Heat Transfer, by J. M. Kay, Cambridge University Press, New York, 1957, xvi + 309 pp. $7.

Reviewed by J. EDWARD SUNDERLAND
Northwestern University

Kay's is a commendable but brief book which integrates a presentation of the fundamental principles of fluid mechanics and heat transfer and applies these principles to a few practical examples.

Although very short, it covers a large amount of material. Following the introductory chapter of the text is a development and application of the continuity equation, the Bernoulli equation and the energy and momentum equations. Chapters are given on dimensional analysis as applied to fluid mechanics, flow in pipes and channels, and pumps and compressors. A chapter entitled "Heat Conduction and Heat Transfer" is followed by a discussion of heat exchangers, dimensional analysis as applied to heat transfer, and heat transfer and skin friction in turbulent flow. A development and some applications of the Navier-Stokes equations are given. A brief presentation of laminar and turbulent boundary layer theory is followed by chapters on turbulent flow, diffusion and mass transfer, the energy equation and heat transfer, forced convection in laminar and turbulent flow, compressible flow in pipes and nozzles, open channel flow, solid particles in fluid flow, flow through packed beds and fluidized solids, and condensation and evaporation. A very short guide to vector analysis is included in the appendix along with sections titled "Equations of Motion for an Inviscid Fluid," "Vorticity and Circulation," "Stress Components in a Viscous Fluid and the Equations of Motion," "Laminar Boundary-layer Flow," and finally, "Heat Transfer with Laminar Flow in a Pipe." Forty problems are given at the end of the book.

In order to cover so much material in such a short book, the author presents the subjects in a very concise form. Vector notation is used throughout the book. The author gives a few references at the end of many of the chapters, but he has failed to bring many of the best references to the reader's attention. Although the presentation of the subject material is rather brief, it is the opinion of the reviewer that a reader who is familiar with vector analysis, but only somewhat acquainted with the fundamental concepts of fluid flow and heat transfer would find the reading of this book very profitable.

Book Notices

Basic Data of Plasma Physics, by Sanborn C. Brown, The Technology Press and John Wiley and Sons, Inc., New York, 1959, viii + 336 pp. $6.50.

This volume is based on lectures by the author and on his technical report "Basic Data of Electrical Discharges." There are sixteen chapters dealing with discharges, collision and emission phenomena. The basic equations are presented, and experimental techniques are described. The volume brings together an enormous amount of data (otherwise found in scattered sources only). Numerous references are cited. Persons involved in plasma physics and its associated applications will find this text very beneficial in locating data.

Periodically Repeated Ignitions by **Shock Waves,** by Paul Schmidt, Arbeitsgemeinschaft fur Forschung des Landes Nordrhein-Westfalen, Heft 82, Westdeutscher Verlag, Koln und Opladen, 1959, 55 pp.

This is a paper presented by the inventor of the V-1 engine at the meeting of the Society for Research of the Northern Rhein-Westfalen Region of West Germany on October 1, 1958, in Dusseldorf. In it the author describes his recent experiments with pulse jet engines, revealing a characteristic dependence of ignition on the natural oscillation of the gas column. The phenomenon is rationalized on the basis of an elementary gas dynamic-kinetic analysis.

Introduction to the Mechanics of the Solar System, by Rudolf Kurth, Pergamon Press, London, 1960, 177 pp. $6.50.

There are not many books available for those who wish to study celestial mechanics. The present volume is very much on the theoretical side and is not an easy book. However, the author does use the simplest approach wherever possible. The Hamilton-Jacobi theory is not used, since it does not help very much for the simple one-body problems with perturbations which occur in the solar system. In this respect the volume differs decidedly from others on theoretical celestial mechanics. This volume should lend itself to a brief graduate course in celestial mechanics.

Technical Literature Digest

M. H. Smith, *Associate Editor*
The James Forrestal Research Center, Princeton University

Propulsion and Power (Combustion Systems)

Propellant Vaporization as a Criterion for Rocket-engine Design: Experimental Effect of Combustor Length, Throat Diameter, Injection Velocity, and Pressure on Rocket Combustor Efficiency, by Bruce J. Clark, *NASA TN* D-258, April 1960, 27 pp.

Analytical and Experimental Studies of Spherical Solid Propellant Rocket Motors, by Joseph G. Thibodaux Jr., Robert L. Swain and George Wright, *NACA Res. Mem.* L57G12a, Aug. 1957, 40 pp. (Declassified by authority of *NASA PA* no. 17, 4/14/60, p. 18.)

Analytical and Experimental Studies of a Divided-flow Ramjet Combustor, by E. E. Dangle, Robert Friedman and A. J. Cervenka, *NACA Res. Mem.* E53KO4, Jan. 1954, 36 pp. (Declassified by authority of *NASA PA* no. 17, 4/14/60, p. 11.)

Effects of Fuel Temperature and Fuel Distribution on the Combustion Efficiency of a 16-inch Ram-jet Engine at Simulated Flight Mach Number of 2.9, by E. E. Dangle, A. J. Cervenka and D. W. Bahr, *NACA Res. Mem.* E52J14, Jan. 1953, 27 pp. (Declassified by authority of *NASA PA* no. 17, 4/14/60, p. 11.)

Flight Test of a Radial-burning Solid-fuel Ram Jet, by Walter A. Bartlett Jr. and H. Rudolph Dettwyler, *NACA Res. Mem.* L52KO3, Dec. 1952, 21 pp. (Declassified by authority of *NASA PA* no. 17, 4/14/60, p. 14.)

Considerations in the Design of Ramjet Engines, by H. Hagen, *Zeitschrift für Flugwissenschaften,* vol. 8, no. 1, Jan. 1960, pp. 17–22. (In German.)

Performance Study of a Piston-type Pump for Liquid Hydrogen, by Arnold E. Biermann and William G. Shinko, *NASA TN* D-276, March 1960, 26 pp.

Criteria for Optimum Mixture-ratio Distribution Using Several Types of Impinging-stream Injector Elements, by G. W. Elverum Jr. and T. F. Morey, *Calif. Inst. Tech., Jet Prop. Lab., Mem.* 30-5, Feb. 1959, 11 pp.

Joint Army-Navy-Air Force Solid Propellant Rocket Static Test Panel, 8th Meeting, Dec. 1959, Bulletin: Addendum, *Solid Propellant Information Agency,*

EDITOR'S NOTE: Contributions from Professors E. R. G. Eckert, J. P. Hartnett, T. F. Irvine Jr. and P. J. Schneider of the Heat Transfer Laboratory, University of Minnesota, are gratefully acknowledged.

Publication SPSTP/8A, March 1960, 119 pp.

Multicomponent Force Measuring System, by T. H. Howell, pp. 89–112.

Digital Data Reduction, by R. E. Williams, pp. 73–78.

Temperature Conditioning and Environmental Temperature Cycling of Solid Rocket Motors, by C. McCarty and R. W. Allen Jr., pp. 79–88.

Calibration Techniques for Digital Instrumentation Systems, by W. W. Holmes, pp. 55–72.

An **Automatic Data Acquisition System for Use in Testing Large Scale Rocket Motors,** by R. W. Armstrong and G. J. Liviakis, pp. 11–22.

Thermodynamic Data for the Calculation of Gas Turbine Performance, by D. Fielding and J. E. C. Topps, *Gt. Brit. Aeron. Res. Council, R & M* 3099, 1959, 115 pp.

Contour Nozzles, by Ellis M. Landsbaum, ARS JOURNAL, vol. 30, March 1960, pp. 244–250.

Nonisentropic Nozzle Flow, by William T. Snyder, ARS JOURNAL, vol. 30, March 1960, pp. 270–271.

A **New Approach to Engine Design,** by Kurt Berman, ASTRONAUTICS, vol. 5, April 1960, pp. 22–24, 100–101.

Multistart Rocket Engines, by Kurt S. Stehling, ASTRONAUTICS, vol. 5, April 1960, pp. 34–37, 102–103.

Contribution to the Problem of the Hot Water Rocket, by Jean-Paul Etheimer, *Forschungsinstitut für Physik der Strahlantriebe E. V., Stüttgart, Mitteilung* 20, Sept. 1959, 65 pp., 20 refs. (In German.)

Advanced Propulsion Systems Symposium, Los Angeles, Dec. 11–13, 1957, **Proceedings,** ed. by Morton Alperin and George P. Sutton, Pergamon Press, N. Y., 1959, 237 pp.

The Liquid Propellant Status Quo, by John F. Tormey, pp. 179–184.

Ozone-Fluorine, by Edward N. Hall, pp. 185–190.

The Use of Metals and Metal Hydrides in Rocket and Jet Propulsion, by James M. Carter, pp. 191–198.

An Experimental Investigation of Unstable Combustion in Solid Propellant Rocket Motors, Part 1, Experimental Results, by W. G. Brownlee, *Calif. Inst. Tech., Jet Prop. Lab., Mem.* 20–187, Dec. 1959, 53 pp.

Noise Radiation from Fourteen Types of Rockets in the 1,000 to 130,000 Pounds Thrust Range, by J. N. Cole and H. E. von Gierke, *Wright Air Dev. Center, Aero Med. Lab., WADC TR*-57-354, Dec. 1957, 72 pp.

Performance Problems in Large Rocket Engines, by S. L. Bragg, *J. Roy. Aeron. Soc.*, vol. 64, March 1960, pp. 131–140.

Final Summary Report on the Development of Monopropellant Test Equipment, by L. Grundeis, *Sundstrand Turbo Div.*, S/TD 1719, July 1959, 105 pp.

Design Method for Spherical Grains, by J. M. Segal, ARS JOURNAL, vol. 30, no. 4, April 1960, pp. 370–371.

Propulsion and Power (Non-Combustion)

Experimental Investigations of Electromagnetically Induced Detonations, Part 1—Parameters Affecting the Formation of the Pinch, by Thomas Donner and Leonard Aronowitz, *Republic Aviation Corp., Plasma Prop. Lab.,* Farmingdale, N. Y., *PPL Rep.* 122, Nov. 1959, 24 pp.

Theoretical Studies for a Problem in Electromagnetically Induced Detonations, by W. Chinitz, K. M. Foreman and L. W. Levin, *Republic Aviation Corp., Plasma Prop. Lab.,* Farmingdale, N. Y., *PPL Rep.* 121, Nov. 1959, 36 pp.

One-dimensional Analysis of Ion Rockets, by Harold R. Kaufman, *NASA TN* D-261, March 1960, 35 pp.

Some Engineering Aspects of the Magnetohydrodynamic Pinch Process for Space Propulsion, by Irving Granet and William J. Guman, *Republic Aviation Corp., Plasma Prop. Lab.,* Farmingdale, N. Y., *PPL Rep.* 120, Nov. 1959, 41 pp.

Advances in Space Science, ed. by Frederick I. Ordway III, vol. 1, 1959, Academic Press, N. Y., 1959, 412 pp.

Power Supplies for Orbital and Space Vehicles, by John H. Huth, pp. 111–159.

Relativistic Theory of Rocket Flight with Advanced Propulsion Systems, by John Huth, ARS JOURNAL, vol. 30, March 1960, pp. 250–253.

A Method for Heat Rejection from Space Powerplants, by Roger C. Weatherston and William E. Smith, ARS JOURNAL, vol. 30, March 1960, pp. 268–269.

Propulsion System for Rendezvous in Space, by Charles J. Kaplan and D. P. Buergin, *Astron. Sci. Rev.*, vol. 1, no. 4, Oct.-Dec. 1959, pp. 11–12, 21.

Non-propulsive Power for Advanced Vehicles, II, by Robert Curran, *Space/Aeron.*, vol. 33, April 1960, pp. 50–53.

Advanced Propulsion Systems Symposium, Los Angeles, Dec. 11–13, 1957, **Proceedings,** ed. by Morton Alperin and George P. Sutton, Pergamon Press, N. Y., 1959, 237 pp.

Ion Propulsion Systems, by S. Naiditch, pp. 1–32.

Experimental Studies on the Thrust from a Continuous Plasma Jet, by Gordon Cann, Adriano Ducati and Vernon Blackman, pp. 33–43.

The Ion Rocket Engine, by Robert H. Boden, pp. 43–70.

Comparison of Propulsion Systems: Solar Heating, Arc-thermodynamics, and Arc-magnetohydrodynamics, by Krafft A. Ehricke, pp. 71–104.

Thrust from Plasma, by Winston H. Bostick, pp. 105–116.

Potential Aircraft Applications of Closed Gas Cycle Nuclear Power Plants, by Rolf D. Buhler and Peter J. Gingo, pp. 117–134.

Speculation About Future Trends in Lightweight Electric Equipment, by R. A. Koehler, pp. 135–144.

Direct Power Conversion—Part I, General Comments, by John H. Huth, pp. 145–150.

Direct Power Conversion—Part II, Fission-electric Reactor, by George Safonov, pp. 151–160.

Electrostatic Generators, by A. John Gale, pp. 161–174.

Magnetohydrodynamic Generators and Propulsive Devices, by Richard J. Rosa, pp. 175–178.

System Considerations Affecting New Propulsion Applications, by Allen F. Donovan, pp. 227–237.

Magnetohydrodynamic Power Generation Using Nuclear Fuel, by Richard J. Rosa, *Avco-Everett Res. Lab., Res. Rep.* 87, 19 pp.

Fuel Cells, by A. M. Moos, *Ind. Engng. Chem.*, vol. 52, April 1960, pp. 391–392.

Fuel Cells as Electrochemical Devices, by H. A. Liebhafsky and D. L. Douglas, *Ind. Engng. Chem.*, vol. 52, April 1960, pp. 293–294.

Carbonaceous Fuel Cells, by H. H. Chambers and A. D. S. Tantram, *Ind. Engng. Chem.*, vol. 52, April 1960, p. 295.

Hydrogen-oxygen Fuel Cells with Carbon Electrodes, by Karl Fordesch, *Ind. Engng. Chem.*, vol. 52, April 1960, pp. 296–297.

Catalysis of Fuel Cell Electrode Reactions, by G. J. Young and R. B. Rozelle, *Ind. Engng. Chem.*, vol. 52, April 1960, pp. 298–300.

Electrode Kinetics, by L. G. Austin, *Ind. Engng. Chem.*, vol. 52, April 1960, p. 300.

The High Pressure Hydrogen-oxygen Fuel Cell, by F. T. Bacon, *Ind. Engng. Chem.*, vol. 52, April 1960, pp. 301–302.

High Temperature Fuel Cells, by G. H. J. Broers and J. A. A. Ketelaar, *Ind. Engng. Chem.*, vol. 52, April 1960, pp. 303–305.

Nature of the Electrode Process, by Everett Gorin and H. L. Recht, *Ind. Engng. Chem.*, vol. 52, April 1960, pp. 306–307.

Molten Carbonate Cells with Gas-diffusion Electrodes, by D. L. Douglas, *Ind. Engng. Chem.*, vol. 52, April 1960, pp. 308–309.

Experimental Magnetohydrodynamic Power Generator, by Richard J. Rosa, *J. Appl. Phys.*, vol. 31, April 1960, p. 735.

Scaling Relations for Plasma Devices, by G. S. Janes, *Avco-Everett Res. Lab., Res. Rep.* 80, Dec. 1959, 11 pp.

Pebble Bed Nuclear Reactors for Space Vehicle Propulsion, by Myron M. Levoy and John J. Newgard, *Aero/Space Engng.*, vol. 19, April 1960, pp. 54–58.

Fuel Cells, by Herman A. Liebhafsky and Leonard W. Niedrach, *J. Franklin Inst.*, vol. 269, April 1960, pp. 257–267.

Considerations in the Design of a Nuclear Rocket, by John J. Newgard and Myron M. Levoy, *Nuclear Sci. & Engng.*, vol. 7, April 1960, pp. 377–386.

Propellants and Combustion

Detonation Parameters for Gaseous Mixtures, by Bernard T. Wolfson and Robert F. Dunn, *Wright Air Dev. Center, Aeron. Res. Lab., TN*-57-309, May 1959, 94 pp.

Property Requirements for Liquid Rocket Propellants, by E. M. Goodger, *Cranfield, Coll. Aeron., CoA Note* 97, Nov. 1959, 19 pp.

Some Instrumentation Techniques for Propellant Detonation Studies, by R. P. Clifford, *Joint Army-Navy-Air Force Solid Propellant Rocket Static Test Panel, 7th Meeting Bull.: Addendum, Oct. 1959, Solid Propellant Information Agency, Pub.* no. SPSTP/7S, pp. 1–10.

Diffusion in a Two-layer Slab with Tables of Concentration, by D. R. Cruise and C. J. Thorne, *NavOrd Rep.* 6439 (*NOTS TP* 2146), May 21, 1959, 400 pp.

Chemical Analysis of Tichloral (TCA) Igniter Mixtures, by B. J. Alley and W. W. Howard, *Army Rocket & Guided Missile Agency, Ordnance Missile Labs. Div., Prop. Lab., Redstone Arsenal, Ala., ARGMA TR* 1D3R, 26 Feb. 1960, 20 pp.

Advanced Propulsion Systems Symposium, Los Angeles, Dec. 11–13, 1957, **Proceedings,** ed. by Morton Alperin and George P. Sutton, Pergamon Press, N. Y., 1959, 237 pp.

Stabilized Free Radicals, by Julius L. Jackson, pp. 205–212.

Research on Free Radicals as Rocket Propellants, by George Moe and Don L. Armstrong, pp. 213–226.

Spectroscopic Studies of Reverse Jet Flame Stabilization, by A. E. Fuhs, ARS JOURNAL, vol. 30, March 1960, pp. 238–243.

Vapor-liquid Equilibria of Ozone-oxygen Systems, by Charles K. Hersh, Robert I. Brabets, Gerald M. Platz, Raymond J. Swehla and Donald P. Kirsh, ARS JOURNAL, vol. 30, March 1960, pp. 264–265.

Thermal Decomposition of Liquid Phase n-propyl Nitrate and Its Compatibility with Various Metals and Other Additives, by Adolph B. Amster and Joseph B. Levy, ARS JOURNAL, vol. 30, March 1960, pp. 280–281.

Detonation Pressure of Liquid TNT, by W. B. Garn, *J. Chem. Phys.*, vol. 32, March 1960, pp. 653–655.

Potential Energy Curves of Hydrogen Fluoride, by Robert J. Fallon, Joseph T. Vanderslice and Edward A. Mason, *J. Chem. Phys.*, vol. 32, March 1960, pp. 698–699.

Investigation of the Tail of a Spinning Detonation, by R. I. Soloukhin and M. E. Topchiyan, *Soviet Physics-Doklady*, vol. 4, no. 4, Feb. 1960, pp. 773–775.

Shape-preserving Flows and a Point Explosion in the Magnetic Gasdynamics of a Gas of Infinite Conductivity, by D. V. Sharikadze, *Soviet Physics-Doklady*, vol. 4, no. 4, Feb. 1960, pp. 789–793.

Studies on Deflagration to Detonation in Propellants and Explosives, by *Bureau of Mines, Explosives Res. Lab., Annual Summary Rep.* 3769, Jan. 1, 1959, to Dec. 31, 1959, 14 pp.

Notes on "Tables for Interior Ballistics," by H. P. Hitchcock, *Aberdeen Proving Ground, Ball. Res. Labs., TN* 1298, Feb. 1960, 11 pp.

A Technical Report on the Mechanism of Ignition of Composite Solid Propellants by Hot Gases, by R. F. McAlevy, P. L. Cowan and M. Summerfield, *Princeton Univ., Dept. Aeron. Engng., Rep.* 505, April 1960, 14 pp. (*AFOSR TN* 60-335.)

Round Robin 19 of the Joint Army-Navy-Air Force Panel on the Analytical Chemistry of Solid Propellants: Evaluation of the Karl Fischer Method for the Determination of Water in Ammonium Perchlorate Using Automatic Titration Equipment, by Eugene A. Burns and Raffaele F. Muraca, *Stanford Res. Inst., Poulter Labs., Tech. Rep.* 002–60, Feb. 1960, 19 pp.

Numerical Computation of Aerodynamic Heating of Liquid Propellants, by John L. Kramer, Herman H. Lowell and William H. Roudebush, *NASA TN* D-273, April 1960, 28 pp.

Joint Army-Navy-Air Force Panel on Liquid Propellant Test Methods, *Liquid Propellant Info. Agency*, March 1960, 1 vol.

Preliminary Investigation of Performance and Starting Characteristics of Liquid Fluorine-Liquid Oxygen Mixtures with Jet Fuel, by Edward A. Rothenberg and Paul M. Ordin, *NACA Res. Mem.* E53J20, Jan. 1954, 21 pp. (Declassified by authority of *NASA PA* no. 17, 4/14/60, p. 11.)

The Interactions Between Nitrogen and Oxygen Molecules, by Willard E. Meador Jr., *NASA Tech. Rep.* R-68, 1960, 52 pp.

A Contribution to the Theory of Laminar Flames with Radial Symmetry, by J. Menkes, *Combustion and Flame*, vol. 4, March 1960, pp. 1–8.

The Effect of Pressure on the Mechanism and Speed of the Hydrazine Decomposition Flame, by G. K. Adams and G. B. Cook, *Combustion and Flame*, vol. 4, March 1960, pp. 9–18.

Carbon Formation in Premixed Flames, by P. H. Daniels, *Combustion and Flame*, vol. 4, March 1960, pp. 45–50.

The Theory of Steady Laminar Spherical Flame Propagation: Equations and Numerical Solution, by D. B. Spalding, *Combustion and Flame*, vol. 4, March 1960, pp. 51–58.

Extinction of a One-dimensional Laminar Flame Between Cooled Porous Plugs, by D. B. Spalding, *Combustion and Flame*, vol. 4, March 1960, p. 93.

One-dimensional Laminar Flame Propagation with an Enthalpy Gradient, by D. B. Spalding and J. Adler, *Combustion and Flame*, vol. 4, March 1960, p. 94.

The Thermal Conductivity of Hydrazine Vapour, by P. Gray and P. G. Wright, *Combustion and Flame*, vol. 4, March 1960, p. 95.

Compilation of Thermodynamic Properties, Transport Properties, and Theoretical Rocket Performance of Gaseous Hydrogen, by Charles R. King, *NASA TN* D-275, April 1960, 71 pp.

Further Studies on the Light Scattering Technique for Determination of Size Distributions in Burning Sprays II: Wide Range Photographic Photometry, by R. A. Dobbins, *Princeton Univ., Dept. Aeron. Engng., Rep.* 498, Feb. 1960, 50 pp.

Consideration of Hydrazine Decomposition, by I. J. Eberstein and I. Glassman, *Princeton Univ., Dept. Aeron. Engng., Rep.* 490, Dec. 1959, 23 pp.

Study of Amine Perchlorates as Ingredients for Fast-burning Propellants, by M. L. Wolfrom and Alan Chaney, *Ohio State Univ., Res. Foundation, RF Project* 675, *Final Rep.*, March 1960, 18 pp.

Mechanisms of the Autodecomposition of Liquid Acetylenic Monopropellants, by U. V. Henderson Jr., *Experiment Inc.*, TM-1152, Jan. 1960, 13 pp.

Basic Investigation of Hybrid Combustion Processes, Quarterly Progress Report for Period Ending 29 Feb. 1960, by C. V. Metzler and W. H. Moberly, *North American Aviation, Inc., Rocketdyne*, R-2267, March 1960, 17 pp.

Ignition Studies, Part V: Study of the Processes Occurring During the Spontaneous Ignition of the Hexane Isomers, by W. A. Affens, J. E. Johnson and H. W. Carhart, *Naval Res. Lab., Rep.* 5437, Jan. 27, 1960, 13 pp.

Dispersing Wave of a Spin Detonation, by R. I. Soloukhin, *Akademiia Nauk SSSR, Izvestiia, Otdelenie Tekhnicheskikh Nauk, Mekhanika i Mashinostroenie*, no. 6, Nov.-Dec. 1959, pp. 145–146. (In Russian.)

Mechanism of the Initiation of the Detonation of Explosive Substance, by K. K. Andreev, *Akademiia Nauk SSSR, Izvestiia, Otdelenie Tekhnicheskikh Nauk, Energetika i Avtomatika*, no. 4, July-Aug. 1959, pp. 188–197. (In Russian.)

Combustion of Highly Reactive Fuels in Supersonic Airstreams, by Edward A. Fletcher, Robert G. Dorsch and Harrison Allen Jr., ARS JOURNAL, vol. 30, no. 4, April 1960, pp. 337–344.

Combustion Intensity in a Heterogeneous Stirred Reactor, by Welby G. Courtney, ARS JOURNAL, vol. 30, no. 4, April 1960, pp. 356–357.

Thermally Induced Bond Stresses in Case-bonded Propellant Grains, by Eric E. Ungar and Bernard W. Shaffer, ARS JOURNAL, vol. 30, no. 4, April 1960, pp. 366–368.

Nonlinear Pressure Oscillations in a Combustion Field, by Gerald Rosen, ARS JOURNAL, vol. 30, no. 4, April 1960, pp. 422–423.

New Method for Studying Polymerization of Solid Propellants and Propellant Binders, by R. W. Warfield, ARS JOURNAL, vol. 30, no. 4, April 1960, pp. 427–428.

Handling Gaseous Fluorine and Chlorine Trifluoride in the Laboratory, by J. Gordon and E. L. Holloway, *Ind. Engng. Chem.*, vol. 52, May 1960, pp. 63A–64A, 66, 69.

Materials and Structures

Welded Titanium Case for Space-probe Rocket Motor, by A. J. Brothers, R. A. Boundy, H. E. Martens and L. D. Jaffe, *Calif. Inst. Tech., Jet Prop. Lab., Rep.* 30-8, Sept. 1959, 8 pp.

Exploratory Studies in Three Dimensional Photothermoelasticity, by Herbert Tramposch and George Gerard, *N. Y. Univ., Coll. Engng., Tech. Rep.* SM 59-5, Sept. 1959, 44 pp.

Rolling-contact Fatigue Life of a Crystallized Glass Ceramic, by Thomas L. Carter and Erwin V. Zaretsky, *NASA TN* D-259, March 1960, 35 pp.

Structural Damage and Other Effects of Solar Plasmas, by L. Reiffel, ARS JOURNAL, vol. 30, March 1960, pp. 258–262.

Analysis of Elastic-plastic Stress Distribution in Thin-wall Cylinders and Spheres Subjected to Internal Pressure and Nuclear Radiation Heating, by Donald F. Johnson, *NASA TN* D-271, April 1960, 34 pp.

Lubricants for Missile Systems, by K. R. Fisch, L. Peale and J. Messina, *Frankford Arsenal, Pitman-Dunn Labs. Group, Rep.* R-1522, Dec. 1959, 40 pp.

Some Problems in the Theory of Heat Resistance and the Development of New, Highly Resistant Titanium Alloys, by I. I. Kornilov, *Akademiia Nauk SSSR, Izvestiia, Otdelenie Tekhnicheskikh Nauk, Metallurgiia i Toplivo*, no. 4, July-Aug. 1959, pp. 190–199. (In Russian.)

Metal Borides and Carbides, Materials of the Future, by W. R. Benn, *Ind. Engng. Chem.*, vol. 52, May 1960, pp. 40A–44A.

Selection, Design, and Use of Super Refractories in High Temperature Operation, by R. W. Brown and R. F. Nering, *Ind. Engng. Chem.*, vol. 52, May 1960, pp. 381–408.

On Small Harmonic Oscillations of a Cylindrical Shell Along the Axis of Which an Ideal Gas Flows with Supersonic Velocity, by B. I. Rabinovich, *PMM: J. Appl. Math. & Mech.*, vol. 23, no. 4, 1959, pp. 1255–1262.

A Statistical Method in the Theory of Stability of Shells, by I. I. Vorovich, *PMM: J. Appl. Math. & Mech.*, vol. 23, no. 4, 1959, pp. 1263–1272.

Fluid Dynamics, Heat Transfer and MHD

Boundary-layer Displacement and Leading-edge Bluntness Effects in High Temperature Hypersonic Flow, by H. K. Cheng, J. G. Hall, T. C. Golian and A. Hertzberg, *Cornell Aeron. Lab., Inc., Rep.* AD-1052-A-9, Jan. 1960, 56 pp.

Rate of Ionization Behind Shock Waves in Air, by S. C. Lin, *Avco-Everett Res. Lab., Res. Note* 170, Dec. 1959, 18 pp.

Theory of the Shock Front, III: Sensitivity to Rate Constants, by J. D. Teare and G. J. Dreiss, *Avco-Everett Res. Lab., Res. Note* 176, Dec. 1959, 17 pp.

A Direct Method of Measuring Density Behind Shock Waves, by D. B. Sleator and M. R. Lewis, *Ball. Res. Labs., Aberdeen Proving Ground, BRL Rep.* 1087, Dec. 1959.

Bibliography on Magnetohydrodynamics, Plasma Physics and Controlled Thermonuclear Processes, by Barbara A. Spence, *Avco-Everett Res. Lab.*, AMP 36, Oct. 1959, 97 pp.

The Blunt Body Viscous Layer Problem with and Without an Applied Magnetic Field, by Hakuro Oguchi, *Wright Air Dev. Center, TN* 60-57, Feb. 1960, 41 pp.

On Carbon Contamination of Air Arcs and Its Effect on Ablation Measurements, by S. Georgiev and P. H. Rose, *Avco-Everett Res. Lab., Res. Rep.* 177, Dec. 1959, 17 pp.

Heat Transfer by Radiation, by H. de L'Estoile and L. Rosenthal, *AGARD Rep.* 211, 1958, 77 pp. (In French.)

Heat Transfer to Cylinders in Crossflow in Hypersonic Rarefied Gas Streams, by Ruth N. Weltmann and Perry W. Kuhns, *NASA TN* D-267, March 1960, 24 pp.

Arc-tangent Fits for Pressure and Pressure-drag Coefficients of Axisymmetric Blunt Bodies at All Speeds, by Ta Li, *J. Aero/Space Sci.*, vol. 27, April 1960, pp. 309–311.

Compressible Flow Tables k = 1.24; Isentropic Process, by C. Hoebich, *Army Rocket & Guided Missile Agency, Ordnance Missile Labs. Div., Design and Dev. Lab., Rtedsone Arsenal, ARGMA TN* 1H1N-9, March 1960, 87 pp.

A Kinetic Theory Description of Rarefied Gas Flows, by Lester Lees, *Calif. Inst. Tech., Guggenheim Aeron. Lab., Hypersonic Res. Proj. Mem.* 51, Dec. 1959, 78 pp.

Convective Flow Due to Acoustic Vibrations in Horizontal Resonant Tubes, by Thomas W. Jackson and Harold L. Johnson, *Georgia Inst. Tech., Engng. Expt. Sta.*, March 1960, 35 pp.

On the Aerodynamic Noise of a Jet, by Sin-I Cheng, *Gen. Appl. Sci. Labs., Inc., Westbury, N. Y., GASL Tech. Rep.* 148, April 1959, 56 pp.

The Oscillation and Noise of an Overpressure Sonic Jet, by Andrew G. Hammitt, *Gen. Appl. Sci. Labs., Inc., Westbury, N. Y., GASL Tech. Rep.* 137, Nov. 1959, 35 pp. (*AFOSR TN* 59-1307.)

Problems of Heat Transfer During a Change of State, ed. by S. S. Kutateladze (trans. from a publication of the State Power Press, Moscow-Leningrad, 1953), *Atomic Energy Comm., Trans. AEC*-tr-3405, 193 pp.

Heat Transfer to a Liquid Freely Flowing over a Surface Heated to a Temperature Above the Boiling Point, by V. M. Borishansky, pp. 109–143.

Recent Advances in Chemical Kinetics of Homogeneous Reactions in Dissociated Air, by Walter G. Zinman, ARS JOURNAL, vol. 30, March 1960, pp. 233–238.

Surface Recombination in the Frozen Compressible Flow of a Dissociated Diatomic Gas Past a Catalytic Flat Plate, by Paul M. Chung and Aemer D. Anderson, ARS JOURNAL, vol. 30, March 1960, pp. 262–264.

Measurements of the Heat Transfer Coefficients for Hydrogen Flowing in a Heated Tube, by J. M. Fowler and C. F. Warner, ARS JOURNAL, vol. 30, March 1960, pp. 266–267.

Navy Symposium on Aeroballistics, 4th, Dahlgren, Va., May 1, 1958, Proceedings, *NavOrd Rep.* 5904, vol. 1 (NPG Rep. 1599), 1 vol.

A High Temperature Wind Tunnel Using a Solid Propellant Rocket as a Source, by H. A. Wallskog, *Paper* 38, 24 pp.

A Magnetogasdynamic Analogy, by M. D. Cowley, ARS JOURNAL, vol. 30, March 1960, pp. 271–273.

Prandtl-Meyer Expansion in Equilibrium Air, by Haim Kennet, ARS JOURNAL, vol. 30, March 1960, pp. 288–289.

Convection in a Fluid at Supercritical Pressures, by J. D. Griffith and R. H. Sabersky, ARS JOURNAL, vol. 30, March 1960, pp. 289–291.

Real Gas Effects in Flow over Blunt Bodies at Hypersonic Speeds, by H. T. Nagamatsu, R. E. Geiger and R. E. Sheer Jr., *J. Aero/Space Sci.*, vol. 27, April 1960, pp. 241–251.

Experimental Study of an Ablating Sphere with Hydromagnetic Effect Included, by John H. Boynton, *J. Aero/-Space Sci.*, vol. 27, April 1960, pp. 306–307.

A Note on the Relation of Biot's Method in Heat Conduction to a Least-squares Procedure, by Stephen J. Citron, *J. Aero/-Space Sci.*, vol. 27, April 1960, pp. 317–319.

First-order Solution to the Compressible

Laminar Boundary Layer in Slip Flow, by Anthony Casaccio, *J. Aero/Space Sci.*, vol. 27, April 1960, pp. 319–320.

The Temperature of Nitrogen and Air Behind Shock Waves, by F. S. Faizullov, N. N. Sobolev and E. M. Kudryavtsev, *Soviet Physics-Doklady*, vol. 4, no. 4, Feb. 1960, pp. 833–836.

Relativistic Transport Equations for a Plasma, I, by Yu. L. Klimontovich, *Soviet Physics-JETP*, vol. 37 (10), no. 3, March 1960, pp. 224–230.

Hydrodynamics of a Two-component Layer as Related to the Theory of Crises in the Process of Boiling, by S. S. Kutateladze and V. N. Moskvicheva, *Soviet Physics-Tech. Phys.*, vol. 4, no. 9, March 1960, pp. 1037–1040.

Ejector-nozzle Flow and Thrust, by H. E. Weber, *J. Basic Engng.* (*ASME Trans. Series D*), vol. 82, no. 1, March 1960, pp. 120–130.

Some Basic Aspects of Magnetohydrodynamic Boundary-layer Flows, by R. V. Hess, *NASA Mem.* N-4-9-59L, April 1959, 42 pp.

Liepmann's Heat Transfer Method in Aerothermochemistry, by Robert Goulard, *Purdue Res. Found., Res. Proj.* 1717, Rep. A-59-5, Aug. 1959, 9 pp.

A Review of Binary Boundary Layer Characteristics, by J. F. Gross, J. P. Hartnett, D. J. Masson and Carl J. Gazley, *The Rand Corp., Engng. Div.*, P-1729, June 1959, 90 pp.

Mass Transfer Cooling in a Steady Laminar Boundary Layer Near the Stagnation Point, by A. A. Hayday, *Heat Tranf. & Fluid Mech. Inst.*, June 1959, pp. 156–170.

Velocity, Temperature, and Heat-transfer Measurements in a Turbulent Boundary Layer Downstream of a Stepwise Discontinuity in Wall Temperature, by D. S. Johnson, *J. Appl. Mech.*, vol. 24, no. 1, March 1957, pp. 2–8

Numerical Solution of Boundary-layer Equations Without Similarity Assumptions, by R. F. Kramer and H. M. Lieberstein, *J. Aero/Space Sci.*, vol. 26, no. 8, Aug. 1959, pp. 508–514.

The Growth of the Thermal Boundary Layer in Laminar Flow Between Parallel Flat Plates, by A. McD. Mercer, *Appl. Sci. Res.*, vol. 8, no. 5, 1959, pp. 357–365

The Effect of the Free-stream Oscillations on the Laminar Layers on a Flat Plate, by Richard J. Nickerson, *U. S. Air Force, WADC Tech. Rep.* 57–481, Dec. 1958, 86 pp.

Experimental Determination of the Turbulent Heat Transfer Rate Distribution along a Slender Blunt Nosed Body from Shock Tube Tests, by E. Offenhartz and H. Weisblatt, *Avco, Res. & Advanced Dev. Div., RAD TR*-9-59-18, May 1959, 24 pp.

An Experimental Study of the Operating Characteristics and Electrode Heat Transfer of a Direct Current Electric Arc in a Pressurized Argon Environment, by George M. Palmer and Frank L. Paris, *Purdue Res. Found, Res. Proj. 1717, Rep.* A-59-10, Aug. 1959, 46 pp.

Chemical Reaction in the Laminar Boundary Layer Instantaneous Reaction, by O. E. Potter, *Trans. Inst. Chem. Engrs.*, vol. 36, no. 6, Dec. 1958, pp. 415–421.

On the Effects of Diffusion and Chemical Reaction in Convective Heat Transfer, by Daniel E. Rosner, *AeroChem. Res. Labs., Inc., TM*-13, June 1959, 7 pp.

Stagnation Point Heat Transfer in a Partially Ionized Gas, by R. W. Rutowski, *Heat Transf. & Fluid Mech. Inst.*, June 1959, pp. 110–125.

Laminar Transfer from Isothermal Spanwise Strips on a Flat Plate, by H. H. Sogin, *J. Appl. Mech.*, vol. 81, no. 4, Feb. 1960, pp. 53–63.

Details of Exact Low Prandtl Number Boundary-layer Solutions for Forced and for Free Convection, by E. M. Sparrow and J. L. Gregg, *NASA Mem.* 2-27-59E, Feb. 1959, 45 pp.

Heat Transfer on Blunt-nosed Bodies in General Three-dimensional Hypersonic Flow, by R. Vaglio-Laurin, *Heat Transf. & Fluid Mech. Inst.*, June 1959, pp. 95–109.

The Experimental Examination of the Local Heat Transfer on the Surface of a Sphere when Subjected to Forced Convective Cooling, by J. Wadworth, *Canada, Nat. Res. Council, Div. Mech. Engng., Rep.* MT-39, Sept. 1958, 56 pp.

Methods of Predicting Laminar Heat Rates on Hypersonic Vehicles, by Richard J. Winsniewski, *NASA TN* D-201, Dec. 1959, 36 pp.

Heat Transfer at a Corner, by Victor Zakkay, *J. Aero/Space Sci.*, vol. 27, no. 2, Feb. 1960, pp. 157–158.

An Experimental Investigation of the Vibration Effect on Heat Transfer in the Process of Boiling, by V. F. Kovalenko, *Teploenergetika*, no. 2, 1958, pp. 76–77. (In Russian.)

Heat Transfer in Film Condensation of Pure Vapors on Vertical Surfaces and Horizontal Pipes, by D. A. Laboontzov, *Teploenergetika*, no. 7, 1957, pp. 72–80. (In Russian.)

The Effect of Vapor Drag on Rotating Condensation, by E. M. Sparrow and J. L. Gregg, *J. Heat Transfer*, vol. 82, no. 1, Feb. 1960, pp. 71–72.

Laminar Condensation Heat Transfer on a Horizontal Cylinder, by E. M. Sparrow and J. L. Gregg, *J. Heat Transfer*, vol. 81, no. 4, Nov. 1959, pp. 291–296.

Dynamic Response of Heat Exchangers Having Internal Heat Sources, Part III, by Vedat S. Arpaci and John A. Clark, *J. Heat Transfer*, vol. 81, no. 4, Nov. 1959, pp. 253–266.

Heat Transfer to Laminar Flow Between Parallel Plates with a Prescribed Wall Heat Flux, by R. D. Cess and E. C. Shaffer, *Appl. Sci. Res.*, vol. 8, no. 5, 1959, pp. 339–344.

Heat Transfer and Friction in Turbulent Vortex Flow, by Frank Kreith and David Margolis, *Appl. Sci. Res.*, vol. 8, no. 6, 1959, pp. 457–473.

The Effect of Surface Roughness on the Convection Heat-transfer Coefficient for Fully Developed Turbulent Flow in Ducts with Uniform Heat Flux, by R. T. Lancet, *J. Heat Transfer*, vol 81, no. 2, May 1959, pp. 168–174.

On Convective Motion of a Conducting Fluid Between Parallel Vertical Plates in a Magnetic Field, by S. A. Regirer, *Soviet Phys.-JETP*, vol. 37 (10), no. 1, Jan. 1960, pp. 149–152.

Effect of a Variable-geometry Diffuser on the Operating Characteristics of a Helium Tunnel Designed for a Mach Number in Excess of 20, by Patrick J. Johnston and Robert D. Witcofski, *NASA TN* D-237, Feb. 1960, 20 pp.

A Study of the Overall Problems of the True-temperature, Hypersonic Wind Tunnel Having Semi-continuous Operation and the Preferred Methods of Solution, *Purdue Univ., School of Aeron. Engng., Rep.* A-59-14, Aug. 1959, 138 pp., 61 refs. plus bibliography, pp. 112–138.

An Experimental Study of the Operating Characteristics and Electrode Heat Transfer of a Direct Current Electrode Arc in a Pressurized Argon Environment, by George M. Palmer and Frank L. Paris Jr., *Purdue Univ., School of Aeron. Engng., Rep.* A-59-5, Aug. 1959, 46 pp.

Radiation from Hot Air and Stagnation Heating, by Bennett Kivel, *Avco-Everett Res. Lab., Res. Rep.* 79, AFBMD-TR-59-2, Oct. 1959, 27 pp.

Fluxes and Non-dimensional Parameters in Radiant Gases, by R. Goulard, *Purdue Univ., School of Aeron. Engng., Rep.* A-59-8, Oct. 1959, 19 pp.

Mass Transfer Cooling Experiments on a Hemisphere at M = 5, by G. E. Anderson, C. J. Scott and D. R. Elgin, *Univ. Minn., Rosemount Aeron. Labs., Res. Rep.* 166, Aug. 1959, 28 pp.

An Analysis of Ablation-shield Requirements for Manned Reentry Vehicles, by Leonard Roberts, *NASA Tech. Rep.* R-62, 1960, 58 pp.

On Base Pressures at High Reynolds Numbers and Hypersonic Mach Numbers, by Jack D. Whittfield and J. Leith Potter, *Arnold Engng. Dev. Center, ARO, Inc.* (*AEDC-TN*-60-61), March 1959, 22 pp.

Application of Various Techniques for Determining Local Heat-Coefficients in a Rocket Engine from Transient Experimental Data, by Curt H. Leibert, James E. Hatch and Ronald W. Grant, *NASA TN* D-277, April 1960, 33 pp.

An Analysis of Nose Ablation for Ballistic Vehicles, by Leonard Roberts, *NASA TN* D-254, April 1960, 30 pp.

End Effects in Magnetohydrodynamic Channel Flow, by Frank Fishman, *Avco-Everett Res. Lab., Res. Rep.* 78 (*AFBMD-TN*-59-5), June 1959, 14 pp.

Heat Transfer from Dissociated Gases in a Shock Tube, by R. A. Hartunian and P. V. Marrone, *Cornell Aeron. Lab., Inc., Rep.* AD-1118-A-7, Nov. 1959, 72 pp.

Heat Transfer in Oscillating Flow, by David T. Harrje and E. J. Croke, *Princeton Univ., Aeron. Engng. Dept., Rep.* 483, Oct. 1959, 34 pp.

Boundary-layer Transition and Heat Transfer in Shock Tubes, by R. A. Hartunian, A. L. Russo and P. V. Marrone, *Cornell Aeron. Lab., Inc., Rep.* AD 1118-A-3, Dec. 1959, 31 pp. (*AFOSR TN* 59-564; *ASTIA AD* 216 759.)

On Some Unsteady Free Molecular Solutions to the Boltzmann Equation; Addendum, by Edward T. Kornowski, *General Electric Co., Missile & Space Vehicle Dept.*, TIS R59SD463 (addendum), Nov. 1959.

A Study of Equilibrium Real-gas Effects in Hypersonic Air Nozzles, Including Charts of Thermodynamic Properties for Equilibrium Air, by Wayne D. Erickson and Helen S. Creekmore, *NASA TN* D-231, April 1960, 179 pp.

Research at the National Physical Laboratory on the Ionization Properties of Gases at High Temperatures, by D. L. Schultz, *Gt. Brit., Nat. Phys. Lab.*, NPL/-Aero/378, June 1959, 12 pp.

Electromagnetic Phenomena in Cosmical Physics (International Astronomical Union Symposium No. 6, Stockholm, Aug. 1956), B. Lehnert, ed., Cambridge, at the University Press, 1958, 545 pp.

Heat Transfer, Fundamentals of Chemical Engineering Review, by E. R. G. Eckert, J. P. Hartnett, T. F. Irvine Jr. and E. M. Sparrow, *Ind. Engng. Chem.*, vol. 52, April 1960, pp. 327–346.

Fluid Dynamics, Fundamentals of Chemical Engineering Review, by C. A. Sleicher Jr., R. A. Stern, L. E. Scriven and A. K. Oppenheim, *Ind. Engng. Chem.*, vol.

52, April 1960, pp. 347–358.

An Experiment on the Stability of Hypersonic Laminar Boundary Layers, by Anthony Demetriades, *J. Fluid Mech.*, vol. 7, March 1960, pp. 385–396.

Electron Diffusion Ahead of Shock Waves in Argon, by H. D. Weymann, *Univ. Maryland, Inst. Fluid Dynam. & Appl. Math., TN* BN-197, March 1960, 16 pp. (*AFOSR TN* 60–334.)

A Method of Calculating Turbulent-boundary-layer Growth at Hypersonic Mach Numbers, by James C. Sivells and Robert G. Payne, *Arnold Engng. Dev. Center, ARO, Inc.*, AEDC-TR-59-3, Feb. 1959, 50 pp.

Magnetohydrodynamic Simple Waves, by J. D. Cole and Y. M. Lynn, *Calif. Inst. Tech., Guggenheim Aeron. Lab.*, Dec. 1959, 51 pp. (*AFOSR TN* 59–1302.)

On the Role of Viscosity and Conductivity in Magnetohydrodynamics, by Meredith C. Gourdine, *Calif. Inst. Tech., Jet Prop. Lab., Tech. Rep.* 32–3, Jan. 1960, 27 pp.

Approximations for the Thermodynamic and Transport Properties of High-temperature Air, by C. Frederick Hansen, *NASA Tech. Rep.* R-50, 1959, 35 pp. (Supersedes *NACA TN* 4150.)

A Method of Forming Continuous Empirical Equations for the Thermodynamic Properties of Air from Ambient Temperatures to 15,000°K, with Applications, by Martin Grabau, *Arnold Engng. Dev. Center, ARO, Inc.*, AEDC-TN-59-102, Aug. 1959, 41 pp.

An Elementary Study of Gas Injection and Sublimation into a Simple Shear Layer, by J. F. Clarke, *Cranfield, Coll. Aeron., CoA Rep.* 126, Feb. 1960, 18 pp.

Ablation Studies of Low Melting Point Bodies in a Preheated Supersonic Air Stream, by J. W. Cleaver and F. Thomson, *Cranfield, Coll. Aeron., CoA Rep.* 127, Feb. 1960 15 pp.

The Performance of Ablation Materials as Heat Protection for Re-entering Satellites, by W. R. Warren and N. S. Diaconis, *General Electric Co., Missile & Space Vehicle Dept.*, TIS R60SD316, Feb. 1960, 26 pp.

Midwestern Conference on Fluid Mechanics, 6th, Austin, Texas, 1959, Proceedings, Austin, University of Texas, 1960, 464 pp.

Recent Progress in Rarefied Gas Dynamics Research, by S. F. Schaaf, pp. 1–15.

On Laminar Heat Transfer to the Stagnation Line Region of a Highly Yawed Cylinder, by Joseph Tsu Chieh Liu, pp. 34–46.

Determination of Convective Heat Transfer to Nonisothermal Surfaces Including the Effect of Pressure Gradient, by J. P. Hartnett, E. R. G. Eckert and Roland Birkebak, pp. 47–60.

Steady State Fusible Body Shapes in a Heated Supersonic Stream, by S. T. Chu and J. D. Lee, pp. 71–80.

Hypersonic Flow Around Bodies of Revolution Which Are Generated by Conic Sections, by Marcel Vinokur, pp. 232–253.

Theoretical and Experimental Study of Heat Transfer by Cellular Convection in the Presence of Impressed Magnetic Fields, by Yoshinari Nakagawa, pp. 417–426.

Canonical Forms, Beltrami Flows and Certain Exact Solutions in Magneto-gas-dynamics, by M. Z. von Krzywoblocki and J. T. Martin, pp. 427–445.

The Wave Motions of Small Amplitude in Radiation-electro-magneto-gasdynamics, by S. I. Pai and A. I. Speth, pp. 446–456.

Further Results on the Flow of a Conducting Fluid Past a Magnetized Sphere, by G. S. S. Ludford and J. D. Murray, pp. 457–465.

Fusion of a Plate in a Supersonic or High-temperature Gas Flow, by A. B. Vatazhin, *Akademiia Nauk SSSR, Izvestiia, Otdelenie Tekhnicheskikh Nauk, Mekhanika i Mashinostroenie*, no. 6, Nov.-Dec. 1959, pp. 7–13. (In Russian.)

Transformation of the System of Equations of Hydrodynamic Approximation of Plasma, by V. S. Tkalich, *Akademiia Nauk SSSR, Izvestiia, Otdelenie Tekhnicheskikh Nauk, Mekhanika i Mashinostroenie* no. 5, Sept.–Oct. 1959, pp. 122–123. (In Russian.)

Superposability in Magnetohydrodynamics, II, by J. N. Kapur, *Appl. Sci. Res.*, vol. 9, Sec. A, 1960, pp. 139–147.

Superposability of Two Axisymmetric Flows Under Axisymmetric Magnetic Fields, by P. Ramamoorthy, *Appl. Sci. Res.*, vol. 9, Sec. A, pp. 153–156.

Transport and Thermodynamic Properties in a Hypersonic Laminar Boundary Layer, Part 2: Applications, by Sinclaire M. Scala and Charles W. Baulknight, ARS JOURNAL, vol. 30, no. 5, April 1960, pp. 329–336.

Estimation of Nonequilibrium Reaction Flight Regimes for Blunt Bodies at Hypersonic Speeds, by T. A. Adamson Jr., ARS JOURNAL, vol. 30, no. 4, April 1960, pp. 358–360.

Short Hypersonic Contour Nozzles, by

R. E. Geiger, ARS JOURNAL, vol. 30, no. 4, April 1960, pp. 368–369.

Forced Convection Heat Transfer to Gaseous Hydrogen at High Heat Flux and High Pressure in a Smooth, Round, Electrically Heated Tube, by J. R. McCarthy and H. Wolf, ARS JOURNAL, vol. 30, no. 4, April 1960, pp. 423–425.

Mass Transfer—Chemical Engineering Fundamentals Review, by C. R. Wilke, J. M. Prausnitz and Andreas Acrivos, *Ind. Engng. Chem.*, vol. 52, May 1960, pp. 441–446.

Molecular Transport Properties of Fluids—Chemical Engineering Fundamentals Review, by E. F. Johnson, *Ind. Engng. Chem.*, vol. 52, May 1960, pp. 447–450.

Thermal Conductivity of Gas Mixtures in Chemical Equilibrium, II, by Richard S. Brokaw, *J. Chem. Phys.*, vol. 32, April 1960, pp. 1005–1006.

Measurements of Skin Friction of the Compressible Turbulent Boundary Layer on a Cone with Foreign Gas Injection, by Constantine C. Pappas and Arthur F. Okuno, *J. Aero/Space Sci.*, vol. 27, May 1960, pp. 321–333.

Magnetohydrodynamic Effects on the Formation of Couette Flow, by L. N. Tao, *J. Aero/Space Sci.*, vol. 27, May 1960, pp. 334–338.

Stagnation-point Heat-transfer Measurements in Hypersonic, Low-density Flow, by S. E. Neice, R. W. Rutowski and K. K. Chan, *J. Aero/Space Sci.*, vol. 27, May 1960, p. 387.

Self-similar Motions of a Gas with Shock Waves, Spreading According to a Power Law into a Gas at Rest, by G. L. Grodzovskii and N. L. Krashchennikova, *PMM: J. Appl. Math. & Mech.*, vol. 23, no. 4, 1959, pp. 1328–1333.

The Measurement of Electron Temperature in High-temperature Plasmas, by R. V. Williams and S. Kaufman, *Proc., Phys. Soc., London*, vol. 57, March 1960, pp. 329–336.

Absorption of Sound and the Width of Shock Waves in Relativistic Hydrodynamics, by M. T. Zhumartbaev, *Soviet Physics-JETP*, vol. 37, no. 4, April 1960, pp. 711–713.

Simple Method for Computing the Mean Range of Radiation in Ionized Gases in High Temperatures, by Yu. P. Raizer, *Soviet Physics-JETP*, vol. 37, no. 4, April 1960, pp. 769–771.

On the Energy Equation in Magneto Gasdynamics, by Ching-Sheng Wu, *Calif. Inst. Tech., Jet Prop. Lab., Tech. Rep.* 32–2, Jan. 1960, 36 pp.

On Chemical Reactions in Internal Flow Systems, by Paul L. Chambré, *Appl. Sci. Res.*, vol. 9, Sec. A, 1960, pp. 157–176.

Experiments on the Departure from Chemical Equilibrium in a Supersonic Flow, by Peter P. Wegener, ARS JOURNAL, vol. 30, no. 4, April 1960, pp. 322–329.

Ablation of Reinforced Plastics in Supersonic Flow, by George W. Sutton, *J. Aero/Space Sci.*, vol. 27, May 1960, pp. 377–386.

Sloshing of Liquids in Cylindrical Tanks of Elliptic Cross Section, by Wen-Hwa Chu, ARS JOURNAL, vol. 30, no. 4, April 1960, pp. 360–363.

Flight Mechanics

Theorem of Image Trajectories in the Earth-moon Space, by Angelo Miele, *Boeing Airplane Co.*, D1-82-0039, Jan. 1960, 10 pp.

Advances in Space Science, ed. by Frederick I. Ordway III, vol. 1, Academic Press, N. Y., 1959, 412 pp.

Interplanetary Rocket Trajectories, by Derek F. Lawden, pp. 1–54.

Ascent from Inner Circular to Outer Co-planar Elliptic Orbits, by L. Rider, ARS JOURNAL, vol. 30, March 1960, pp. 254–258.

Some Characteristics of the Planar Satellite Orbit, by Josef S. Pistiner, ARS JOURNAL, vol. 30, March 1960, pp. 275–277.

Symmetry of the Earth's Figure, by J. L. Brenner, R. Fulton and N. Sherman, ARS JOURNAL, March 1960, pp. 278–279.

Iterative Solution of the N-body problem for Real Time, by L. M. Rauch, ARS JOURNAL, March 1960, pp. 284–286.

Some Aspects of a Three-body Problem, by G. K. Oertel and S. F. Singer, *Astronautica Acta*, vol. 5, no. 6, 1959, pp. 356–366.

On the Flight Path of a Hypervelocity Glider Boosted by Rockets, by A. Miele, *Astronautica Acta*, vol. 5, no. 6, 1959, p. 367.

Rendezvous Compatible Orbits, by Norman V. Petersen and Robert S. Swanson, *Astron. Sci. Rev.*, vol. 1, no. 4, Oct.–Dec. 1959, pp. 13–14, 20.

An Orbital Rendezvous Simulator, by E. Levin and J. Ward, *Astron. Sci. Rev.*, vol. 1, no. 4, Oct.–Dec. 1959, pp. 15–16, 21.

Orbital Plane-change Maneuver, by Daniel B. DeBra, *Astron. Sci. Rev.*, vol. 1, no. 4, Oct.–Dec. 1959, pp. 19–21.

A Class of Optimum Trajectory Problems in Gravitational Fields, by E. W. Graham, *J. Aero/Space Sci.*, vol. 27, April 1960, pp. 296–303.

Dynamics of Flight—the Resonance of Spinning Missiles, by M. Bismut, *Recherche Aéron.*, no. 74, Jan.–Feb. 1960, pp. 3–11. (In French.)

Optimum Trajectories with Atmospheric Resistance, by E. W. Graham and B. J. Beane, *Douglas Aircr. Co., Rep.* SM-23-745, Nov. 1959, 44 pp.

A New Coordinate System for Satellite Orbit Theory, by J. L. Brenner, G. E. Laita and M. Weisfeld, *Stanford Res. Inst., Interim Tech. Rep.* 2, June 15, 1959, 86 pp.

The Capture Problem in the Three-body Restricted Orbital Problem, by V. A. Yegorov, *NASA Tech. Transl.* F-9, April 1960, 16 pp.

Minimum Time Flight Paths, by G. M. Schindler, ARS JOURNAL, vol. 30, no. 4, April 1960, pp. 352–355.

Curves of Rapid Determination of Orbital Transfer Requirements, by Philip J. Bonomo, ARS JOURNAL, vol. 30, no. 4, April 1960, pp. 371–372, 421.

Two Analytical Results of Fin-stabilized Rocket Trajectory Under Quadratic Drag Law, by K. S. Sung and C. Park, *J. Aero/Space Sci.*, vol. 27, May 1960, pp. 388–389.

Vehicle Design, Testing and Performance

Navy Symposium on Aeroballistics, 4th, Dahlgren, Va., May 1, 1958, Proceedings, *NavOrd Rep.* 5904, vol. 1 (*NPG Rep.* 1599).

A Glide Missile Study, by A. A. Fojt, *Paper* 5, 23 pp.

Mathematical Models Used in the Analysis of Third Stage Vanguard, by Charles H. Frick and Elbert C. Hubbard, *Paper* 25, 12 pp.

Joint Army-Navy-Air Force Solid Propellant Rocket Static Test Panel, 7th Meeting, Bulletin, Addendum, *Solid Propellant Information Agency, Publication* SPSTP/7A, Oct. 1959, 31 pp.

Straight-pipe Diffuser Thrust Stand for Measuring High Altitude Rocket Performance, pp. 11–31.

Advances in Space Science, ed. by Frederick I. Ordway III, vol. 1, Academic Press, N. Y., 1959, 412 pp.

Manned Space Cabin Systems, by Eugene B. Konecci, pp. 159–265.

Recovery of Guided Weapons, by S. B. Jackson, *Aircr. Engng.*, vol. 32, March 1960, pp. 73–76.

Mass Considerations in Ring Supported Solar Sails, by W. E. Jahsman, ARS JOURNAL, vol. 30, March 1960, pp. 287–288.

Observation Satellites: Problems and Prospects, by Amron H. Katz, ASTRONAUTICS, vol. 5, April 1960, pp. 26–29, 74, 76, 78, 80.

Thermal Protection of Space Vehicles, by Peter E. Glaser, ASTRONAUTICS, vol. 5, April 1960, pp. 40–41, 105.

Flight Testing of Manned Orbital Vehicles, *Soc. of Exptl. Test Pilots*, vol. 4, no. 2, Winter 1960, pp. 83–88.

A Study of Methods for Simulating the Atmosphere Entry of Vehicles with Small-scale Models, by Byron L. Swenson, *NASA TN* D-90, April 1960, 51 pp.

An Analysis of the Impact Motion of an Inflated Sphere Landing Vehicle, by E. Dale Martin and John T. Howe, *NASA TN* D-314, April 1960, 45 pp.

Gas Dynamics of an Inflated Sphere Striking a Surface, by John T. Howe and E. Dale Martin, *NASA TN* D-315, April 1960, 49 pp.

Maximum - effort—Minimum - support Simulated Space Flight, by George T. Hauty, *Aero/Space Engng.*, vol. 19, April 1960, pp. 44–47.

Mercury Capsule and Its Flight Systems, by Maxine A. Faget and Robert O. Piland, *Aero/Space Engng.*, vol. 19, April 1960, pp. 48–53.

Thermal Control of the Explorer Satellites, by Gerhard Heller, ARS JOURNAL, vol. 30, no. 4, April 1960, pp. 344–352.

Simple Formula for Prediction and Automatic Scrutation, by R. J. Duffin and T. W. Schmidt, ARS JOURNAL, vol. 30, no. 4, April 1960, pp. 364–365.

Experimental and Analytical Study of Rolling-velocity Amplification During the Thrusting Process for Two 10-inch-diameter Spherical Rocket Motors in Free Flight, by C. William Martez and Robert L. Swain, *NASA Tech. Mem.* X-75, Sept. 1959, 36 pp. (Declassified by authority of *NASA TPA* 17, 4/14/60, p. 20.)

Guidance and Control

Analog Computer Technique for Plotting Frequency Response, by John L. Webster and David N. Schultz, ARS JOURNAL, vol. 30, March 1960, pp. 273–275.

On Mid-course Guidance in Satellite Interception, by G. W. Morgenthaler, *Astronautica Acta*, vol. 5, no. 6, 1959, pp. 328–346.

A Unified Analytical Description of Satellite Attitude Motions, by R. E. Roberson, *Astronautica Acta*, vol. 5, no. 6, 1959, pp. 347–355.

Terminal Guidance for Rendezvous in Space, by Raymond S. Wiltshire and W. H. Clohessy, *Astron. Sci. Rev.*, vol. 1, no. 4, Oct.–Dec. 1959, pp. 9–10.

Orbital Propulsion System for Space Maneuvering, by Sterge T. Demetriades, *Astron. Sci. Rev.*, vol. 1, no. 4, Oct.–Dec. 1959, pp. 17–18, 26.

Magnetometer System for Orientation in Space, by H. E. DeBolt, *Electronics*, vol. 33, April 8, 1960, pp. 55–58.

Design of a Final Calibration Stand for a Pendulous Integrating Gyroscope, by George E. Sontag and John L. Perample, *General Motors Engng. J.*, vol. 7, Jan.–March 1960, pp. 13–16.

Bang-bang Versus Linear Control of a Second-order Rate-type Servomotor, by P. F. Meyfarth, *J. Basic Engng.* (*ASME Trans., Series D*), vol. 82, no. 1, March 1960, pp. 66–72.

Influence of Pitching on the Critical Oscillation Velocity of Missiles, by C. Beatrix, *Recherche Aéron.*, no. 74, Jan.–Feb. 1960, pp. 55–59. (In French.)

Precision Gyro Operation Through Torque Averaging, by Martin S. Klemes, Arthur W. Lane and Edgar L. Zeigler, *Sperry Engng. Rev.*, vol. 12, Dec. 1959, pp. 23–27.

Exploratory Statistical Analysis of Planet Approach-phase Guidance Schemes Using Range, Range-rate, and Angular-rate Measurements, by David P. Harry III and Alan L. Friedlander, *NASA TN* D-268, March 1960, 81 pp.

Control System Analysis and Design via the "Second Method" of Liapunov, by R. E. Kalman and J. E. Bertram, *RIAS, Inc., Monograph* 59-13, 1959, 37 pp. (National Automatic Control Conference, Dallas, Nov. 4–5, 1959, *Paper* 59-NAC-2 and 3.)

Recent Soviet Contributions to Ordinary Differential Equations and Non-linear Mechanics, by Joseph P. LaSalle and Solomon Lefshetz, *RIAS, Inc., Tech. Rep.* 59-3, April 1959, 47 pp. (*AFOSR TN* 59-308; *ASTIA AD* 213 092.)

National Electronics Conference, 15th, Chicago, Oct. 1959, Proceedings, Chicago, The Conference, 1960, 1089 pp.

Trends in Adaptive Control Systems, by John G. Truxal, pp. 1–16.

Multidimensional Adaptive Control, by John E. Gibson, pp. 17–26.

On the Philosophy of Adaptive Control for Plant Adaptive Systems, by M. Margolis and C. T. Leondas, pp. 27–33.

Use of Cross Correlation in an Adaptive Control System, by G. W. Anderson, R. N. Buland and G. R. Cooper, pp. 34–45.

Modern Navigation—A Survey, by C. W. Draper, pp. 761–768.

A Glance at the Salient Points of Space Guidance, by Bernard Lee, pp. 769–783.

The Synthesis of Velocity Inertial Navigation Systems, by F. V. Johnson, pp. 784–793.

High Speed Inertial Platform Stabilization and Control, by Martin Finke, pp. 794–806.

Radar Target Angular Scintillation in Tracking and Guidance Systems Based on Echo Signal Phase Front Distortion, by Dean D. Howard, pp. 840–849.

Designing Control Circuits for Objects with Pure Lags, by E. L. Itskovich, *Automation and Remote Control* (*trans. of Avtomatika i Telemekhanika*), vol. 20, no. 8, Aug. 1959, pp. 983–991.

The Equation and Certain Properties of an Automatic Control System's Root Locus, by N. N. Mikhailov, *Automation and Remote Control* (*trans. of Avtomatika i Telemekhanika*), vol. 20, no. 8, Aug. 1959, pp. 1063–1070.

On a Tracking Drive with Gyroscopes on an Oscillating Platform, by S. G. Kolesnichenko, *Automation and Remote Control* (*trans. of Avtomatika i Telemekhanika*), vol. 20, no. 8, Aug. 1959, pp. 1071–1078.

Precision Tracking with Monopulse Radar, by J. H. Dunn and D. D. Howard, *Electronics*, vol. 33, April 22, 1960, pp. 51–56.

Cockpit Presentation and Controls for Space Vehicles, *Soc. Exptl. Test Pilots*, vol. 4, no. 2, Winter 1960, pp. 39–107.

Fundamentals of Astrodynamics, by Robert M. L. Baker Jr. and Maud W. Makemson, *Univ. Calif., Los Angeles, Astrodynam. Rep.* 6, Sept. 1959, 336 pp. (*AFOSR TN* 59-1045.)

Dynamics of a Gyroscope with Two Degrees of Freedom, by M. Z. Litvin-Sedoi, *Akademiia Nauk SSSR, Izvestiia, Otdelenie Tekhnicheskikh Nauk, Mekhanika i Mashinostroenie*, no. 5, Sept.-Oct. 1959, pp. 72–78. (In Russian.)

Motion Stability of a Gyroscope in Gimbals, by L. M. Karkhashov, *Akademiia Nauk SSSR, Izvestiia, Otdelenie Tekhnicheskikh Nauk, Mekhanika i Mashinostroenie*, no. 5, Sept.-Oct. 1959, pp. 79–83. (In Russian.)

Integral Quality Indicators in the Theory of Automatic Control and Estimate of the Behavior of a Function by Means of the Known Value of the Functional, by L. I. Rozonoer, *Akademiia Nauk SSSR, Izvestiia, Otdelenie Tekhnicheskikh Nauk, Energetika i Avtomatika*, no. 4, July-Aug. 1959, pp. 93–96. (In Russian.)

Effect of Vibrational Interferences on the Stability and Dynamic Qualities of Nonlinear Automatic Control Systems, by E. P. Popov, *Akademiia Nauk SSSR, Izvestiia, Otdelenie Tekhnicheskikh Nauk, Energetika i Avtomatika*, no. 4, July-Aug. 1959, pp. 97–105. (In Russian.)

One Method of Determining the Transition Component of Motion of An Automatic Control System with Arbitrary Excitation, by P. I. Chinaev, *Akademiia Nauk SSSR, Izvestiia, Otdelenie Tekhnicheskikh Nauk, Energetika i Avtomatika*, no. 4, July-Aug. 1959, pp. 105–111. (In Russian.)

Calculation of a Self-adapting Servosystem Having Two-step Parameter Control, by Iu. M. Kozlov, *Akademiia Nauk SSSR, Izvestiia, Otdelenie Tekhnicheskikh Nauk, Energetika i Avtomatika*, no. 4, July-Aug. 1959, pp. 112–115. (In Russian.)

Microminiaturizing a Space Vehicle Computer; the Problems Involved and an Approach to Solve Them, by E. Keonjian, *Electronics*, vol. 33, April 29, 1960, pp. 95–98.

The Theory of Gyrocompass, by V. N. Koshliakov, *PMM: J. Appl. Math. & Mech.*, vol. 23, no. 4, 1959, pp. 1164–1173.

On the Equations of the Precessional Theory of a Gyroscope in the Form of Equations of Motion of the Pole in the Phase Plane, by A. Iu. Ishlinskii, *PMM: J. Appl. Math. & Mech.*, vol. 23, no. 4, 1959, pp. 1153–1163.

A Particular Solution of the Problem of the Motion of a Gyroscope on Gimbals, by A. A. Bogoiavlenskii, *PMM: J. Appl. Math. & Mech.*, vol. 23, no. 4, 1959, pp. 1365–1369.

The Accelerated Placing of a Gyroscopic Compass in a Meridian, by Ia. N. Roitenberg, *PMM: J. Appl. Math. & Mech.*, vol. 23, no. 4, 1959, pp. 1370–1374.

Motion of Stabilized Gyroscopic Systems on a Moving Base, by V. S. Novoselov, *PMM: J. Appl. Math. & Mech.*, vol. 23, no. 4, 1959, pp. 1375–1381.

Investigation of the Stability of a Gyroscope Taking into Account the Dry Friction on the Axis of the Inner Cardan Ring (Gimbal), by V. V. Krementulo, *PMM: J. Appl. Math. & Mech.*, vol. 23, no. 4, 1959, pp. 1382–1386.

The Theory of Quality of Nonlinear Control Systems, by Shzhan Sy-In, *PMM: J. Appl. Math. & Mech.*, vol. 23, no. 4, 1959, pp. 1387–1392.

Problems of Interplanetary Navigation and Atmospheric Re-entry, by T. R. F. Nonweiler, *J. Royal Aeron. Soc.*, vol. 64, March 1960, pp. 155–160.

Instrumentation and Communications

Communication, Navigation, and Range Facilities Required for Space Exploration, *Soc. Exptl. Test Pilots*, vol. 4, no. 2, Winter 1960, pp. 51–82.

Sensitive Thermal Conductivity Gas Analyzer, by John R. Purcell and R. N. Keeler, *Rev. Sci. Instr.*, vol. 31, March 1960, pp. 304–305.

The Synthesis of Atmospheric Forms and the Effective Parameters of the Lower Part of the Ionosphere at Low Frequencies, by Ia. L. Al'pert and D. S. Fligel, *Radio Engng. and Electronics* (*trans. of Radiotekhnika i Elektronika*), vol. 4, no. 2, 1959, pp. 65–77.

On an Approximate Method for Synthesizing Optimal Linear Systems for Separating Signal from Noise, by Yu. P. Leonov, *Automation and Remote Control* (*trans. of Avtomatika i Telemekhanika*), vol. 20, no. 8, Aug. 1959, pp. 1039–1048.

National Electronics Conference, 15th, Chicago, Oct. 1959, Proceedings, Chicago, The Conference, 1960, 1089 pp.

Performance Improvement in Single Channel Voice Communication Radio System in Space, by Leang P. Yeh, pp. 151–162.

Synchronous Reception in a PCM/PS Telemetry System, by H. Rasllard and H. N. Putschi, pp. 163–172.

Instrumentation for a Heat Budget Earth Satellite, by R. J. Parent and Wayne B. Swift, pp. 824–829.

The Theory and Design of a Clamped-diaphragm Composite-dielectric, Variable-capacitance Transducer, by K. Posel, *Univ. Witwatersrand, Johannesburg, S. Africa, Dept. Mech. Engng., Rep.* 1/59, Dec. 1959, 36 pp.

Advances in Space Science, ed. by Frederick I. Ordway III, vol. 1, Academic Press, N. Y., 1959, 412 pp.

Interplanetary Communications, by J. R. Pierce and C. C. Cutler, pp. 55–110.

Comments on Far Field Scattering from Bodies of Revolution, by K. M. Siegel, R. D. Goodrich and V. H. Weston, *Appl. Sci. Res., Sect. B*, vol. 8, no. 1, 1959, pp. 8–12.

Refraction Correction Techniques in Earth Satellite Optical Tracking for Precision Prediction, by Albert D. Wasel, ARS JOURNAL, vol. 30, no. 3, March 1960, pp. 282–284.

A Rocket Borne Video Telescope for Observing Mars, by D. H. Robey, *Astronautica Acta*, vol. 5, no. 6, 1959, pp. 313–327.

Camera Control System for Rocket Sled Tests, by F. M. Gardner and L. R. Hawn, *Electronics*, vol. 33, April 1, 1960, pp. 63–65.

Characteristics of Infrared Detectors, by S. F. Jacobs, *Electronics*, vol. 33, April 1, 1960, pp. 72–73.

Index to Advertisers

Optimum Frequencies for Outer Space Communication, by George W. Haydon, *J. Res., Nat. Bur. Standards, D., Radio Propagation,* vol. 64D, no. 2, March–April 1960, pp. 105–110.

Nonresonance Absorption of Electromagnetic Waves in a Magnetoactive Plasma, by B. N. Gershman, *Soviet Physics-JETP,* vol. 37(10), no. 3, March 1960, pp. 497–503.

A Review of Infrared Developments, by Barton J. Howell, *Sperry Engng. Rev.,* vol. 12, Dec. 1959, pp. 28–38.

Directional Sensitivity for a Finite Hot-wire Anemometer, by S. Corrsin, *Johns Hopkins Univ., Mech. Engng. Dept.,* 1960, 10 pp.

A Transistorized Galvanometer Current Limiter, by P. L. Clemens and R. L. Ledford, *Arnold Engng. Dev. Center, ARO, Inc.,* AEDC-TN-59-110, Nov. 1959, 19 pp.

The Effect of Nuclear Radiation on Electronic Components, by H. Cary, J. F. Hansen, W. E. Chapin, E. N. Wyler and H. S. Scheffler, *Battelle Mem. Inst., Radiation Effects Info. Center, REIC Rep.* 8, July 1959, 24 pp.

The Manometer Error Caused by Small Leaks in the Casing of a Satellite, by S. A. Kuchay, *NASA Tech. Transl.* F-14, April 1960, 7 pp.

Midwestern Conference on Fluid Mechanics, 6th, Austin, Texas, 1959, Proceedings, Austin, University of Texas, 1960, 464 pp.

An Electro-mechanical Transducer for Measuring Dynamic Pressures in Fluids, by Donald A. Gilbrech, pp. 320–330.

High Temperature Semiconductor Thermocouples, by P. S. Kislyi and G. V. Samsonov, *Akademiia Nauk SSSR, Izvestiia, Otdelenie Tekhnicheskikh Nauk, Metallurgiia i Toplivo,* no. 6, Nov.-Dec. 1959, pp. 133–136. (In Russian.)

Effect of Magnetodielectric Media on the Distribution of Electromagnetic Waves in a Spiral Wave-guide Located in a Magnetodielectric, by B. M. Bulgakov and V. P. Shestopalov, *Akademiia Nauk SSSR, Izvestiia, Otdelenie Tekhnicheskikh Nauk, Energetika i Avtomatika,* no. 4, July-Aug. 1959, pp. 166–176. (In Russian.)

Recent Advances in Space Solar Observatory Instrumentation, by William S. Rense, ARS JOURNAL, vol. 30, no. 4, April 1960, pp. 313–322.

Foucault Pendulum Effect in a Schuler-tuned System, by Charles Boxmeyer, *J. Aero/Space Sci.,* vol. 27, May 1960, pp. 343–347.

Millimicrosecond Pulsing—Its Application and Technique, by W. M. Good, *Nuclear Instr. & Methods,* vol. 6, March 1960, pp. 323–330.

Atmospheric and Space Physics

Measurements of Flux of Small Extraterrestrial Particles, by H. A. Cohen, *Air Force Cambridge Res. Center, Geophys. Res. Directorate, Res. Notes* 28, *AFCRC-TN-59-647,* Jan. 1960, 11 pp.

The Composition of Outer Space, by Francis S. Johnson, ASTRONAUTICS, vol. 5, April 1960, pp. 30–31, 92, 94.

Production of K Mesons by Cosmic-ray Protons at 3250 m Above Sea Level, by M. Ya. Balats, P. I. Lebedev and Yu. V. Obukhov, *Soviet Physics-JETP,* vol. 37 (10), no. 3, March 1960, pp. 417–421.

Taking Account of the Gravitational Energy, by D. D. Ivanenko and N. V. Mitskevich, *Soviet Physics-JETP,* vol. 37(10), no. 3, March 1960, pp. 618–619.

On Linear Theories of Gravitation, by V. I. Pustovoit, *Soviet Physics-JETP,* vol. 37(10), no. 3, March 1960, pp. 619–620.

Upper Atmosphere and Satellite Drag, by R. J. Stirton, *Smithsonian Contribs. to Astrophys.,* vol. 5, no. 2, 1960, pp. 9–15.

"The Astronomical Unit" and the Solar Parallax, by Samuel Herrick, George Westrom and Maud W. Makemson, *Univ. Calif., Los Angeles, Astrodynam. Rep.* 5, Sept. 1959, 25 pp. (*AFOSR TN* 59-1044.)

The Meteoric Heat Echo, by Allan F. Cook and Gerald S. Hawkins, *Smithsonian Contribs. to Astrophys.,* vol. 5, no. 1, 1960, pp. 1–7.

The Structure of the Sunspot Zone, by Barbara Bell, *Smithsonian Contribs. to Astrophys.,* vol. 5, no. 3, 1960, pp. 17–28.

Temperature Fluctuations in the Atmospheric Boundary Layer, by C. H. B. Priestley, *J. Fluid Mech.,* vol. 7, March 1960, pp. 373–384.

Solar Flare Connected with an Increase of Intensity of Cosmic Rays, by L. Křivský, J. Hladký, P. Mokrý et al., *Nuovo Cimento,* vol. 15, no. 4, Feb. 16, 1960, pp. 695–699.

Electromagnetic Phenomena in Cosmical Physics (International Astronomical Union Symposium No. 6, Stockholm, Aug. 1956), B. Lehnert, ed., Cambridge, at the University Press, 1958, 545 pp.

Planetary Astronomy from Satellite-substitute Vehicles, by John D. Strong, G. H. de Vaucouleurs and Fritz Zwicky, *Air Force Missile Dev. Center, Holloman Air Force Base, New Mex.,* March 1960, 169 pp., 144 refs. (*AFMDC-TR-60-6.*)

Some Results of the Measurement of the Spectrum Mass of Positive Ions by the 3d Artificial Earth Satellite, by V. G. Istomin, *NASA Tech. Transl.* F-7, April 1960, 19 pp.

The Determination of the Density of the Atmosphere at an Altitude of 430 Kilometers by the Sodium Vapor Diffusion Method, by I. S. Shklovskiy and V. G. Kurt, *NASA Tech. Transl.* F-15, April 1960, 13 pp.

Twisted Ray Paths in the Ionosphere, by C. B. Haselgrove and Jenifer Haselgrove, *Proc., Phys. Soc., London,* vol. 75, March 1960, pp. 357–363.

Human Factors and Bioastronautics

The Role of a Human Operator in Space Flight Development, *Soc. Exptl. Test Pilots,* vol. 2, no. 2, Winter 1960, pp. 3–27.

Physiological and Psychological Rigors of Space Travel, *Soc. Exptl. Test Pilots,* vol. 4, no. 2, Winter 1960, pp. 28–50.

Advances in Space Science, ed. by Frederick I. Ordway III, vol. 1, Academic Press, N. Y., 1959, 412 pp.

Radiation and Man in Space, by Hermann J. Schaefer, pp. 267–339.

Nutrition in Space Flight, by Robert G. Tischer, p. 341.

Advanced Propulsion Systems Symposium, Los Angeles, Dec. 11–13, 1957, **Proceedings,** ed. by Morton Alperin and George P. Sutton, Pergamon Press, N. Y., 1959, 237 pp.

Human Hazards of Space Flight, by Homer J. Steward, pp. 199–204.

Extraterrestrial Life, by Harlow Shapley, ASTRONAUTICS, vol. 5, April 1960, pp. 32–33, 50, 52.